

TOHOKU UNIVERSITY
Graduate School of Engineering

Dynamics and Control of Space Manipulators
During a Satellite Capturing Operation

A dissertation submitted for the degree Doctor of Philosophy (Engineering)

Department of Aerospace Engineering

by

Dimitar DIMITROV

08 February 2005

To my best friend Chika.

And in memory of my mother and father

Acknowledgments

It is a great pleasure for me to acknowledge the people who have helped and inspired me during my development as a researcher.

I would like to begin by expressing my gratitude to my thesis supervisor and advisor, Prof. Kazuya Yoshida, for his guidance during the course of my Ph.D. study here in Tohoku University - Japan. I have benefited greatly from his valuable advises and believe that the freedom I had in my research, changed my perspective and understanding about “what research really is”. The discussions that we had, formed me (I believe) as a good researcher, and will influence me in the years to come. I am honored to be his student.

I would like to give special thanks to the members of the thesis examination committee for their support and valuable comments: Prof. Kazuya Yoshida (Chairman of the committee), Prof. Masaru Uchiyama, Prof. Kazuhiro Kosuge, and especially to Prof. Dragomir Nenchev, who’s detailed remarks, not only led to the reshaping of this thesis, but broadened my perspective as well.

I would like to thank again Prof. Dragomir Nenchev, who was my adviser during my stay in Hirosaki University. His determination and style of scientific pursuit, left a mark in my behavior not only as a researcher but as an individual. Now, writing these lines, makes me remember that he was the one who led me to the idea of pursuing my Ph.D. here at Tohoku University. On a personal note, I would like to thank him and his wife (Mariana), for helping me to find a part time job, and assisting me greatly during the first six months of my stay in Hirosaki, when I was self supported.

It gives me a great pleasure to thank Prof. Veselin Pavlov, who was my adviser during my university years in the Technical University - Sofia. His inspiring lectures on kinematics and synthesis of robotic manipulators were very helpful in my work. I would like to thank him for his extraordinary patience, and enduring optimism, at a time when I was very frustrated and stuck in my research. His encouragement and understanding were very stimulating. I owe him an apology for letting him down, and not finishing my doctoral dissertation in my home University, where I was enrolled in the Ph.D. program for almost two years.

Special thanks are due to all my colleagues from the Space Robotics Laboratory at To-

hoku University. The research environment was incredible guys. I am particularly grateful to Hikoki Nakanishi, Satoko Abiko and Gabriele Gilardi, for the many hours of discussion, advice, and assistance. Special credit is due to Yoichiro Sato, Hiromitsu Watanabe and Kaori Shoji who developed a real time dynamic simulation environment, which proved to be helpful for my research. I also thank Genya Ishigami and Marco Antonio Chacin Torres, for helping me with useful suggestions in many cases, and especially Tomohisa Oki, who assisted me very much during the preparation of this thesis.

It is really impossible for this acknowledgment to be complete without thanking Nikolai Angelov (Boncho), with whom we developed a shared MS graduation thesis. The joint research was very important experience for me.

My stay in Tohoku University was possible thanks to the support I received from the Japanese Government (Monbukagakusyo scholarship), for which I am grateful.

On a personal note, I would like to thank my aunt Elka and my cousin Dragomir, who were helping me from Bulgaria during my stay in Japan. I am very grateful to my grandmothers who are always supporting me.

I also would like to thank my girlfriend Chika, who is my guide in this 不思議の国 Japan.

Finally, I must acknowledge my parents Veska and Nikolai, who dedicated their lives to me and my brother.

Abstract

Free-flying manipulator systems are envisioned to perform servicing, inspection and assembling operations in orbit. The control of such systems is a challenging task, since the equations that govern their motion are highly nonlinear. Furthermore, unlike fixed-base manipulators a free-floating robot exhibits nonholonomic behavior as a result of the nonintegrability of the angular momentum conservation law.

Much effort has already been dedicated to free-flying and free-floating systems from the viewpoint of inertia coupling effects between the manipulator and base motion. In many cases such coupling effects are beneficial (base vibration suppression control using the manipulator system), in others they impose great difficulties for the control algorithms (applications related to reactionless motion planning). Extensive analysis of this phenomenon is necessary since it can extend the capabilities of space manipulators. In this thesis, different problems typically appearing as a result of the above mentioned dynamic coupling effects are discussed.

The work is divided into six parts. Chapter 1 is introductory and outlines some of the typically appearing difficulties during the utilization of free-flying and free-floating systems. It is organized as a short literature survey that makes an overview of some of the dynamic modeling, planning and control strategies introduced up to now.

Chapter 2 develops the dynamic equations governing the motion of a general manipulator system with open or closed-loop structure that is mounted on a free-floating base. The formulation presented is used as a framework for the remaining chapters of this thesis.

Chapter 3 makes an outline of some of the fundamental concepts and strategies used for the control of free-floating systems. It is intended to be a review of some of the existing methods, closely related to the problems studied in this thesis.

The main topic addressed in this study is the capture of a tumbling satellite using a robotic manipulator. In recent years, such operation has been recognized to be a priority task, since its solution is expected to be applied to a variety of space missions, involving servicing, inspection, and repairing operations. The approaching motion of a manipulator arm to a target satellite and the resulting post-impact motion of the system are discussed in Chapters 4 and 5, respectively. The aims of the analysis made can be outlined as

follows;

- (1) to provide further insight into the problems occurring while capturing a tumbling satellite;
- (2) to propose a new method for planning reactionless end-effector paths to a desired point in Cartesian space;
- (3) to propose a strategy using bias angular momentum that can facilitate the trajectory planning and post-impact control;
- (4) to propose two control laws for the post-impact phase that can manage the momentum in the system in a desired way.

The main contributions of Chapter 4 are: (i) introduction of the *Holonomic Distribution Control*, which can be utilized for reactionless path planning to a stationary target satellite; (ii) the introduction of the *Bias Momentum Approach*, methods for its application and discussion on its influence on the post-impact motion of the system.

In Chapter 5, analysis of manipulator motions that result in maintaining the stationary state of the spacecraft's base in the presence of external wrenches is made. The *Distributed Momentum Control* is introduced and compared with existing post-impact control strategies.

The final chapter consists of conclusions and remarks for possible future work.

The utilization of the three new concepts introduced in this thesis;

(**c**¹) *Holonomic Distribution Control*;

(**c**²) *Bias Momentum Approach*;

(**c**³) *Distributed Momentum Control*,

can be beneficial for the solution of variety of practical problems. In each section, notes on the practical implementation of those concepts are made. In addition, numerical simulations are performed in order to verify and demonstrate their usefulness.

Contents

Acknowledgments	i
Abstract	iii
1 Introduction	1
1.1 Space manipulator systems	1
1.2 Current State-Of-The-Art	3
1.2.1 Kinematics and dynamics modeling for space manipulators	3
1.2.2 Trajectory and path planning for space manipulators	4
1.2.3 Satellite capturing operation	5
1.3 Contribution statement	8
2 Dynamics of free-flying manipulator systems	9
2.1 Choice of coordinates	10
2.1.1 Independent coordinates	10
2.1.2 Dependent coordinates	11
2.1.2.1 Relative coordinates	11
2.1.2.2 Reference point coordinates (Cartesian)	12
2.1.2.3 Natural coordinates (fully Cartesian)	13
2.2 Space of allowable motions (SAM)	14
2.3 Role of SAM in the dynamic analysis	16
2.3.1 Example: Lagrange multipliers elimination	16
2.4 Formulation in independent coordinates	19
2.4.1 Open-loop systems	20
2.4.1.1 Computation of the non-linear term \mathbf{c}_n and matrix \mathbf{R}^o	22
2.4.2 Closed-loop systems	27
2.4.2.1 Coordinate partitioning	29
2.4.2.2 Constraint equations and matrix Φ_z^c for a cut rotational joint	30
2.4.2.3 Forming \mathbf{R}^c and calculation of the dependent velocities	32

2.4.2.4	Calculation of the dependent accelerations	33
2.4.2.5	Computation algorithm	34
2.5	Summary	35
3	Fundamental control concepts and strategies	37
3.1	Subspace of reactionless motions	38
3.1.1	Solution for the joint variables	41
3.1.1.1	Pseudoinverse approach	43
3.1.1.2	Coordinate partitioning approach	44
3.1.1.3	Task space augmentation approach	45
3.1.2	Torque based reactionless manipulation	46
3.2	Multiple tasks	47
3.2.1	Task performance measure	49
4	Approaching phase of a satellite capturing operation	51
4.1	Problem definition and assumptions	53
4.2	The coupling wrench theorem	54
4.3	Reduced form of the equations of motion	55
4.4	Approaching maneuver to a stationary target satellite	58
4.4.1	Pfaffian constraints	59
4.4.2	Holonomic Distribution Control	63
4.4.3	Application of the Holonomic Distribution Control	65
4.4.4	Simulation Study	66
4.5	Approaching maneuver to a tumbling target satellite	71
4.5.1	The Bias Momentum Approach	73
4.5.1.1	Non-bias distribution	73
4.5.1.2	Bias angular momentum in the manipulator	74
4.5.1.3	Angular momentum management	76
4.5.2	Planning of approaching trajectory when BMA is utilized	76
4.5.2.1	<i>Step A</i> - Choice of manipulator initial configuration	77
4.5.2.2	<i>Step B</i> - Determining the Momentum Profile	78
4.5.2.3	Simulation Study	79
4.5.3	Comparison between different state variables	85
4.5.3.1	Simulation Study	86
4.5.4	Bias Momentum Approach - verification by simulation	92

5 Post-impact motion control issues	97
5.1 Reaction Null Space Control	97
5.2 Distributed Momentum Control	99
5.3 Application to single arm manipulator	101
5.3.1 Utilization of gas/jet thrusters for attitude control	106
5.4 Application to dual manipulator system	111
6 Conclusions and future work	113
6.1 Summary	113
6.2 Future work	115
Bibliography	117
Biography and List of Publications	126
A Derivation of \dot{B}_i and \dot{b}_i	131
B Example for coordinate partitioning	133
C Momentum conservation equation	135
D Components of the inertia matrix H	141
E Reduced equation of motion	145
F Parameters of the manipulators used	149
F.1 3D 7 DOF manipulator	149
F.2 Planar 6 DOF dual-arm system	152

List of Figures

1.1	Japanese Experimental Module Remote Manipulator System (JEM-RMS) (Courtesy of JAXA)	2
1.2	Chaser and target satellites.	5
2.1	Comparison between different types of coordinates	11
2.2	Two consecutive bodies connected by a rotational joint. All vectors are expressed in the inertial coordinate frame.	23
2.3	A tree manipulator system mounted on a free-floating base.	25
2.4	System containing a closed loop.	31
2.5	Dimensions of the matrices involved during the stages of the dynamic for- mulation.	36
3.1	Coupling motion between the base and manipulator system.	38
3.2	Mapping of the joint velocities on the base motion in the case when $\mathcal{L}_0 = 0$. $C(\cdot)$ represents the <i>range space</i> (column space) and $N(\cdot)$ is the null space of a matrix.	42
4.1	Four phases of a capturing operation. During the <i>closing in phase</i> , the chaser spacecraft performs an orbital maneuver to the target satellite (this maneuver can be referred to as approach, nevertheless, we want to make a clear distinction between global motion of the spacecraft, and local motion of the manipulator, hence, the term <i>approach</i> will be used only regarding the manipulator's motion). During the approach (case B), the robot arm follows a predefined trajectory profile and reaches a grasping point posi- tioned on the target satellite. During the <i>impact phase</i> , a griper system establishes a firm grip on the grasping facility. The final phase covers the post-impact motion of the system.	52
4.2	Model of a n DOF space robot capturing a target.	56
4.3	Unicycle constraints.	60

4.4	Cartesian paths when using different <i>primitives</i> for a three DOF planar manipulator mounted on a free-floating base.	64
4.5	End-effector path in Cartesian space. The manipulator configuration is depicted at the initial, intermediate and final positions.	68
4.6	Profiles of the joint angles and joint angular velocities.	70
4.7	Model of a space robot capturing a target, where \mathbf{L}_{bm} denotes the coupling angular momentum between the manipulator arm and the base of the chaser satellite, and \mathbf{L}_t stands for the angular momentum in the target satellite. .	72
4.8	Four cases of pre-impact angular momentum distribution.	74
4.9	Angular momentum management among the reaction wheels and the manipulator.	75
4.10	End-effector position and velocity in cases \mathbf{S}_A and \mathbf{S}_{AB} (x , y , z axis).	82
4.11	Profile of the torques in the reaction wheels derived using <i>Step A</i> and <i>Step B</i> from the trajectory planning procedure.	83
4.12	Manipulator configuration at t_0 and t_f for case \mathbf{S}_{AB}	83
4.13	Motion profile of the manipulator from t_0 to t_f for case \mathbf{S}_{AB} (the view angle is different from the one in Fig. 4.12).	84
4.14	Position and linear velocity of the end-effector.	89
4.15	Profile of the torque in the reaction wheels (x , y and z axis).	90
4.16	Joint velocities.	91
4.17	Comparison of the base attitude change in case of full-bias and non-bias momentum distributions (x , y and z axis).	94
4.18	Angular momentum distribution for the full-bias and non-bias cases (x , y and z axis).	95
5.1	Angular momentum “flow” when DMC is used.	100
5.2	Angular momentum distribution when DMC and RNSC are used during the post-impact phase (x , y and z axis).	102
5.3	Base attitude comparison when DMC and RNSC are used (x , y and z axis).	103
5.4	Joint (1-6) velocity rates when DMC and RNSC are used.	104
5.5	Joint (7-10) velocity rates when DMC and RNSC are used.	105
5.6	Comparison of angular momentum distributions in case of DMC, and attitude control via thrusters.	108
5.7	Comparison of the base attitude deviations in case of DMC, and attitude control via thrusters.	109
5.8	Torque applied by the thrusters.	110
5.9	Angular momentum distribution for the dual-arm case.	111

5.10	Base attitude deviation for the dual-arm case.	112
5.11	Initial and final manipulator configurations in the post-impact phase.	112
C.1	Angular momentum expressed around different points. \mathbf{r}_0 and \mathbf{r}_g stand for the vectors from the inertial frame to the base and center of mass of the entire system, respectively.	137
F.1	3D 7DOF manipulator	150
F.2	2D 6DOF dual-arm	150

Chapter 1

Introduction

This chapter makes a brief review of some of the research activities and accomplishments made in the area of dynamic modeling, planning and control of space robotic systems. Many of the problems to be considered uniquely appear only in the case of moving base robots. Nevertheless, when possible, a parallel between such systems and ground-fixed manipulators will be made.

1.1 Space manipulator systems

Free-flying manipulator systems are envisioned to perform servicing, inspection and assembling operations in orbit. Equipped with highly dexterous tools and carried by transporter vehicles, their application in orbit is indispensable. However, in order the potential of manipulator systems for space applications to be fully utilized, a number of technical challenges need to be solved first. Those challenges arise in number of areas, including dynamics and control. In many cases it is not possible to directly use the already developed control strategies for fixed-base manipulators because the nature of the problems occurring are unique to space robots. In the sequel, some of the typical difficulties experienced in many space applications will be discussed. Ways for overcoming them by means of using articulated manipulator systems will be the main objective of this research.

The practical utilization of manipulator systems in space is already fact. In 1997 NASDA's ETS-VII satellite successfully demonstrated the rendezvous and docking with a cooperative target [127]. Other examples include the Canadian Special Purpose Dexterous Manipulator (SPDM), mounted on the space station remote manipulator system (SSRMS); the Japanese Experimental Module Remote Manipulator System (JEM-RMS), which consists of a macro and micro manipulator Fig. 1.1¹.

Utilization of *free-flying* manipulator systems for accomplishment of different space missions have already been proposed [16], [93]. The advantages of such systems are em-

¹The launching of JEM-RMS will be fact in the near future.

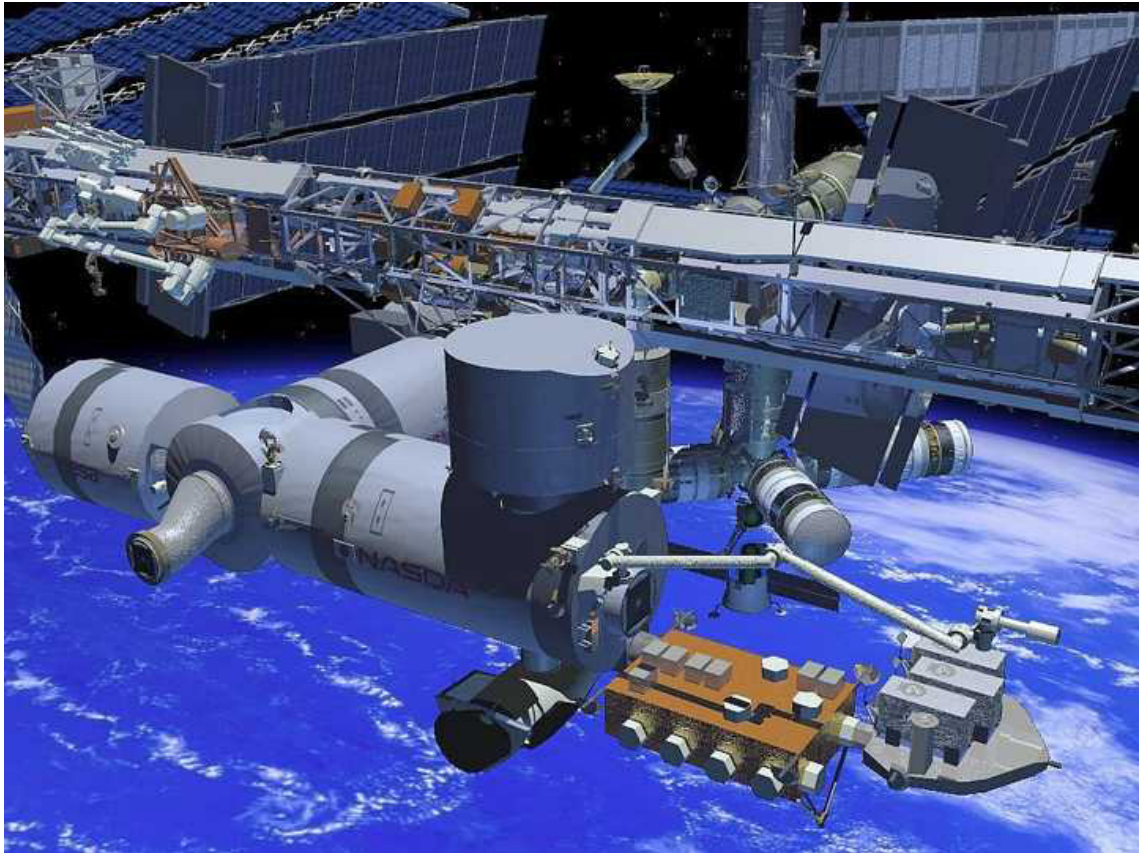


Figure 1.1: Japanese Experimental Module Remote Manipulator System (JEM-RMS) (Courtesy of JAXA)

phasized from the viewpoint of unlimited workspace and high level of redundancy. The linear and attitude motions of the spacecraft's base of a *free-flying* system are assumed to be actively controlled using reaction jets (thrusters) during the arm motion. Such approach, though simple and with straightforward implementation has a considerable disadvantage, since it leads to reduction of the life of a satellite system. This reduction comes from the fact that the amount of reaction jet's fuel is nonrenewable and limited resource in space. This problem is very challenging for the research community since its solution requires planning and control algorithms to be properly addressed.

As opposed to *free-flying* systems, the spacecraft of *free-floating* robot manipulators is not actively controlled during the process of manipulation. Since in such case the momentum is conserved², the arm motion will induce reactions to the base body. Especially, the angular reactional motion is mostly undesirable, since loss of communication with the ground-base and other problems can occur. A number of control strategies that cope with

²If the environmental disturbances are assumed negligible for the duration of the manipulator motion.

these difficulties are already introduced and will be outlined in the sequel. Furthermore, as noted in [89], [87] *free-floating* systems suffer from the so called *dynamic singularities*, which makes the analysis even more challenging. Clearly, the *free-flying* and *free-floating* modes can be employed during different phases of a mission.

1.2 Current State-Of-The-Art

This section is intended to be a short literature survey. An overview of some of the dynamic modeling, planning and control strategies (related to a satellite capturing operation) introduced up to now is made. A common starting point for such survey is from issues related to kinematic and dynamic modeling. This is an important aspect since in order suitable control algorithms to be designed and implemented, good understanding of robot dynamics is needed.

1.2.1 Kinematics and dynamics modeling for space manipulators

Dynamics of multibody systems is a field that have been studied by many researchers. A variety of approaches which differ in complexity and level of efficiency are available. Main focus of most of them is on Newton-Euler, Lagrangian or Kane's formulations [60], [37], [50]. Most of the research has been conducted mainly with respect to fixed-base manipulator systems, nevertheless majority of the methods available could be adopted for the case when the base body is free-floating.

Wittenburg [119], [96] was among the first to propose the use of the concept of reduced tree system to tackle the problems of dynamics for systems having close-loop structure. In the case when no external forces act on the system, simplifications to the dynamical model could be obtained by using the *virtual manipulator approach* proposed in [113], [114]. In [87], using barycentric vectors a study on the kinematics and dynamics of systems in *free-floating* mode is made. In [66], the idea of *direct path method* which results in more compact equations of motion was introduced, the authors discussed the *barycentric vector approach* as well. A detailed discussion on the dynamics of multibody systems is made in Chapter 2 where systematic derivation of a dynamic model for space manipulators with open and closed-loop structure is included.

Notes on kinematic modeling for multibody systems in space are made in [100], [21], [30]. In [112], the generalized Jacobian matrix³ is introduced. It is utilized by the authors in [19], where solution algorithms for the inverse kinematics of space manipulator systems are presented.

³In Appendix E the structure of the generalized Jacobian matrix is derived.

1.2.2 Trajectory and path planning for space manipulators

Trajectory planning for systems under nonholonomic constraints is a well known research field. A robotic manipulator mounted on a free-floating satellite exhibits nonholonomic behavior as a result of the nonintegrability of the angular momentum equation.

Up until now, different solutions to the path and trajectory planning problems for space manipulators have been proposed. As mentioned in the previous subsection, the concept of the generalized Jacobian matrix was introduced in [112]. It can be used for continuous control of the end-effector without controlling the vehicle's motion. A bidirectional approach for motion planning of free-floating space robots was proposed in [73]. It was shown that the final values of the state variables describing the system, depend not only on the n joint variables but also on the history of their trajectories and do not remain confined on a n -dimensional manifold. Such result clearly implies that, the end-effector can reach a desired position and orientation with different values of the state variables, even if only six joint are available. This indicates the presence of redundancy, in [75] the authors call it nonholonomic redundancy and propose ways for its utilization for facilitating the trajectory planning problem. In [115] Vafa and Dubowsky proposed the novel concept of a *virtual manipulator* which simplifies the kinematics and dynamics of a space robot system. By solving the motion of a virtual manipulator (fixed in the center of mass of the entire system) for a given end-effector trajectory, the motion of the base \leftrightarrow robot arm system can be obtained straightforwardly. Furthermore, using this approach they formulated a tool called “disturbance map” and then extended the notation to an “extended disturbance map” [110], [29] which suggests paths that result in low attitude fuel consumption⁴. Using optimization techniques for performing reactionless trajectory planning, as proposed in [20], [94] does not always converge to satisfactory results, where providing initial guess for the optimization algorithm is of great importance. In [90], the authors propose a manipulator design that provides a larger “reactionless workspace” and address the null space planning problem. In [88], [92], configuration and path planning for nonholonomic systems are discussed. The utilization of optimal control for redundant systems is discussed in [1], [71], [99]. Almost smooth time-invariant control for planar space manipulators is proposed in [67], where the authors discuss a stabilization technique without disregarding the existence of dynamic singularities. In addition, controllability issues related to serial space robot systems are discussed. A measure of the dynamic coupling of space robot systems based on the momentum conservation law is introduced in [120]. Such measure (based on a matrix relating the end-effector and base motions) can

⁴The application of the *extended disturbance map* for manipulators with more than 3 DOF is however difficult.

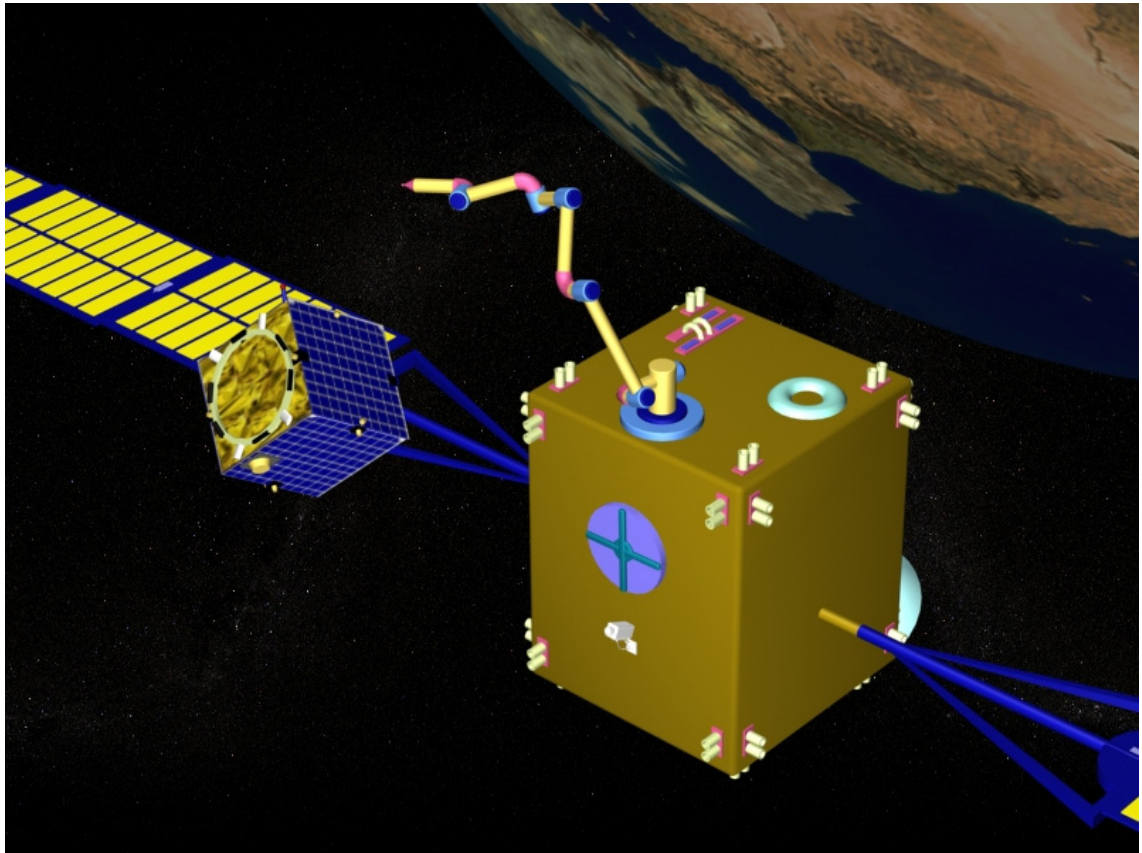


Figure 1.2: Chaser and target satellites.

be employed in order to aid the planning process.

1.2.3 Satellite capturing operation

In recent years, the capture of a free-floating target in orbit (Fig. 1.2) has been recognized as a priority task. Its importance is apparent from the fact that in most cases capturing operation should precede missions like servicing, inspection and assembly which are critical for the survival of existing satellites in orbit. Here, some of the main approaches related to satellite capture are outlined.

There has been a great deal of fundamental research in the area of space robotics and though capturing a tumbling object in space is a well known problem, it is difficult to distinguish one of the solutions proposed up to now, which can solve it readily. Discussing the whole process from the trajectory planning to the post-impact control is an arduous task. The nature of the problems occurring in the different phases of the capture can be completely different so most of the researchers tend to separate the operation into closing

in maneuver, approach⁵, impact and post-impact motion.

Most of the solutions presented up to now are from the viewpoint of force impulse generated during the contact. Different strategies for its estimation and minimization are presented in [130], [124], [117]. The concept of joint resistance model was introduced in [125], furthermore, the authors proposed the so called *impulse index* and *impulse ellipsoid* which adequately describe the force impulse characteristics. The effect of a “payload impact” on the dynamics of a flexible-link space robot is discussed in [23]. The application of impedance control when capturing a non-cooperative target is proposed in [128]. The condition which guarantees that the target will not be pushed away after the contact is clarified. A comprehensive discussion about the usage of the “*reaction null space*” is made in [82], [83]. The authors utilize the null space of the coupling inertia matrix in order to decouple the base and manipulator dynamics. Furthermore, they showed that obtaining joint velocities using this approach does not influence the momentum distribution whatsoever. A detailed discussion on a *momentum distribution* in a space manipulator is made in Chapter 4.

Other possible solutions to the capturing problem can be derived from the viewpoint of the angular momentum of the target object. Grasping a target satellite without considering its momentum will impose difficulties for the post-impact control and most probably the capturing operation will fail. Different solutions are proposed up to now. One of them utilizes a device with controllable momentum wheels (“space leech”), which has to be attached to the target [116] and absorb the angular momentum. In [64], the idea of rotational motion-damper is proposed. Using a *contact/push* based method, the angular momentum from the target is transferred to the chaser satellite in portions. This could result however, in separation from the target after each contact and therefore, the usage of gas-jet thrusters for linear motion is unavoidable. This method might be useful if the tumbling rate of the target is very large and direct capture is not possible. A similar method using “impulsive control” is proposed by Yoshikawa et al. [131]. A verification of the above strategy using experiment, is reported in [52]. In [76], Nakamura et al. utilize a “tethered retriever” which is guided to the target through the tension force in the tether and thrusters positioned on the retriever. In the post-impact phase, the angular momentum of the target is “absorbed” in attitude devices positioned on the retriever. In [111], the chaser satellite makes a fly-around maneuver in such a way that the capturing operation can be conducted with small relative motion between the two systems. The authors propose a “free motion path method,” which enables us to completely ignore the non-linearity effect in the dynamics by taking advantage of the conservative quantities of

⁵Here, with *approach*, the approaching motion of a manipulator arm to a target satellite is implied.

the system. In [69] using an extended Kalman filter, estimation of the target's motion is made. The authors assume that the inertia parameters of the target are known or can be estimated. At a next step the centroid of the chaser satellite is repositioned (using thruster power) to be along the angular momentum vector of the target satellite, and the spacecraft is actuated in order to obtain a certain angular velocity which can facilitate the manipulator approaching motion. In addition, experimental results are presented.

Other references include studies related to planning safe kinematic trajectories during the closing in maneuver to a target object [63], [41], [42]. Some control aspects of a capturing operation are studied in [39], [77], [62], [40], [91], [32]. The path planning problem to a free-floating target for a manipulator with angular momentum is addressed in [121], [122]. The capture of a spinning object using a dual flexible arm manipulator is studied in [123]. A development of a laboratory simulator for motion study of free-floating robots in relation to a target object is reported in [2]. Using this laboratory simulator, design issues related to free-floating planar robotic systems in view of optimal chasing and capturing operation, are addressed in [5]. Utilization of two free flyers for capture and manipulation of an object in space is presented in [25]. Notes on dynamical modeling and control of spacecraft-mounted manipulators during a capturing operation are made in [24].

1.3 Contribution statement

The main contributions of this thesis are listed as follows:

- Systematic derivation of the equations of motion for open and closed-loop free-flying manipulator systems.
- Provide further insight into the problems occurring while capturing a tumbling satellite.
- The *Holonomic Distribution Control* is introduced for planning reactionless Cartesian paths to a stationary target satellite.
- Strategy using bias angular momentum (the *Bias Momentum Approach*) that can facilitate the trajectory planning and post-impact motion is introduced.
- Trajectory generation procedure in the case when the *Bias Momentum Approach* is utilized, is proposed. Different state variables for the optimization algorithm employed are compared.
- *Distributed Momentum Control* to be used during the post-impact phase of a capturing operation is introduced. It manages the momentum in the system in such a way that no base angular motions occur.
- Utilization of the *Reaction Null Space Control* for base attitude control during the post-impact phase (the form of the control used is different from the initially proposed one).

Chapter 2

Dynamics of free-flying manipulator systems

Dynamics of mechanical systems is a well studied field in which many books have been written [119], [107], [45], [102], [51], [38], [4], [68], [101], [57], [22], [7]. Building a dynamical model is of great interest since it provides a relation between the joint actuator torques and the motion of the structure. A variety of formulations which differ in complexity and level of efficiency are available. The creation of most of them came as a solution to practical problems. It is interesting to note that, the differential equations governing the motion of a multibody system have been known since the time of Newton and Lagrange, however, their application for solving practical problems began not more than 40 years ago when the automobile industry and projects related to space exploration demanded precise mathematical models to be used for prediction of the motion of the systems of interest. Since the multibody structure of a spacecraft could not be ignored, there was a considerable interest in doing the dynamic analysis before the actual system is constructed and flown. The “design and try” strategy was unacceptable, therefore the development of highly reliable algorithms for dynamic simulations was a priority issue.

Investigation of multibody models of spacecraft vehicles on one hand, and models from the automobile industry on the another, gave birth to two different classes of formulations. The first one, referred here as *global formulations*, treat all kinds of mechanical systems (open-loop, close-loop, loosely or severely constrained) in the same way. Such formulations are simple and robust. They treat each component of a system separately and interconnect it to the others through constraint equations. They have a large range of applications, however, their efficiency is low [97].

The second class of formulations is referred to as *topological formulations*. They are developed in a way that takes advantage of the system’s topology. This does not only increase the efficiency of the dynamic simulations, but gives important insight for solving problems related to the behavior of the particular system under examination. The latter

advantage is of great importance since it can facilitate the search for solutions to problems related to planning and control.

The goal of this chapter is to present a systematic derivation of the equations of motion for both open and closed-loop free-flying manipulator systems. The approach presented can be considered to be a part of the group of *topological formulations*. Its implementation is straightforward and will create a framework for the rest of the thesis. A big part of the formulation presented is based on the work in [45].

For obvious reasons it is not possible to cover the entire spectrum of problems arising while the equations of motion are formulated. This is not the aim here, henceforth only issues relevant to the main topic of this thesis will be included.

This chapter is organized as follows. In Section 2.1 the most commonly used coordinates for the formulation of the dynamical equations of a multibody system are outlined. In Sections 2.2 and 2.3 the role played by the *subspace of allowable motions* in the dynamical formulation is discussed. Section 2.4 contains derivation of the motion equations for both open and closed-loop systems. Finally, in Section 2.5 a summary of the main variables used in the dynamical formulation is made.

2.1 Choice of coordinates

The first dilemma encountered when one needs to choose a way to describe the configuration and motion of a multibody system is what kind of coordinates should be utilized. This choice is not unique, and depends on the particular structure of the system of interest. The first practical systems studied were with open-chain topology and relative coordinates were the best choice. However, for a general system, where closed-loops are present, considering the advantages that different sets of coordinates present is beneficial. Next an outline of the commonly used coordinates is made. The advantages and disadvantages of each set are emphasized.

2.1.1 Independent coordinates

One of the most important characteristics of independent coordinates is that their number coincides with the number of degrees of freedom of the system, and hence, this is the minimal possible representation that could be utilized. One advantage that this type of coordinates provide, is that there is no need for the Lagrange multipliers to be calculated, and hence, a big part of the calculation burden is dropped. The equations are compact and constraint stabilization problems do not occur. Furthermore, very efficient explicit integrators could be utilized [46].

The case when independent coordinates are used has two main disadvantages. First,

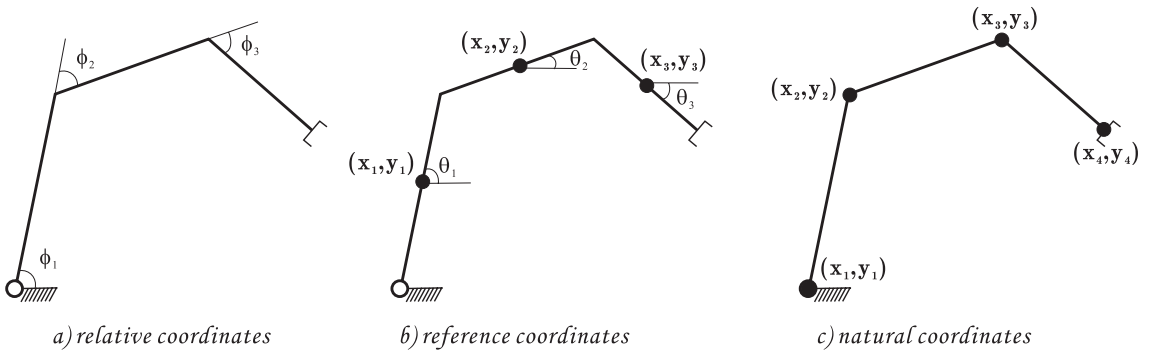


Figure 2.1: Comparison between different types of coordinates

such coordinates must be selected, and changed every time when they become inappropriate¹. This procedure is closely related to the particular integration algorithm utilized and leads to restarting it each time a change of coordinates occur [45] p. 172. The second problem is related to the calculation of positions, velocities and accelerations for the remaining parts of the multibody system, which depend on the current choice of independent coordinates. The positions of the dependent coordinates are usually calculated using methods that iteratively find a solution close to a given initial guess (the most commonly used one is the Newton-Raphson method). In practice, since the configuration of a mechanical system at time t is known, it can be used as an initial guess, hence, finding the correct solution for $t + \Delta t$ is practically guaranteed, however, this iterative calculation process slows down the simulation. On the other hand, finding the velocities and accelerations of the dependent coordinates (with independent velocities and accelerations known) is a far easier problem.

2.1.2 Dependent coordinates

One way to overcome the problems stated in the previous subsection is to use different type of coordinates. In particular, coordinates that describe the motion of each body of the mechanical system. This will clearly eliminate the need of solving the *positioning problem* at the end of each iteration. The main difference between independent and dependent coordinates is that the latter ones are interconnected with constraint equations. Three different types of dependent coordinates will be outlined in the sequel.

2.1.2.1 Relative coordinates

Relative coordinates define the position of each element (link) in relation to the previous one in the kinematic chain by using the parameters corresponding to the relative DOF

¹With “inappropriate” it is implied that they no longer describe uniquely the motion of the system.

allowed by the joint linking these elements. Fig 2.1 (a) shows an example of a manipulator system described using relative coordinates. As can be seen, they represent a system with a minimal number of dependent coordinates. In the particular case of open-chain systems, the number of relative coordinates coincides with the number of DOF, hence, they are independent and no constraint equations are necessary.

Advantages:

- (1) Reduced number of coordinates. Especially suited for open-chain systems.
- (2) The consideration of the DOF of each joint. This is an important advantage when the joint has an actuator attached, since it can be controlled directly.

Disadvantages:

- (1) Since the absolute motion of each body depends on the motion of the lower links of the manipulator chain, the mathematical formulation can be more involved.
- (2) They lead to equations of motion with matrices which, although small, are dense, and hence, expensive to evaluate.
- (3) They require some preprocessing work to determine the independent constraint equations (in case of a closed-loop system).

Even though the mass matrix of the system is dense, the evolution of recursive computational techniques makes it possible to factorize and invert it in an efficient way [6].

2.1.2.2 Reference point coordinates (Cartesian)

The reference coordinates try to overcome the difficulties of the relative coordinates by directly defining the position and orientation of each element with respect to the inertial frame (Fig 2.1 (b))

Advantages:

- (1) The position and orientation of each element is directly determined.
- (2) The matrices appearing in the equations of motion are sparse.

Disadvantages:

- (1) Much larger number of variables is required.
- (2) In the 3D case the definition of orientation for each element is complicated.

2.1.2.3 Natural coordinates (fully Cartesian)

Natural coordinates represent an interesting alternative to the previous two sets of coordinates. Also called *fully Cartesian coordinates* they were first introduced by Garcia de Jalón [43], [44]. The idea is to use a set of points on each element to define the position of the system. The minimal set of points for each element is two. Note that since each body has two points, its position and orientation are fully determined, hence, there is no need to use an additional variable representing orientation as in the reference point coordinates. The rules for choosing the set of points are explained in details in [45]. As can be seen in Fig 2.1 (c), if the points on each element are positioned in the joints then two adjacent elements can share one point. In general, the number of natural coordinates tends to be an average between the number of relative coordinates and the number of reference coordinates. In Fig 2.1 (a) the number of coordinates is three, in Fig 2.1 (b) it is nine and Fig 2.1 (c) it is six (note that in the case depicted, the position (x_1, y_1) is constant).

Advantages:

- (1) The constraint equations that arise are quadratic (or linear), hence, their Jacobian matrix is a linear (or constant) function of the natural coordinates.
- (2) The natural coordinates are composed by purely Cartesian variables and therefore are easy to define and represent geometrically.

Disadvantages:

- (1) The constraint equations corresponding to different angular quantities in the same mechanical structure might be different [45] p. 31.

Coordinates to be utilized:

Through the thesis, a set of relative coordinates will be used to describe the manipulator motion. Such choice allows for an important class of mechanical systems to be simulated without constraint equations. Of particular interest are manipulators used in orbit which in most cases are with open-loop structure. When constraints do arise they will be fewer in number, making it much easier to solve them efficiently. Closed loops can appear when a target object is captured using a dual-manipulator system (such example will be discussed in Section 5.4). In this particular case, using independent relative coordinates for the manipulator motion can give an important insight which can be helpful for the application of different control strategies. In addition, the base motion will be described using a set of *reference point coordinates*.

2.2 Space of allowable motions (SAM)

Up to now, a distinction between independent and dependent sets of coordinates was presented. In this section, the relation between them will be made. In other words, the problem of extracting an independent set of coordinates if a dependent one is given will be discussed. This is a purely kinematical problem, however, it constitutes very important points for the multibody dynamic formulation to be used hereafter.

In this section, it will be shown that the dependent velocities of the components of a constrained multibody system ($\dot{\mathbf{Y}} \in R^k$) belong to a very particular vector space called the *space of allowable motions*. It will be shown that this vector space coincides with the *null space* of the Jacobian matrix of the constraint equations. The case when the system of interest is *scleronomous*² will be examined.

Let us consider a system of m independent holonomic constraints that can be expressed using the following algebraic equation:

$$\Phi(\mathbf{Y}_c) = 0 \in R^m \quad (2.1)$$

where \mathbf{Y}_c is a set of dependent Cartesian coordinates describing the configuration of the system.

Remark:

It should be noted that, it is not necessary for the components of the Cartesian velocity vector $\dot{\mathbf{Y}}$ to be the derivatives, term by term, of \mathbf{Y}_c ([119], [38], Section 2.3). For example, the velocity $\dot{\mathbf{Y}}_j$ of body j can be described using \mathbf{v}_j and $\boldsymbol{\omega}_j$, which stand for the linear velocity of a reference point on body j and angular velocity, respectively. On the other hand, the configuration of body j can be represented by the position of a reference point, and a set of Euler angles whose derivatives are not equivalent to $\boldsymbol{\omega}_j$. Bear in mind that $\boldsymbol{\omega}_j$ is a nonintegrable variable, in other words, the derivatives of no set of three parameters form the components of the angular velocity vector. The dimension of \mathbf{Y}_c is not going to be even specified, since different sets for attitude description like *Euler parameters*, *quaternions*, *direction cosine matrix* can be used. Hereafter, it is assumed that the derivatives of the dependent coordinates $\dot{\mathbf{Y}}_c$ can always be related to the velocity vector $\dot{\mathbf{Y}}$ by using a positive-definite matrix $\mathbf{U}(\mathbf{Y}_c)$ (see [38], Table 2.3), hence:

$$\dot{\mathbf{Y}}_c = \mathbf{U}(\mathbf{Y}_c)\dot{\mathbf{Y}} \quad (2.2)$$

The importance of equation (2.2) will be emphasized in Section 2.4.1 and at the end of this chapter, where a short note on integration of the motion equations is made.

From the above discussion it is clear that the definition of a variable $\mathbf{Y} \in R^k$, who's derivative is equal to $\dot{\mathbf{Y}}$ is not possible in the general case. Nevertheless, it will be employed to represent partial derivative of a generic function F with respect to the k system dependent Cartesian coordinates ($\partial F / \partial \mathbf{Y}$). Bear in mind that the actual

²The constraint equations do not depend explicitly on the time variable.

computation of the partial derivatives will be made using $(\partial \dot{F} / \partial \dot{\mathbf{Y}})$, however the latter notation is not intuitive. For more details see Section 2.4.2.2 and equation (2.50).

Differentiating (2.1) twice with respect to time leads to (the chain rule is used):

$$\Phi_Y \dot{\mathbf{Y}} = 0 \quad (2.3)$$

$$\Phi_Y \ddot{\mathbf{Y}} = -\dot{\Phi}_Y \dot{\mathbf{Y}} = \mathbf{c} \quad (2.4)$$

where $\Phi_Y \in R^{m \times k} = \partial \Phi / \partial \mathbf{Y}$ is the Jacobian matrix of the constraint equations. Note that $f = k - m > 0$ are the degrees of freedom (DOF) of the system. It can be seen that in order $\dot{\mathbf{Y}}$ to satisfy equation (2.3) it must be in the null space of Φ_Y . This space (to be denoted by $\mathbf{R} \in R^{k \times f}$) is spanned by f independent vectors of dimension k . From linear algebra it is known that in order for a vector to belong to a given vector space \mathbf{V} it should be a linear combination of the members of \mathbf{V} . Hence, $\dot{\mathbf{Y}}$ can be formed in the following way (for a comprehensive discussion on linear spaces see [109]):

$$\dot{\mathbf{Y}} = \mathbf{R}_1 \dot{z}_1^i + \mathbf{R}_2 \dot{z}_2^i \dots + \mathbf{R}_f \dot{z}_f^i = \sum_{j=1}^f \mathbf{R}_j \dot{z}_j^i \quad (2.5)$$

where \mathbf{R}_j is the j^{th} column of \mathbf{R} and the coefficients of (2.5) form the vector of independent velocities \dot{z}^i . Hence, it can be concluded that the dimension of the *space of allowable motions* which coincides with the number of vectors that span the null space of Φ_Y , is equal to the DOF of the multibody system³. This fact is very useful, because it provides a way to project the vector of independent velocities \dot{z}^i onto the null space of Φ_Y and obtain the dependent velocity vector $\dot{\mathbf{Y}}$. This can be expressed by the following equation of paramount importance:

$$\dot{\mathbf{Y}} = \mathbf{R} \dot{z}^i \quad (2.6)$$

where

$$\Phi_Y \mathbf{R} = 0 \quad (2.7)$$

The discussion can be made with respect to any set of dependents velocities, nevertheless for clarity, $\dot{\mathbf{Y}}$ is assumed to be a set of Cartesian velocities, including angular velocity $\boldsymbol{\omega}_i$ of body i , and the linear velocity of its center of mass \mathbf{v}_i .

We are particularly interested in ways to compute the *space of allowable motions* \mathbf{R} . In view of the fact that, the columns of \mathbf{R} span the null space of Φ_Y , the authors of [106] proposed the direct utilization of the SV (singular value) decomposition for the computation of \mathbf{R} . As noted in [45] p. 101, such an iterative method can gradually decrease

³For example, for an open chain manipulator system mounted on a free-floating base, the dimensions of \mathbf{R} will be $(6n + 6) \times (n + 6)$, where n is the number of available joints.

the efficiency of the simulation, and its application is not desired at each iteration step. This fact although important, from the viewpoint of simulation efficiency, is not the only reasoning for not using SV decomposition for the direct computation of \mathbf{R} . As noted by the authors of [132], [33], [68] p. 422-433 (see **Example A.26.**), viewing a mathematical model of a physical system only as numbers and arrays of numbers, masks the physics of the problem, and can lead to lost insight. When arrays with dimensionally nonuniform components are used (as is the case with Φ^4), a consistent analysis to avoid errors should be made. For example, the summation of two vectors a and b , characterized by different dimensional units (such as meter, second) is physically meaningless, and hence, disallowed. Furthermore, a and b do not form a vector space (for an exact definition see [34]), therefore the definition of *orthogonality* (tangent space), or *magnitude*, of an array of numbers containing a and b is not possible. The problems outlined above typically appear when motion planning algorithms have to be implemented [57], [58].

In general, without knowledge of the specific structure of the matrix Φ_Y , the definition of its null space (although numerically possible), should not be considered. Furthermore, the understanding of the physical properties standing behind a given matrix \mathbf{R} is very important, as will become apparent in the following chapters.

Hereafter, \mathbf{R} will play an important role in the formulation of the dynamical equations, hence, we find it necessary to examine some of its properties first.

2.3 Role of SAM in the dynamic analysis

Matrix \mathbf{R} has been implicitly or explicitly referred to by many authors. Among them Kane and Levinson [51], Nakamura [72], Garcia de Jalón and Bayo [45], Kamman and Huston [49] and others. The best way to demonstrate its role for facilitating the dynamic formulation is by the following example.

2.3.1 Example: Lagrange multipliers elimination

In general, the dynamics of a manipulator system can be expressed using its kinetic (T) and potential (V) energy. By forming the Lagrangian $L_a = T - V$ and then using Hamilton's principle, one arrives at the famous Lagrange formulation of the equation of motion [37]:

$$\frac{d}{dt}\left(\frac{\partial L_a}{\partial \dot{\mathbf{Y}}}\right) - \frac{\partial L_a}{\partial \mathbf{Y}} + \Phi_Y^T \lambda = \mathbf{Q}_{ex} \quad (2.8)$$

where \mathbf{Q}_{ex} is the vector of generalized external forces acting along the dependent coordinates. Φ_Y is the Jacobian matrix of the constraint equations, $\lambda \in R^m$ is a vector of unknown Lagrange multipliers and $(\cdot)^T$ denotes a matrix transpose operator. The third

⁴Depending on the type of constraints imposed.

term on the left-hand-side (LHS) of equation (2.8) accounts for the constraint forces in the system. The kinetic energy of a multibody system can be expressed as follows:

$$T = \frac{1}{2} \dot{\mathbf{Y}}^T \mathbf{M}(\mathbf{Y}_c) \dot{\mathbf{Y}}$$

where \mathbf{M} is symmetric, positive-definite and (in general) configuration dependent matrix containing mass and inertia properties. With such notation, equation (2.8) can be expressed as:

$$\mathbf{M} \ddot{\mathbf{Y}} + \Phi_Y^T \lambda = \mathbf{Q} \quad (2.9)$$

where \mathbf{Q} accounts for the external forces plus all the velocity-dependent inertial terms. The solution of (2.9) is not a trivial problem. It can be done using a number of different methods, and each method leads to different complexity and accuracy.

Equations (2.9) represents k equations in $k + m$ unknowns (the k elements of vector $\ddot{\mathbf{Y}}$ and the m elements of vector λ). In order to have a sufficient number of equations, it is necessary to supply m more. One possible choice is to use (2.9) in combination with (2.1). This results in a system of *index 3* differential algebraic equations (DAE)⁵. In order to avoid *index 3* DAE, equation (2.4) can be utilized instead, leading to:

$$\begin{bmatrix} \mathbf{M} & \Phi_Y^T \\ \Phi_Y & \mathbf{0} \end{bmatrix} \begin{bmatrix} \ddot{\mathbf{Y}} \\ \lambda \end{bmatrix} = \begin{bmatrix} \mathbf{Q} \\ \mathbf{c} \end{bmatrix} \quad (2.10)$$

which is a system with $k + m$ equations in $k + m$ unknowns. (2.10) can be solved simultaneously for the accelerations and Lagrange multipliers by directly taking the inverse of the leading matrix, or alternatively, first equation (2.9) can be solved to obtain:

$$\ddot{\mathbf{Y}} = \mathbf{M}^{-1} \mathbf{Q} - \mathbf{M}^{-1} \Phi_Y^T \lambda \quad (2.11)$$

then by substituting (2.11) into (2.4) and solving for the Lagrange multipliers one obtains:

$$\lambda = (\Phi_Y \mathbf{M}^{-1} \Phi_Y^T)^{-1} (\Phi_Y \mathbf{M}^{-1} \mathbf{Q} - \mathbf{c}) \quad (2.12)$$

Consequently, introducing (2.12) into (2.11) gives the solution for the accelerations $\ddot{\mathbf{Y}}$.

The main advantage of this method is that it permits the computation of the force associated with the constraints with a minimum additional effort. Equation (2.12) yields λ directly without having to solve the inverse dynamics problem. However, a drawback can be found in the fact that if the system of interest is with an open-loop structure, the computation of Lagrange multipliers is an unnecessary burden.

⁵DAE's are classified according to their *differential index* or simply *index*, defined as the number of times that the DAE has to be differentiated to obtain a standard set of ODE. The higher the index the more complex the integration becomes. Nonlinear DAE can be classified in two major groups: *implicit* and *semi-explicit* the latter one is the type of equation that arises commonly in constrained multibody systems, optimal control and trajectory planning problems.

Utilization of \mathbf{R}

Apart from increasing the equations in the system (as done above), an alternative approach by decreasing the number of unknowns can be taken. Multiplying equation (2.9) from the left by \mathbf{R}^T , the following equation is obtained:

$$\mathbf{R}^T \mathbf{M} \ddot{\mathbf{Y}} + \mathbf{R}^T \Phi_Y^T \lambda = \mathbf{R}^T \mathbf{Q} \quad (2.13)$$

However, by virtue of equation (2.7) the term containing the Lagrange multipliers can be canceled, for one to obtain:

$$\mathbf{R}^T \mathbf{M} \ddot{\mathbf{Y}} = \mathbf{R}^T \mathbf{Q} \quad (2.14)$$

Combining (2.14) with the constrained equation (2.4) (as done in (2.10)), one arrives at:

$$\begin{bmatrix} \mathbf{R}^T \mathbf{M} \\ \Phi_Y \end{bmatrix} \ddot{\mathbf{Y}} = \begin{bmatrix} \mathbf{R}^T \mathbf{Q} \\ \mathbf{c} \end{bmatrix} \quad (2.15)$$

This is a system with k equations in k unknowns which can be solved for the dependent accelerations $\ddot{\mathbf{Y}}$. Equation (2.15) does not explicitly contain any independent coordinates, rather they are implicitly considered via the matrix \mathbf{R} (this notation was initially introduced by Kamman and Huston [49]).

It should be noted that by using \mathbf{R} it was possible to eliminate the Lagrange multipliers from the equation of motion, and decrease the dimensions of the system to be solved. The solution of both (2.10) and (2.15) suffer from stabilization problems as a result of the fact that the constraints are defined only using equation (2.4), and the state variables are dependent. In theory, this should not be a problem, and (2.10) or (2.15) should guarantee that the constraint equations are satisfied at any time, however, in practice constraint violations occur. The reason for this is the existence of a round-off error during the integration process, which is accumulated and increases with time. Therefore a *Baumgarte* [15], *Penalty method* or other type of stabilization algorithms should be employed (for more information see [8], [9], [10]). Nevertheless, it should be noted that (2.15) has to be stabilized only for long simulations. As far as (2.10) is concerned, if stabilization is not applied the results are unacceptable for all but short simulations.

Even though (2.15) is not the form of equation of motion that will be utilized here, it gives a clear idea about how the dimensions of the system can be reduced. This is important since our goal is to derive the dynamic equations only with respect to a set of independent variables.

There are two main problems of the formulation in (2.15) that should be distinguished:

- (1) Even if the system of interest is with open-loop structure, the constraints Φ and their Jacobian matrix Φ_Y has to be formed.

- (2) Computation of the matrix \mathbf{R} that relates the dependent Cartesian velocities with an independent set of variables using factorization of Φ_Y is not efficient. As already noted, the direct application of SV decomposition for obtaining the null space of Φ_Y , is not applicable in general (see Section 2.2).

In order to find a solution to these problems and acquire a better understanding, in the next section the derivation of the equations of motion with respect to an independent set of coordinates is performed in four stages:

S1) The motion equations and the constraints of a mechanical system are formulated in Cartesian coordinates.

S2) All the closed-loops in the system are opened⁶, and the constraint equations are partitioned in two groups. The first one corresponds to the constraints of the open-chain system, and the second one is formed by the constraints needed to close the loops previously opened.

S3) A *velocity transformation*⁷ switches from Cartesian velocities to *relative velocities* corresponding to the open-chain system. Hence, the only constraints left are the one for the cut joints.

S4) A second *velocity transformation* that keeps only a subset of independent velocities is applied.

2.4 Formulation in independent coordinates

In order to express the four stages explained in the previous section in mathematical fashion, the following notation is introduced: The constraints that correspond to the open-loop multibody system will be denoted by $\Phi^o \in R^{m^o \times k}$, and the constraints that close the opened loops will be denoted by $\Phi^c \in R^{m^c \times k}$, with m^o and m^c being the number of constraint equations ($m^o + m^c = m$). Consequently, (2.3) can be rewritten as:

$$\begin{bmatrix} \Phi_Y^o \\ \Phi_Y^c \end{bmatrix} \dot{\mathbf{Y}} = 0 \quad (2.16)$$

Taking into consideration the partitioning above, equation (2.9) becomes:

$$\mathbf{M} \ddot{\mathbf{Y}} + \Phi_Y^{oT} \lambda^o + \Phi_Y^{cT} \lambda^c = \mathbf{Q} \quad (2.17)$$

where λ^o and λ^c are the Lagrange multipliers associated with Φ_Y^o and Φ_Y^c , respectively.

$$\lambda = \begin{bmatrix} \lambda^o \\ \lambda^c \end{bmatrix} \quad \mathbf{M} = \text{diag}(\mathbf{M}_0, \mathbf{M}_1, \dots, \mathbf{M}_n) \quad \mathbf{Q} = [\mathbf{Q}_0^T, \mathbf{Q}_1^T, \dots, \mathbf{Q}_n^T]^T$$

⁶The standard way to open a loop is by cutting a joint [72], however, some researchers [56] proposed to cut a link. The reasoning for this is that in a cut joint friction cannot be modeled.

⁷*Velocity transformation* means transformations from one set of velocities, describing the system's motion to another.

$$\mathbf{M}_i = \begin{bmatrix} m_i \mathbf{E}_3 & \mathbf{0} \\ \mathbf{0} & \mathbf{I}_i \end{bmatrix} \quad \mathbf{Q}_i = \begin{bmatrix} \mathbf{F}_i \\ \mathbf{N}_i - \hat{\boldsymbol{\omega}}_i \mathbf{I}_i \boldsymbol{\omega}_i \end{bmatrix}$$

In the equations above, m_i is the mass and \mathbf{I}_i is the inertia tensor of body i ($i = 0$ represents the base body) about its center of mass (expressed in the inertial frame). \mathbf{F}_i and \mathbf{N}_i are the forces and torques applied to the center of mass of body i , (\cdot) denotes a skew-symmetric representation of a three dimensional vector and $\mathbf{E}_p \in R^{p \times p}$ ($p = 3$) is a unit matrix.

Next, an efficient two step procedure for the solution of (2.17) that deals separately with the constraints Φ^o and Φ^c will be presented.

2.4.1 Open-loop systems

In this subsection, it is assumed that the manipulator system of interest has a tree structure. If closed-loops are intrinsic in its design, they are opened through cutting a joint. For simplicity each joint will be assumed to have only one translational or rotational DOF. This does not impose a limitation on the formulation, since complicated joints with more than one DOF can be modeled using those two primitives. Furthermore, the manipulator is mounted on a free-floating base with three translational and three rotational degrees of freedom.

First, the upper part of equation (2.16) will be considered. It implies that the vector of dependent Cartesian velocities $\dot{\mathbf{Y}}$ should belong to the *subspace of allowable motions*, spanned by the null space of Φ_Y^o . This space will be denoted by \mathbf{R}^o , and hence, the following relation should hold true:

$$\Phi_Y^o \mathbf{R}^o = 0 \quad (2.18)$$

As discussed in Section 2.2, the vector of dependent Cartesian velocities $\dot{\mathbf{Y}}$ can be related to an independent set of velocities $\dot{\mathbf{z}}$ by means of \mathbf{R}^o , where the dimension of $\dot{\mathbf{z}}$ coincides with the DOF of the open-loop system, hence:

$$\dot{\mathbf{Y}} = \mathbf{R}^o \dot{\mathbf{z}} \quad (2.19)$$

Equation (2.19) represent a *velocity transformation* between the dependent *Cartesian velocities* and a set of independent velocities $\dot{\mathbf{z}}$. Note that since a free-floating base is considered as well, $\dot{\mathbf{z}}$ consists of the manipulator *relative velocities* plus a set of six Cartesian velocities for the base body, hence:

$$\dot{\mathbf{z}} = \begin{bmatrix} \dot{\mathbf{x}}_b \\ \dot{\boldsymbol{\phi}} \end{bmatrix} \quad (2.20)$$

since $\dot{\mathbf{x}}_b$ is included in $\dot{\mathbf{Y}}$ as well, the entries of \mathbf{R}^o corresponding to the base will be trivial.

Differentiation of (2.19) with respect to time leads to:

$$\ddot{\mathbf{Y}} = \mathbf{R}^o \ddot{\mathbf{z}} + \dot{\mathbf{R}}^o \dot{\mathbf{z}} \quad (2.21)$$

Substitution of (2.21) in (2.17) and multiplication from the left with \mathbf{R}^{oT} results in:

$$\mathbf{R}^{oT} \mathbf{M}(\mathbf{R}^o \ddot{\mathbf{z}} + \dot{\mathbf{R}}^o \dot{\mathbf{z}}) + \mathbf{R}^{oT} \Phi_Y^{oT} \lambda^o = \mathbf{R}^{oT} \mathbf{Q}$$

Note that since the system is considered to have a tree structure, the term $\Phi_Y^{cT} \lambda^c$ does not appear in the equation. After some formula manipulation, noting that $\mathbf{R}^{oT} \Phi_Y^{oT} = (\Phi_Y^o \mathbf{R}^o)^T = 0$ one obtains:

$$\mathbf{R}^{oT} \mathbf{M} \mathbf{R}^o \ddot{\mathbf{z}} + \mathbf{R}^{oT} \mathbf{M} \dot{\mathbf{R}}^o \dot{\mathbf{z}} - \mathbf{R}^{oT} \mathbf{Q} = \mathbf{0}$$

Using the definition of \mathbf{Q} , the above equation can be represented in a more convenient way:

$$\mathbf{R}^{oT} \mathbf{M} \mathbf{R}^o \ddot{\mathbf{z}} + \mathbf{R}^{oT} \mathbf{M} \dot{\mathbf{R}}^o \dot{\mathbf{z}} - \mathbf{R}^{oT} \mathbf{Q}_{ex} = \mathbf{R}^{oT} \mathbf{Q}_{ex} \quad (2.22)$$

where

$$\mathbf{Q}_{n_i} = \begin{bmatrix} \mathbf{0} \\ -\hat{\boldsymbol{\omega}}_i \mathbf{I}_i \boldsymbol{\omega}_i \end{bmatrix} \quad \mathbf{Q}_{ex_i} = \begin{bmatrix} \mathbf{F}_i \\ \mathbf{N}_i \end{bmatrix} \quad (i = 0, 1, \dots, n)$$

The component on the RHS of equation (2.22) represents a map of the column vector of external wrenches $\mathbf{Q}_{ex} \in R^{(6n+6)}$ on the equivalent joint torques and base forces/torques. Hence, it can be concluded that \mathbf{R}^o has the structure of a Jacobian matrix. More precisely, it contains the partial derivatives of the k dependent Cartesian coordinates with respect to the motion of the base body and manipulator joints (and will be referred to as *augmented* Jacobian matrix). Its computation can be performed in a straightforward fashion, as will be shown in the following subsection.

Since in our notation as generalized coordinates are chosen the n manipulator joints and six base motions, the only way the external forces \mathbf{Q}_{ex} can alter the momentum of the system (in the simulation) is if they are properly mapped as forces/torques applied to the base body⁸. Such mapping is successfully performed by the *augmented* Jacobian matrix \mathbf{R}^o . Without any abuse to the notation in (2.22) one can add a separate component for the joint torque ($\boldsymbol{\tau}$) to obtain:

$$\mathbf{H} \begin{bmatrix} \ddot{x}_b \\ \ddot{\phi} \end{bmatrix} + \mathbf{c}_n = \begin{bmatrix} \mathbf{0} \\ \boldsymbol{\tau} \end{bmatrix} + \mathbf{R}^{oT} \mathbf{Q}_{ex} \quad (2.23)$$

where

$$\mathbf{H} = \mathbf{R}^{oT} \mathbf{M} \mathbf{R}^o \quad \mathbf{c}_n = \mathbf{R}^{oT} \mathbf{M} \dot{\mathbf{R}}^o \dot{\mathbf{z}} - \mathbf{R}^{oT} \mathbf{Q}_{ex}$$

⁸The torques applied in the manipulator joints do not alter the momentum of the manipulator system.

This is the final form of the equations of motion of a tree system formulated with respect to a set of independent coordinates, where $\ddot{\mathbf{x}}_b$ stands for the base linear and angular accelerations. Equation (2.23) does not contain any constraint equations and adapts well to both implicit and explicit integrators [97]. In order to find the solution for the acceleration vector $\ddot{\mathbf{z}}$, once the external and joint torques are known, the leading matrix \mathbf{H}^9 has to be inverted to obtain:

$$\begin{bmatrix} \ddot{\mathbf{x}}_b \\ \ddot{\phi} \end{bmatrix} = \mathbf{H}^{-1} \left(\begin{bmatrix} \mathbf{0} \\ \boldsymbol{\tau} \end{bmatrix} + \mathbf{R}^{oT} \mathbf{Q}_{ex} - \mathbf{c}_n \right) \quad (2.24)$$

It should be noted that integration of $\ddot{\mathbf{z}}$ leads to obtaining the system's velocities $\dot{\mathbf{z}}$, which however cannot be directly integrated to yield positions. This comes from the fact that $\dot{\mathbf{x}}_b$ contains the base angular velocity, which is known to be nonintegrable. In order to overcome this problem one can use a transformation as in equation (2.2), which will lead to a set of integrable variables. In [38], Table 2.3, eight alternatives for such transformation are included. Among them are the derivatives of: Direction cosines, Axis/angle variables, Euler-Rodriguez parameters, Euler parameters, Euler angles. Choosing a particular one is related to the nature of the problem to be solved, and integration routine utilized. Some additional notes regarding integration of the equations of motion will be made at the end of this chapter.

2.4.1.1 Computation of the non-linear term \mathbf{c}_n and matrix \mathbf{R}^o

The computation of the derivative of \mathbf{R}^o in order to obtain the non-linear term \mathbf{c}_n is quite an expensive procedure. Fortunately, it does not need to be computed numerically. From equation (2.21) it can be noted that if the independent accelerations $\ddot{\mathbf{z}}$ are set equal to zero, the term $\dot{\mathbf{R}}^o \dot{\mathbf{z}}$ can be computed recursively as the vector of dependent Cartesian accelerations $\ddot{\mathbf{Y}}$. The components of the vector $\ddot{\mathbf{Y}}$ were already defined to be the angular velocity $\boldsymbol{\omega}_i$ of body i and the linear velocity of its center of mass \mathbf{v}_i .

$$\ddot{\mathbf{Y}}_i = \begin{bmatrix} \mathbf{v}_i \\ \boldsymbol{\omega}_i \end{bmatrix}$$

It should be noted that, simplifications could be achieved using different representations [79], [97], [53]. The computation of $\dot{\mathbf{Y}}$ (for simplicity only revolute joint will be considered) can be performed as follows (see Fig. 2.2):

$$\boldsymbol{\omega}_i = \boldsymbol{\omega}_k + \mathbf{u}_i \dot{\phi}_i \quad (2.25)$$

⁹Since $\mathbf{H} = \mathbf{R}^{oT} \mathbf{M} \mathbf{R}^o$ is symmetric and positive-definite its inverse exists. Each component of \mathbf{H} is defined in Appendix D.

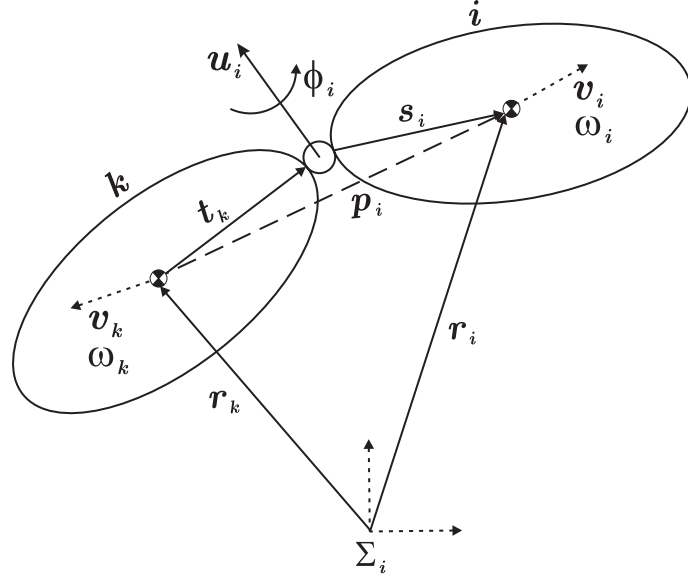


Figure 2.2: Two consecutive bodies connected by a rotational joint. All vectors are expressed in the inertial coordinate frame.

$$\begin{aligned}
 \mathbf{v}_i &= \mathbf{v}_k + \boldsymbol{\omega}_k \times \mathbf{t}_k + \boldsymbol{\omega}_i \times \mathbf{s}_i \\
 \mathbf{v}_i &= \mathbf{v}_k + \boldsymbol{\omega}_k \times \mathbf{t}_k + (\boldsymbol{\omega}_k + \mathbf{u}_i \dot{\phi}_i) \times \mathbf{s}_i \\
 \mathbf{v}_i &= \mathbf{v}_k + \boldsymbol{\omega}_k \times \mathbf{t}_k + \boldsymbol{\omega}_k \times \mathbf{s}_i + \mathbf{u}_i \times \mathbf{s}_i \dot{\phi}_i \\
 \mathbf{v}_i &= \mathbf{v}_k + \boldsymbol{\omega}_k \times (\mathbf{t}_k + \mathbf{s}_i) + \mathbf{u}_i \times \mathbf{s}_i \dot{\phi}_i
 \end{aligned}$$

$$\mathbf{t}_k + \mathbf{s}_i = \mathbf{r}_i - \mathbf{r}_k = \mathbf{p}_i$$

$$\mathbf{v}_i = \mathbf{v}_k + \boldsymbol{\omega}_k \times \mathbf{p}_i + \mathbf{u}_i \times \mathbf{s}_i \dot{\phi}_i \quad (2.26)$$

Note that, the indices i and k need not be consecutive numbers. Link k is the lower connection of link i (a link can have only one lower and multiple upper connections). Combining equations (2.25) and (2.26) leads to:

$$\dot{\mathbf{Y}}_i = \begin{bmatrix} \mathbf{v}_i \\ \boldsymbol{\omega}_i \end{bmatrix} = \begin{bmatrix} \mathbf{E}_3 & -\hat{\mathbf{p}}_i \\ \mathbf{0} & \mathbf{E}_3 \end{bmatrix} \begin{bmatrix} \mathbf{v}_k \\ \boldsymbol{\omega}_k \end{bmatrix} + \begin{bmatrix} \mathbf{u}_i \times \mathbf{s}_i \\ \mathbf{u}_i \end{bmatrix} \dot{\phi}_i \quad (2.27)$$

where $-\hat{\mathbf{p}}_i \boldsymbol{\omega}_k = \boldsymbol{\omega}_k \times \mathbf{p}_i$. Equation (2.27) can be rewritten as:

$$\dot{\mathbf{Y}}_i = {}^k \mathbf{B}_i \dot{\mathbf{Y}}_k + \mathbf{b}_i \dot{\phi}_i \quad (2.28)$$

$${}^k \mathbf{B}_i = \begin{bmatrix} \mathbf{E}_3 & -\hat{\mathbf{p}}_i \\ \mathbf{0} & \mathbf{E}_3 \end{bmatrix} \quad \mathbf{b}_i = \begin{bmatrix} \mathbf{u}_i \times \mathbf{s}_i \\ \mathbf{u}_i \end{bmatrix}$$

Before the vector of dependent Cartesian accelerations $\ddot{\mathbf{Y}}$ is derived, a parallel between equations (2.28) and (2.19) will be made. Let us consider the tree system depicted

in Fig. 2.3. It consists of six links mounted on a free-floating base body. Writing the components of (2.28) for this system results in:

$$\begin{aligned}\dot{\mathbf{Y}}_0 &= \mathbf{E}_6 \dot{\mathbf{Y}}_0 \\ \dot{\mathbf{Y}}_1 &= {}^0\mathbf{B}_1 \dot{\mathbf{Y}}_0 + \mathbf{b}_1 \dot{\phi}_1 \\ \dot{\mathbf{Y}}_2 &= {}^1\mathbf{B}_2 \dot{\mathbf{Y}}_1 + \mathbf{b}_2 \dot{\phi}_2 = {}^1\mathbf{B}_2 {}^0\mathbf{B}_1 \dot{\mathbf{Y}}_0 + {}^1\mathbf{B}_2 \mathbf{b}_1 \dot{\phi}_1 + \mathbf{b}_2 \dot{\phi}_2 \\ \dot{\mathbf{Y}}_3 &= {}^2\mathbf{B}_3 \dot{\mathbf{Y}}_2 + \mathbf{b}_3 \dot{\phi}_3 = {}^2\mathbf{B}_3 {}^1\mathbf{B}_2 {}^0\mathbf{B}_1 \dot{\mathbf{Y}}_0 + {}^2\mathbf{B}_3 {}^1\mathbf{B}_2 \mathbf{b}_1 \dot{\phi}_1 + {}^2\mathbf{B}_3 \mathbf{b}_2 \dot{\phi}_2 + \mathbf{b}_3 \dot{\phi}_3 \\ \dot{\mathbf{Y}}_4 &= {}^2\mathbf{B}_4 \dot{\mathbf{Y}}_2 + \mathbf{b}_4 \dot{\phi}_4 = {}^2\mathbf{B}_4 {}^1\mathbf{B}_2 {}^0\mathbf{B}_1 \dot{\mathbf{Y}}_0 + {}^2\mathbf{B}_4 {}^1\mathbf{B}_2 \mathbf{b}_1 \dot{\phi}_1 + {}^2\mathbf{B}_4 \mathbf{b}_2 \dot{\phi}_2 + \mathbf{b}_4 \dot{\phi}_4 \\ \dot{\mathbf{Y}}_5 &= {}^0\mathbf{B}_5 \dot{\mathbf{Y}}_0 + \mathbf{b}_5 \dot{\phi}_5 \\ \dot{\mathbf{Y}}_6 &= {}^5\mathbf{B}_6 \dot{\mathbf{Y}}_5 + \mathbf{b}_6 \dot{\phi}_6 = {}^5\mathbf{B}_6 {}^0\mathbf{B}_5 \dot{\mathbf{Y}}_0 + {}^5\mathbf{B}_6 \mathbf{b}_5 \dot{\phi}_5 + \mathbf{b}_6 \dot{\phi}_6\end{aligned}$$

where $\dot{\mathbf{Y}}_0 = [\mathbf{v}_0^T \quad \boldsymbol{\omega}_0^T]^T$ are the velocities of the base body. For the computation of $\dot{\mathbf{Y}}_4$, $\dot{\mathbf{Y}}_2$ was used as a lower body connection, since the motion of *link 4* does not depend on the motion of *link 3* and *joint 3* (at least in kinematical sense). Writing the above equations in a matrix form results in:

$$\begin{bmatrix} \dot{\mathbf{Y}}_0 \\ \dot{\mathbf{Y}}_1 \\ \dot{\mathbf{Y}}_2 \\ \dot{\mathbf{Y}}_3 \\ \dot{\mathbf{Y}}_4 \\ \dot{\mathbf{Y}}_5 \\ \dot{\mathbf{Y}}_6 \end{bmatrix} = \begin{bmatrix} {}^b\mathbf{J}_b & {}^b\mathbf{J}_m \\ \mathbf{J}_b & \mathbf{J}_m \end{bmatrix} \begin{bmatrix} \dot{\mathbf{Y}}_0 \\ \dot{\phi}_1 \\ \dot{\phi}_2 \\ \dot{\phi}_3 \\ \dot{\phi}_4 \\ \dot{\phi}_5 \\ \dot{\phi}_6 \end{bmatrix} \quad (2.29)$$

where ${}^b\mathbf{J}_m \in R^{6 \times n}$ is the Jacobian of the base with respect to the motion of the links and is a zero matrix (since the base is the lowest link in the kinematic chain). ${}^b\mathbf{J}_b \in R^{6 \times 6} = \mathbf{E}_6$ is the Jacobian of the base with respect to the base motion. \mathbf{J}_b and \mathbf{J}_m are the Jacobian matrices of each link with respect to the base and other links motion, respectively.

$$\mathbf{J}_b \in R^{6n \times 6} = \begin{bmatrix} {}^0\mathbf{B}_1 & & & & & \\ {}^1\mathbf{B}_2 {}^0\mathbf{B}_1 & & & & & \\ {}^2\mathbf{B}_3 {}^1\mathbf{B}_2 {}^0\mathbf{B}_1 & & & & & \\ {}^2\mathbf{B}_4 {}^1\mathbf{B}_2 {}^0\mathbf{B}_1 & & & & & \\ {}^0\mathbf{B}_5 & & & & & \\ {}^5\mathbf{B}_6 {}^0\mathbf{B}_5 & & & & & \end{bmatrix}$$

$$\mathbf{J}_m \in R^{6n \times n} = \begin{bmatrix} \mathbf{b}_1 & \mathbf{0} & \mathbf{0} & \mathbf{0} & \mathbf{0} & \mathbf{0} \\ {}^1\mathbf{B}_2 \mathbf{b}_1 & \mathbf{b}_2 & \mathbf{0} & \mathbf{0} & \mathbf{0} & \mathbf{0} \\ {}^2\mathbf{B}_3 {}^1\mathbf{B}_2 \mathbf{b}_1 & {}^2\mathbf{B}_3 \mathbf{b}_2 & \mathbf{b}_3 & \mathbf{0} & \mathbf{0} & \mathbf{0} \\ {}^2\mathbf{B}_4 {}^1\mathbf{B}_2 \mathbf{b}_1 & {}^2\mathbf{B}_4 \mathbf{b}_2 & \mathbf{0} & \mathbf{b}_4 & \mathbf{0} & \mathbf{0} \\ \mathbf{0} & \mathbf{0} & \mathbf{0} & \mathbf{0} & \mathbf{b}_5 & \mathbf{0} \\ \mathbf{0} & \mathbf{0} & \mathbf{0} & \mathbf{0} & {}^5\mathbf{B}_6 \mathbf{b}_5 & \mathbf{b}_6 \end{bmatrix}$$

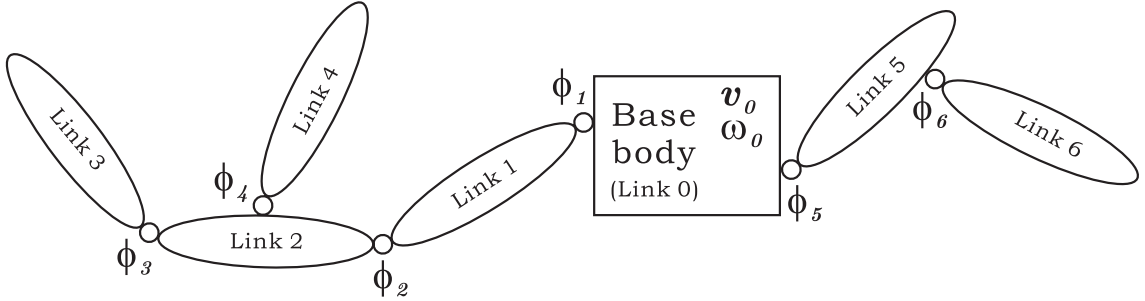


Figure 2.3: A tree manipulator system mounted on a free-floating base.

Comparison of equations (2.29) and (2.19) yields the contents of matrix \mathbf{R}^o :

$$\mathbf{R}^o = \begin{bmatrix} {}^b\mathbf{J}_b & {}^b\mathbf{J}_m \\ \mathbf{J}_b & \mathbf{J}_m \end{bmatrix} \quad (2.30)$$

The matrix \mathbf{B} has the following properties:

$${}^j\mathbf{B}_i \cdot {}^k\mathbf{B}_j = {}^k\mathbf{B}_i \quad {}^i\mathbf{B}_i = \mathbf{E}_6 \quad {}^k\mathbf{B}_i^T = {}^i\mathbf{B}_k \quad (2.31)$$

If the nonzero entries of the Jacobian matrix \mathbf{R}^o are substituted with *ones*¹⁰, the *path connectivity* matrix \mathbf{P}_c for the system in Fig. 2.3 is obtained (it is also called *accessibility matrix* [119], [118]). The i^{th} row of \mathbf{P}_c represents link i , and the columns stand for the joints that influence its motion (in the representation below, in squares are included the indices of the rows and columns, where $[i=0]$ and $[j=0]$ refer to the base). The matrix \mathbf{P}_c can be constructed at a preprocessing stage (before the actual simulation) only from information about the connectivity structure of the system, and can be useful for the kinematic and dynamic analysis.

$$\mathbf{P}_c = \left[\begin{array}{c|cccccc|c} 1 & 0 & 0 & 0 & 0 & 0 & 0 & i=0 \\ \hline 1 & 1 & 0 & 0 & 0 & 0 & 0 & i=1 \\ 1 & 1 & 1 & 0 & 0 & 0 & 0 & i=2 \\ 1 & 1 & 1 & 1 & 0 & 0 & 0 & i=3 \\ 1 & 1 & 1 & 0 & 1 & 0 & 0 & i=4 \\ 1 & 0 & 0 & 0 & 0 & 1 & 0 & i=5 \\ 1 & 0 & 0 & 0 & 0 & 1 & 1 & i=6 \\ \hline j=0 & j=1 & j=2 & j=3 & j=4 & j=5 & j=6 & \square \end{array} \right]$$

Note that, since the numbering of the n joints and links is made from the “roots” to the “leaves” of the kinematic tree, the upper triangular part of \mathbf{P}_c is always filled with zeros¹¹.

¹⁰The components of \mathbf{J}_b and \mathbf{J}_m are with dimensions 6×6 and 6×1 , respectively. Each of them is substituted by a scalar (zero or one).

¹¹A notation using opposite numbering can be utilized as well, as suggested by Negrut, Serban and Potra [79].

Using the entries of matrix \mathbf{P}_c , the general formulation for the computation of the variable components of \mathbf{R}^o becomes (the first property of \mathbf{B} from equation (2.31) is used):

$$\mathbf{J}_b^i \in R^{6 \times 6} = {}^0\mathbf{B}_i \quad (2.32)$$

$$\mathbf{J}_m^{(i,j)} \in R^{6 \times 1} = {}^j\mathbf{B}_i \mathbf{b}_j \quad (2.33)$$

for $(i, j = 1, 2, \dots, n)$ such that $\mathbf{P}_c^{i,j} = 1$ (only combinations of i and j that correspond to element 1 in matrix \mathbf{P}_c).

The so constructed matrix \mathbf{R}^o satisfies equation (2.18). Note that the formulation of the constraint equations Φ^o was not even necessary. The method presented is general and systematic. It is not recursive and can be applied independently for the computation for each body, hence, it can take full advantage of parallel computer architectures. The procedure in equations (2.32) and (2.33) is computationally efficient, and most importantly reveals the structure of the null space of Φ_Y^o . At a next step, \mathbf{J}_m can be represented as a product of two matrices $\mathbf{J}_m = \mathbf{J}_m^n \mathbf{J}_m^d$

$$\mathbf{J}_m^n = \begin{bmatrix} \mathbf{E}_6 & \mathbf{0} & \mathbf{0} & \mathbf{0} & \mathbf{0} & \mathbf{0} \\ {}^1\mathbf{B}_2 & \mathbf{E}_6 & \mathbf{0} & \mathbf{0} & \mathbf{0} & \mathbf{0} \\ {}^1\mathbf{B}_3 & {}^2\mathbf{B}_3 & \mathbf{E}_6 & \mathbf{0} & \mathbf{0} & \mathbf{0} \\ {}^1\mathbf{B}_4 & {}^2\mathbf{B}_4 & \mathbf{0} & \mathbf{E}_6 & \mathbf{0} & \mathbf{0} \\ \mathbf{0} & \mathbf{0} & \mathbf{0} & \mathbf{0} & \mathbf{E}_6 & \mathbf{0} \\ \mathbf{0} & \mathbf{0} & \mathbf{0} & \mathbf{0} & {}^5\mathbf{B}_6 & \mathbf{E}_6 \end{bmatrix}$$

$$\mathbf{J}_m^d = \begin{bmatrix} b_1 & \mathbf{0} & \mathbf{0} & \mathbf{0} & \mathbf{0} & \mathbf{0} \\ \mathbf{0} & b_2 & \mathbf{0} & \mathbf{0} & \mathbf{0} & \mathbf{0} \\ \mathbf{0} & \mathbf{0} & b_3 & \mathbf{0} & \mathbf{0} & \mathbf{0} \\ \mathbf{0} & \mathbf{0} & \mathbf{0} & b_4 & \mathbf{0} & \mathbf{0} \\ \mathbf{0} & \mathbf{0} & \mathbf{0} & \mathbf{0} & b_5 & \mathbf{0} \\ \mathbf{0} & \mathbf{0} & \mathbf{0} & \mathbf{0} & \mathbf{0} & b_6 \end{bmatrix}$$

where \mathbf{J}_m is called the *natural orthogonal complement* (NOC) (the terminology is introduced by Angeles and Lee [3]) and the product $\mathbf{J}_m^n \mathbf{J}_m^d$ is called the *decoupled natural orthogonal complement* (DeNOC) (introduced by Saha [98]). Though such separation does not introduce changes in the form of the equations of motion (2.23), it brings further insight into the problem.

As already mentioned, further simplifications could be achieved by a different choice for the components of $\dot{\mathbf{Y}}$. Merely by using different dependent Cartesian velocities, the authors of [46] are able to simplify the structure of \mathbf{R}^o (in their notation the coupling elements below the main diagonal disappear), leading to a more concise and faster dynamic formulation.

Finally, the dependent Cartesian accelerations are found through differentiation of equation (2.28):

$$\ddot{\mathbf{Y}}_i = {}^k\mathbf{B}_i \ddot{\mathbf{Y}}_k + {}^k\dot{\mathbf{B}}_i \dot{\mathbf{Y}}_k + \mathbf{b}_i \ddot{\phi}_i + \dot{\mathbf{b}}_i \dot{\phi}_i \quad (2.34)$$

$${}^k\dot{\mathbf{B}}_i = \begin{bmatrix} \mathbf{0} & -\frac{d}{dt}\hat{\mathbf{p}}_i \\ \mathbf{0} & \mathbf{0} \end{bmatrix} \quad \dot{\mathbf{b}}_i = \begin{bmatrix} \frac{d}{dt}(\mathbf{u}_i \times \mathbf{s}_i) \\ \frac{d}{dt}(\mathbf{u}_i) \end{bmatrix}$$

The components of ${}^k\dot{\mathbf{B}}_i$ and $\dot{\mathbf{b}}_i$ are derived in Appendix A.

In order to demonstrate the simplicity and validity of the formulation presented in this section, a library of Matlab functions that perform the dynamic computation for a multibody system was developed. They can be downloaded at:

<http://www.astro.mech.tohoku.ac.jp/~mitko>

2.4.2 Closed-loop systems

The approach adopted in the previous subsection is very convenient because the equations of motion can be extended to the case when closed-loops exist with a minimal effort. Recall that up to now only the open loop constraints Φ^o were considered. It was assumed that the manipulator system is with open tree structure, or if closed-loops are intrinsic in the design they are opened through cutting a joint. Hereafter, the remaining constraints Φ^c which correspond to the joints that were cut will be imposed.

Equation (2.23) was formulated with respect the independent coordinates in case of a tree structure. If closed-loops exist the *relative coordinates* cease to be independent and the DOF of the system are decreased. Hereafter, the following notation will be utilized:

$$\dot{\mathbf{z}} = \begin{bmatrix} \dot{\mathbf{z}}^d \\ \dot{\mathbf{z}}^i \end{bmatrix} \quad (2.35)$$

where $\dot{\mathbf{z}}^i$ are a set of truly independent velocities. Again, starting point for the discussion is equation (2.16). Its lower part implies that the dependent Cartesian velocity vector $\dot{\mathbf{Y}}$ should be a linear combination of the vectors spanning the null space of Φ_Y^c . In order for the new constraints (Φ^c) to be accounted for, they should be included in the equation of motion (2.23). Starting from equation (2.17) and performing again the derivation process from the previous subsection, however, this time considering the term $\Phi_Y^{cT} \lambda^c$ as well, results in:

$$\mathbf{H}\ddot{\mathbf{z}} + \mathbf{c}_n + \Phi_z^{cT} \lambda^c = \begin{bmatrix} \mathbf{0} \\ \boldsymbol{\tau} \end{bmatrix} + \mathbf{R}^{oT} \mathbf{Q}_{ex} \quad (2.36)$$

where $\Phi_z^c = \Phi_Y^c \mathbf{R}^o$ can be interpreted as the Jacobian of the closed loop constraints with respect to the independent coordinates describing the tree system. In the same fashion

as discussed regarding \mathbf{Y} in Section 2.2 (see the *Remark*) it can be concluded that, the definition of a variable $\mathbf{z} \in R^{n+6}$ who's derivative is equal to $\dot{\mathbf{z}}$ is not possible, because of the nonintegrability of ω_0 . Nevertheless, \mathbf{z} will be employed to represent a partial derivative with respect to the n relative coordinates and six base reference coordinates, as in $\Phi_z^c = \partial\Phi^c/\partial\mathbf{z}$.

As in case of (2.10) and (2.15), there are different ways to solve equation (2.36). Here, a second *velocity transformation* from $\dot{\mathbf{z}}$ to $\dot{\mathbf{z}}^i$ will be used, that will result in elimination of the term $\Phi_z^{cT}\lambda^c$. Again as in the previous section the relation between the dependent and independent set of velocities is made through the null space of the Jacobian matrix of the constraint equations (in this case Φ_z^c), hence:

$$\dot{\mathbf{z}} = \mathbf{R}^c \dot{\mathbf{z}}^i \quad (2.37)$$

where

$$\Phi_z^c \mathbf{R}^c = 0 \quad \text{and} \quad \Phi_z^c \dot{\mathbf{z}} = 0 \quad (2.38)$$

Differentiation of (2.37) leads to:

$$\ddot{\mathbf{z}} = \mathbf{R}^c \ddot{\mathbf{z}}^i + \dot{\mathbf{R}}^c \dot{\mathbf{z}}^i \quad (2.39)$$

Now substituting (2.39) into (2.36) and multiplying from the left with \mathbf{R}^{cT} gives:

$$\mathbf{R}^{cT} \mathbf{H} \mathbf{R}^c \ddot{\mathbf{z}}^i + \mathbf{R}^{cT} \mathbf{H} \dot{\mathbf{R}}^c \dot{\mathbf{z}}^i + \mathbf{R}^{cT} \mathbf{c}_n + \mathbf{R}^{cT} \Phi_z^{cT} \lambda^c = \mathbf{R}^{cT} \begin{bmatrix} \mathbf{0} \\ \boldsymbol{\tau} \end{bmatrix} + \mathbf{R}^{cT} \mathbf{R}^{oT} \mathbf{Q}_{ex}$$

or

$$\mathbf{H}^i \ddot{\mathbf{z}}^i + \mathbf{c}_n^i = \begin{bmatrix} \mathbf{0} \\ \boldsymbol{\tau}^i \end{bmatrix} + \mathbf{Q}_{ex}^i \quad (2.40)$$

where

$$\begin{aligned} \mathbf{H}^i &= \mathbf{R}^{cT} \mathbf{H} \mathbf{R}^c ; \quad \mathbf{Q}_{ex}^i = \mathbf{R}^{cT} \mathbf{R}^{oT} \mathbf{Q}_{ex} \\ \begin{bmatrix} \mathbf{0} \\ \boldsymbol{\tau}^i \end{bmatrix} &= \mathbf{R}^{cT} \begin{bmatrix} \mathbf{0} \\ \boldsymbol{\tau} \end{bmatrix} \end{aligned} \quad (2.41)$$

$$\begin{aligned} \mathbf{c}_n^i &= \mathbf{R}^{cT} \mathbf{H} \dot{\mathbf{R}}^c \dot{\mathbf{z}}^i + \mathbf{R}^{cT} \mathbf{c}_n \\ &= \mathbf{R}^{cT} \mathbf{R}^{oT} \mathbf{M} \mathbf{R}^o \dot{\mathbf{R}}^c \dot{\mathbf{z}}^i + \mathbf{R}^{cT} \mathbf{R}^{oT} \mathbf{M} \dot{\mathbf{R}}^o \mathbf{R}^c \dot{\mathbf{z}}^i - \mathbf{R}^{cT} \mathbf{R}^{oT} \mathbf{Q}_n \\ &= \mathbf{R}^{cT} \mathbf{R}^{oT} \mathbf{M} (\mathbf{R}^o \dot{\mathbf{R}}^c + \dot{\mathbf{R}}^o \mathbf{R}^c) \dot{\mathbf{z}}^i - \mathbf{R}^{cT} \mathbf{R}^{oT} \mathbf{Q}_n \\ &= \mathbf{R}^{cT} \mathbf{R}^{oT} \mathbf{M} \frac{d}{dt} (\mathbf{R}^o \mathbf{R}^c) \dot{\mathbf{z}}^i - \mathbf{R}^{cT} \mathbf{R}^{oT} \mathbf{Q}_n \end{aligned} \quad (2.42)$$

Equation (2.40) is of particular interest because of a number of reasons. It is formulated with respect to a truly independent set coordinates, and its solution is stable to numerical drift. The mass matrix \mathbf{H}^i is symmetric and positive-definite as opposed to the leading matrix of (2.10) which is only symmetric. No constraints explicitly appear in the system of equations, but rather they are imposed implicitly through the utilization of matrices \mathbf{R}^o and \mathbf{R}^c . It can be seen that by multiplication with \mathbf{R}^{cT} , the torques in the manipulator joints $\boldsymbol{\tau}$ can be mapped into $\boldsymbol{\tau}_i$, which are the torques only in the independent relative coordinates. Such map is very useful for the computation of the inverse dynamics problem as pointed out by Nakamura in [72].

The computation of the nonlinear term \mathbf{c}_n^i can be done following a procedure similar to the one presented in the previous subsection. From the equation that relates the dependent Cartesian velocities to the independent ones

$$\dot{\mathbf{Y}} = \mathbf{R}^o \dot{\mathbf{z}} = \mathbf{R}^o \mathbf{R}^c \dot{\mathbf{z}}^i$$

the relationship of accelerations can be expressed as follows:

$$\ddot{\mathbf{Y}} = \mathbf{R}^o \mathbf{R}^c \ddot{\mathbf{z}}^i + \frac{d}{dt}(\mathbf{R}^o \mathbf{R}^c) \dot{\mathbf{z}}^i \quad (2.43)$$

Hence, the term $\frac{d}{dt}(\mathbf{R}^o \mathbf{R}^c) \dot{\mathbf{z}}^i$ can be directly computed as the Cartesian accelerations ($\ddot{\mathbf{Y}}$) that would be produced by the independent relative velocities $\dot{\mathbf{z}}^i$ and null relative independent accelerations ($\ddot{\mathbf{z}}^i = 0$). Note that for the actual (recursive) computation of $\frac{d}{dt}(\mathbf{R}^o \mathbf{R}^c) \dot{\mathbf{z}}^i$ one needs to know the dependent relative velocities and accelerations ($\dot{\mathbf{z}}^d, \ddot{\mathbf{z}}^d$) as well (their computation will be derived at the end of this subsection).

One obstacle imposed by the presented approach is that a set of independent variables describing the motion of the system has to be provided at any time. Since this is of paramount importance for the application of equation (2.40), a coordinate partitioning method will be discussed next.

2.4.2.1 Coordinate partitioning

Finding an independent set of variables that describe the motion of a mechanical system is not a problem with unique solution. It should be noted that in general, no set of independent coordinates is adequate through the entire motion of the system. Hence, finding such a set, and being able to detect when a given set is not independent any more, are two problems of transcendental importance. One can readily use the properties of the Jacobian matrix of the constraints Φ_z^c in order to solve both of them.

There are different methods that can be used to partition the state variables into independent and dependent components [45]. In general, they can be divided into two

groups: *orthogonal* and *projection* methods. Here, a *projection* method based on the *Gauss Jordan elimination* with partial pivoting will be utilized [103]. It decomposes the Jacobian matrix Φ_z^c as follows:

$$\Phi_z^c = \begin{bmatrix} \Phi_z^d & \Phi_z^i \end{bmatrix} \quad (2.44)$$

where $\Phi_z^d \in R^{m^c \times m^c}$ is a square matrix containing the columns of Φ_z^c in which pivots have appeared during the partitioning procedure, m^c is the number of constraint equations (it is assumed that the constraints are independent). $\Phi_z^i \in R^{m^c \times f}$ includes the remaining $f = n + 6 - m^c$ columns (n it the number of manipulator joints, 6 is the DOF of the base body). The variables associated with the columns of Φ_z^i and Φ_z^d are called independent and dependent, respectively. In general, for the solution of a system of linear equations with a leading matrix as in (2.44) it is necessary to specify values for the independent variables, and then compute the dependent ones. Once the *Gauss Jordan elimination* is performed on matrix Φ_z^c , f from the elements of $\dot{\mathbf{z}}$ can be chosen to form the independent subset $\dot{\mathbf{z}}^i$. In Appendix B a simple example that demonstrates the above procedure is included.

2.4.2.2 Constraint equations and matrix Φ_z^c for a cut rotational joint

In this subsection, the constraint equations that occur when a rotational joint is cut will be outlined. In order to impose a closed-loop condition for the system shown in Fig. 2.4 the following equations must be established:

$$\mathbf{r}_i - \mathbf{r}_k = 0 \quad (2.45)$$

$$\mathbf{u}_i - \mathbf{u}_k = 0 \quad (2.46)$$

(2.45) has three independent equations and (2.46) has two independent equations¹². Writing (2.45) and (2.46) in a general form leads to:

$$\Phi^r(\mathbf{r}_i, \mathbf{r}_k) = 0 \quad (2.47)$$

$$\Phi^u(\mathbf{u}_i, \mathbf{u}_k) = 0 \quad (2.48)$$

It is necessary to compute the **Jacobian matrix** of the above two constraints with respect to the coordinate vector \mathbf{z} , hence, using the chain rule one obtains:

$$\begin{aligned} \frac{\partial \Phi^r}{\partial \mathbf{z}} &= \frac{\partial \Phi^r}{\partial \mathbf{r}_i} \frac{\partial \mathbf{r}_i}{\partial \mathbf{z}} + \frac{\partial \Phi^r}{\partial \mathbf{r}_k} \frac{\partial \mathbf{r}_k}{\partial \mathbf{z}} = \Phi_{r_i}^r \frac{\partial \mathbf{r}_i}{\partial \mathbf{z}} + \Phi_{r_k}^r \frac{\partial \mathbf{r}_k}{\partial \mathbf{z}} \\ \frac{\partial \Phi^u}{\partial \mathbf{z}} &= \frac{\partial \Phi^u}{\partial \mathbf{u}_i} \frac{\partial \mathbf{u}_i}{\partial \mathbf{z}} + \frac{\partial \Phi^u}{\partial \mathbf{u}_k} \frac{\partial \mathbf{u}_k}{\partial \mathbf{z}} = \Phi_{u_i}^u \frac{\partial \mathbf{u}_i}{\partial \mathbf{z}} + \Phi_{u_k}^u \frac{\partial \mathbf{u}_k}{\partial \mathbf{z}} \end{aligned}$$

¹²The rotational joint has one DOF which is around the coinciding axis \mathbf{u}_i and \mathbf{u}_k .

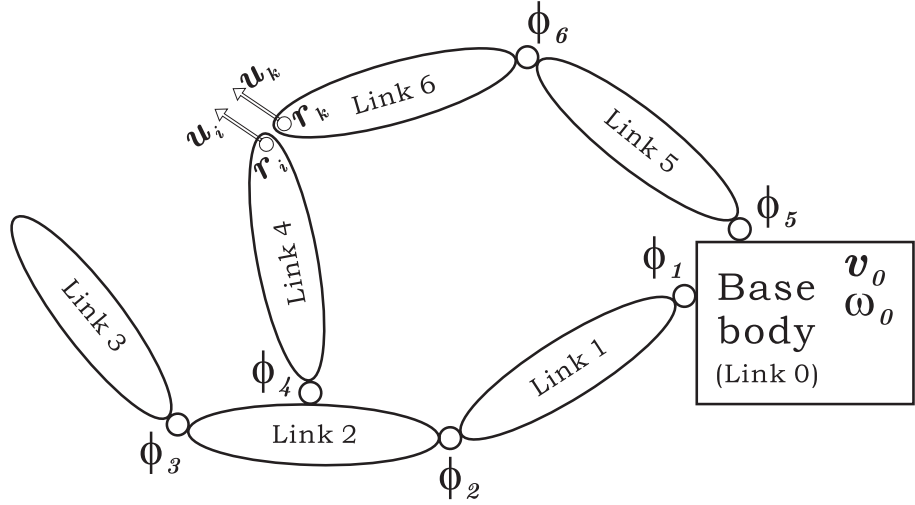


Figure 2.4: System containing a closed loop.

where

$$\begin{aligned}\Phi_{r_i}^r &= \frac{\partial \mathbf{r}_i}{\partial \mathbf{r}_i} - \frac{\partial \mathbf{r}_k}{\partial \mathbf{r}_i} = \mathbf{E} \\ \Phi_{r_k}^r &= \frac{\partial \mathbf{r}_i}{\partial \mathbf{r}_k} - \frac{\partial \mathbf{r}_k}{\partial \mathbf{r}_k} = -\mathbf{E} \\ \Phi_{u_i}^u &= \frac{\partial \mathbf{u}_i}{\partial \mathbf{u}_i} - \frac{\partial \mathbf{u}_k}{\partial \mathbf{u}_i} = \mathbf{E} \\ \Phi_{u_k}^u &= \frac{\partial \mathbf{u}_i}{\partial \mathbf{u}_k} - \frac{\partial \mathbf{u}_k}{\partial \mathbf{u}_k} = -\mathbf{E}\end{aligned}$$

The derivative of the position vectors \mathbf{r}_i and \mathbf{r}_k with respect to a generic coordinate z_j can be computed as the velocities of these points induced by a unit velocity in \dot{z}_j . For instance, if joint j is revolute and is determined by a point \mathbf{r}_j and a unit vector \mathbf{u}_j , located between the base body and point \mathbf{r}_i , the velocity of point i originated by a unit relative velocity in joint j can be expressed as:

$$\frac{\partial \dot{\mathbf{r}}_i}{\partial \dot{z}_j} = \mathbf{u}_j \times (\mathbf{r}_i - \mathbf{r}_j) \quad (2.49)$$

note that

$$\begin{aligned}\frac{\partial \dot{\mathbf{r}}_i}{\partial \dot{z}_j} &= \frac{\partial}{\partial \dot{z}_j} \left(\frac{\partial \mathbf{r}_i}{\partial z_j} \frac{dz_j}{dt} \right) \\ &= \frac{\partial}{\partial \dot{z}_j} \left(\frac{\partial \mathbf{r}_i}{\partial z_j} \right) \frac{dz_j}{dt} + \frac{\partial \mathbf{r}_i}{\partial z_j} \frac{\partial}{\partial \dot{z}_j} \left(\frac{dz_j}{dt} \right) \\ &= \frac{\partial}{\partial \dot{z}_j} \left(\frac{\partial \mathbf{r}_i}{\partial z_j} \right) \dot{z}_j + \frac{\partial \mathbf{r}_i}{\partial z_j} \frac{\partial \dot{z}_j}{\partial \dot{z}_j} = \frac{\partial \mathbf{r}_i}{\partial z_j}\end{aligned} \quad (2.50)$$

where

$$\frac{\partial \dot{z}_j}{\partial \dot{z}_j} = 1 \quad \text{and} \quad \frac{\partial}{\partial \dot{z}_j} \left(\frac{\partial \mathbf{r}_i}{\partial z_j} \right) = 0$$

The last equality follows from the fact that the term in the brackets does not explicitly depend on \dot{z}_j .

The derivative of the unit vectors (\mathbf{u}_i and \mathbf{u}_k) with respect to a generic coordinate z_j can be computed in the same fashion, for example:

$$\frac{\partial \mathbf{u}_i}{\partial z_j} = \frac{\partial \dot{\mathbf{u}}_i}{\partial \dot{z}_j} = \mathbf{u}_j \times \mathbf{u}_i \quad (2.51)$$

The Jacobian matrix Φ_z^c becomes:

$$\Phi_z^c = \begin{bmatrix} \Phi_z^r \\ \Phi_z^u \end{bmatrix} \quad (2.52)$$

where

$$\Phi_z^r = \frac{\partial \Phi^r}{\partial \mathbf{z}} \quad \Phi_z^u = \frac{\partial \Phi^u}{\partial \mathbf{z}}$$

2.4.2.3 Forming \mathbf{R}^c and calculation of the dependent velocities

Once Φ_z^c is formed, using the coordinate partitioning method based on the *Gauss Jordan elimination* with partial pivoting (see Section 2.4.2.1) it is possible to reformulate (2.38) to arrive at the following partitioned velocity equation:

$$\begin{bmatrix} \Phi_z^d & \Phi_z^i \end{bmatrix} \begin{bmatrix} \dot{\mathbf{z}}^d \\ \dot{\mathbf{z}}^i \end{bmatrix} = 0 \quad (2.53)$$

Matrix Φ_z^d is non-singular because its columns contain the pivots of Φ_z^c , hence, it is invertible. From the above equation it follows that:

$$\dot{\mathbf{z}}^d = -(\Phi_z^d)^{-1} \Phi_z^i \dot{\mathbf{z}}^i \quad (2.54)$$

$$\begin{bmatrix} \dot{\mathbf{z}}^d \\ \dot{\mathbf{z}}^i \end{bmatrix} = \begin{bmatrix} -(\Phi_z^d)^{-1} \Phi_z^i \\ \mathbf{E} \end{bmatrix} \dot{\mathbf{z}}^i \quad (2.55)$$

Equations (2.55) and (2.37) are equivalent, therefore

$$\mathbf{R}^c = \begin{bmatrix} -(\Phi_z^d)^{-1} \Phi_z^i \\ \mathbf{E} \end{bmatrix} \quad (2.56)$$

As demonstrated in Appendix B, when the *Gauss Jordan elimination* with partial pivoting is performed, Φ_z^d is constructed to be a unit matrix with proper dimensions. This guarantees that it is full rank, and most importantly its inverse is no longer needed, hence, the above expression for \mathbf{R}^c can be expressed as:

$$\mathbf{R}^c = \begin{bmatrix} -\Phi_z^i \\ \mathbf{E} \end{bmatrix}$$

Equation (2.56) is generally valid no matter what coordinate partitioning method is used, hence, it will be utilized hereafter.

From practical point of view, expressing the dependent velocities $\dot{\mathbf{z}}^d$ from equation (2.53) can be done using the least square formulation (matrix $\Phi_z^{dT} \Phi_z^d$, [109] p. 153), hence, (2.54) becomes :

$$\dot{\mathbf{z}}^d = -(\Phi_z^{dT} \Phi_z^d)^{-1} (\Phi_z^{dT} \Phi_z^i) \dot{\mathbf{z}}^i \quad (2.57)$$

Utilization of equation (2.57) is convenient in cases when the matrix Φ_z^d becomes close to singular. Such situations can occur if the utilization of a particular set of coordinates is desirable, even if they are close to a singular configuration.

2.4.2.4 Calculation of the dependent accelerations

In order to compute the dependent relative accelerations $\ddot{\mathbf{z}}^d$, equation (2.53) is differentiated with respect to time to obtain:

$$\begin{bmatrix} \Phi_z^d & \Phi_z^i \end{bmatrix} \begin{bmatrix} \ddot{\mathbf{z}}^d \\ \ddot{\mathbf{z}}^i \end{bmatrix} + \begin{bmatrix} \dot{\Phi}_z^d & \dot{\Phi}_z^i \end{bmatrix} \begin{bmatrix} \dot{\mathbf{z}}^d \\ \dot{\mathbf{z}}^i \end{bmatrix} = 0$$

substituting $\ddot{\mathbf{z}}^i = 0$ in the above equation and solving for $\ddot{\mathbf{z}}^d$ leads to:

$$\ddot{\mathbf{z}}^d = -(\Phi_z^d)^{-1} \dot{\Phi}_z^c \dot{\mathbf{z}} \quad (2.58)$$

the solution of equation (2.58) can be found using the least squares method as pointed out in the previous subsection.

· Computation of matrix $\dot{\Phi}_z^c$.

Again let us consider the constraint equations separately as in (2.47) and (2.48). Their Jacobian with respect to \mathbf{z} was found to be:

$$\begin{aligned} \Phi_z^r &= \Phi_{r_i}^r \frac{\partial \mathbf{r}_i}{\partial \mathbf{z}} + \Phi_{r_k}^r \frac{\partial \mathbf{r}_k}{\partial \mathbf{z}} \\ \Phi_z^u &= \Phi_{u_i}^u \frac{\partial \mathbf{u}_i}{\partial \mathbf{z}} + \Phi_{u_k}^u \frac{\partial \mathbf{u}_k}{\partial \mathbf{z}} \end{aligned}$$

The above equations can be differentiated to obtain:

$$\begin{aligned} \dot{\Phi}_z^r &= \dot{\Phi}_{r_i}^r \frac{\partial \mathbf{r}_i}{\partial \mathbf{z}} + \Phi_{r_i}^r \frac{d}{dt} \left(\frac{\partial \mathbf{r}_i}{\partial \mathbf{z}} \right) + \dot{\Phi}_{r_k}^r \frac{\partial \mathbf{r}_k}{\partial \mathbf{z}} + \Phi_{r_k}^r \frac{d}{dt} \left(\frac{\partial \mathbf{r}_k}{\partial \mathbf{z}} \right) \\ \dot{\Phi}_z^u &= \dot{\Phi}_{u_i}^u \frac{\partial \mathbf{u}_i}{\partial \mathbf{z}} + \Phi_{u_i}^u \frac{d}{dt} \left(\frac{\partial \mathbf{u}_i}{\partial \mathbf{z}} \right) + \dot{\Phi}_{u_k}^u \frac{\partial \mathbf{u}_k}{\partial \mathbf{z}} + \Phi_{u_k}^u \frac{d}{dt} \left(\frac{\partial \mathbf{u}_k}{\partial \mathbf{z}} \right) \end{aligned}$$

However, $\dot{\Phi}_{r_i}^r$, $\dot{\Phi}_{r_k}^r$, $\dot{\Phi}_{u_i}^u$ and $\dot{\Phi}_{u_k}^u$ are equal to zero and $\Phi_{r_i}^r$, $-\Phi_{r_k}^r$, $\Phi_{u_i}^u$ and $-\Phi_{u_k}^u$ are equal to \mathbf{E} , hence:

$$\begin{aligned}\dot{\Phi}_z^r &= \frac{d}{dt} \left(\frac{\partial \mathbf{r}_i}{\partial \mathbf{z}} \right) - \frac{d}{dt} \left(\frac{\partial \mathbf{r}_k}{\partial \mathbf{z}} \right) = \frac{d}{dt} \left(\frac{\partial \dot{\mathbf{r}}_i}{\partial \dot{\mathbf{z}}} \right) - \frac{d}{dt} \left(\frac{\partial \dot{\mathbf{r}}_k}{\partial \dot{\mathbf{z}}} \right) \\ \dot{\Phi}_z^u &= \frac{d}{dt} \left(\frac{\partial \mathbf{u}_i}{\partial \mathbf{z}} \right) - \frac{d}{dt} \left(\frac{\partial \mathbf{u}_k}{\partial \mathbf{z}} \right) = \frac{d}{dt} \left(\frac{\partial \dot{\mathbf{u}}_i}{\partial \dot{\mathbf{z}}} \right) - \frac{d}{dt} \left(\frac{\partial \dot{\mathbf{u}}_k}{\partial \dot{\mathbf{z}}} \right)\end{aligned}$$

Therefore, differentiation of (2.49) and (2.51) leads to:

$$\begin{aligned}\frac{d}{dt} \left(\frac{\partial \dot{\mathbf{r}}_i}{\partial \dot{\mathbf{z}}_j} \right) &= \frac{d}{dt} (\mathbf{u}_j) \times (\mathbf{r}_i - \mathbf{r}_j) + \mathbf{u}_j \times \frac{d}{dt} (\mathbf{r}_i - \mathbf{r}_j) \\ &= (\boldsymbol{\omega}_j^p \times \mathbf{u}_j) \times (\mathbf{r}_i - \mathbf{r}_j) + \mathbf{u}_j \times (\dot{\mathbf{r}}_i - \dot{\mathbf{r}}_j)\end{aligned}\quad (2.59)$$

$$\begin{aligned}\frac{d}{dt} \left(\frac{\partial \dot{\mathbf{u}}_i}{\partial \dot{\mathbf{z}}_j} \right) &= \frac{d}{dt} (\mathbf{u}_j) \times \mathbf{u}_i + \mathbf{u}_j \times \frac{d}{dt} (\mathbf{u}_i) \\ &= (\boldsymbol{\omega}_j^p \times \mathbf{u}_j) \times \mathbf{u}_i + \mathbf{u}_j \times (\boldsymbol{\omega}_i \times \mathbf{u}_i)\end{aligned}\quad (2.60)$$

where $\boldsymbol{\omega}_j^p$ is the angular velocity of the body with output joint j .

2.4.2.5 Computation algorithm

1.) Start at time t , when the positions and independent velocities¹³ are known.

$$\mathbf{y} = \begin{bmatrix} \mathbf{z}_c \\ \dot{\mathbf{z}}^i \end{bmatrix}$$

where \mathbf{z}_c are position variables describing the configuration of the tree system. As noted in Section 2.2 (see the *Remark*) $\dot{\mathbf{z}}_c \neq \dot{\mathbf{z}}$.

2.) Using \mathbf{z}_c , calculate in a recursive process the new dependent Cartesian positions \mathbf{Y}_c , solving an open-chain position problem.

3.) The constraint equations of the closed-loop system (corresponding to the cut joints) are formed. The Jacobian matrix Φ_z^c is calculated using equation (2.52)¹⁴. The dependent velocities $\dot{\mathbf{z}}^d$ are calculated from the independent ones $\dot{\mathbf{z}}^i$ using equation (2.54) or (2.57). Matrix \mathbf{R}^c is formed.

4.) From the velocities $\dot{\mathbf{z}}$, calculate in a recursive process the new dependent Cartesian velocities $\dot{\mathbf{Y}}$, solving an open-chain problem.

5.) Using equation (2.58), calculate the dependent accelerations $\ddot{\mathbf{z}}^d$. Note that the independent accelerations were set equal to zero $\ddot{\mathbf{z}}^i = 0$.

¹³Note that the initial independent velocities $\dot{\mathbf{z}}^i$ are the only velocities that can be specified by the user. The dependent ones should be calculated using the constraint equations like in (2.54).

¹⁴This is in the case when the cut joint rotational.

- 6.) Calculate the term $\frac{d}{dt}(\mathbf{R}^o \mathbf{R}^c) \dot{\mathbf{z}}^i$ from (2.43) as the Cartesian accelerations $\ddot{\mathbf{Y}}$ (open chain system) evaluated with $\ddot{\mathbf{z}}^i = 0$. In the process $\ddot{\mathbf{z}}^d$, calculated in step 5 is necessary.
- 7.) Form the terms \mathbf{H}^i , c^i , \mathbf{Q}_{ex}^i and solve (2.40) for $\ddot{\mathbf{z}}^i$.
- 8.) From $\dot{\mathbf{z}}$ form an integrable velocity vector $\dot{\mathbf{z}}_I$, using a relation as the one in (2.2).
- 9.) From the obtained independent accelerations $\ddot{\mathbf{z}}^i$ and the velocities $\dot{\mathbf{z}}_I$ form $\dot{\mathbf{y}}$.

$$\dot{\mathbf{y}} = \begin{bmatrix} \dot{\mathbf{z}}_I \\ \ddot{\mathbf{z}}^i \end{bmatrix}$$

Integration of $\dot{\mathbf{y}}$ gives \mathbf{y} and the algorithm can start again from step 1. As an alternative, one can integrate only an independent set of $\dot{\mathbf{z}}_I$ ($\dot{\mathbf{z}}_I^i$). The solution for the position of the dependent coordinates, however, has to be found at each step using an iterative procedure (like Newton-Raphson), which can gradually slow down the simulation. When $\dot{\mathbf{z}}_I$ is integrated, the components of \mathbf{z}_c are directly obtained and the stabilization problem is not critical because the round-off errors do not tend to increase with time (although they accumulate and can slow down the integration) see [45] p. 174).

Although not discussed here, selecting a suitable integration method is very important for the actual dynamic computation using the formulation presented in this chapter. A choice between *stability* \leftrightarrow *accuracy* \leftrightarrow *efficiency* has to be made, which in general depends on the type of the problem to be solved. A comprehensive discussion can be found in [31], [104].

2.5 Summary

A systematic derivation of the equations of motion for a multibody systems with open and closed-loop structure was presented. The formulation was made with respect to an independent set of coordinates. A number of advantages and disadvantages of this approach were outlined.

As a conclusion to the discussion, a summary of the main variables used in the dynamic formulation will be made. In Fig. 2.5 some of the essential matrix operations are depicted. The dimensions used are defined as follows:

n - number of manipulator joints.

k - ($k = 6n + 6$) is the number of the dependent Cartesian variables¹⁵

m^o - open loop constraints

m^c - closed loop constraints (for closing the cut joints)

¹⁵Six variables for each link and 6 for the base body.

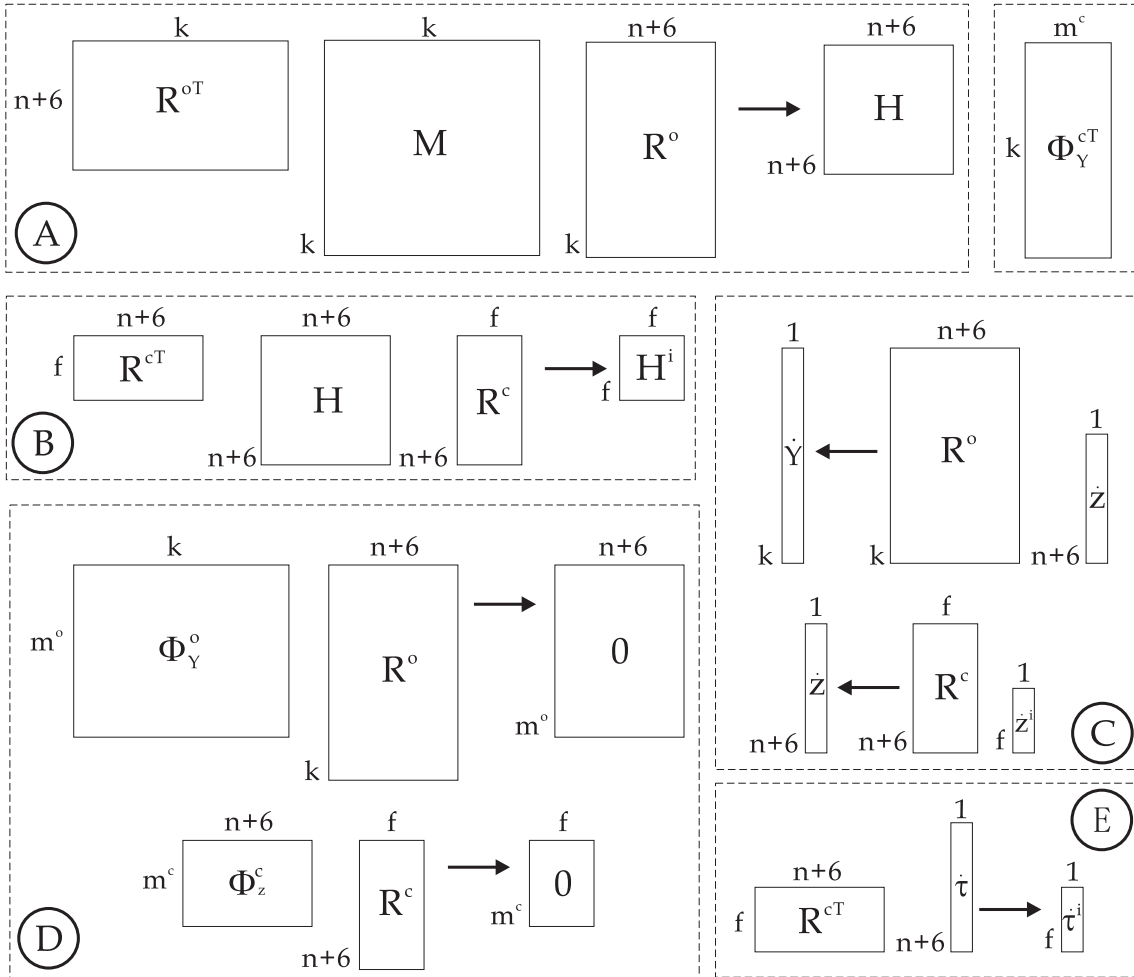


Figure 2.5: Dimensions of the matrices involved during the stages of the dynamic formulation.

$$f \quad - \quad (f = k - m^o - m^c) \text{ DOF of the system}$$

Fig. 2.5 **A** and **B** depict the first and second velocity transformations. It can be seen how the dimensions of the mass matrix changes ($\mathbf{M} \rightarrow \mathbf{H} \rightarrow \mathbf{H}^i$). The corresponding change of the state variables is depicted in **C** (equations (2.19) and (2.37)). Fig. 2.5 **D** depicts the fact that the columns of \mathbf{R}^o and \mathbf{R}^c span the null space of the Jacobian matrix of the constraint equations (equations (2.18) and (2.38)). Finally **E** demonstrates that \mathbf{R}^{cT} is a map between the torques in all manipulator joints τ and the torques only in the independent relative coordinates τ^i . This concept can be used for an *elegant* computation of the inverse dynamics of a closed-loop system as pointed out in [72].

Chapter 3

Fundamental control concepts and strategies

This chapter reviews some of the fundamental concepts and control strategies typically used in the field of space robotics. It is organized as follows. In Section 3.1 the concept of *reactionless manipulation* is outlined. The *coupling momentum*, and its importance for the solution of a variety of problems typically related to space robots are discussed. In addition, some of the commonly used redundancy resolution techniques are overviewed. In Section 3.2 the concept of task priority is outlined. A manipulability measure that can facilitate a task priority based control is examined.

Using the framework established in the previous chapter, the general form of the dynamic equations that govern the motion of a manipulator system with a tree structure, can be expressed in the following form (see (2.23));

$$\begin{bmatrix} \mathbf{H}_b & \mathbf{H}_c \\ \mathbf{H}_c^T & \mathbf{H}_\phi \end{bmatrix} \begin{bmatrix} \ddot{\mathbf{x}}_b \\ \ddot{\boldsymbol{\phi}} \end{bmatrix} + \begin{bmatrix} \mathbf{c}_b \\ \mathbf{c}_\phi \end{bmatrix} = \begin{bmatrix} \mathbf{0} \\ \boldsymbol{\tau} \end{bmatrix} + \mathbf{R}^{oT} \mathbf{Q}_{ex} \quad (3.1)$$

where the components of the global inertia matrix \mathbf{H} are derived in Appendix D. In addition, the nonlinear term \mathbf{c}_n is divided into two parts with subscripts $(\cdot)_b$ and $(\cdot)_m$, corresponding to the base and manipulator, respectively:

$$\mathbf{H} = \begin{bmatrix} \mathbf{H}_b & \mathbf{H}_c \\ \mathbf{H}_c^T & \mathbf{H}_\phi \end{bmatrix} \quad \mathbf{c}_n = \begin{bmatrix} \mathbf{c}_b \\ \mathbf{c}_m \end{bmatrix}$$

The external wrenches \mathbf{Q}_{ex} acting on the center of mass of each component of the multi-body system, are projected as joint torques ($\boldsymbol{\tau}$) and base wrenches using the *augmented* Jacobian matrix \mathbf{R}^{oT} , which forms the space of allowable motions of the system (see Section 2.2). The matrices $\mathbf{H}_b(\mathbf{x}_b, \boldsymbol{\phi})$ and $\mathbf{H}_\phi(\boldsymbol{\phi})$ are the global inertia of the base body and manipulator, respectively. The off-diagonal element $\mathbf{H}_c(\mathbf{x}_b, \boldsymbol{\phi}_m)$ contains the coupling inertia terms between the base and manipulator system.

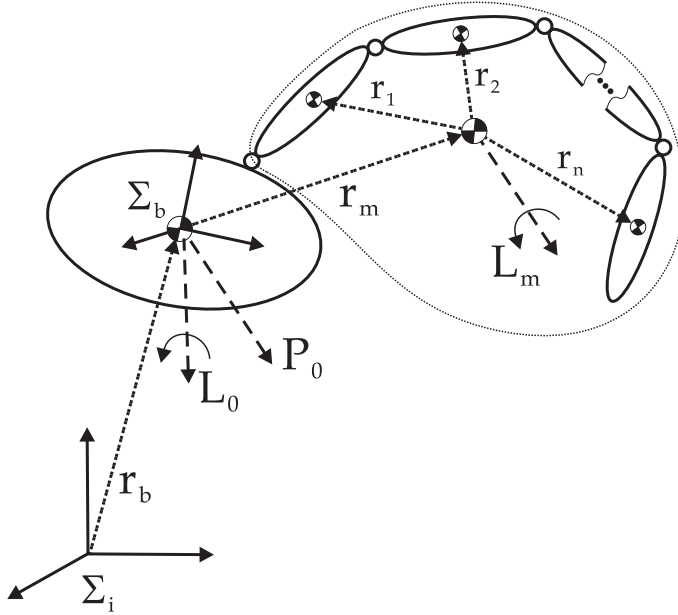


Figure 3.1: Coupling motion between the base and manipulator system.

The two sets of equations in (3.1), namely the one for the base and manipulator motions are dynamically coupled. Hence, due to the motion of the robot arm, forces and torques are transmitted to the spacecraft system, resulting in reaction motion. The investigation of this phenomenon is one of the main concerns hereafter.

Of particular interest are the properties of the coupling inertia matrix H_c , which can be used to uniquely determine a relation between the manipulator and base motions. In general, H_c and H_b are functions of the joint and base variables. However, in the absence of external forces, they depend only on ϕ . Hence, by solely controlling the robot arm, a desired spacecraft's base behavior can be ensured [86]. Of particular interest here is finding a subspace of manipulator motions that ensures zero base reactions, hence, a subspace in which decoupled behavior can be observed [83].

3.1 Subspace of reactionless motions

In order to obtain a better understanding, first a clear physical interpretation of the problem at hand will be made. Consider a manipulator system mounted on a free-floating base body as depicted in Fig. 3.1. We want to find manipulator joint velocities that result in zero base motion. It is reasonable to assume that if such velocities exist, they will be a member of a vector space (to be denoted by R^n) which is a subspace of R^o . In order to find R^n and make use of it, the same approach as the one used in Chapter 2 will be employed. It can be outlined in the following five steps;

- (S1) first the constraint equations that guarantee fulfilment of a given desired criteria are formed;
- (S2) at a second step the Jacobian of the constraint equations is found;
- (S3) using the properties of the above calculated Jacobian matrix, partitioning of the manipulator joint velocities into dependent and independent sets is made;
- (S4) the null space (if it exists) of this Jacobian matrix is constructed;
- (S5) once the independent velocities are specified the dependent ones are calculated.

First, the constraints for zero base reaction will be considered. As for now, it will be assumed that the external forces/torques are zero, and initially the base is at rest. The easiest way to form the constraints in this particular case is by making use of the conservative quantities of the system (Fig. 3.1), namely its momentum, hence, we have;

$$\mathbf{P}_0 = w_m \dot{\mathbf{r}}_m = 0 \quad (3.2)$$

$$\mathbf{L}_0 = \mathbf{L}_m + \mathbf{r}_m \times w_m \dot{\mathbf{r}}_m = 0 \quad (3.3)$$

where \mathbf{L}_m is the angular momentum of the manipulator around its center of mass and w_m is the manipulator's total mass (note that the derivative of \mathbf{r}_m has to be computed in Σ_b). Evidently, \mathbf{L}_0 is simply \mathbf{L}_m expressed around the base centroid and \mathbf{P}_0 is the linear momentum of the arm as seen from Σ_b . If \mathbf{P}_0 and \mathbf{L}_0 are equal to zero the stationary state of the base will be maintained. Comparison of equations (3.2) and (3.3) with the expressions for the momentum of the system derived in Appendix C (C.11) leads to the following relation:

$$\mathbf{H}_c \dot{\boldsymbol{\phi}} = \begin{bmatrix} w_m \dot{\mathbf{r}}_m \\ \mathbf{L}_m + \mathbf{r}_m \times w_m \dot{\mathbf{r}}_m \end{bmatrix}$$

In [83], this is called the coupling momentum of the system. The above relation is of paramount importance, and will be extensively used hereafter. Rewriting the constraint equations using the newly introduced quantity leads to:

$$\mathcal{L} = \mathbf{H}_c \dot{\boldsymbol{\phi}} = 0 \quad (3.4)$$

Note that, the above constraint is at velocity level and judging from equation (C.16), \mathbf{H}_c has a structure of a Jacobian matrix, however, it includes the mass and inertia characteristics of the system as well. Note again, that the constraints could not be defined explicitly as a function of the manipulator joint positions because the system of interest has a nonholonomic structure and (in general) for the same manipulator configuration the base position and orientation can be arbitrary.

The vector $\dot{\phi}$ that satisfies (3.4) belongs to the subspace of manipulator reactionless motions which coincides with the null space of the coupling inertia matrix. It is orthogonal to the *row space* of \mathbf{H}_c and will be denoted by \mathbf{R}^n , hence:

$$\mathbf{H}_c \mathbf{R}^n = 0 \quad (3.5)$$

Differentiation of (3.4) leads to:

$$\frac{d}{dt} \mathcal{L} = \mathcal{F}_b^m = \mathbf{H}_c \ddot{\phi} + \dot{\mathbf{H}}_c \dot{\phi} = 0 \quad (3.6)$$

Equation (3.6) implies that in order to maintain the stationary state of the base, the wrenches \mathcal{F}_b^m transmitted from the motion of the manipulator to the base should be zero¹. Alternatively the condition in (3.6) could be obtained by substituting zeros for the base velocities \dot{x}_b ² and accelerations \ddot{x}_b in the upper part of the equation of motion (3.1).

An alternative interpretation of (3.6) leads us to a very important conclusion, which was first introduced in [83]. It will be stated in the following theorem:

Theorem 1:

In the absence of active external disturbances, the motion of the manipulator does not induce any reactions to the base if and only if the coupling momentum is conserved ($\mathcal{L} = \text{const}$).

Proof: The proof follows from the direct examination of (3.6). □

Hereafter, manipulator motion that results in conservation of \mathcal{L} will be referred to as *reactionless manipulation*. This is a key concept, that can be applied for the solution of a number of practical problems, some of which will be discussed in the following chapters. Note that \mathcal{L} does not necessarily need to be equal to zero for *Theorem 1* to be valid. Only its rate of change is an important factor³. Taking this into account, a general form of equation (3.4) can be obtained as follows:

$$\mathcal{L}_0 = \mathbf{H}_c \dot{\phi}(t) \quad (3.7)$$

where $\mathcal{L}_0 = \mathbf{H}_c \dot{\phi}(t_0)$ is the initial value of the coupling momentum. It is obvious that if $\mathcal{L}(t) = \mathbf{H}_c \dot{\phi}(t) = \mathcal{L}_0$ for all $t \geq 0$ no base motion will occur (equation (3.7) could be obtained by integration of 3.6). It should be noted that a scenario where the base is

¹From the viewpoint of the base body, \mathcal{F}_b^m are external forces, although they do not change the momentum of the system.

² \dot{x}_b appears in the nonlinear term c_b .

³From practical point of view, in order for the manipulator to perform a stable motion there is always an upper limit for the value of \mathcal{L} . It depends on the mass and inertial characteristics of the system.

stationary and the coupling momentum is different from zero implies that the momentum of the entire system is non-zero.

The *coupling momentum* concept outlined above requires further treatment. When external disturbances act on the system (as in most practical cases), *Theorem 1* needs to be reformulated. The situation when the system encounters momentum change is of particular interest here, since it can occur during the contact with a target satellite. The discussion will be extended in Chapter 4, where the *coupling wrench theorem* will be introduced. At a next step, in Chapter 5, application of the *coupling wrench theorem* during the post-impact phase of a satellite capturing operation is discussed.

Next, the general solution of equations (3.6) and (3.7) will be examined.

3.1.1 Solution for the joint variables

Recall that in Chapter 2, the number of truly independent coordinates describing the motion of a given system was referred to as degrees of freedom (DOF). The DOF of a system were defined as the difference between the *dependent coordinates* describing its motion, and the number of imposed constraints. Those constraints were dependent from the manipulator structure, and were solely used for interconnecting the elements of a multibody system. It is convenient to make a distinction between them and the *task constraints* to be used hereafter⁴. Henceforth, an open-loop manipulator with n joints will be assumed to have n DOF, regardless of the imposed *task constraints* (m^t). The difference between the DOF and the *task constraints* will be called degree of redundancy (DOR) and will be denoted by f^r , hence, $f^r = n - m^t$. Note that, the above formulation of DOR does not include the DOF of the base body, because it is assumed that the base is not actively actuated.

Let us consider first equation (3.7). In general, the existence of solution for $\dot{\phi}$ that results in *reactionless motion* is not guaranteed. If both the translational and attitude motion of the base need to be controlled, the number of task constraints imposed is $m^t = 6$. Hence, in order for a solution to exist the manipulator should have six or more actuated joints ($n \geq m^t$). In the case when $n = m^t$ and the coupling momentum $\mathcal{L}_0 = 0$ the only possible solution is the trivial one. The reasoning for this can be inferred from the following well known relation from linear algebra (see [109] p. 138):

Definition 1:

$$\dim(\text{row space}) + \dim(\text{null space}) = \text{number of columns.}$$

⁴Although it is difficult for this distinction to be formulated in a mathematical fashion, when a system is controlled aiming to satisfaction of given criteria, the resulting constraints will be called *task constraints*.

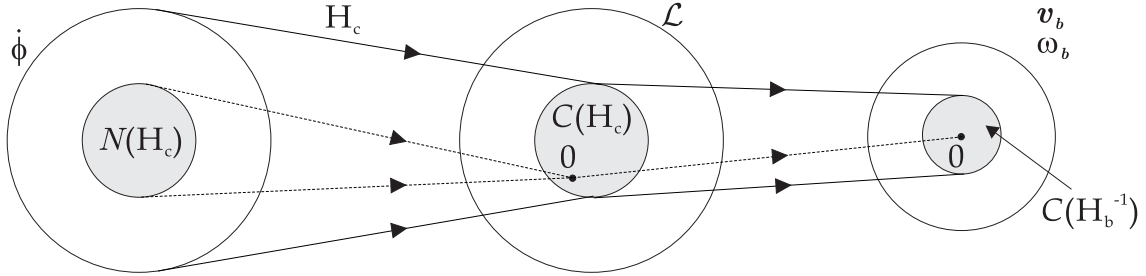


Figure 3.2: Mapping of the joint velocities on the base motion in the case when $\mathcal{L}_0 = 0$. $C(\cdot)$ represents the *range space* (column space) and $N(\cdot)$ is the null space of a matrix.

For the case discussed above, the *row space* of $\mathbf{H}_c \in R^{m^t \times n}$ is formed by the m^t constraint equations imposed. It forms a subspace in the R^n dimensional space of allowable motions for $\dot{\phi}$. The dimension of the *null space* component coincides with the DOR of the system. *Definition 1* actually states that $m^t + f^r = n$. It is obvious that if $n = m^t \Rightarrow f^r = 0$, hence, the solution of (3.7) with $\mathcal{L}_0 = 0$ is trivial. On the other hand if $n > m^t$ and again $\mathcal{L}_0 = 0$ the solutions belong to a f^r dimensional subspace of R^n .

Although most of the discussion here is made regarding $\mathcal{L}_0 = 0$ ⁵, it is worth answering the question: *what is the range of obtainable values for \mathcal{L} as a result of the manipulator's motion*. From linear algebra it is known that a system of equations as (3.7), can be solved for any vector \mathcal{L} which is in the column space (also called *range space*) of the leading matrix \mathbf{H}_c . This means that \mathcal{L} has to be a linear combination of the columns of \mathbf{H}_c , hence:

$$\mathcal{L} = \mathbf{H}_c^1 \dot{\phi}_1 + \mathbf{H}_c^2 \dot{\phi}_2 + \dots + \mathbf{H}_c^n \dot{\phi}_n \quad (3.8)$$

The space spanned by the columns of any matrix is called *column space*, and will be denoted by $C(\cdot)$. In the robotics related literature, $C(\cdot)$ is commonly referred to as *manipulable space* [74]. For equation (3.8), the *manipulable space* of \mathbf{H}_c consists of all the mappings for every $\dot{\phi}$, hence, providing information, whether given \mathcal{L} could be realized as a result of the motion of the manipulator. For example, if a planar (x,y axis) system, with no external disturbances is considered, no motion of the manipulator will result in nonzero x and y components of the coupling angular momentum \mathcal{L} . Because of its straightforward interpretation, the *manipulable space* proves to be useful in the analysis of manipulator systems [129]. It should be noted that the dimensions of the *column* and *row space* of a matrix are identical [109], hence, *Definition 1* can be rewritten in the following convenient form:

$$\dim C(\mathbf{H}_c) + \dim N(\mathbf{H}_c) = n$$

⁵Chapters 4 and 5 will deal with the case when $\mathcal{L}_0 \neq 0$.

with $N(\cdot)$ representing the null space of a matrix. Fig. 3.2 illustrates the influence of the manipulator joint velocities on the base motion. As can be seen, joint velocities derived from the null space of the coupling inertia matrix \mathbf{H}_c , result in zero coupling angular momentum \mathcal{L} , as well as in zero change of the base velocity. On the other hand, if $\dot{\phi}$ is a component of the range space of \mathbf{H}_c , the manipulator motion results in nonzero coupling momentum and base velocity.

In most cases, only particular base motions need to be restricted. For example, if the manipulator is mounted on a flexible structure, from practical point of view, some of the directions of base motion can be considered to be stiff enough, hence, leading to a smaller number of task constraints m^t [81]. The formulation of the *reactionless manipulation problem* with respect only to a given set of base motions is called *selective reaction-null space* [83].

The first way to find $\dot{\phi}$ discussed here, solves (3.7) in a way that locally guarantees minimal norm for the joint velocities (in least squares sense). The derivation of this solution follows:

3.1.1.1 Pseudoinverse approach

The following cost function is considered:

$$g(\dot{\phi}) = \frac{1}{2}(\dot{\phi} - \dot{\xi})^T(\dot{\phi} - \dot{\xi}) \quad (3.9)$$

where $\dot{\xi}$ is a vector of arbitrary (at least for the moment) joint velocities to be projected on the null space of \mathbf{H}_c . In order to minimize $(\dot{\phi} - \dot{\xi})$, the method of *Lagrange multipliers* will be used. The cost function is altered to include the unknown *multipliers* λ_p that will incorporate the constraints from (3.7):

$$g^c(\dot{\phi}, \lambda_p) = \frac{1}{2}(\dot{\phi} - \dot{\xi})^T(\dot{\phi} - \dot{\xi}) + \lambda_p^T(\mathbf{H}_c\dot{\phi} - \mathcal{L}_0) \quad (3.10)$$

The solution has to satisfy the following *necessary condition* [95]:

$$\left(\frac{\partial g^c}{\partial \dot{\phi}} \right)^T = 0$$

hence, one obtains:

$$\dot{\phi} = \mathbf{H}_c^T \lambda_p + \dot{\xi} \quad (3.11)$$

which if substituted in (3.7) leads to:

$$\lambda_p = (\mathbf{H}_c \mathbf{H}_c^T)^{-1}(\mathcal{L}_0 - \mathbf{H}_c \dot{\xi})$$

substituting the expression for λ_p back in (3.11) gives:

$$\dot{\phi} = \mathbf{H}_c^+ \mathcal{L}_0 + (\mathbf{E} - \mathbf{H}_c^+ \mathbf{H}_c) \dot{\xi} \quad (3.12)$$

with $\mathbf{H}_c^+ = \mathbf{H}_c^T (\mathbf{H}_c \mathbf{H}_c^T)^{-1}$ representing the right *pseudoinverse* of matrix \mathbf{H}_c . In the literature it is typically referred to as *the Moore-Penrose generalized inverse*. Equation (3.12) is the general solution to (3.7) [18]. Its latter term is of particular interest, since it is decoupled from \mathcal{L}_0 . This can be demonstrated by substituting (3.12) back into (3.7) to obtain:

$$\mathcal{L}_0 = \mathbf{H}_c \mathbf{H}_c^+ \mathcal{L}_0 + \mathbf{H}_c (\mathbf{E} - \mathbf{H}_c^+ \mathbf{H}_c) \dot{\xi}$$

The above equation is valid for any choice of $\dot{\xi}$, since $\mathbf{H}_c \mathbf{H}_c^+ = \mathbf{E}$ and

$$\mathbf{H}_c (\mathbf{E} - \mathbf{H}_c^+ \mathbf{H}_c) = 0 \quad (3.13)$$

Comparing equations (3.13) and (3.5) leads to the following expression for \mathbf{R}^n :

$$\mathbf{R}^n = (\mathbf{E} - \mathbf{H}_c^+ \mathbf{H}_c) \quad (3.14)$$

From the discussion above, it becomes clear that $\dot{\xi}$ projected on the null space \mathbf{R}^n results in joint velocities that does not violate the constraints in (3.7). Furthermore, in the particular case when $\mathcal{L}_0 = 0$ the component $\mathbf{R}^n \dot{\xi}$ is the only possible solution which results in *reactionless manipulation*.

Using the pseudoinverse of \mathbf{H}_c the solution to (3.6) is:

$$\ddot{\phi} = -\mathbf{H}_c^+ \dot{\mathbf{H}}_c \dot{\phi} + (\mathbf{E} - \mathbf{H}_c^+ \mathbf{H}_c) \ddot{\xi} \quad (3.15)$$

For more information about computation and properties of pseudoinverse of a matrix see [18], [55].

3.1.1.2 Coordinate partitioning approach

The approach using pseudoinverse outlined in the previous subsection is attractive, since it guarantees minimum joints velocities norm (at least in local sense). Nevertheless, problems related to kinematic singularities are not avoided. Close to such configurations the joint velocities can become arbitrary large as noted by the authors of [13]. Many alternatives to this solution have been proposed, including weighting methods [18], methods based on gradient projection [129], [28], such that utilize task augmentation [85], [14], and others.

Here, following the procedure in Section 2.4.2, the *Gauss Jordan elimination* with partial pivoting will be utilized in order to find solution to (3.7). As already shown, (Section 2.4.2) the coupling inertia matrix \mathbf{H}_c can be partitioned as follows [103], [17]:

$$\mathbf{H}_c = \begin{bmatrix} \mathbf{H}_c^d & \mathbf{H}_c^i \end{bmatrix} \quad (3.16)$$

where $\mathbf{H}_c^d \in R^{m^t \times m^t}$ is a full rank square matrix containing the columns of \mathbf{H}_c in which pivots have appeared during the partitioning procedure (forming the column space of \mathbf{H}_c), $\mathbf{H}_c^i \in R^{m^t \times f^r}$ includes the remaining $f^r = n - m^t$ columns (forming the null space of \mathbf{H}_c). The variables associated with the columns of \mathbf{H}_c^i and \mathbf{H}_c^d are called independent and dependent, respectively (for more information see the example in Appendix B). Hence, equation (3.7) can be rewritten as follows:

Case A ($\mathcal{L}_0 = 0$)

$$\begin{bmatrix} \mathbf{H}_c^d & \mathbf{H}_c^i \end{bmatrix} \begin{bmatrix} \dot{\phi}^d \\ \dot{\phi}^i \end{bmatrix} = 0 \quad (3.17)$$

Solving equation (3.17) for the dependent joint velocities leads to:

$$\dot{\phi}^d = -\mathbf{H}_c^{d-1} \mathbf{H}_c^i \dot{\phi}^i \quad (3.18)$$

This method is convenient, because it makes a clear distinction between a set of dependent and independent joint velocities. The number of elements in $\dot{\phi}^i$ is equal to the DOR of the system, and plays identical role as $\dot{\xi}$ in (3.12). Evidently, if $\dot{\phi}^i = 0$, manipulator motion does not occur.

Case B ($\mathcal{L}_0 \neq 0$)

In the case when the initial value of the coupling momentum is different from zero, equation (3.17) becomes:

$$\begin{bmatrix} \mathbf{H}_c^d & \mathbf{H}_c^i \end{bmatrix} \begin{bmatrix} \dot{\phi}^d \\ \dot{\phi}^i \end{bmatrix} = \mathcal{L}_0^p \quad (3.19)$$

where \mathcal{L}_0^p is the altered \mathcal{L}_0 during the partitioning of \mathbf{H}_c ⁶. Solving (3.19) for $\dot{\phi}^d$ leads to:

$$\dot{\phi}^d = \mathbf{H}_c^{d-1} (\mathcal{L}_0^p - \mathbf{H}_c^i \dot{\phi}^i) \quad (3.20)$$

It can be noted that even if $\dot{\phi}^i = 0$ the motion of the dependent part of $\dot{\phi}$ will guarantee zero base deviation. The particular case when $\dot{\phi}^i = 0$ will result in reactionless manipulation using only m^t number of joints. This corresponds to the particular solution in (3.12) (the resultant joint velocities are different, however).

3.1.1.3 Task space augmentation approach

As opposed to the method discussed in the previous subsection, where the state vector was partitioned by means of the *Gauss Jordan elimination*, the technique to be outlined here

⁶In order to preserve the same system of equations, all arithmetic procedures applied to the rows of \mathbf{H}_c are performed to the RHS as well.

is based on projection of the n dimensional vector of joint velocities into a f^r dimensional space using a time independent matrix $W \in R^{f^r \times n}$ [46], [45].

$$\dot{\xi} = W\dot{\phi} \quad (3.21)$$

Before revealing the structure of W , equations (3.21) and (3.7) will be joined to form the following system:

$$\begin{bmatrix} \mathbf{H}_c \\ W \end{bmatrix} \dot{\phi} = \begin{bmatrix} \mathcal{L}_0 \\ \dot{\xi} \end{bmatrix} \quad (3.22)$$

Equation (3.22) will have a unique solution if and only if the leading matrix is square and the rows of W are linearly independent from each other and from the rows of \mathbf{H}_c . Let us assume that there is a matrix W that meets the above requirements. Hence, $T_{Aug} = [\mathbf{H}_c^T \quad W^T]^T$ can be inverted to obtain:

$$\dot{\phi} = \begin{bmatrix} \mathbf{H}_c \\ W \end{bmatrix}^{-1} \begin{bmatrix} \mathcal{L}_0 \\ \dot{\xi} \end{bmatrix} \quad (3.23)$$

Denoting the first m^t columns of T_{Aug}^{-1} with \mathbf{P} and the remaining f^r column with \mathbf{R}^n , the following relation can be obtained:

$$\begin{bmatrix} \mathbf{H}_c \\ W \end{bmatrix} \begin{bmatrix} \mathbf{H}_c \\ W \end{bmatrix}^{-1} = \begin{bmatrix} \mathbf{H}_c \\ W \end{bmatrix} [\mathbf{P} \quad \mathbf{R}^n] = \begin{bmatrix} \mathbf{H}_c \mathbf{P} & \mathbf{H}_c \mathbf{R}^n \\ W \mathbf{P} & W \mathbf{R}^n \end{bmatrix} = \begin{bmatrix} \mathbf{E} & \mathbf{0} \\ \mathbf{0} & \mathbf{E} \end{bmatrix}$$

As can be seen, the columns of \mathbf{R}^n span the null space of \mathbf{H}_c . The solution of (3.22) becomes:

$$\dot{\phi} = \mathbf{P}\mathcal{L}_0 + \mathbf{R}^n\dot{\xi} \quad (3.24)$$

Equation (3.24) has similar structure to (3.12), where the former and latter terms represent the particular and homogenous solutions, respectively.

Matrix W plays an important role in the above formulation. It actually represents f^r independent constraints relating the independent variables of the problem. As long W is chosen so that T_{Aug} is full rank, the solution of (3.22) can be readily found. The important aspect of this formulation is that once W is determined, it need not be changed until its rows are independent from the rows of \mathbf{H}_c . For a good example demonstrating this see [45] p. 102 (Example 3.13).

3.1.2 Torque based reactionless manipulation

In the previous section, control strategies for performing reactionless manipulation at velocity and acceleration level were outlined. The same concept can be formulated directly

regarding the input joint torque. Considering zero external disturbances and solving the upper part of (3.1) for the joint accelerations leads to:

$$\ddot{\boldsymbol{\phi}} = -\mathbf{H}_c^+ (\mathbf{H}_b \ddot{\boldsymbol{x}}_b + \mathbf{c}_b) + (\mathbf{E} - \mathbf{H}_c^+ \mathbf{H}_c) \ddot{\boldsymbol{\xi}}$$

Substituting the above equation into the lower part of (3.1) leads to:

$$\boldsymbol{\tau} = \mathbf{H}_\phi (\mathbf{E} - \mathbf{H}_c^+ \mathbf{H}_c) \ddot{\boldsymbol{\xi}} + \mathbf{c}_\phi - \mathbf{H}_\phi \mathbf{H}_c^+ \mathbf{c}_b \quad (3.25)$$

where as a desired condition the base acceleration $\ddot{\boldsymbol{x}}_b$ was set to zero. In all (3.12), (3.15), (3.24) and (3.25) appears the *arbitrary* vector $\ddot{\boldsymbol{\xi}}$. If properly chosen it can result in realization of additional tasks without disturbing the base stationary state. A method for determining $\ddot{\boldsymbol{\xi}}$ is outlined in the next subsection.

3.2 Multiple tasks

In many cases, a manipulator system is bound to work in a multi-task environment. Its ability to perform more than one task at a time is essential from the viewpoint of performance efficiency and reliability. Furthermore, for achieving optimal performance, the decomposition of a given task into sub-tasks with priority is necessary. As a simple and very common example, the position and orientation of the robot hand can be considered. In order to enlarge the reachable workspace of the *first priority* task (usually position), a trade-off resulting in incompleteness of the secondary task has to be made. The idea of *tasks with order of priority* was introduced by Nakamura [70].

Henceforth, it is assumed that the manipulator of interest is kinematically redundant with respect to the imposed task constraints ($f^r = n - m^t > 0$). The task priority approach determines the way such redundancy has to be utilized (in order certain conditions to be satisfied), based only on present information. Its application is computationally inexpensive, and suitable for real-time implementation. Nevertheless, problems related to *conflicts* between the different tasks impose quite a challenge, since their occurrence is not related to the kinematic or dynamic parameters of the system. Such *task conflicts* are usually referred to as *algorithmic singularities*, since they represent solely the incompatibility of the simultaneously used control algorithms [80].

Here, the idea will be demonstrated with an example. In the case when a manipulator system needs to perform an approaching maneuver to a target satellite, it is usually necessary to control the base motion in a desired way. Hence, two types of constraints need to be imposed;

(C1) base motion constraint;

(C2) end-effector motion constraint.

From practical point of view, the satisfaction of six base and six end-effector conditions is not feasible. For that reason, the formulation will be made only with respect to the base attitude (no change is desired) and end-effector linear motion profile. The former one is assumed to be with first priority. In order to account only for the base rotation, equation (3.7) will take the following form:

$$\mathbf{L}_c = \tilde{\mathbf{H}}_c \dot{\boldsymbol{\phi}} \quad (3.26)$$

where \mathbf{L}_c is called the *coupling angular momentum* [82]. For more details on the transition between (3.7) and (3.26) see Appendix C, equation (C.18).

The C2 task is defined using:

$$\mathbf{v}_h = \mathbf{J}_{\phi h}^v \dot{\boldsymbol{\phi}} + \mathbf{v}_b \quad (3.27)$$

with \mathbf{v}_h and \mathbf{v}_b being the linear velocities of the end-effector and base, respectively. $\mathbf{J}_{\phi h}^v$ represents the linear part of the Jacobian matrix of the end-effector ($\mathbf{J}_{\phi h}$).

Solving (3.26) for $\dot{\boldsymbol{\phi}}$ (using redundancy resolution based on the pseudoinverse of $\tilde{\mathbf{H}}_c$), gives:

$$\dot{\boldsymbol{\phi}} = \tilde{\mathbf{H}}_c^+ \mathbf{L}_c + (\mathbf{E} - \tilde{\mathbf{H}}_c^+ \tilde{\mathbf{H}}_c) \dot{\boldsymbol{\xi}} \quad (3.28)$$

substituting $\dot{\boldsymbol{\phi}}$ from (3.28) into (3.27) leads to:

$$\mathbf{v}_h = \mathbf{J}_{\phi h}^v \tilde{\mathbf{H}}_c^+ \mathbf{L}_c + \mathbf{J}_{\phi h}^v (\mathbf{E} - \tilde{\mathbf{H}}_c^+ \tilde{\mathbf{H}}_c) \dot{\boldsymbol{\xi}} + \mathbf{v}_b$$

solving the above equation for $\dot{\boldsymbol{\xi}}$, one obtains:

$$\dot{\boldsymbol{\xi}} = \bar{\mathbf{J}}^+ (\mathbf{v}_h - \mathbf{v}_b - \mathbf{J}_{\phi h}^v \tilde{\mathbf{H}}_c^+ \mathbf{L}_c) + (\mathbf{E} - \bar{\mathbf{J}}^+ \bar{\mathbf{J}}) \dot{\boldsymbol{\xi}}_2$$

where $\bar{\mathbf{J}} = \mathbf{J}_{\phi h}^v (\mathbf{E} - \tilde{\mathbf{H}}_c^+ \tilde{\mathbf{H}}_c)$ is a restricted Jacobian matrix typically appearing in redundancy resolution schemes [80]. Finally substituting $\dot{\boldsymbol{\xi}}$ back into (3.28), gives:

$$\dot{\boldsymbol{\phi}} = \tilde{\mathbf{H}}_c^+ \mathbf{L}_c + \bar{\mathbf{J}}^+ \Psi + (\mathbf{E} - \tilde{\mathbf{H}}_c^+ \tilde{\mathbf{H}}_c) (\mathbf{E} - \bar{\mathbf{J}}^+ \bar{\mathbf{J}}) \dot{\boldsymbol{\xi}}_2 \quad (3.29)$$

where $\dot{\boldsymbol{\xi}}_2$ is an arbitrary vector with proper dimensions, $\Psi = \mathbf{v}_h - \mathbf{v}_b - \mathbf{J}_{\phi h}^v \tilde{\mathbf{H}}_c^+ \mathbf{L}_c$ and $(\mathbf{E} - \tilde{\mathbf{H}}_c^+ \tilde{\mathbf{H}}_c) \bar{\mathbf{J}}^+ = \bar{\mathbf{J}}^+$. The last relation follows directly from the idempotency⁷ and symmetry of $(\mathbf{E} - \tilde{\mathbf{H}}_c^+ \tilde{\mathbf{H}}_c)$, and the properties of the pseudoinverse.

The term $\tilde{\mathbf{H}}_c^+ \mathbf{L}_c$ is the particular solution for the task with first priority. The second term represents the projection of the secondary task on the null space of $\tilde{\mathbf{H}}_c$. Hence, joint

⁷A square matrix \mathbf{A} is idempotent if $\mathbf{A} = \mathbf{A}^2$.

velocities that perform end-effector control are derived only from the orthogonal space of the row space of $\tilde{\mathbf{H}}_c$, therefore, they will not influence the base control subtask whatsoever. The last term accounts for the remaining degrees of redundancy.

If $\mathbf{L}_c = 0$ and $\dot{\xi}_2 = 0$ ⁸ are assumed, (3.29) becomes:

$$\dot{\phi} = \bar{\mathbf{J}}^+ (\mathbf{v}_h - \mathbf{v}_b) \quad (3.30)$$

As can be seen, the restricted Jacobian matrix $\bar{\mathbf{J}}$ is the key to the method described above. In the particular example considered, it contains information about the end-effector kinematics (via $\mathbf{J}_{\phi h}^v$) and the manipulator \leftrightarrow base dynamic coupling (via $\tilde{\mathbf{H}}_c$). If $\bar{\mathbf{J}}$ is well conditioned, the solution of (3.30) will provide joint velocities that satisfy the end-effector velocity constraints, while providing zero base attitude deviation. In many cases, however, the generation of a singularity-free solutions is not possible as a result of *task contradiction*, in other words even though each task could be performed separately, their simultaneous application is not possible. In terms of the three matrices $\tilde{\mathbf{H}}_c$, $\mathbf{J}_{\phi h}^v$ and $\bar{\mathbf{J}}$ this means that:

$$\{rank(\bar{\mathbf{J}}) < rank(\bar{\mathbf{J}})^{max} \mid rank(\tilde{\mathbf{H}}_c) = rank(\tilde{\mathbf{H}}_c)^{max}, rank(\mathbf{J}_{\phi h}^v) = rank(\mathbf{J}_{\phi h}^v)^{max}\}$$

The above expression is an interpretation of *algorithmic singularity*.

3.2.1 Task performance measure

Avoiding situations when the restricted Jacobian $\bar{\mathbf{J}}$ is singular is of particular interest from the viewpoint of planning and control. Apart as a result of algorithmic singularities, rank deficiency of $\bar{\mathbf{J}}$ can occur at manipulator configurations where $rank(\mathbf{J}_{\phi h}^v) < rank(\mathbf{J}_{\phi h}^v)^{max}$ as well. The first step in avoiding singularities is to locate them in joint space. This can be successfully performed using a measure similar to the one proposed by Yoshikawa [129] ($S_J = \sqrt{\det [\mathbf{J}_{\phi h}^v \mathbf{J}_{\phi h}^{vT}]}$). As introduced in [80] such measure can have the following form:

$$S_{\bar{\mathbf{J}}} = \sqrt{\det [\bar{\mathbf{J}} \bar{\mathbf{J}}^T]} \quad (3.31)$$

When the scalar S_J becomes equal to zero and $\mathbf{J}_{\phi h}^v$ is full rank ($S_J \neq 0$), the performance of the secondary task in combination with the first one becomes impossible.

Using the fact that $(\mathbf{E} - \tilde{\mathbf{H}}_c^+ \tilde{\mathbf{H}}_c)(\mathbf{E} - \tilde{\mathbf{H}}_c^+ \tilde{\mathbf{H}}_c)^T = (\mathbf{E} - \tilde{\mathbf{H}}_c^+ \tilde{\mathbf{H}}_c)$, equation (3.31) can be rewritten in a more convenient form:

$$S_{\bar{\mathbf{J}}} = \sqrt{\det [\mathbf{J}_{\phi h}^v (\mathbf{E} - \tilde{\mathbf{H}}_c^+ \tilde{\mathbf{H}}_c) \mathbf{J}_{\phi h}^{vT}]} \quad (3.32)$$

⁸No additional redundancy is available or the introduction of additional constraints (third task) is not desirable.

In general, $S_{\bar{J}} < S_J$, since $S_{\bar{J}}$ represents the restricted manipulability measure that defines the ability of the manipulator to perform the end-effector task, when joint velocities only from the null space of $\tilde{\mathbf{H}}_c$ are used. Although likely, it is not necessary that $S_{\bar{J}}$ becomes smaller when the dimension of $(\mathbf{E} - \tilde{\mathbf{H}}_c^+ \tilde{\mathbf{H}}_c)$ decreases. However, from (3.32) it can be directly observed that in the case when $(\mathbf{E} - \tilde{\mathbf{H}}_c^+ \tilde{\mathbf{H}}_c)$ does not exist $S_{\bar{J}}$ will be equal to zero.

An alternative, and very helpful interpretation of (3.32) can be made. It can be represented as a product of the elements of $\bar{\mathbf{J}}$ obtained by its singular value decomposition $\bar{\mathbf{J}} = \bar{\mathbf{U}} \bar{\Sigma} \bar{\mathbf{V}}^T$, where $\bar{\mathbf{U}} \in R^{m_2^t \times m_2^t}$ and $\bar{\mathbf{V}} \in R^{n \times n}$ with m_2^t being the number of secondary constraints⁹. $\bar{\Sigma} = \text{diag}(\sigma_1, \sigma_2, \dots, \sigma_{m_2^t}) \in R^{m_2^t \times n}$ contains the singular values of $\bar{\mathbf{J}}$ ($\sigma_1 \geq \sigma_2 \geq \dots \geq \sigma_{m_2^t} \geq 0$), hence:

$$S_{\bar{J}} = \sqrt{\det [\bar{\mathbf{U}} \bar{\Sigma} \bar{\mathbf{V}}^T \bar{\mathbf{V}} \bar{\Sigma}^T \bar{\mathbf{U}}^T]} \quad (3.33)$$

Taking into account that $\bar{\mathbf{U}}$ and $\bar{\mathbf{V}}$ are orthogonal matrices, the above equation becomes:

$$S_{\bar{J}} = \sqrt{\det [\bar{\Sigma} \bar{\Sigma}^T]} = \prod_{i=1}^{m_2^t} \sigma_i \quad (i = 1, 2, \dots, m_2^t) \quad (3.34)$$

When matrix $\bar{\mathbf{J}}$ loses rank, at least one of its singular values σ_i becomes zero, hence, leading to $S_{\bar{J}} = 0$.

From the discussion above it can be concluded that the inverse of the restricted manipulability measure $S_{\bar{J}}$ has similar properties as the *condition number*¹⁰ of $\bar{\mathbf{J}}$.

The manipulability measure outlined above, relies on the Euclidean metric on R^3 (only the end-effector linear velocity was considered), which is not invariant under change of coordinate frames. As noted in [68] p. 429, care should be exercised when one applies this measure to manipulator design and control (see **Example A.26**). Additional references related to this problem can be found in [132], [102], [33].

⁹In the example considered here, these are the end-effector motions to be controlled.

¹⁰The condition number of a matrix is defined as the ratio between the biggest and smallest singular value ($\sigma_1/\sigma_{m_2^t}$).

Chapter 4

Approaching phase of a satellite capturing operation

In recent years, the capture of a tumbling satellite has been recognized as a priority task. Its solution is expected to be applied to a variety of space missions, involving servicing, inspection, and repairing operations [126], [54], [84], [39], [16], [93]. Furthermore, the removal of space debris from orbit is a mission that should be considered seriously. In order the realization of each task to be possible, a capturing operation should be performed.

There has been a great deal of fundamental research in the area of space robotics (see Chapter 1) and though capturing a tumbling object in space is a well known problem, it is difficult to distinguish one of the solutions proposed up to now, which can solve it readily. Discussing the whole process from the trajectory planning to the post-impact control is an arduous task. The nature of the problems occurring in the different phases of the capture can be completely different, so most of the researchers tend to separate the operation into closing in maneuver, approach¹, impact and post-impact motion (Fig. 4.1).

In this chapter, the approaching motion of a space manipulator to a target satellite is discussed. It is assumed that the *closing in maneuver* of the chaser spacecraft has already finished and the target object is within the reachable space of the robotic arm. Solutions to typical problems that can occur during this phase are studied. The application of a strategy based on momentum redistribution is introduced. It will be shown that its utilization is beneficial from the viewpoint of trajectory planning when constraints on the base attitude motion are imposed. Furthermore, in Chapter 5 the effects of the above mentioned strategy over the post-impact motion of the system are discussed.

The outline of this chapter is as follows: Problem definition and assumptions are presented in Section 4.1. The treatment of the fundamental concept of reactionless manipulation outlined in the previous chapter will be extended here.

¹Here, with *approach*, the approaching motion of a manipulator arm to a target object is implied.

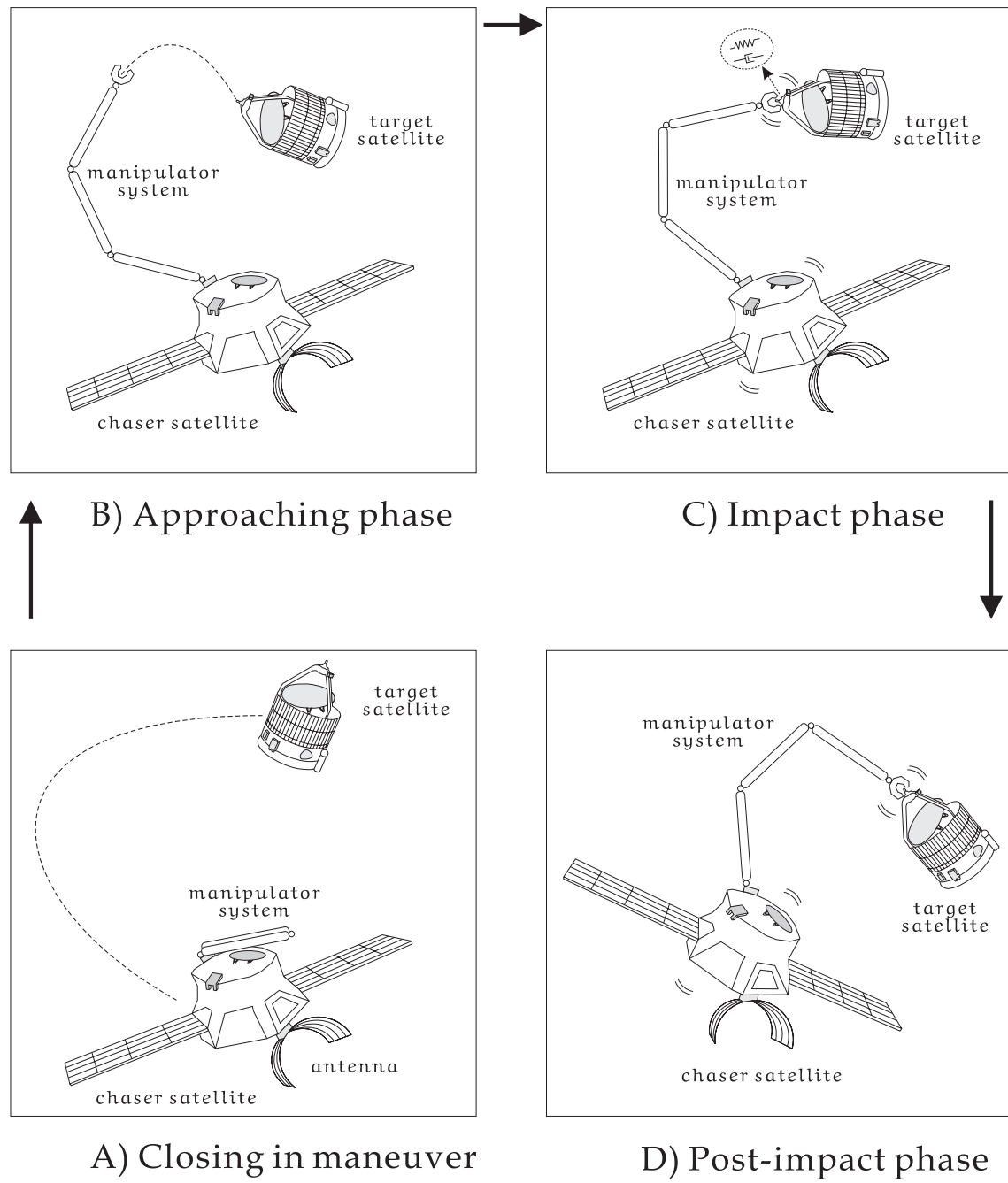


Figure 4.1: Four phases of a capturing operation. During the *closing in phase*, the chaser spacecraft performs an orbital maneuver to the target satellite (this maneuver can be referred to as approach, nevertheless, we want to make a clear distinction between global motion of the spacecraft, and local motion of the manipulator, hence, the term *approach* will be used only regarding the manipulator's motion). During the approach (case **B**), the robot arm follows a predefined trajectory profile and reaches a grasping point positioned on the target satellite. During the *impact phase*, a griper system establishes a firm grip on the grasping facility. The final phase covers the post-impact motion of the system.

Theorem 1 (see Section 3.1) will be reformulated for the case when external disturbances act on the system. This new formulation (referred to as the *coupling wrench theorem*), proves to be useful for all phases of the capturing operation. Preliminaries and basic equations to be used are summarized in Section 4.3, where a reduced form of the equation of motion is derived.

In Section 4.4, a discussion regarding the manipulator approaching motion to a non-tumbling satellite is made. Considering such *stationary* case, gives additional insight on the satellite capturing problem, as will become apparent in the sequel. In Section 4.4.2 the *holonomic distribution control* is introduced, and the problem of planning a reactionless end-effector path to a desired point in Cartesian space is studied.

In Section 4.5 a discussion regarding the manipulator approaching motion to a tumbling satellite is made. The *bias momentum approach* (BMA) is introduced in Section 4.5.1. Different pre-impact momentum distributions are compared, and angular momentum redistribution strategy is developed. The trajectory planning problem when BMA is utilized, is address in Section 4.5.2. A two step planning procedure and different ways for its implementation are discussed. Mission scenario, and results from numerical simulations that verify the usefulness of the proposed strategies are in Section 4.5.4.

4.1 Problem definition and assumptions

As mentioned at the beginning of this chapter, the problems occurring in the four phases of a capturing operation are different. Solutions that look useful when applied for overcoming a specific difficulty during the approach however, might turn out to be a burden for the stages to come. That is why the usefulness of the strategies to be proposed hereafter is assessed from the viewpoint of the entire capturing operation. The aim of the study in this chapter is threefold;

- (1) to provide further insight into the problems occurring while capturing a tumbling satellite;
- (2) to utilize the *holonomic distribution control* for planning reactionless end-effector paths to a desired position in Cartesian space;
- (3) to propose a strategy using bias angular momentum that can facilitate the trajectory planning and post-impact motion control.

More specifically, the main focus is on finding such motion profile for the manipulator arm (during the approach) that minimizes the reactions transferred to the chaser's satellite base, before and after the contact with the target. The assumptions made can be outlined as follows.

Assumptions:

In this study, a robotic manipulator mounted on a chaser satellite is assumed to capture a target object. We assume that;

- a₁) the target undergoes constant linear and angular motion and its angular momentum is known in advance (precise estimation is not necessary) [59], [61], [35], [47];
- a₂) there are no external forces acting on the entire system (chaser plus target). No gas-jet thrusters are used on the chaser's base². For attitude stabilization only reaction wheels are utilized;
- a₃) there is no relative linear motion between the mass centroids of the chaser and target;
- a₄) the inertial frame Σ_i is fixed in the center of mass of the entire system;
- a₅) the manipulator is redundant with respect to the base angular motion task;
- a₆) the capturing operation is successfully completed when the angular momentum from the target is transferred in the reaction wheels on the chaser satellite.

4.2 The coupling wrench theorem

In Section 3.1 an overview of the already introduced [81] concept of *coupling momentum*, and its utilization for reactionless manipulation was made. The discussion however, was restricted only to the case when the momentum of the system is constant, hence, the external disturbances acting on the system are zero. Such assumption, although valid in many cases, cannot be made when a contact with a tumbling target satellite is to be performed. In this section a generalization of *Theorem 1* (see Section 3.1) will be proposed.

Coupling wrench theorem:

The stationary state of the base will be maintained if and only if the coupling wrench $\mathcal{F}_c(t) = \frac{d}{dt}\mathcal{L}(t)$ is equal to the sum of all external wrenches projected along the coordinates of the base at time t , for all t .

If $\mathcal{F}_b^\Sigma(t)$ is the sum of all external wrenches projected along the coordinates of the base at time t , the *coupling wrench theorem* (CWT) states that $\mathcal{F}_c(t) = \mathcal{F}_b^\Sigma(t)$, for all t . It can be seen that CWT does not contradict with *Theorem 1*, since when no external forces act on the system $\frac{d}{dt}\mathcal{L}(t) = 0 \Rightarrow \mathcal{L} = \text{const.}$

Proof:

²An exception is made in Section 5.3.1 where for the sake of comparison a case when gas/jet thrusters are used, is included.

The validity of the above theorem follows directly from the upper part of equation (3.1), when the base velocities $\dot{\mathbf{x}}_b$ and accelerations $\ddot{\mathbf{x}}_b$ are set equal to zero. Let us rewrite the right hand side of (3.1) in the following way:

$$\begin{bmatrix} {}^b\mathbf{J}_b & {}^b\mathbf{J}_m \\ \mathbf{J}_b & \mathbf{J}_m \end{bmatrix}^T \begin{bmatrix} \mathbf{Q}_{ex}^b \\ \mathbf{Q}_{ex}^m \end{bmatrix} \quad (4.1)$$

where the expression for \mathbf{R}^o follows from equation (2.30), and the column vector of external wrenches \mathbf{Q}_{ex} , is divided into wrenches acting on the base (\mathbf{Q}_{ex}^b) and on the links of the manipulator arm (\mathbf{Q}_{ex}^m). Next, combining the upper part of equations (4.1) and (3.1) leads to:

$$\mathbf{H}_b \ddot{\mathbf{x}}_b + \mathbf{H}_c \ddot{\phi} + \dot{\mathbf{H}}_b \dot{\mathbf{x}}_b + \dot{\mathbf{H}}_c \dot{\phi} = \mathbf{Q}_{ex}^b + \mathbf{J}_b^T \mathbf{Q}_{ex}^m \quad (4.2)$$

where the nonlinear term $\mathbf{c}_b = \dot{\mathbf{H}}_b \dot{\mathbf{x}}_b + \dot{\mathbf{H}}_c \dot{\phi}$, and ${}^b\mathbf{J}_b$ is a unit matrix was used. Setting the base velocities $\dot{\mathbf{x}}_b$ and accelerations $\ddot{\mathbf{x}}_b$ equal to zero, and adopting $\mathcal{F}_b^\Sigma = \mathbf{Q}_{ex}^b + \mathbf{J}_b^T \mathbf{Q}_{ex}^m$ leads to:

$$\frac{d}{dt} \mathcal{L} = \mathcal{F}_b^\Sigma \quad (4.3)$$

where equation (3.6) was used.

□

Corollary:

The *coupling wrench theorem* establishes a clear condition which if satisfied, the stationary state of the base will be maintained in the presence of external forces/torques. In theory, evaluation of the magnitude and direction of the external disturbances is possible, however, in practice such measurements can contain high level of noise, hence, direct implementation of equation (4.3) might be difficult.

Proposition 1: If the change of the *coupling momentum* (\mathcal{L}) is equal to the momentum change of the system, then the base stationary state will be maintained.

Proof: The proof follows directly from equation (4.3).

□

Through the rest of this chapter, as well as in Chapter 5, *Proposition 1* will be used extensively. It appears to be useful both for the approach and post-impact motion control of the system, as it will become apparent in the sequel.

4.3 Reduced form of the equations of motion

The dynamical equations governing the motion of a free-flying space robot as a multibody system are in general expressed as in equation (3.1). The formulation is not limited

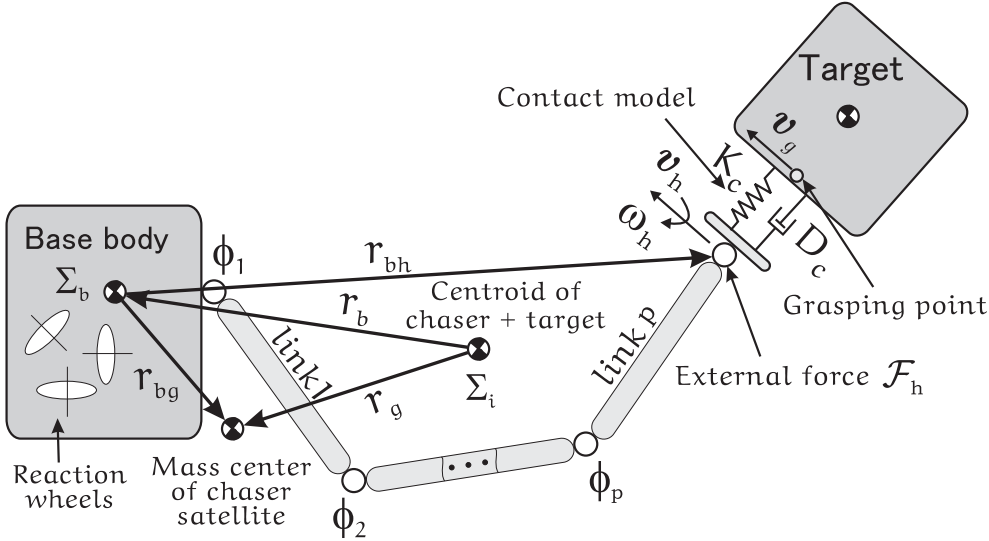


Figure 4.2: Model of a n DOF space robot capturing a target.

to a single manipulator arm, and for the derivations in this chapter we assume a serial manipulator with p degrees of freedom (DOF), in combination with a system of three reaction wheels (RW), mounted on a base body as shown in Fig. 4.2 ($n = p + 3$). Points of interest are Σ_i and Σ_b , which represent the origin of the inertial frame and the frame fixed in the base centroid, respectively.

During the impact and post-impact phases of a capturing operation, momentum is “exchanged” between the chaser and a tumbling target satellite. Especially, the angular component of this momentum can be quite harmful. For a satellite-based chaser system, it can lead to attitude destabilization. When the robot is mounted on a flexible supporting structure, high amplitude vibrations will be induced. On the other hand, linear momentum (if it exists) can be compensated by external forces only, therefore it will not be discussed here. Taking into consideration that at the beginning of the approaching phase there is no relative linear velocity between the centroids of the chaser and target satellites (as assumed in Section 4.1), (3.1) can be reformulated with respect to the base attitude only. Eliminating the linear base acceleration from the upper part of (3.1), results in a system of equations where $\dot{\mathbf{v}}_b$ ³ is implicitly accounted for.

$$\begin{bmatrix} \tilde{\mathbf{H}}_b & \tilde{\mathbf{H}}_{bm} & \tilde{\mathbf{H}}_{br} \\ \tilde{\mathbf{H}}_{bm}^T & \tilde{\mathbf{H}}_m & \mathbf{0} \\ \tilde{\mathbf{H}}_{br}^T & \mathbf{0} & \tilde{\mathbf{H}}_r \end{bmatrix} \begin{bmatrix} \dot{\boldsymbol{\omega}}_b \\ \ddot{\boldsymbol{\phi}}_m \\ \ddot{\boldsymbol{\phi}}_r \end{bmatrix} + \begin{bmatrix} \tilde{\mathbf{c}}_b \\ \tilde{\mathbf{c}}_m \\ \tilde{\mathbf{c}}_r \end{bmatrix} = \begin{bmatrix} \mathbf{0} \\ \boldsymbol{\tau}_m \\ \boldsymbol{\tau}_r \end{bmatrix} + \begin{bmatrix} \tilde{\mathbf{J}}_{bh}^T \\ \tilde{\mathbf{J}}_{mh}^T \\ \tilde{\mathbf{J}}_{rh}^T \end{bmatrix} \mathcal{F}_h \quad (4.4)$$

where sub-indices m and r denote variables of the manipulator and reaction wheels, respectively. For simplicity, only external wrenches acting at the tip of the end-effector

³Hereafter, for convenience, variables that describe the base body will be denoted by subscript b (for the derivations in Chapter 2, subscript 0 was used).

(\mathcal{F}_h) are considered. $\tilde{\mathbf{J}}_{bh}$, $\tilde{\mathbf{J}}_{mh}$ and $\tilde{\mathbf{J}}_{rh}$ are Jacobian matrices which, together with the remaining sub-matrices of (4.4) are defined in Appendix E. Note that the coupling inertia matrix $\tilde{\mathbf{H}}_c$ is divided into two parts:

$$\tilde{\mathbf{H}}_c = [\tilde{\mathbf{H}}_{bm} \ \tilde{\mathbf{H}}_{br}] \in R^{3 \times n}$$

where $\tilde{\mathbf{H}}_{bm} \in R^{3 \times p}$ and $\tilde{\mathbf{H}}_{br} \in R^{3 \times 3}$ are the coupling inertia matrices between the base and manipulator, and base and reaction wheels, respectively.

Integrating the upper part of (4.4) yields the angular momentum conservation law:

$$\mathbf{L} = \tilde{\mathbf{H}}_b \boldsymbol{\omega}_b + \tilde{\mathbf{H}}_{bm} \dot{\boldsymbol{\phi}}_m + \tilde{\mathbf{H}}_{br} \dot{\boldsymbol{\phi}}_r + \mathbf{L}_p \quad (4.5)$$

where $\mathbf{L}_p = \hat{\mathbf{r}}_{bg} \mathbf{P} + \mathbf{r}_b \times \mathbf{P} = \mathbf{r}_g \times \mathbf{P}$, with \mathbf{P} representing the linear momentum of the spacecraft, and \mathbf{r}_b is the distance from the inertial coordinate frame (Σ_i) to the base centroid (Fig. 4.2). In equation (4.5) \mathbf{L} is the angular momentum around the origin of Σ_i (see Appendix C). From assumptions **(a2)** and **(a4)** it follows that before the contact, the linear momentum of the two systems with respect to Σ_i will be zero. Each of the three remaining components on the right hand side of (4.5) defines a partial angular momentum of the system. The first term represents the angular momentum of the base body as a result of its attitude change, the second one is related to the manipulator motion and is called the *coupling angular momentum* [83] (between the base and the manipulator). The third term is the angular momentum in the reaction wheels.

$$\mathbf{L}_b = \tilde{\mathbf{H}}_b \boldsymbol{\omega}_b \quad \mathbf{L}_{bm} = \tilde{\mathbf{H}}_{bm} \dot{\boldsymbol{\phi}}_m \quad \mathbf{L}_r = \tilde{\mathbf{H}}_{br} \dot{\boldsymbol{\phi}}_r$$

In Section 3.1, $\mathcal{L} = \mathbf{H}_c \dot{\boldsymbol{\phi}}$ was called the *coupling momentum*. It includes both linear and angular parts (\mathcal{L}^P and \mathcal{L}^L). It should be noted that $\mathcal{L}^L \neq \mathbf{L}_{bm}$ because \mathcal{L}^L is expressed around the base centroid, while \mathbf{L}_{bm} is expressed around the mass center of the chaser system (see Appendix C and the definition of the symbols appearing in equation (C.18)). In the sequel, mostly the *coupling angular momentum* \mathbf{L}_{bm} will be used. Sometimes when it is clear from the context, for simplicity \mathbf{L}_{bm} will be referred to as *coupling momentum*.

By applying internal torques in the manipulator joints and reaction wheels, the three partial angular momenta can change in a desired way. This change is called momentum redistribution. In other words, though the amount of \mathbf{L} present in the chaser system is constant, its distribution over the base, manipulator and reaction wheels can vary. In Section 4.5.1, it will be shown that the momentum distribution before the contact with the target is closely related to the base attitude deviation after the contact. With a proper choice of the three partial angular momenta, one can facilitate the post-impact attitude control. Furthermore, the process of angular momentum redistribution results in manipulator motion, which will be utilized in order to generate a feasible end-effector approaching trajectory in Section 4.5.2.

4.4 Approaching maneuver to a stationary target satellite

In this chapter, the approaching motion of a space manipulator to a stationary target satellite is discussed. With *stationary* it is implied that the target does not undergo rotational motion. From assumption *a₃* made in Section 4.1 it follows that, from the viewpoint of the chaser satellite, the grasping point appears to be stationary. Furthermore, it is assumed that the *closing in maneuver* has already finished, and the target object is within the reachable space of the robotic arm.

In the case of a *stationary* target, the capturing problem reduces to planning an approaching path for the end-effector to a given grasping point (on the target satellite) fixed in inertial coordinates. Since the end-effector motion profile can be designed in such a way, that the magnitude of the contact forces during the impact phase are very close to zero [128], the post-impact motion of the system can be assumed negligible. Hence, in this section only the motion of the chaser systems during the approaching phase will be considered. Furthermore, it is assumed that the spacecraft's base is in a free-floating mode, hence, no attitude control is performed.

As already mentioned in Chapter 1, in 1997 the NASDA's ETS VII satellite was successful to demonstrate the rendezvous and docking with a cooperative target [127]. One of the problems encountered was keeping the spacecraft's base attitude profile within predefined limits during the manipulator motion. In order to be able to satisfy this requirement, the motion profile for the robot arm should be designed using the concept of *reactionless manipulation*, introduced in [81]. In this section the main focus will be on determining end-effector Cartesian paths that result in minimal spacecraft's base attitude change.

In Chapter 1 some of the main techniques for path planning applied to space robots have been outlined. This chapter introduces a new such technique (referred to as *holonomic distribution control*) that permits planning of reactionless paths to a desired point in Cartesian space. It has certain similarities with a strategy previously employed for solving the inverse kinematics problem for a redundant manipulator arm, by partitioning the Jacobian matrix into *full rank* minors [36]. The resemblance is in light of the fact that, a decomposition in joint space which leads to certain advantages from the viewpoint of planning and control is made. The main differences are; (i) we consider the system's dynamical characteristics as well; (ii) the joint space is decomposed into sets with redundancy *one* with respect to the base angular motion; (iii) the application considered is reactionless path planning, hence the nature of the problems that need to be dealt with is different. Some of them are related to the fact that a free-floating manipulator is a system under nonholonomic constraints; (iv) for the implementation of our approach a

mesh adaptive direct search algorithm is utilized.

Next, a brief discussion on the types of constraints that need to be dealt with, and a short overview of some basic concepts from differential geometry that are needed for the formulation of the *holonomic distribution control*, are made.

4.4.1 Pfaffian constraints

In this subsection, a brief treatment of two types of Pfaffian constraints (integrable and nonintegrable) is made. Both appear typically when free-floating systems are studied. It is assumed that the system of interest is *drift free*, in other words the angular momentum is equal to zero (under the present assumptions this condition is satisfied during the approaching motion).

In Section 2.2, for the formulation of the dynamical equations of a free-floating manipulator system, a set of holonomic (*scleronomous*) constraints were used. They were defined using a set of algebraic functions in the following form:

$$h_i(\mathbf{q}) = 0, \quad i = 1, \dots, m^t \quad (4.6)$$

where $\mathbf{q} \in R^n$ is a vector that uniquely represents the configuration of the system of interest. After the constraints in (4.6) are imposed, the motion of the system evolves on a $f^r = n - m^t$ dimensional manifold (for a definition of *manifold* see [58] p. 132, [68] p. 403). As it was noted in Section 2.2, the solution to the equations of motion with constraints can be facilitated if the constraints are represented at velocity or acceleration level (see equations (2.3), (2.4)). Such transition is straightforward and most importantly, reversible ([68] p. 318). Let us write this in the following fashion:

$$h_i(\mathbf{q}) = 0 \quad \Rightarrow \quad \frac{\partial h_i}{\partial \mathbf{q}} \dot{\mathbf{q}} = \nu_i(\mathbf{q}) \dot{\mathbf{q}} = 0 \quad \Rightarrow \quad h_i(\mathbf{q}) = 0 \quad (4.7)$$

The set of equations:

$$\nu_i(\mathbf{q}) \dot{\mathbf{q}} = 0 \quad (4.8)$$

are called Pfaffian constraints. A set of Pfaffian constraints is said to be integrable, if it is equivalent to a set of algebraic constraints. With *equivalent*, it is implied that the Pfaffian constraints span the same smooth hypersurface in configuration space as the set of algebraic constraints. It is customary to refer to integrable Pfaffian constraints as holonomic, although they are expressed at velocity level, while holonomic constraints are defined by a set of algebraic functions.

In many cases, the formulation of the constraint equations can be done directly (only) at velocity level, hence, forming a set of Pfaffian constraint. This was done in Section

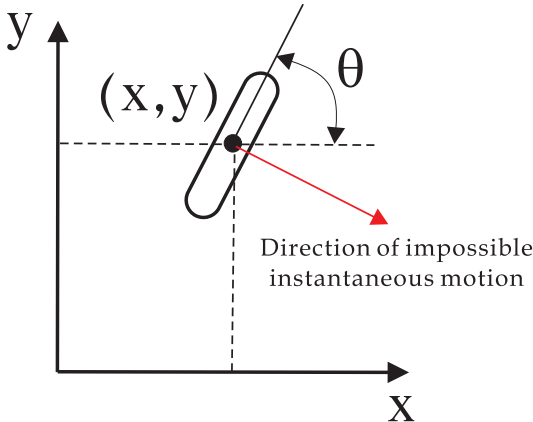


Figure 4.3: Unicycle constraints.

3.1, where the structure of the *coupling momentum* \mathcal{L} [83] was derived. When $\nu_i(\mathbf{q})_i$ is not defined as the differential of an algebraic function, determining whether the resulting constraint is holonomic is not straightforward [68], [57], [102]. A single constraint of the form in equation (4.8) is said to be *nonholonomic* if it is nonintegrable, hence, it is not equivalent to an algebraic function (defining a holonomic constraint). Perhaps, the simplest example demonstrating a system under nonholonomic constraint is the unicycle.

Unicycle example:

The unicycle in Fig. 4.3 is characterized by the (x, y) position of its center point (denoted by a dot), and by the angle θ between the x axis and the axis of the unicycle. Let us assume that the unicycle cannot move sideways. In Fig. 4.3 a red line depicts the direction of impossible instantaneous motion. The corresponding constraint can be defined as follows:

$$[\sin(\theta), -\cos(\theta), 0] \begin{bmatrix} \dot{x} \\ \dot{y} \\ \dot{\theta} \end{bmatrix} = 0 \quad (4.9)$$

Since the unicycle can have an arbitrary configuration with the same velocity $\dot{\mathbf{q}}$, the above constraint cannot be integrated analytically to yield the (x, y) position and angle θ . Equation (4.9) is a typical example of a nonintegrable Pfaffian constraint. It should be noted that a nonholonomic constraint does not limit the configuration space of the system, but only imposes a *local* velocity restriction. Evidently, the unicycle can reach any point in the plane with arbitrary orientation θ .

□

Discussing integrability in the presence of multiple Pfaffian constraints becomes much more involved. The reason comes from the fact that, even if each of the m^t constraints in (4.8) is nonintegrable, the combination of two or more of them might lead to an integrable (holonomic) set of constraints. This fact will be fully utilized in the *holonomic distribution control* that will be introduced in the next section.

In many cases, it is convenient to convert a given problem with nonholonomic constraints in another form. By examining the system not from the viewpoint of the *directions of impossible instantaneous motion*, but rather from the viewpoint of the directions in which we are free to move, in other words the *space of allowable motions*. In Section 2.2 a detailed analysis on the usage of the *space of allowable motions* for the definition of the system dynamics was made. In addition, in Section 3.1 we used the term *subspace of reactionless motions*, which represented manipulator motions that result in zero reaction forces transmitted to the base spacecraft. Following the derivation made in Section 2.2, we choose a basis for the right null space (to be denoted by $g_j(\mathbf{q})$) of the constraints in (4.8), which satisfies the following relation:

$$\nu_i(\mathbf{q})g_j(\mathbf{q}) = 0, \quad i = 1, \dots, m^t, \quad j = 1, \dots, n - m^t \quad (4.10)$$

Hence, the subspace of allowable motions can be written as:

$$\dot{\mathbf{q}} = g_1(\mathbf{q})u_1 + g_2(\mathbf{q})u_2 + \dots + g_{f^r}(\mathbf{q})u_{f^r} \quad (4.11)$$

where $f^r = n - m^t$ can be interpreted as the degree of redundancy of a system with n DOF, and m^t applied task constraints. The column vector $\mathbf{u} \in R^{f^r}$ (containing all the u 's) represents the control input of the system in (4.11).

The application of the above approach to the unicycle example is straightforward.

Unicycle example (continued a):

The *space of allowable motions* for the unicycle characterized by equation (4.9) can be expressed as follows:

$$g_1(\mathbf{q}) = \begin{bmatrix} 0 \\ 0 \\ 1 \end{bmatrix} \quad g_2(\mathbf{q}) = \begin{bmatrix} \cos(\theta) \\ \sin(\theta) \\ 0 \end{bmatrix} \quad (4.12)$$

It should be noted that although the unicycle can reach every configuration (x, y, θ) , the dimension of the *space of allowable motions* is two, because at a given instant only two system motions are allowed: (i) change of the angle θ , and (ii) translation along the unicycle axis. □

At the end of this subsection, it is convenient to adopt some notation from differential geometry, which will be used in Section 4.4.2. The following definitions are adopted from [68].

Definition 1: A *vector field* on R^n is a smooth map which assigns to each point $\mathbf{q} \in R^n$ a tangent vector $\dot{\mathbf{q}} \in T_q R^n$. Where $T_q R^n$ stands for the *tangent space* to point \mathbf{q} .

Definition 2: A *distribution*⁴ is a smooth map assigning a linear subspace of $T_q R^n$ to each configuration $\mathbf{q} \in R^n$.

⁴The term “distribution” defined here is different from the term “distribution” used through the thesis, where the latter one is used to express mainly an angular momentum distribution.

Example for a *distribution* is the linear span of the *vector fields* $g_1(\mathbf{q})$ and $g_2(\mathbf{q})$ in the unicycle example above. In general we will denote a *distribution* as:

$$\Delta = \text{span}\{g_1(\mathbf{q}), \dots, g_{f^r}(\mathbf{q})\} \quad (4.13)$$

Evaluated at any point $\mathbf{q} \in R^n$ the *distribution* defines a linear subspace of the tangent space $T_q R^n$:

$$\Delta_q = \text{span}\{g_1(\mathbf{q}), \dots, g_{f^r}(\mathbf{q})\} \subset T_q R^n \quad (4.14)$$

Definition 3: A *distribution* Δ is said to be *regular* if the dimension of Δ_q does not vary with \mathbf{q} .

Definition 4: A *distribution* is *involutive* if it is closed under the *Lie bracket*.

The *Lie bracket* between two *vector fields* a and b on R^n is a new *vector field*, denoted by $[a, b]$, defined by:

$$[a, b](\mathbf{q}) = \frac{\partial b}{\partial \mathbf{q}} a(\mathbf{q}) - \frac{\partial a}{\partial \mathbf{q}} b(\mathbf{q}) \quad (4.15)$$

Lie bracket satisfies (i) Skew-symmetry, (ii) Jacobi identity, (iii) Chain rule [68] p. 325. Hence, it can be concluded that *Lie bracket* on R^3 coincides with the vector cross product.

Unicycle example (continued b):

For the unicycle in Fig. 4.3, the *distribution* Δ is obviously *regular*, since at each configuration \mathbf{q} , $\Delta_q = 2$ (note that in equation (4.12), $g_1(\mathbf{q})$ and $g_2(\mathbf{q})$ are decoupled).

The *distribution*, is not *involutive*, since if it were, according to Frobenius' theorem (*A regular distribution is integrable if and only if it is involutive*) it should be concluded that the constraints are integrable (which is not the case). Even though for that simple example it was possible to determine the nonintegrability only by inspection, it is worth confirming it using *Definition 4* as well.

Computing the Lie bracket of $g_1(\mathbf{q})$ and $g_2(\mathbf{q})$ (see equation (4.12)), using (4.15) leads to:

$$\frac{\partial g_1(\mathbf{q})}{\partial \mathbf{q}} g_2(\mathbf{q}) = \begin{bmatrix} 0 & 0 & 0 \\ 0 & 0 & 0 \\ 0 & 0 & 0 \end{bmatrix} \begin{bmatrix} \cos(\theta) \\ \sin(\theta) \\ 0 \end{bmatrix}; \quad \frac{\partial g_2(\mathbf{q})}{\partial \mathbf{q}} g_1(\mathbf{q}) = \begin{bmatrix} 0 & 0 & -\sin(\theta) \\ 0 & 0 & \cos(\theta) \\ 0 & 0 & 0 \end{bmatrix} \begin{bmatrix} 0 \\ 0 \\ 1 \end{bmatrix}$$

$$g_3 = [g_1, g_2] = \begin{bmatrix} -\sin(\theta) \\ \cos(\theta) \\ 0 \end{bmatrix}$$

The *vector field* g_3 is linearly independent of g_1 and g_2 , and violates the constraint (4.9). Hence, it can be concluded that the *distribution* Δ is not *involutive*. This confirms that (4.9) is a nonholonomic constraint. Similar approach can be used in order to discuss holonomy and nonholonomy of free-floating space systems [73].

□

4.4.2 Holonomic Distribution Control

Reactionless motion of a manipulator system in combination with achieving a desired motion profile of the end-effector can be performed by using the task priority approach outlined in Section 3.2. In order for both tasks to be successfully carried out without occurrence of *algorithmic singularities*, the parameter $\dot{\xi}$ in equation (3.28) has to be defined properly. Specifying $\dot{\xi}$ in a way that satisfies given path constraints is not a trivial problem, however. Using optimization techniques for the direct determination of $\dot{\xi}$ is very much dependent on the initial-guess specified, and yields satisfactory results only in limited number of cases. In this study we propose the *holonomic distribution control* (HDC) in order to simplify the path planning problem. Its main concept is outlined hereafter.

The HDC is defined to be a control in the form of equation (4.11), that utilizes a one dimensional *distribution* $\Delta^1 \subset \Delta$. The dimension of the *distribution* Δ coincides with the degree of redundancy of the system, which is $f^r = n - m^b$, where n is determined by the manipulator joint variables (the system of interest is assumed to be in a free-floating mode), and m^b represents the base task constraints. The reasoning for using only one dimensional *distribution* is based on the fact that, in any configuration \mathbf{q} , the solutions which lead to reactionless manipulation evolve from a one dimensional manifold. By using Lie bracket on the columns of the reaction null space of the coupling inertia matrix $\tilde{\mathbf{H}}_{bm}$ (which span the *distribution* Δ), an *involutivity* of Δ^1 can be established [83]. In addition, if the coupling inertia matrix does not loose rank, the *distribution* Δ (and hence $\Delta^1 \subset \Delta$) can be shown to be *regular*. Once *involutivity* of a *regular distribution* Δ^1 is established, its integrability follows directly from the Frobenius' theorem.

By choosing different combinations of *vector fields* (members of Δ) in order to form distinct one dimensional *distributions* Δ^1 , the motion of the system can be steered in different directions. Furthermore, the constraints corresponding to Δ^1 are holonomic, hence, each of the instantaneously available motion directions, lie on a smooth one dimensional manifold in joint space. Such approach can facilitate the planning problem as will be shown in the sequel.

Remark:

Above, an assumption that the coupling inertia matrix does not loose rank was made. This assumption can be shown to be always valid, if the system of interest has *strong inertial coupling* [108], [65].

One way of defining distinct one dimensional *distributions*, is to partition the manipulator joint variables into a number of sets, referred to as *primitives*. Each *primitive* consists of $m^b + 1$ joint variables (m^b is the number of base rotational motions to be controlled). For example, if a three DOF planar manipulator mounted on a free-floating base is considered, its *primitives* can be defined as depicted in Fig. 4.4. Since $m^b = 1$, each *primitive* consists

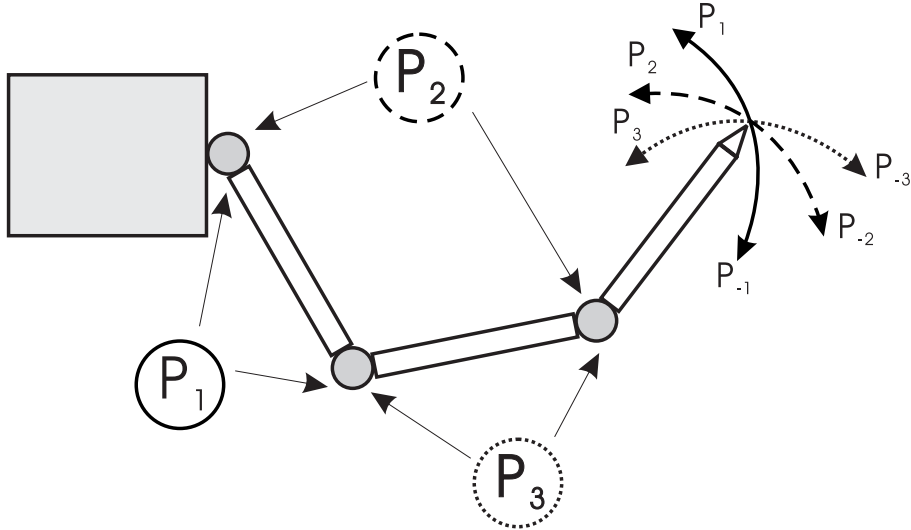


Figure 4.4: Cartesian paths when using different *primitives* for a three DOF planar manipulator mounted on a free-floating base.

of only two joints. For example, primitive 1 is formed by joints 1 and 2. Let us assume that for a time period $t + \Delta t$ just one *primitive* is actuated and the remaining joints are servo locked. Hence, at a given time t each *primitive* defines a direction for the reactionless end-effector motion in Cartesian space⁵ (Fig. 4.4). It is clear that these directions are just a subspace of the possible end-effector reactionless motions from a given manipulator configuration. Nevertheless, the decomposition utilized here facilitates the path planning problem, because manipulator motion derived from one dimensional null space of the coupling inertia matrix $\tilde{\mathbf{H}}_{bm}$, results in a curve in Cartesian and joint space (not a surface). Hence, at each manipulator configuration the end-effector motion resulting from a given *primitive* is unique⁶. Using HDC regarding systems in three dimensional space is possible. In the case of a 3D five DOF manipulator for example, when $m^b = 3$ five *primitives* exist (each of them consists of four joint variables). In the case of a six DOF manipulator the *primitives* are fifteen.

Once a *primitive* is chosen the joint space is separated into actuated (ϕ^a) and stationary (ϕ^s) joints.

$$\begin{bmatrix} \tilde{\mathbf{H}}_{bm}^s & \tilde{\mathbf{H}}_{bm}^a \end{bmatrix} \begin{bmatrix} \dot{\phi}^s \\ \dot{\phi}^a \end{bmatrix} = 0 \quad (4.16)$$

Hence, the motion rate of ϕ^a can be calculated as follows:

$$\dot{\phi}^a = -\tilde{\mathbf{H}}_{bm}^{a+}\tilde{\mathbf{H}}_{bm}^s\dot{\phi}^s + (\mathbf{E} - \tilde{\mathbf{H}}_{bm}^{a+}\tilde{\mathbf{H}}_{bm}^a)\dot{\xi}^a \quad (4.17)$$

⁵For the example discussed above there will be six such directions.

⁶In the case when the manipulator motion is derived using a *distribution* with two or higher dimensions, the reactionless paths lie on a two or higher dimensional surface. Choosing a direction on this surface is not a trivial problem, and that is precisely what we want to avoid.

If $\dot{\phi}^s = 0$ is assumed, the above equation becomes:

$$\dot{\phi}^a = (\mathbf{E} - \tilde{\mathbf{H}}_{bm}^{a+} \tilde{\mathbf{H}}_{bm}^a) \dot{\xi}^a \quad (4.18)$$

where $(\mathbf{E} - \tilde{\mathbf{H}}_{bm}^{a+} \tilde{\mathbf{H}}_{bm}^a)$ represents the null space of the coupling inertia matrix $(\tilde{\mathbf{H}}_{bm}^a)$ corresponding to the actuated joints, and $\dot{\xi}^a \in R^{(m^b+1)}$ is an arbitrary column vector. It should be noted that, end-effector paths resulting from joint velocities calculated from (4.18) does not depend on the magnitude of $\dot{\xi}^a$ (assuming that it is not equal to zero). The reasoning for this comes from the fact that the null space of $\tilde{\mathbf{H}}_{bm}^a$ is one dimensional. Hence, $\dot{\xi}^a$ can influence only the end-effector velocity on a given path. Since trajectory planning is not the issue here, $\dot{\xi}^a$ will be considered to be with constant magnitude. Nevertheless, its sign can determine the direction of motion and needs to be accounted for.

Using the fact that the Cartesian paths are independent from the magnitude of $\dot{\xi}^a$, the path planning problem reduces to finding a sequence of *primitives*, in combination with durations Δt for the actuation of each *primitive*. A way to determine them will be discussed in the following section.

4.4.3 Application of the Holonomic Distribution Control

The problem of finding feasible sequence of *primitives* and times for their actuation that satisfy given path constraints is essential for the successful planning. For simplicity, hereafter only one path constraint will be considered, namely a desired final position for the end-effector. Furthermore, it is assumed that the initial manipulator configuration is known. In this section the reactionless path planning is defined as an optimization problem. The state variables are chosen to be a sequence of h *primitives* $P = [P_i^1, P_i^2, P_i^3, \dots, P_i^h]$, and the time for actuation of each of them $T = [\Delta t^1, \Delta t^2, \Delta t^3, \dots, \Delta t^h]$, where $i = 0, \pm 1, \pm 2, \dots, \pm z$. Note that P_z stands for the last available *primitive* (z), and P_{-z} accounts for the motion in the *opposite* direction⁷. Choosing P_0 will result in a stationary system. It is not necessary to include all *primitives*, in some cases for example, the motion in the *opposite* direction will clearly be unnecessary, hence, it could be disregarded in order to facilitate the optimization solver.

Apart from the already mentioned path constraint (final position of the end-effector), the solution to the optimization problem should satisfy the following geometric condition:

$$\phi^{min} \leq \phi \leq \phi^{max} \quad (4.19)$$

It should be noted that, constraints for the base attitude are not necessary since the manipulator motion is derived from equation (4.18).

⁷For the case of the three DOF manipulator in Fig. 4.4 $i = 0, \pm 1, \pm 2, \pm 3$.

Judging from the state variables (T and P) and constraints defined above, the problem that has to be solved is a typical nonlinear mixed-variables optimization problem. T represent h *continuous* variables, and P represents h *categorical* variables⁸.

Solution of a mixed-variables problem can be found using different techniques, here a *mesh adaptive direct search* (MADS) algorithm is utilized. It is very similar to *generalized pattern search* algorithm, however, presents some advantages, since the local exploration of the space of variables is not restricted to a finite number of directions (called *poll* directions). For more details see [12], [11].

Calculation of the manipulator motion and constraints can be performed at kinematical level⁹. For given vectors P and T the process can be described as follows:

Step ① Initialize counter $j = 1$, and time $t = 0$.

Step ② At time t from the known positions and velocities of the generalized coordinates of the system (\mathbf{r}_b , \mathbf{v}_b , $\boldsymbol{\phi}$ and $\dot{\boldsymbol{\phi}}$), compute the coupling inertia matrix $\tilde{\mathbf{H}}_{bm}$ (the state variables describing the angular motion of the base are not considered since no attitude change will occur).

Step ③ If $t > \Delta t^j$, increment j with one.

Step ④ Use P^j to derive the motion rates for the actuated joints ($\dot{\boldsymbol{\phi}}^a$) from the null space of $\tilde{\mathbf{H}}_{bm}^a$.

Step ⑤ Knowing $\dot{\boldsymbol{\phi}}$ (note that $\dot{\boldsymbol{\phi}}^s = 0$), find the base linear velocity (\mathbf{v}_b) from the momentum conservation equation (see Appendix C).

Step ⑥ Integrate \mathbf{v}_b and $\dot{\boldsymbol{\phi}}$ to obtain \mathbf{r}_b and $\boldsymbol{\phi}$.

Step ⑦ Increment t with δt (integration step size).

Step ⑧ If $j \leq h$ goto **Step ①**.

When the above calculation is over the optimization procedure can evaluate the difference between the real and desired end-effector position as well as the geometric condition (4.19) and generate new entries for P and T if necessary.

In general, more entries (state variables for the optimization procedure) in P and T result in more precise path planning. The same applies for the number of available *primitives*, since they provide a diversity of the solution at a local level. On the other hand the size of h and z affect the convergence rate of the optimization solver, hence, they should be chosen carefully considering the characteristics of the problem to be solved.

4.4.4 Simulation Study

In this section the results from numerical simulation of a 3 DOF planar manipulator mounted on a free-floating base body are presented. The parameters of the system are in Tab. 4.1. The simulation is performed in Matlab 7.0, and the Matlab toolbox Nomadm

⁸Variables whose values must always come from a predefined list. For example, color, shape, or in the case discussed here, *primitive* number.

⁹Since external forces and torques are assumed equal to zero, computation of the system dynamics is not necessary.

Table 4.1: Model parameters

	Base	Link 1	Link 2	Link 3
m [kg]	40	2	2	2
l [m]	1.0	1.0	1.0	1.0
I [kgm ²]	25	0.5	0.5	0.5

[134], that implements MADS algorithm is used as an optimization solver. The results presented hereafter, demonstrate the ability to generate a reactionless Cartesian path for the end-effector from a given initial manipulator configuration to a desired final position. The initial manipulator configuration is taken to be $\dot{\phi} = [15, 15, -25]$ [deg]. The position of the grasping point of the target satellite in inertial coordinates is assumed to be [1, 1, 0] m. This is taken as a desired end-effector final position. The available *primitives* are chosen to be:

$$i = 0, 1, 2, 3$$

The specified initial guess for the optimization procedure is:

$$P = [0, 0, 0, 0, 0, 0, 0, 0, 0, 0] \quad T = [8, 8, 8, 8, 8, 8, 8, 8, 8] \text{ sec.}$$

The vector $\dot{\xi}^a$ used is $[0, 0.5]^T$, and the joint limitations are $\phi^{min} = -150$ [deg] and $\phi^{max} = 150$ [deg]. The result from the optimization procedure is:

$$P = [1, 2, 3, 1, 2, 1, 1, 2, 3, 0]$$

$$T = [17.47, 12.4, 11.06, 6.27, 4.39, 6.17, 14.07, 3.38, 2.77, 7] \text{ sec.}$$

If the above sequence of *primitives* in P is used, with time durations the entries of T , the manipulator will reach the desired position in Cartesian space. Fig. 4.5 depicts three manipulator configurations (initial, intermediate and final one). It can be observed (Fig. 4.5) that during the motion of the manipulator, the base body undergoes translational motion. This is expected, since only the base attitude was controlled.

The joint angle and joint angular velocity profiles are depicted in Fig. 4.6. They clearly show the switching from one *primitive* to another. The x axis represents the currently used primitive. The nonsmooth profile of the joint velocities is a result of the constant magnitude of the parameter $\dot{\xi}^a$. Such constant magnitude of $\dot{\xi}^a$ was used in order to facilitate the optimization solver. Once a feasible Cartesian path is obtained however, a smooth joint velocity profile can be generated in a straightforward fashion. Hence, the time profile of the end-effector on the reactionless path can be additionally specified.

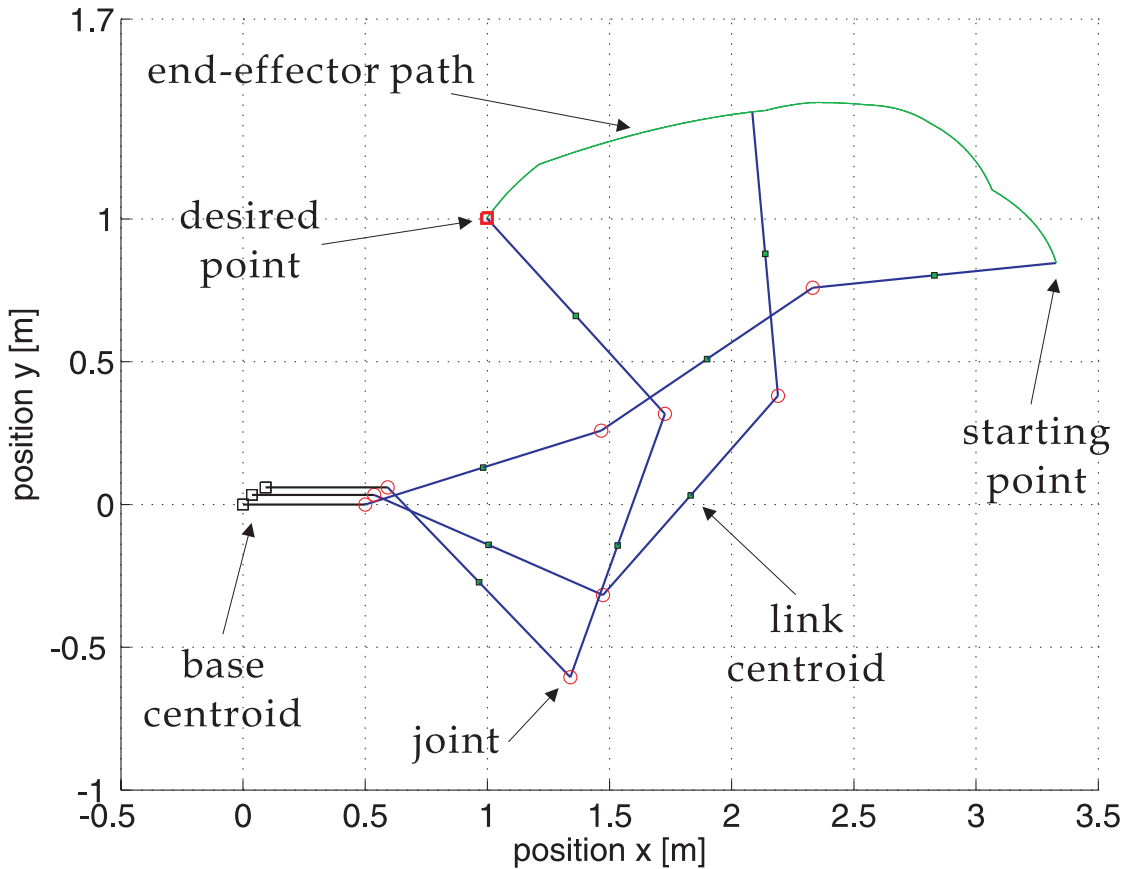


Figure 4.5: End-effector path in Cartesian space. The manipulator configuration is depicted at the initial, intermediate and final positions.

In addition, it should be noted that servo locking the joints not included in the currently used *primitive* is just one possible option. Alternatively using predefined profile for their motion can result in a completely different manipulator behavior. This might prove to be useful in cases when the currently available *primitives* cannot provide a desired manipulator motion.

After obtaining a solution for P and T , the resultant trajectory might be unsatisfactory. In some cases, discontinuities can be observed during transitions between two *primitives*. This fact though unwelcome is by far not unexpected since only a subspace of the space of possible reactionless motions was utilized. Once a feasible path is obtained however, it can be used as an initial-guess for a new optimization procedure, where criteria regarding the smoothness of a given path segment can be included. This new procedure does not need to use *holonomic distribution control*. Once a good initial-guess is available most of the optimization algorithms can converge to satisfactory results.

The merit of the HDC can be found in the fact that it decomposes the entire set of available solutions into small subsets, that can be utilized much easier. If using one

subset does not yield satisfactory results it can be changed, and a different one could be utilized. Finding a solution can not be guaranteed since the nature of the problem is highly non-linear, however, the HDC provides a reasonable simplification for the path planning problem. It is worth mentioning that even though the initial guess specified for the example here was trivial, providing a meaningful one is possible. In some cases, experienced user can use HDC and by try and error, reach an adequate solution.

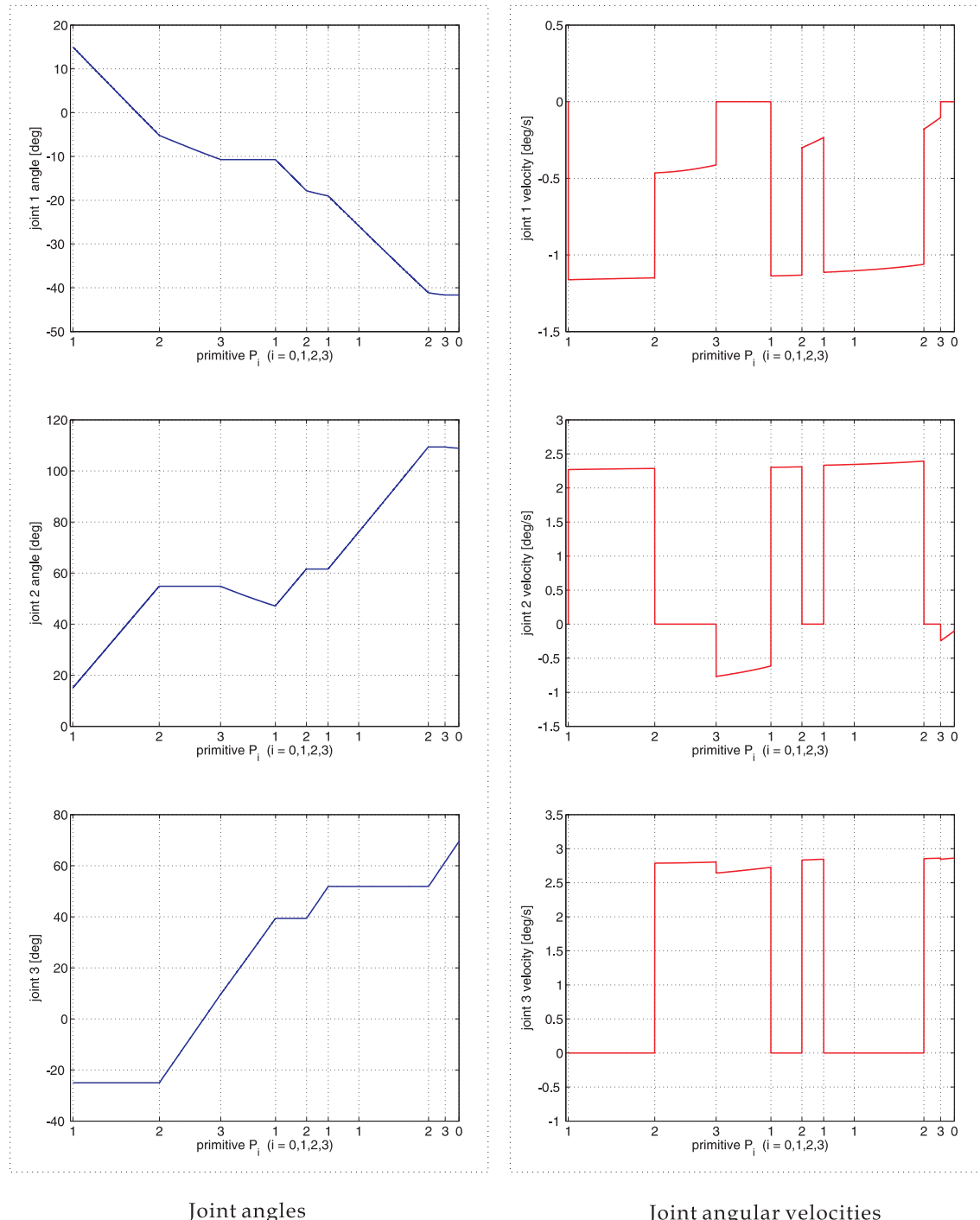


Figure 4.6: Profiles of the joint angles and joint angular velocities.

4.5 Approaching maneuver to a tumbling target satellite

In the previous section, the target satellite was assumed to be stationary as seen from the inertial frame fixed in the center of mass of the entire system (chaser plus target). This assumption simplifies the problem because; (i) estimation of the motion of the grasping point is not necessary; (ii) before the contact between the end-effector and the grasping point, there is sufficient time in order to guarantee a soft contact (using impedance control for example [128]); (iii) if the approaching motion is interrupted as a result of an unexpected problem, the input conditions for the motion planner remain the same, hence, it is easy to restart the approach; (iv) after the contact the motion of the system is negligible, hence, if a problem occurs, the target satellite can be safely released, with no risk for collision with the chaser spacecraft. Furthermore, the utilization of attitude devices (as a result of the capture) is not necessary.

When the assumption of stationary target is dropped, the discussion of the capturing problem becomes involved. As compared to the stationary case; (i) estimation of the motion profile of the grasping point is necessary. When the inertia characteristics of the target are unknown, obtaining a long term estimation is challenging [35], [48], [59], [61], [78]; (ii) the planning algorithm has to design a feasible approaching trajectory, that minimizes the contact forces during the impact-phase, as well as the reactions transferred to the base during the manipulator approaching motion; (iii) if the approach is interrupted, reliable estimation should be performed again; (iv) during the post-impact phase the momentum initially stored in the target satellite, transfers to the chaser and imposes difficulties from the viewpoint of base attitude control. Furthermore, releasing the target satellite leads to collision risks with the manipulator links and spacecraft's base. Management of the momentum of the target has to be performed. If methods for such management are not examined before the approaching motion, the capturing operation could fail. In [64], [131], [52] a strategy for such momentum management based on a *contact/push* based method is proposed. Such strategy is useful when the momentum stored in the target satellite is large, and direct capture is not possible. If *contact/push* based method is used, each contact with the target can be approximated as an impulsive force applied to the end-effector. In such case, planning of pre-impact arm configuration for minimization of the base reactions is advantageous [125], [82], [23], [117], [124]. If however, the manipulator and grasping point (positioned on the tumbling target) are in continuous contact, planning of pre-impact arm configuration has to be replaced with planning of pre-impact momentum distribution [26], [27], as will be discussed in the sequel.

In this section we present a possible solution to some of the difficulties outlined above. As already mentioned at the beginning of this chapter, we focus on minimizing the base

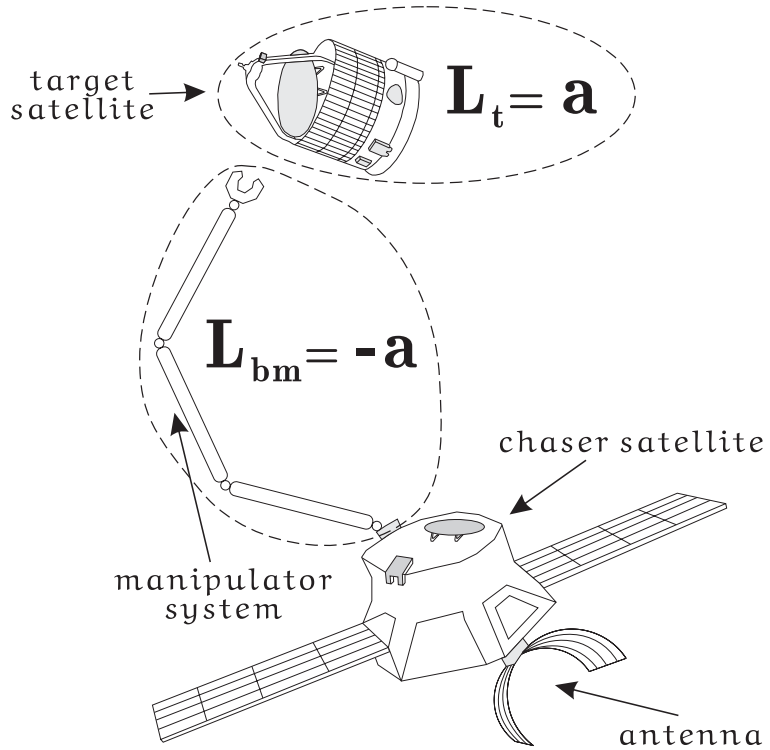


Figure 4.7: Model of a space robot capturing a target, where L_{bm} denotes the coupling angular momentum between the manipulator arm and the base of the chaser satellite, and L_t stands for the angular momentum in the target satellite.

attitude reactions during the approaching and post-impact motion. It should be noted that, although it is tempting to use powerful gas/jet thrusters for this purpose, important insights are obtained from a familiarity with the “external-torque-free” motion of the entire system, before and after the contact with the tumbling target object.

The capturing strategy proposed in Section 4.5.1, is based on obtaining a desired angular momentum distribution in the chaser satellite during the approaching phase in order to facilitate the base attitude control in the post-impact phase. Furthermore, it is shown that this strategy, referred to as the *bias momentum approach* (BMA), can be utilized in order to facilitate the solution of the trajectory planning problem. In Fig. 4.7 is depicted the most favorable case, when the BMA is utilized, namely when the bias momentum preloaded in the manipulator during the approaching motion, is with equal magnitude and opposite direction to the one in the target satellite. Hence, after the capture the manipulator and target will have angular momentum equal to zero. In the case when such favorable distribution cannot be obtained the management of the remaining momentum during the post-impact phase could be carried out using two control laws introduced in Chapter 5. The first one is at acceleration and the second one at velocity level. In both Chapter 5, and the following subsection we make use of the *coupling wrench*

theorem formulated in Section 4.2.

4.5.1 The Bias Momentum Approach

One of the main characteristics of a capturing operation in orbit is the momentum conservation if there are no external forces. If just the chaser or target system is considered, it might undergo momentum change, however, in the entire system the conservation law will hold. Under the present assumptions, during the approaching phase, the angular momentum in the entire system can be sufficiently defined by four variables, namely \mathbf{L}_{bm} , \mathbf{L}_r , \mathbf{L}_b , and the angular momentum of the target satellite \mathbf{L}_t (see Section 4.3). The amount of momentum stored in each of them plays an important role for the successful completion of the capturing operation. The zero attitude change restriction can be expressed as $\mathbf{L}_b = 0$. In Fig. 4.8 four typical distributions (at the start of the post-impact phase) are depicted. Next, a comparison among them will be made. In order to do so, it will be assumed that the manipulator joints are servo locked after the contact with the target, and a simple PD feedback attitude control via reaction wheels is utilized¹⁰.

4.5.1.1 Non-bias distribution

The distribution depicted in Fig. 4.8 **Case A** is with coupling angular momentum equal to zero. This case is referred to as “non-bias”. After the contact, \mathbf{L}_t distributes over the entire system. How fast it will be transferred to the base depends on factors like: pre-impact configuration, force impulse that occurs during the impact phase, post-impact control. In order to keep the base attitude stationary, the attitude stabilization devices¹¹ should work to compensate its deviation. As a result of the maximum torque restriction, the reaction wheels will most likely fail to accommodate the angular momentum transferred to the base in a short time. Hence, base rotational motion will occur.

One way for obtaining a distribution as the one depicted in **Case A** is using *reactionless manipulation* during the approach to the target. Planning of such reactionless trajectory however, is not a trivial problem (for more details see Chapter 4.4). A different way for obtaining $\mathbf{L}_{bm} = 0$ before the contact with the target is by performing momentum redistribution as depicted in Fig. 4.9. At a first step angular momentum with magnitude a is redistributed between the robot arm and reaction wheels. At a second step the initial momentum distribution is obtained. Such manipulation results in change of the arm’s configuration. This is a typical behavior of a system under nonholonomic constraints.

If at the start of the capturing operation angular momentum is already stored in the

¹⁰This is clearly not the best possible control strategy for the post-impact phase, however, it permits easy comparison.

¹¹Note that only reaction wheels are utilized for base attitude control.

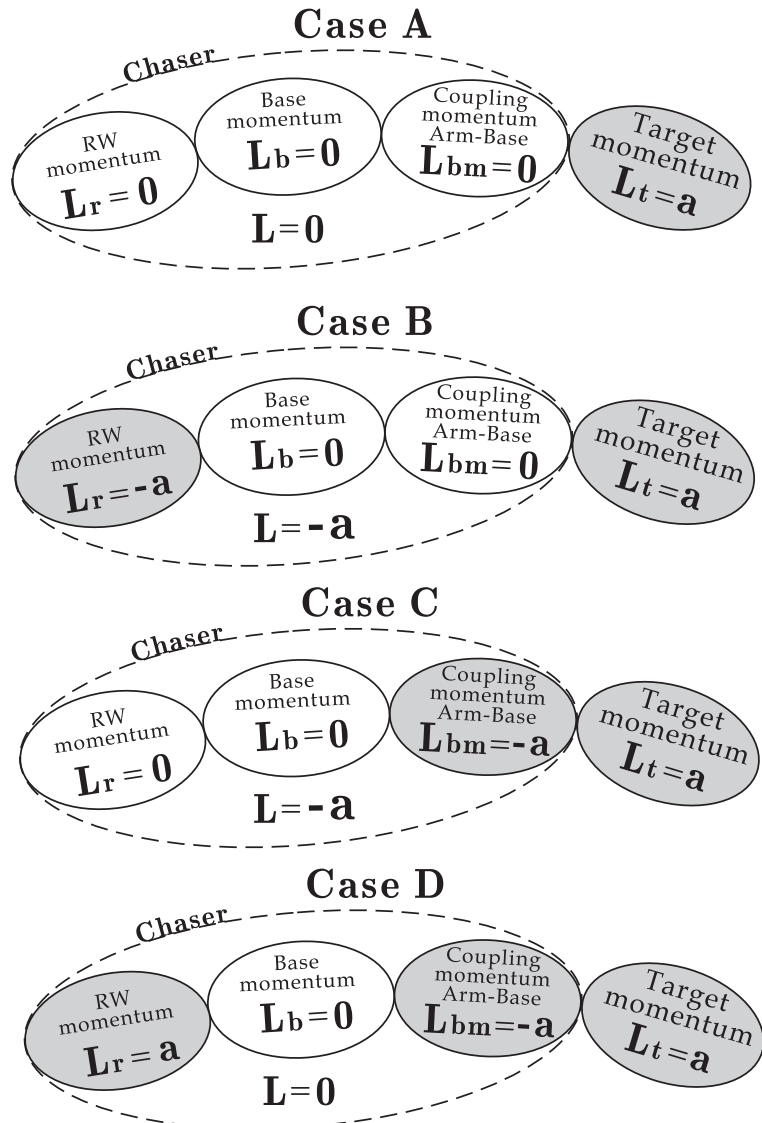


Figure 4.8: Four cases of pre-impact angular momentum distribution.

reaction wheels and it is with equal magnitude and opposite direction to the one in the target, see **Case B**, the momentum of the entire system will be equal to zero, however, the transfer rate of L_t towards the attitude devices during the post-impact phase will be the same as in **Case A**. Hence, both distributions will yield identical results from the viewpoint of base attitude change.

4.5.1.2 Bias angular momentum in the manipulator

In both **Case B** and **Case C** the angular momentum of the entire system is equal to zero, however, the latter distribution leads to some advantages from the viewpoint of base attitude control after the contact with the target. **Case C** provides different alternatives

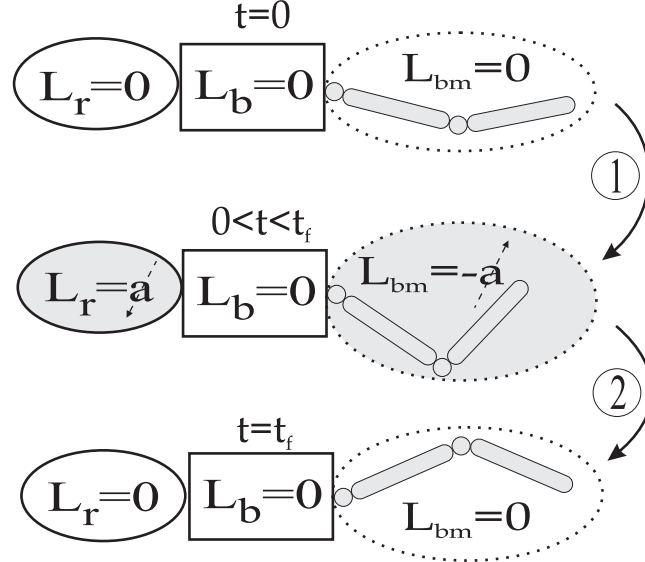


Figure 4.9: Angular momentum management among the reaction wheels and the manipulator.

for post-impact system control. One of them is again using the reaction wheels in order to compensate the base attitude change. An alternative approach uses the fact that after the contact, the angular momentum from the target could be canceled out with the one preloaded in the manipulator arm (\mathbf{L}_{bm}). Therefore, in the post-impact phase just the remaining amount of angular momentum in the base, manipulator and target should be redistributed in order the system to come to a complete stop. Since in this particular case the angular momentum that needs to be redistributed is actually zero, even locking the manipulator joints will lead to a successful completion of the capturing operation (see assumption a_6 in Section 4.1). We should note however, that if no post-impact control is applied, base attitude deviation might occur as a result of the impact force generated during the contact. In order to be successful in controlling the base attitude, such control has to satisfy the condition in the *coupling wrench theorem* formulated in Section 4.2.

Since \mathbf{L} is constant during the approach, cases **B** and **C** imply that momentum was already stored in the reaction wheels before the start of the approaching phase. This however, is not necessary (for the application of BMA), as can be seen from the distribution depicted in **Case D**. In general the definition of a favorable angular momentum distribution can be summarized as follows:

$$\left. \begin{array}{l} |\mathbf{L}_{bm}^c| \leq |\mathbf{L}_t^c| \\ \mathbf{L}_t^c \mathbf{L}_{bm}^c < 0 \end{array} \right\} \quad (4.20)$$

where $c = \{x, y, z\}$ stand for the x , y and z components of a three dimensional vector. Equation (4.20) actually states that the momentum that should be preloaded in the manipulator has to be with smaller or equal magnitude and opposite direction to the one in

the target. The limiting case when $\mathbf{L}_{bm} = -\mathbf{L}_t$, is referred to as “*full*” bias distribution and obtaining it is not always possible. Nevertheless this case will be included in the analysis as well, since it can give important insight into the problem. A bias momentum distribution which is not “*full*” and satisfies (4.20) will be called “*partial*”.

4.5.1.3 Angular momentum management

Here, the problem of obtaining a desired angular momentum distribution in the chaser system during the approaching phase is discussed. Under the current assumptions, \mathbf{L} remains constant during the approach to the target. However, it will not necessarily be equal to zero. In the general case, the system of reaction wheels is used for compensation of environmental torques, therefore before the start of the approach to the target $\tilde{\mathbf{H}}_{br}\dot{\phi}_r$ can have a value different from zero. Solving (4.5) for the joint velocity rates, using $\omega_b = 0$ (desired condition) and $\mathbf{P} = 0$, one obtains:

$$\dot{\phi}_m = \tilde{\mathbf{H}}_{bm}^+ (\mathbf{L} - \tilde{\mathbf{H}}_{br}\dot{\phi}_r) + (\mathbf{E}_p - \tilde{\mathbf{H}}_{bm}^+ \tilde{\mathbf{H}}_{bm})\dot{\xi}_p \quad (4.21)$$

where $(\mathbf{E}_p - \tilde{\mathbf{H}}_{bm}^+ \tilde{\mathbf{H}}_{bm})$ is the projector onto the null space of $\tilde{\mathbf{H}}_{bm}$ and $\dot{\xi}_p \in R^p$ is an arbitrary vector. For more details see Section 3.1.1. One important property of the null space component that was already mentioned is that joint velocities derived from it do not influence the momentum distribution whatsoever. Since \mathbf{L} is constant during the approach, the only member of (4.21) that can redistribute the momentum in the chaser satellite is $\tilde{\mathbf{H}}_{br}\dot{\phi}_r$. From the constraint $\mathbf{L}_b = 0$ it follows that, joint velocities obtained from (4.21) will result in such manipulator motion, that the rate of change of \mathbf{L}_{bm} will be equal to the rate of change of $-\tilde{\mathbf{H}}_{br}\dot{\phi}_r$.

The second component of (4.21) can be utilized in order to additionally constrain the manipulator motion (see Section 3.2). In the context of this section, a necessary secondary constraint is the velocity profile of the end-effector. Determination of such profile for $\dot{\xi}_p$ that avoids algorithmic singularity with the first task (using only local optimization via the pseudoinverse) however, is an arduous problem. On the other hand the solution to the planning problem is crucial for the successful completion of the capturing operation, that is why in the next subsection we present a motion planning strategy, based on the fact that the bias momentum approach is utilized. It should be noted that, the above mentioned strategy does not make use of the latter term of equation (4.21), in other words, the null space solution is not employed for the trajectory planning process.

4.5.2 Planning of approaching trajectory when BMA is utilized

Trajectory planning for systems under nonholonomic constraints is a well known research field. The system under discussion, exhibits nonholonomic behavior as a result of the

nonintegrability of the angular momentum equation (4.5). In Chapter 1, some of the commonly used planning strategies for space robots were outlined. Here, the angular momentum redistribution performed in the chaser satellite during the approaching phase is utilized for the formulation of a *two step* strategy for the determination of approaching trajectory to a tumbling target. When capturing a tumbling object two main factors should be considered;

- f₁**) the angular momentum of the target object;
- f₂**) the velocity change of the grasping point.

The second one (**f₂**) implies that the approaching trajectory should be designed in such a way that at the moment of contact, the linear velocities of the grasping point and end-effector are the same, in order to avoid high impact forces. The consideration of both factors is critical for the successful completion of a capturing operation. As discussed in Section 4.5.1, if the BMA is utilized, and momentum redistribution is performed during the approaching motion of the manipulator, the management of \mathbf{L}_t during the post-impact phase can be facilitated. Note that, such momentum redistribution should not be considered as additional burden to the trajectory planning. Since, if no momentum is redistributed (BMA is not utilized), the only possibility for manipulator motion (if zero base attitude change is desired) is in the null space of the coupling inertia matrix $\tilde{\mathbf{H}}_{bm}$. Hence, due to the utilization of the BMA during the approaching phase, some new alternatives arise.

The momentum to be redistributed during the approach can be determined using two criteria. The first one is equation (4.20) and the second one is:

$$\left. \begin{array}{l} \mathbf{r}_h(t_f) = \mathbf{r}_g(t_f) \\ \dot{\mathbf{r}}_h(t_f) = \dot{\mathbf{r}}_g(t_f) \end{array} \right\} \quad (4.22)$$

where $\mathbf{r}_h(t_f)$ and $\mathbf{r}_g(t_f)$ are the positions of the end-effector and grasping point (with respect to Σ_i), respectively, and t_f is the final time for the approaching maneuver. Next, two steps of a planning strategy that account for both criteria in (4.20) and (4.22) are presented. The first step deals only with the position constraint (upper part of (4.22)) and determines a manipulator initial configuration, while at a second step, the velocity constraint as well as the momentum profile to be redistributed are considered.

4.5.2.1 Step A - Choice of manipulator initial configuration

Here, the motion of the reaction wheels is considered as a control input for the motion of the robot arm. In other words, the manipulator moves in a way that guarantees zero attitude change, by absorbing the angular momentum transferred from the reaction wheels

to the base body. Such motion can be obtained using the former component of (4.21). Hence, specifying the torque profile to be applied in the attitude devices during the approach, determines the manipulator motion from initial configuration $\phi_m(t_0)$ to a final one $\phi_m(t_f)$ ¹².

With a fixed input command¹³, one can satisfy the condition in the upper part of (4.22) by choosing a proper initial configuration for the manipulator arm ($\phi_m(t_0)$). Here, the search for appropriate $\phi_m(t_0)$ is defined as a standard optimization problem, with the p initial joint angles as state variables, objective function:

$$Y_{ob}^A = \mathbf{r}_h(t_f) - \mathbf{r}_g(t_f) \quad (4.23)$$

and the following geometric constraint:

$$\phi_m^{min} \leq \phi_m \leq \phi_m^{max} \quad (4.24)$$

Note that this is just an intermediate step whose aim is to determine initial manipulator configuration that accounts for the specific input command defined, and the upper part of (4.22). The objective function (Y_{ob}^A) does not necessarily need to converge to zero (error tolerance is admissible). Fine-tuning is performed at a second step. The torque profile of the reaction wheels should be defined such, that result in obtaining a favorable momentum distribution, as defined in (4.20). If obtaining a desired momentum distribution is not necessary, choosing a particular manipulator initial configuration is not required. In such a case, the planning can be made directly using *Step B*, which will be discussed next.

4.5.2.2 Step B - Determining the Momentum Profile

In this step the condition of fixed torque profile is dropped, and finding such input command that results in manipulator motion satisfying both constraints in (4.22) is desired. For this purpose, the trajectory planning problem is defined as; planning a point-to-point motion from a known initial end-effector position in Cartesian space $\mathbf{r}_h(t_0)$ ¹⁴ to $\mathbf{r}_g(t_f)$, with the following nonlinear velocity constraints:

$$\dot{\mathbf{r}}_h(t_f) - \dot{\mathbf{r}}_g(t_f) = 0 \quad (4.25)$$

Furthermore, apart from the geometric restrictions in (4.24) the following dynamic constraints should be satisfied as well:

$$\tau_r^{min} \leq \tau_r \leq \tau_r^{max} \quad (4.26)$$

¹²This motion could be altered using the null space component in (4.21), however at this stage it will not be considered.

¹³The input command is the profile of the torque in the reaction wheels.

¹⁴Which corresponds to the initial manipulator configuration, determined in *Step A*.

The torque profile of the reaction wheels are chosen as state variables¹⁵. As can be seen in the constraint equations (4.24), (4.25) and (4.26) there is no term that accounts for base attitude minimization. This is because zero spacecraft attitude is guaranteed merely by the fact that the manipulator is controlled using (4.21). Hence, the objective function can be chosen to satisfy some different criteria (for example minimal path length.).

$$Y_{ob}^B = \int_{t_0}^{t_f} \sqrt{\dot{\mathbf{r}}_h^T \dot{\mathbf{r}}_h} dt \quad (4.27)$$

If the initial manipulator configuration is chosen arbitrary not using the algorithm in *Step A*, *Step B* can still be utilized for finding the torque profile of the reaction wheels that satisfy the position and velocity constraints. The resulting momentum redistribution during the approach however, will not be easily predictable.

It is obvious that for the problem at hand, using techniques from optimal control, cannot guarantee solution in each case. Evidently, combination of *Step A* and *Step B* cannot always yield a favorable momentum distribution as in (4.20). We however, observed that for “reasonable” choice of position and velocity constraints, the solutions are very sensitive to the length of the approaching maneuver t_f and the constraint in equation (4.26). Since the torque limitation of the reaction wheels is a constraint that cannot be altered (in a practical case), varying the time for the approach (t_f) in many cases is sufficient for the optimization algorithm to converge to satisfactory results¹⁶. Example that shows the results from both optimization procedures is presented next.

4.5.2.3 Simulation Study

Here, the trajectory planning sequence discussed in the previous subsection is applied for a seven DOF manipulator mounted on a free-floating base. It is assumed to make contact at $t_f = 30$ sec. with a target satellite which is rotating with constant angular velocity $\omega_{bt} = [-0.02, -0.02, -0.02]^T$ rad/s and has angular momentum $\mathbf{L}_t = [-3, -3, -3]^T$ Nms. The grasping point is positioned at $\mathbf{r}_g^b = [-0.5, -0.5, 0.5]^T$, where \mathbf{r}_g^b is expressed in the target body fixed frame. The torque limitation of the reaction wheels is 0.2 Nm. The parameters of the chaser system are in Appendix F. Two cases are considered:

S_A determining the manipulator initial configuration using *Step A*;

S_{AB} trajectory planning using *Step A* and *Step B*.

¹⁵In Section 4.5.3 the choice of state variables and their influence over the result of the optimization procedure is discussed.

¹⁶Note that, the time duration of the approaching motion can be arbitrary specified.

The position and linear velocity of the grasping point at $t_f = 30$ are determined to be:

$$\begin{aligned}\mathbf{r}_g(t_f) &= [2, -1.2, 1.54]^T \text{ m} \\ \dot{\mathbf{r}}_g(t_f) &= [-0.0002, 0.0201, -0.0199]^T \text{ m/s}\end{aligned}$$

The evaluation of the constraints and objective function is done using a simulation at kinematical level. Since no external forces are acting during the approach, computation of the system dynamics is not necessary¹⁷. The computational sequence used is outlined next:

Simulation at kinematic level:

Step ① Start at time $t = 0$ when positions and velocities of the generalized coordinates of the system are known (\mathbf{A}_b , \mathbf{r}_b , \mathbf{v}_b , ϕ , $\dot{\phi}$), and compute the inertia matrices \mathbf{H}_b and \mathbf{H}_c (\mathbf{A}_b is the rotational matrix of the base).

Step ② Using equation (4.21), from the known values of the input variables $\dot{\phi}_r$, determine the manipulator joint velocities ($\dot{\phi}_m$). This particular motion of the manipulator and reaction wheels will result in zero base attitude change.

Step ③ Find the linear velocity of the base solving equation (C.17) (note that ω_b is not considered, since it is equal to zero).

Step ④ Integrate \mathbf{v}_b and ϕ to obtain \mathbf{r}_b and ϕ .

Step ⑤ Using \mathbf{A}_b , \mathbf{r}_b , ϕ and $\dot{\phi}$ the computation of the constraint equations (4.22), (4.24), as well as the objective functions (4.27) or (4.23) is straightforward.

Step ⑥ Goto **Step ①**.

Note that since the torques of the reaction wheels are chosen to be state variables for the optimization procedure in *Step B*, $\dot{\phi}_r$ should be computed by numerical integration of $\ddot{\phi}_r$, which is given as:

$$\ddot{\phi}_r = \tilde{\mathbf{H}}_{br}^{-1} \boldsymbol{\tau}_r$$

In Fig. 4.10 a comparison between the results from cases \mathbf{S}_A and \mathbf{S}_{AB} is made. The input command (profile of the torque in the reaction wheels) for case \mathbf{S}_A is chosen to be $\boldsymbol{\tau}_r = [-0.1, -0.1, -0.1]^T \text{ Nm}$ during the entire approaching phase, hence, loading the manipulator with $\mathbf{L}_{bm} = [3, 3, 3]^T \text{ Nms}$, which is a “full-bias” momentum distribution. The initial guess for the optimization routine was specified to be:

$$\dot{\phi}_m^{ig} = [-10, 20, 25, -35, -160, 30, 20]^T \text{ deg},$$

which was arbitrary chosen in order to position the manipulator end-effector in the vicinity of the grasping point. The solution obtained is:

$$\dot{\phi}_m(t_0) = [-10.3, 22.6, 14.9, -35.6, -150.6, 32.2, 16.6]^T \text{ deg},$$

Note that since in this case, just the end-effector positioning subtask is considered the linear velocities (case \mathbf{S}_A) do not converge to the values of $\dot{\mathbf{r}}_g(t_f)$ (Fig. 4.10).

¹⁷This is done in order to achieve computational savings.

Using the manipulator initial configuration calculated above, in *Step B* of the trajectory planning procedure, the torque profile of the reaction wheels is altered in a way that satisfies the velocity constraints as well. The initial guess for the profile of $\boldsymbol{\tau}_r$ (state variables for this optimization routine) is the same as the one used in case S_A . The resultant profile is depicted in Fig. 4.11. Both end-effector position and velocity constraints for case S_{AB} are satisfied, and the momentum distribution obtained meets the requirements of (4.20) ($\mathbf{L}_{bm} = [2.46, 1.43, 0.41]^T \text{ Nms}$)¹⁸. The manipulator configuration in case S_{AB} at t_0 and t_f is depicted in Fig. 4.12. A small base translational motion can be observed, which is expected since it is not controlled. The manipulator motion sequence is depicted in Fig. 4.13.

¹⁸The results from both *Step A* and *Step B* are obtained using Matlab's Optimization Toolbox (*fmincon*) [133].

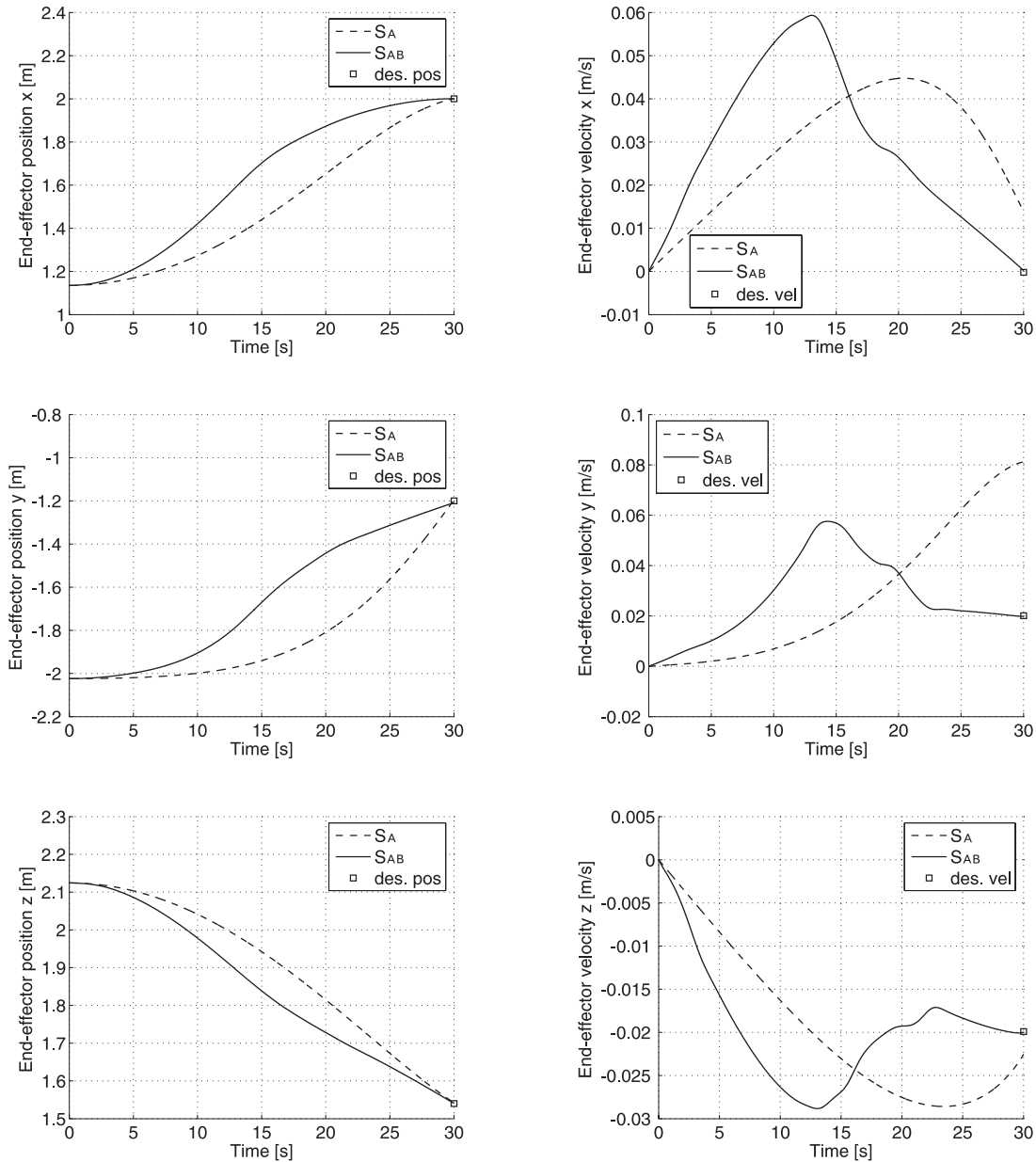


Figure 4.10: End-effector position and velocity in cases S_A and S_{AB} (x , y , z axis).

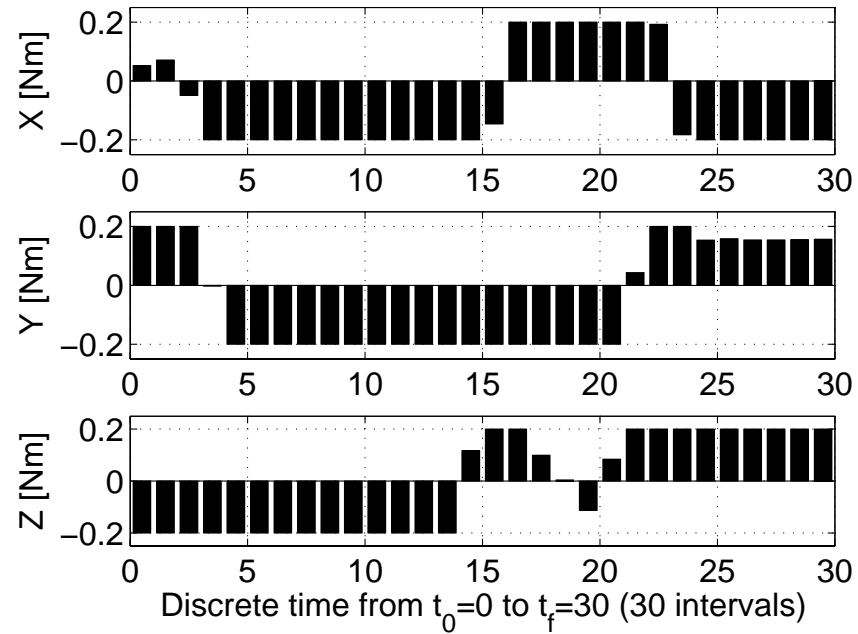


Figure 4.11: Profile of the torques in the reaction wheels derived using *Step A* and *Step B* from the trajectory planning procedure.

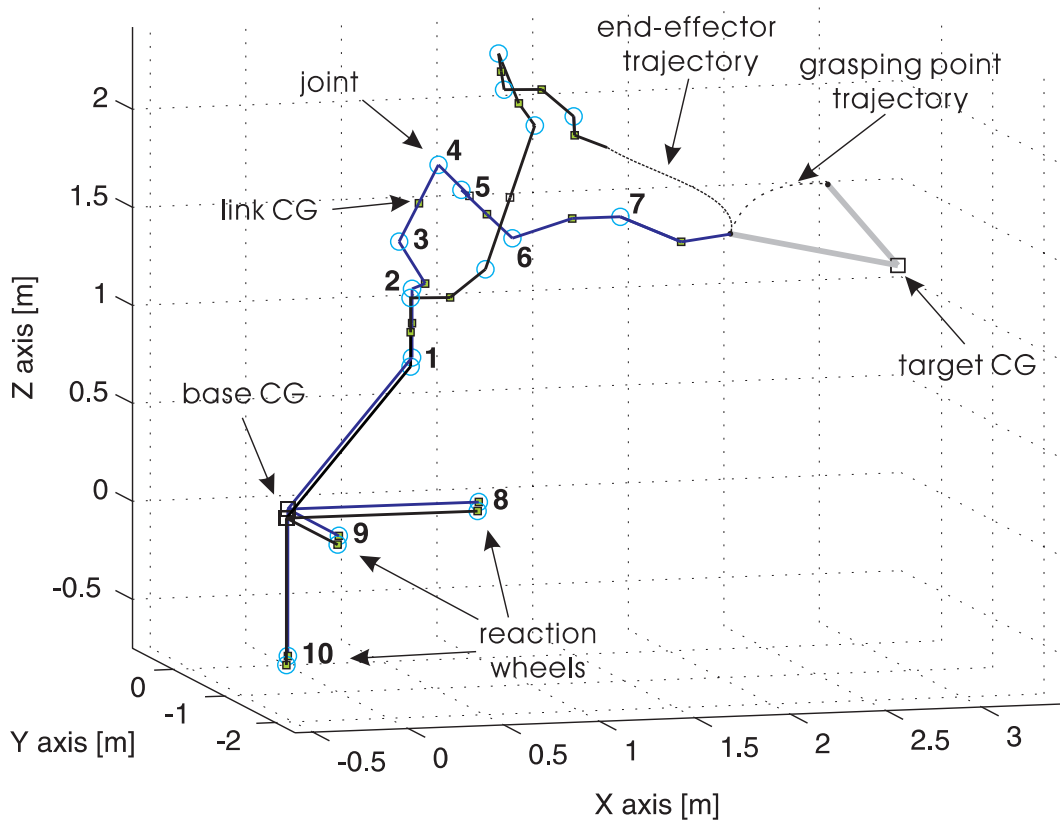


Figure 4.12: Manipulator configuration at t_0 and t_f for case S_{AB} .

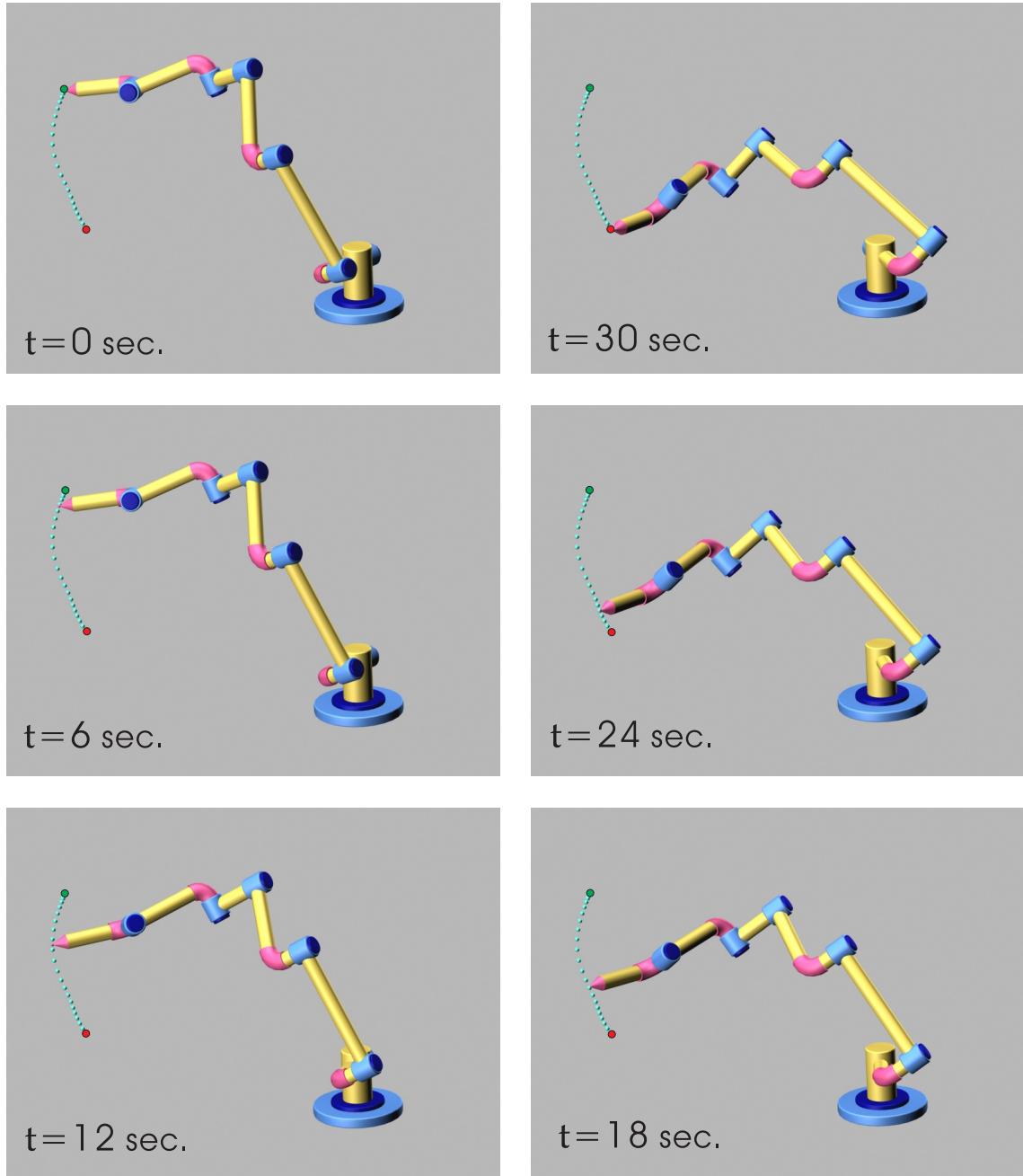


Figure 4.13: Motion profile of the manipulator from t_0 to t_f for case S_{AB} (the view angle is different from the one in Fig. 4.12).

4.5.3 Comparison between different state variables

In the previous subsection a two step trajectory planning sequence was utilized for defining the manipulator approaching motion. In *Step B*, optimization solver was used to determine the torque profile to be applied in the reaction wheels. Once this profile is known, using equation¹⁹ (4.21) the manipulator motion can be determined. Here, an alternative approach will be adopted, namely the manipulator joint velocities will be chosen as state variables for the optimization procedure, and the velocities of the reaction wheels will be determined using:

$$\dot{\phi}_r = -\mathbf{H}_{br}^{-1} \mathbf{H}_{bm} \dot{\phi}_m \quad (4.28)$$

The two alternatives;

- \mathbf{A}_r) torque in the reaction wheels as state variables;
- \mathbf{A}_m) velocity of the manipulator joints as state variables;

lead to different solutions for the system motion (using the same optimization solver), and will be compared hereafter. The reason for choosing case \mathbf{A}_r in Section 4.5.2.2 is discussed.

There are two main drawbacks when the manipulator joint velocities are chosen to be state variables for the optimization procedure:

- a.) The number of state variables increases proportionally to the number of DOF of the manipulator. Hence the space in which solutions are being sought is larger.
- b.) The optimization solver changes directly the profile of $\dot{\phi}_m$.

Obtaining reasonable motion profile for the manipulator joints is as important as finding satisfactory Cartesian trajectory for the end-effector. Specific motion in joint space may be desirable for overcoming limitations related to the manipulator structure, like kinematic singular configurations. In many cases obtaining solutions with minimal joint velocity norm is preferred. Furthermore, it might be necessary to separate the joint space in two sets of components, which perform different tasks. If state variables as in case \mathbf{A}_m above are chosen, the solution of such problems might be possible if additional constraints to the optimization solver are imposed. This however, is not the best possible solution as it will be pointed out next.

Once $\dot{\phi}_m$ are chosen for the current step of the optimization algorithm (case \mathbf{A}_m), the motion of the entire system is predetermined, (see equation (4.28)), hence, the solution is very much dependent on the solver type. One way to deal with this problem is to use a different set of state variables. A good candidate is the torque in the reaction wheels.

¹⁹In the case when base attitude motion does not occur, a direct relation between the torques applied in the reaction wheels and the resultant change of their angular velocities can be made (non-linear effects do not occur).

If the motion rates of the reaction wheels are known, motion of the manipulator that satisfies specific requirements can be found by using the following equation (similar to (4.21)):

$$\dot{\phi}_m = -\tilde{\mathbf{H}}_{bm}^{\#} \tilde{\mathbf{H}}_{br} \dot{\phi}_r + (\mathbf{E}_p - \tilde{\mathbf{H}}_{bm}^{\#} \tilde{\mathbf{H}}_{bm}) \dot{\xi}_p \quad (4.29)$$

where $(\cdot)^{\#}$ denotes a generalized inverse of a matrix. Different requirements can be imposed by changing the type of generalized inverse, or by using the null space component. Using a particular relation between $\dot{\phi}_r$ and $\dot{\phi}_m$ permits additional adjustments to be made. In other words, the optimization solver interacts with $\dot{\phi}_m$ through a “filter” (the type of generalized inverse employed), that can be specified by the user. That is one of the reasons for the torques of the reaction wheels to be chosen as state variables for the optimization procedure in Section 4.5.2.2. Next, a numerical example that illustrates the discussion above is made.

4.5.3.1 Simulation Study

In this section a comparison through numerical simulation between two different sets of state variables for the optimization procedure used in Section 4.5.2.2 is made. The constraints in equations (4.22) and (4.26) are imposed. Minimal path length determines the value of the objective function (4.27). The simulations are performed in Matlab 7.0, and the solver *fmincon* from the Matlab Optimization Toolbox [133] is utilized.

Three cases are discussed:

C1: The manipulator joint velocities are the state variables.

C2: The joint torques of the reaction wheels are state variables,
(pseudoinverse is utilized, without null space solution).

C3: The joint torques of the reaction wheels are state variables.
(coordinate partitioning²⁰ is utilized, without null space solution).

For the three cases the following parameters are the same:

$$\begin{aligned}\tau_r^{max} &= [0.2, 0.2, 0.2]^T \text{ Nm} \\ \tau_r^{min} &= [-0.2, -0.2, -0.2]^T \text{ Nm} \\ \mathbf{r}_g(t_f) &= [1.8, -1.8, 1.7]^T \text{ m} \\ \dot{\mathbf{r}}_g(t_f) &= [0.0031, 0.0033, -0.0025]^T \text{ m/s} \\ \phi(t_0) &= [-10, 20, 25, -35, -160, 30, 20, 0, 0, 0] \text{ deg}\end{aligned}$$

²⁰The method for coordinate partitioning utilized is described in Section 3.1.1.2 *Case B* (with the values of the independent joint velocities $\dot{\phi}^i = 0$.)

The results from the three optimization procedures are depicted as follows (the initial guess for all of them is trivial):

Fig. 4.14 shows the Cartesian positions and velocities of the end-effector. With the specific constraints imposed, the solutions for the end-effector motion from the three procedures are very similar²¹. There is almost no difference, between Y_{ob}^B in cases **C1**, **C2** and **C3** as well. Although for the case discussed here such observation can be made, in general, such resemblance can not be achieved²², as will be discussed in the sequel.

Fig. 4.15 depicts the torque profile of the reaction wheels. Fig. 4.16 contains the manipulator joint velocities for all three cases. Let us consider first case **C2**. As a result of the utilization of pseudoinverse, the solution to the optimization problem yields (locally) minimal manipulator joint velocity norm (see Tab. 4.2 S_m) for a given motion of the reaction wheels. It is evident that in case **C2** the norm of the torque profile (S_r) is the highest one. In some cases, system motion where fast velocity change of the reaction wheels results in slow motion of the manipulator might not be desirable. Nevertheless, in other this effect is mostly helpful. For example, when momentum needs to be redistributed (between the reaction wheels and manipulator) in a way that results in low manipulator joint velocity rates, the utilization of redundancy resolution based on pseudoinverse is advantageous. If approach as in **C1** is adopted, in order to ensure low value for S_m , additional constraints need to be imposed. Such constraints can degrade the convergence rate of the optimization solver, furthermore, the resultant output is very sensitive to the specified initial guess. Even though the pseudoinverse approach guarantees only local minimum of S_m , in many cases it is sufficient enough.

Table 4.2: Output from the optimization procedures.

	C1	C2	C3
S_m	14.85	9.29	11.31
S_r	51.9791	84.1925	79.7115
Y_{ob}^B	0.7031	0.7058	0.7029

$$S_m = \sum_{i=0}^{i=t_f} \|\dot{\phi}_m(t_i)\| \quad ; \quad S_r = \sum_{i=0}^{i=t_f} \|\tau_r(t_i)\|$$

In case **C1** the overall torque applied to the attitude devices is less than the one applied for cases **C2** and **C3**. (see Tab. 4.2 S_r). Furthermore, the norm of the manipulator joint velocities in **C1** is higher than the one in cases **C2** and **C3** (see Tab. 4.2 S_m). This shows that the routine based on equation (4.28) found system motion, where fast ma-

²¹In all three cases the constraints are satisfied as well.

²²For the sake of comparison, a case when **C1**, **C2** and **C3** converge to a solution is presented.

nipulator movement corresponds to small reaction wheels torques. This effect, however, was not intended, and if different constraints are imposed the solution can easily change. A numerical simulation was performed with end-effector constraints as the one used in Section 4.5.2.2, and the algorithm in case **C1** (with trivial initial guess) did not converge to satisfactory results. Even when initial guess was properly specified, the time for convergence was long. In addition, considering the joint velocity profile for case **C1**, it can be noted that $\dot{\phi}_m$ is not “smooth”²³. This results from the fact that the optimization solver changes it directly. As mentioned at the beginning of this section the generalized inverse works as a filter for the manipulator motion. This can be seen from the profiles of the joint velocities in cases **C2** and **C3**.

The utilization of different generalized inverse in (4.29) can result in constraining the system in a different way. As an example, coordinate partitioning (case **C3**) is utilized via equation (3.20) (see Section 3.1.1.2 *Case B*). The values of the independent joint velocities are set to zero. The first three joints of the manipulator are chosen to be the dependent set of coordinates which will be used to control the system. As evident from Fig. 4.16 (B), joints number 4, 5, 6 and 7 are not actuated in case **C3**. Only the motion of joints 1, 2 and 3 is sufficient to perform base attitude control and end-effector positioning control simultaneously (proven that the torque profile of the reaction wheels is chosen appropriately). The unactuated joints can be utilized for the satisfaction of additional requirements. From the above discussion it can be noted, that the 7 DOF manipulator has four DOR, although six constraints are imposed (base attitude, and end-effector Cartesian position). The reason for this is that the motion of the three reaction wheels is used as a control input for the manipulator motion (hence, they provide three additional DOF). The desired momentum to be redistributed can be considered to be a nonholonomic constraint, since it does not decrease the dimension of the configuration space, but rather imposed an instantaneous velocity condition.

Finally, it should be noted, that the computational time for case **C1** is the highest one, which is to be expected since the number of state variables used for the optimization procedure is higher. Nevertheless, since all three cases are intended for off-line computation, this is not a critical issue. Using both sets of state variables (manipulator joint velocities and joint torque) leads to some advantages, and their combined use might be beneficial. For example, planning based on state variables as in **C2** is performed first, at a next step, the obtained result is used as an initial guess for a procedure based on state variables as in **C1**. In such a way it might be possible to refine the results.

²³Here, the term “smooth” is used to express consistency, or regularity.

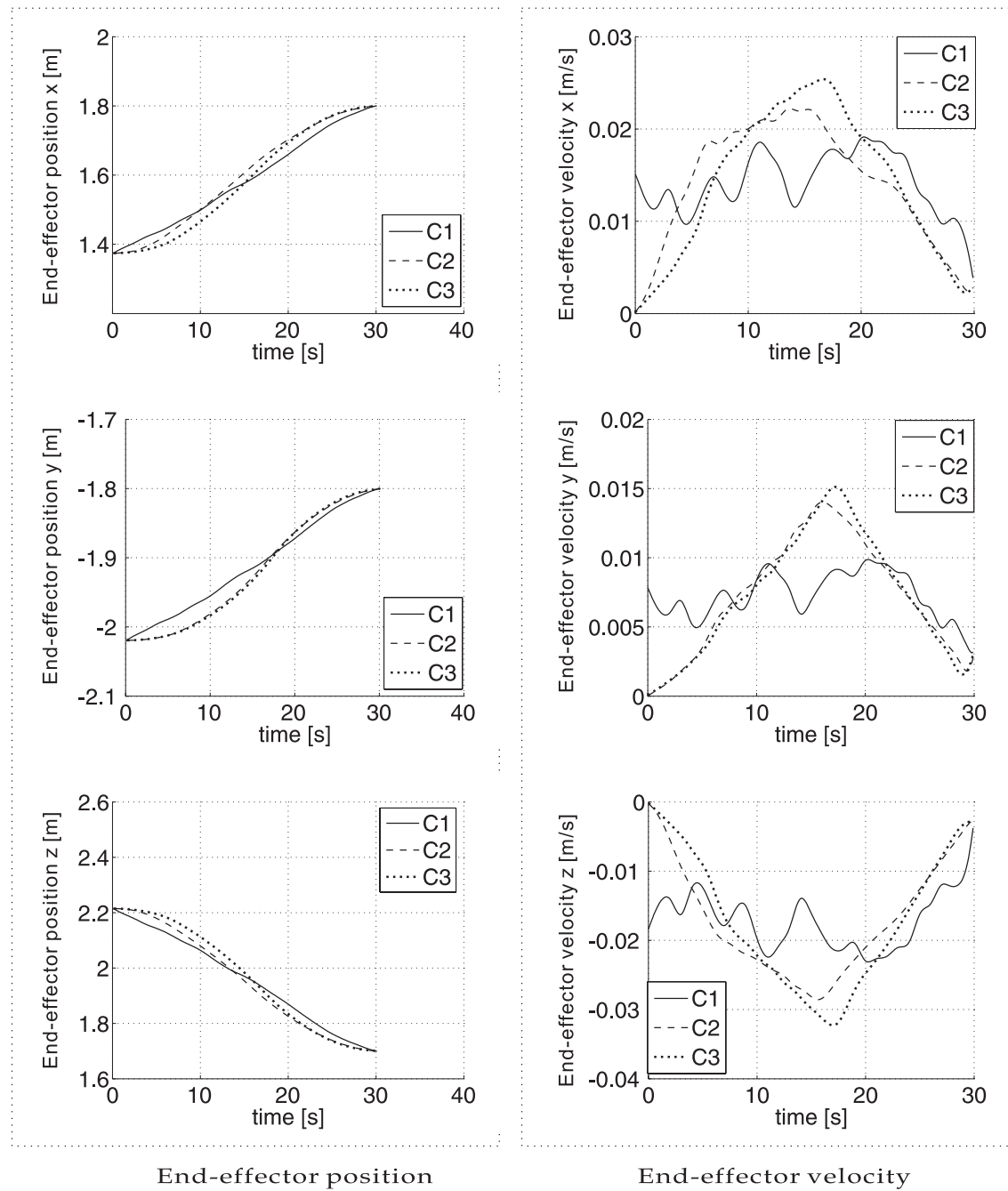


Figure 4.14: Position and linear velocity of the end-effector.

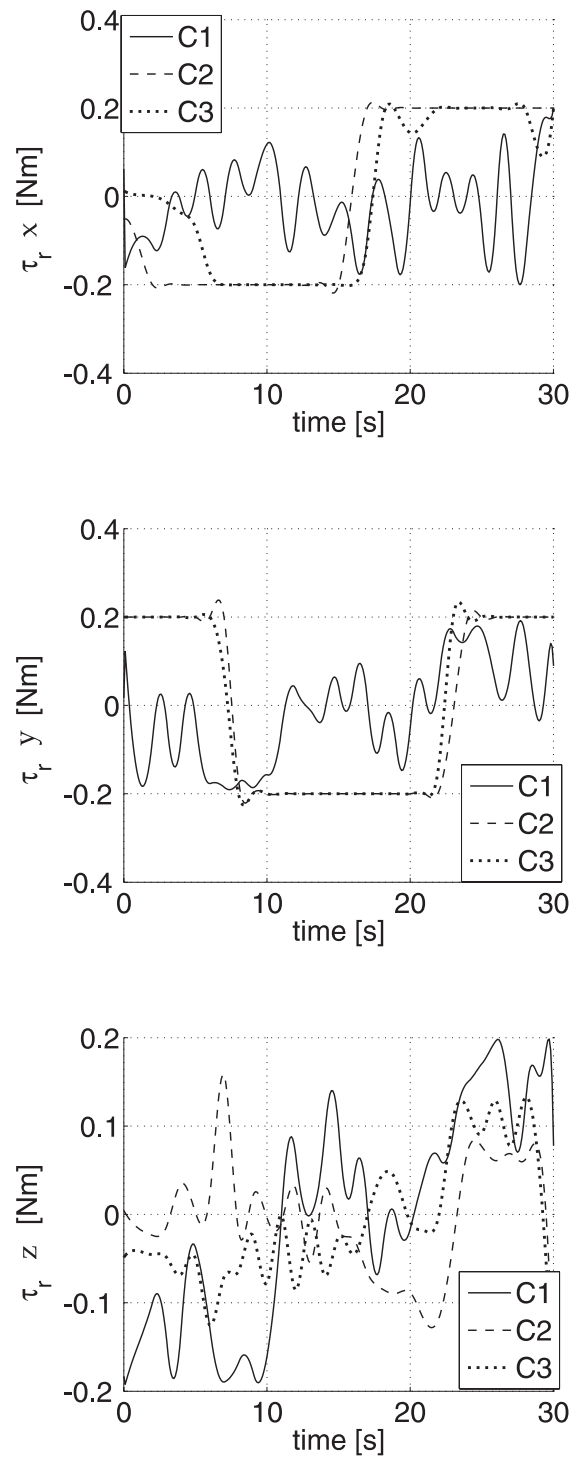
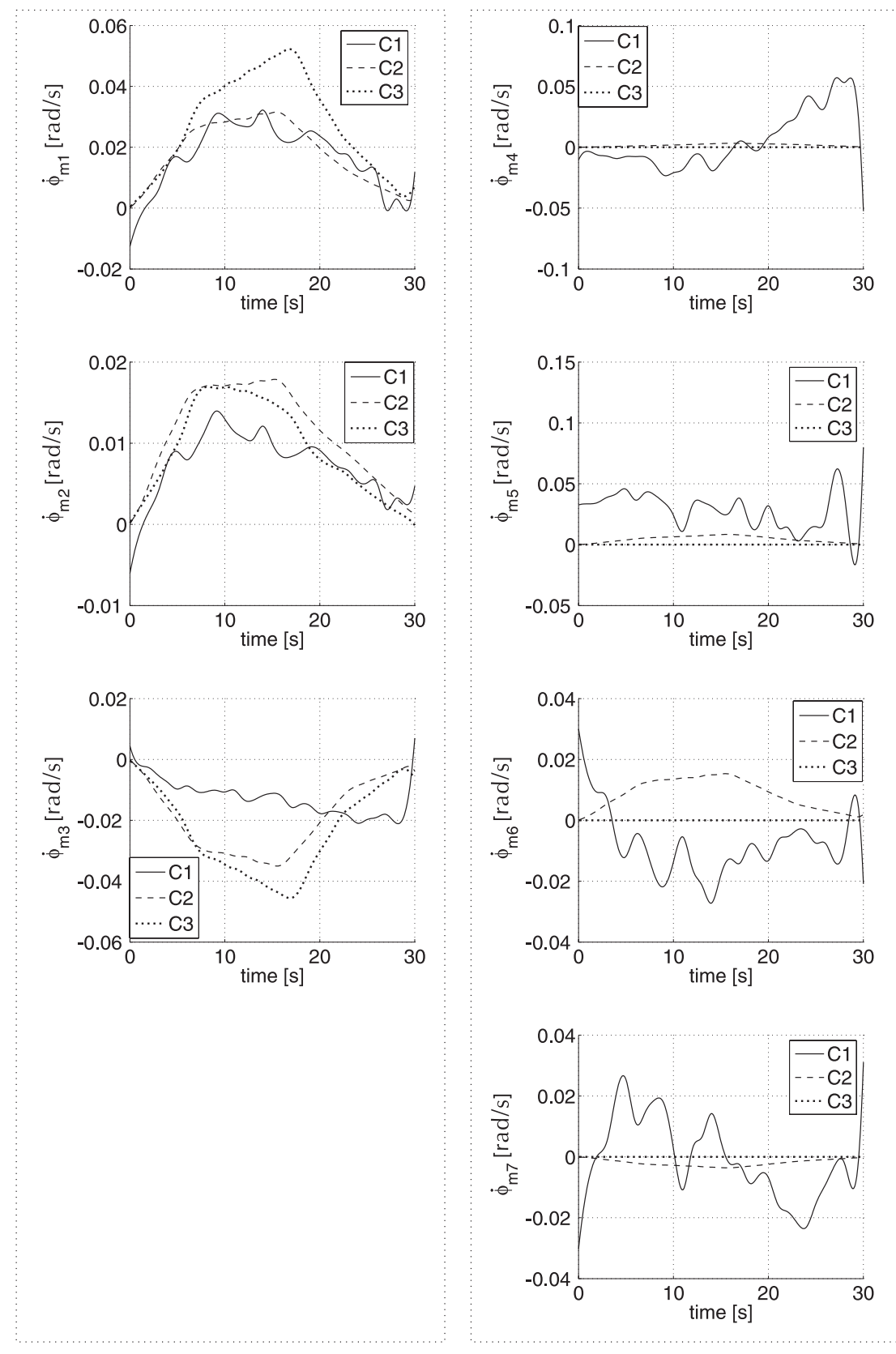


Figure 4.15: Profile of the torque in the reaction wheels (x , y and z axis).



(A) Actuated joints (1,2,3)

(B) Stationary joints (4,5,6,7)

Figure 4.16: Joint velocities.

4.5.4 Bias Momentum Approach - verification by simulation

In this subsection, simulation results that verify the strategy presented in Section 4.5.1 are presented. Two cases will be considered:

- F** *approaching phase:* full bias momentum
post-impact phase: the manipulator joints are locked
(no attitude control);
- N** *approaching phase:* non-bias momentum
post-impact phase: the manipulator joints are locked
(attitude control via reaction wheels);

As noted in Section 4.5.1, locking the manipulator joints at the start of the post-impact phase and using only reaction wheels for base attitude control is clearly not the best possible strategy to be taken. Nevertheless, it allows a comparison between *bias* and *non-bias* momentum distributions to be made.

In case **F** input command for the reaction wheels as in S_A is used, which results in obtaining a “full-bias” momentum distribution in the chaser satellite. As mentioned in 4.5.1, if “full-bias” momentum distribution is obtained, locking the manipulator joints during the post-impact phase leads to a successful completion of the capturing operation, as a result of the cancelation of \mathbf{L}_{bm} and \mathbf{L}_t . The base attitude profile in cases **F** and **N** is depicted in Fig. 4.17. Note that the base attitude change in the “full-bias” case right after the contact with the target is a result from the impact force generated ($\dot{\mathbf{r}}_h \neq \dot{\mathbf{r}}_g$ for the trajectory in S_A see Fig. 4.10). As can be seen, in the *non-bias* case angular momentum is transferred repeatedly to the base body, and due to the torque limitation, the reaction wheels are unable to compensate it. Recall that in case **N**, $\mathbf{L}_{bm} = 0$ at the moment of contact with the target satellite²⁴.

The profile of the angular momentum before and after the contact with the target is depicted in Fig. 4.18.

As it becomes evident from the results above, the method of obtaining a favorable momentum distribution in the manipulator when a tumbling target has to be captured, resembles the method of obtaining a pre-impact arm configuration for base reactions minimization, when an infinitesimal force impulse is applied at the end-effector [82]. The similarity is in view of the fact the both methods make preparation during the approaching phase. The aim of such preparation is to facilitate the post-impact base motion control.

²⁴In order to make a fair comparison, the manipulator configuration at the beginning of the post-impact phase should be identical for both cases. Defining a trajectory for the non-bias case that results in such configuration is difficult, that's why case **N** is considered just during the post-impact phase.

It should be noted that, in the case of a tumbling target the magnitude and direction of the contact forces has to be assumed unknown and constantly changing, hence, a particular pre-impact manipulator configuration does not provide significant advantages. As for the angular momentum, it is a conservative quantity and does not depend on the internal wrenches in the system. Note, that the contact forces/torques are internal from the viewpoint of the entire system consisted of the chaser and target satellites.

Apart from occurring as a result of intentional control, servo lock of the manipulator joints can happen in case of manipulator failure. In such a case, the utilization of a *full-bias* angular momentum distribution will guarantee the safe completion of the capturing operation.

The above discussion treats only the case of *full* and *non-bias* momentum distributions. In practice, however, they are most unlikely to appear²⁵. The application of the former one depends on the manipulator mass and inertia characteristics. In general, they might not be sufficient in order for the arm to store a *full-bias* momentum distribution because:

- the angular momentum in the target object can be large;
- the manipulator joint velocity rates have to be kept in reasonable range.

The application of the latter case (\mathbf{N}) leads to difficulties during the planning phase. The generation of an end-effector reactionless trajectory to a generic point in Cartesian space, for a 6 or 7 DOF manipulator is still a challenge (approach for reactionless path planning is discussed in Chapter 4.4). From the above discussion it can be assumed that the most likely momentum distribution at the beginning of the post-impact phase is a *partial* one. Its treatment will be extended in Chapter 5.

²⁵Nevertheless, the discussion of cases \mathbf{F} and \mathbf{N} gives valuable insight into the problems appearing during a capturing operation.

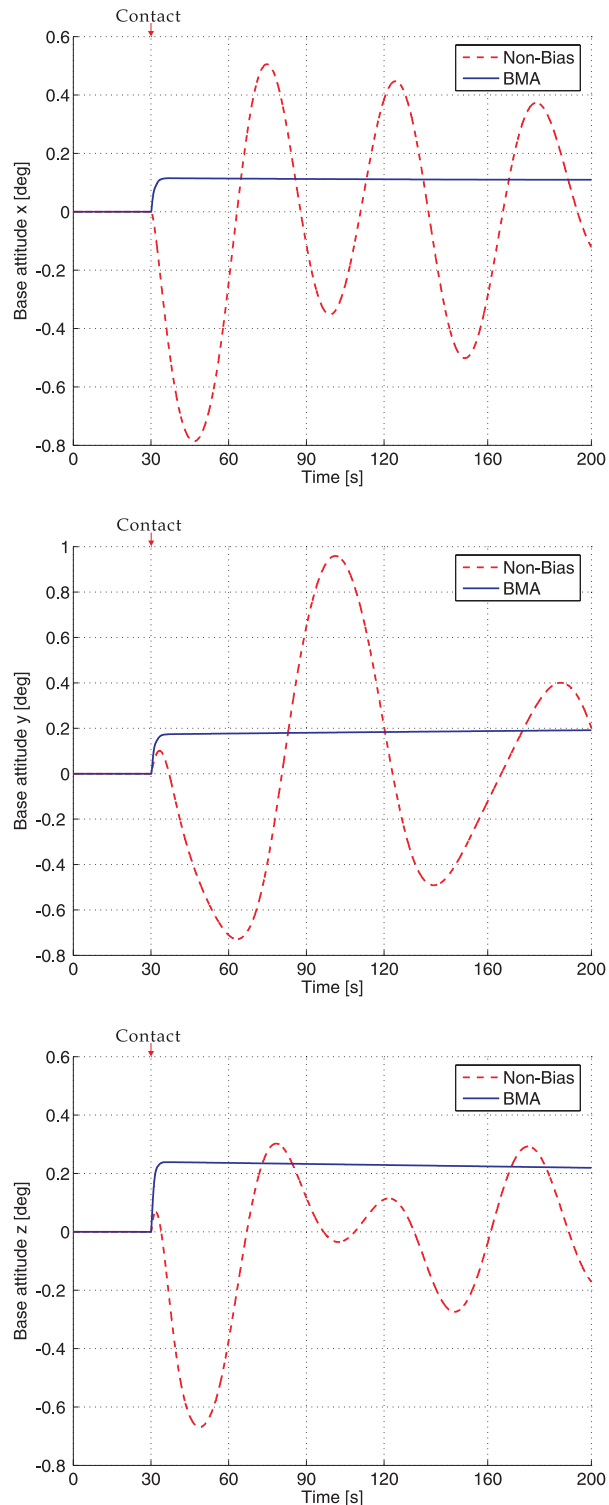


Figure 4.17: Comparison of the base attitude change in case of full-bias and non-bias momentum distributions (x , y and z axis).

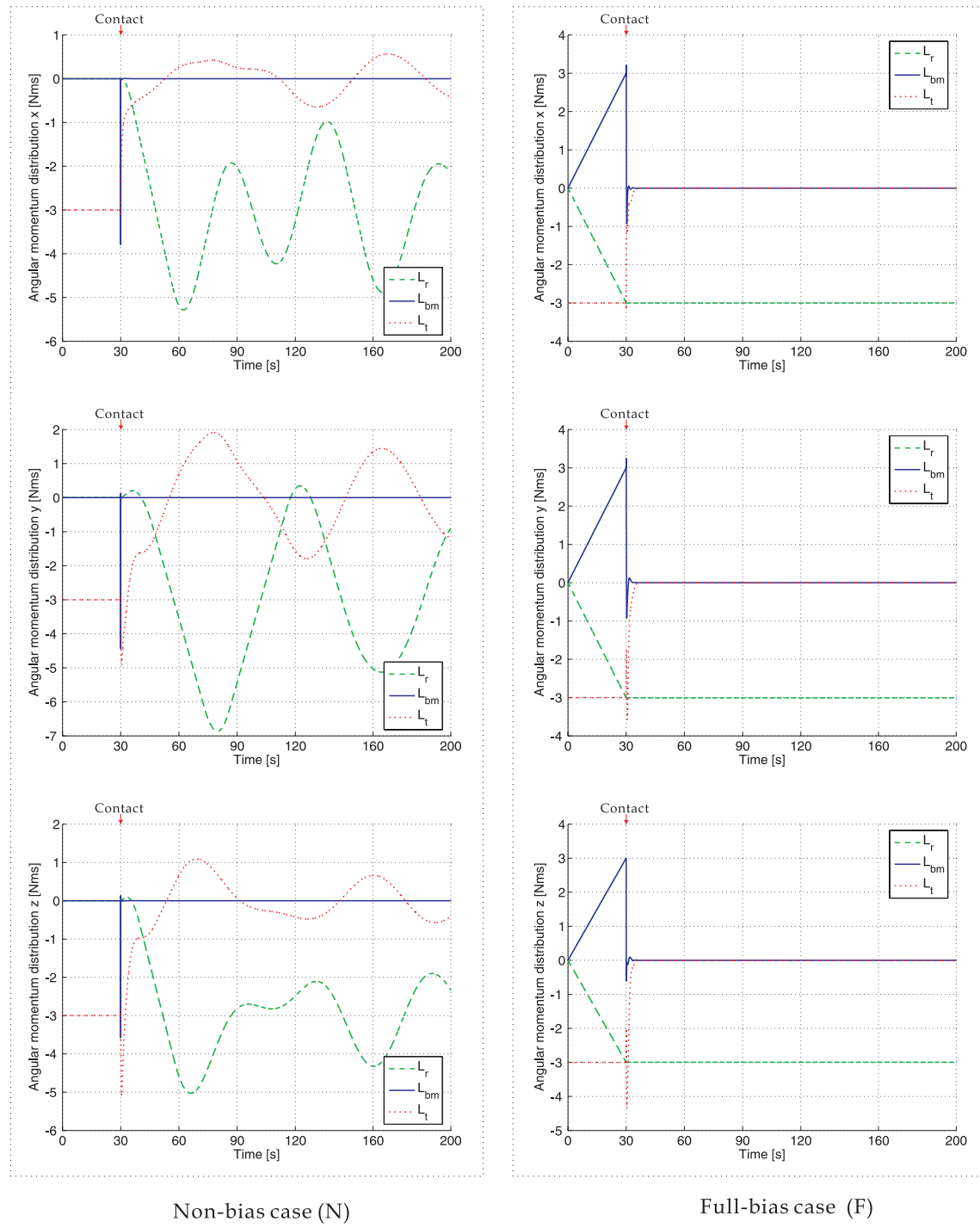


Figure 4.18: Angular momentum distribution for the full-bias and non-bias cases (x , y and z axis).

Chapter 5

Post-impact motion control issues

In Chapter 4 the approaching motion of the chaser system was discussed. A *bias momentum approach* that utilizes momentum redistribution between the robot arm and a system of reaction wheels was introduced. It proved to be useful for planning an approaching trajectory to the target satellite as well as for facilitating the post-impact control. It was demonstrated that in the case when *full bias* momentum distribution is obtained, even locking the manipulator joints leads to a successful completion of the capturing operation (with minimal base attitude change). In many cases, however, achieving such favorable momentum distribution is not possible. In those cases relying only on the attitude devices may not be the optimal solution [27]. The treatment of problems that can occur after the contact with the target object is extended in this chapter.

After establishing contact with the target, \mathbf{L}_t distributes over the chaser satellite. The objective is to manage the momentum in the entire system in such a way that it does not affect the base attitude motion. Two control laws that satisfy this desired condition are proposed. Both of them achieve minimal base attitude change exploiting the dynamic coupling between the manipulator and spacecraft. The first one is at acceleration and the second one at velocity level. Note that, information about the forces acting between the end-effector and grasping point is not needed.

5.1 Reaction Null Space Control

The transition between the approaching phase and the post-impact phase can change the degree of redundancy¹ of the system. Since there is no more need to follow a desired trajectory, the system can be constraint in a different way.

The primary task will be again keeping the base attitude zero and let the secondary one be minimization of the joint velocities. Extracting the first equation from (4.4) and

¹The term DOR was defined as the difference between the DOF of the system and the task constraints imposed.

solving it for $\ddot{\phi}_m$ we obtain:

$$\ddot{\phi}_m = -\tilde{\mathbf{H}}_{bm}^+(\tilde{\mathbf{H}}_b\dot{\omega}_b + \tilde{\mathbf{H}}_{br}\ddot{\phi}_r + \tilde{\mathbf{c}}_b - \tilde{\mathbf{J}}_{bh}^T\mathcal{F}_h) + \tilde{\mathbf{R}}^n\ddot{\xi}_p \quad (5.1)$$

where the second term denotes the joint accelerations from the angular reaction null space $\tilde{\mathbf{R}}^n$ ($\ddot{\xi}_p \in R^p$ is an arbitrary vector). Expressing $\ddot{\phi}_r$ from the third equation of (4.4) and substituting it together with $\ddot{\phi}_m$ from (5.1) into the middle part of (4.4), one obtains:

$$\bar{\mathbf{H}}\dot{\omega}_b - \bar{\mathbf{H}}_r\tau_r + \bar{\mathbf{c}}_n + \tilde{\mathbf{H}}_m\tilde{\mathbf{R}}^n\ddot{\xi}_p = \tau_m + \bar{\mathbf{H}}_f\mathcal{F}_h \quad (5.2)$$

where the new matrices are defined as follows:

$$\begin{aligned} \bar{\mathbf{H}} &= \tilde{\mathbf{H}}_{bm}^T - \tilde{\mathbf{H}}_m\tilde{\mathbf{H}}_{bm}^+\tilde{\mathbf{H}}_b + \bar{\mathbf{H}}_r\tilde{\mathbf{H}}_{br}^T \\ \bar{\mathbf{H}}_r &= \tilde{\mathbf{H}}_m\tilde{\mathbf{H}}_{bm}^+\tilde{\mathbf{H}}_{br}\tilde{\mathbf{H}}_r^{-1} \\ \bar{\mathbf{H}}_f &= \tilde{\mathbf{J}}_{mh}^T - \tilde{\mathbf{H}}_m\tilde{\mathbf{H}}_{bm}^+\tilde{\mathbf{J}}_{bh}^T + \bar{\mathbf{H}}_r\tilde{\mathbf{J}}_{rh}^T \\ \bar{\mathbf{c}}_n &= \tilde{\mathbf{c}}_m - \tilde{\mathbf{H}}_m\tilde{\mathbf{H}}_{bm}^+\tilde{\mathbf{c}}_b + \bar{\mathbf{H}}_r\tilde{\mathbf{c}}_r \end{aligned}$$

The nonlinear feedback

$$\tau_m^{rnsc} = \bar{\mathbf{H}}\mathbf{u}_b - \bar{\mathbf{H}}_r\tau_r + \bar{\mathbf{c}}_n + \tilde{\mathbf{H}}_m\tilde{\mathbf{R}}^n\mathbf{u}_m \quad (5.3)$$

defines a feedback linearizing controller for equation (5.2), where \mathbf{u}_b and \mathbf{u}_m are new control input variables. Using (5.3), the closed-loop equation becomes:

$$\bar{\mathbf{H}}(\dot{\omega}_b - \mathbf{u}_b) + \tilde{\mathbf{H}}_m\tilde{\mathbf{R}}^n(\ddot{\xi}_p - \mathbf{u}_m) = \bar{\mathbf{H}}_f\mathcal{F}_h \quad (5.4)$$

Equation (5.4) represents a superposition of two decoupled dynamical subsystems. With the assumption that the system of interest has a *strong inertial coupling* [108], which implies that the matrix $\bar{\mathbf{H}} \in R^{n \times 3}$, has full rank, with proper choice of the control inputs \mathbf{u}_b and \mathbf{u}_m , two control tasks could be performed simultaneously;

- (a) satellite base attitude control using $\bar{\mathbf{H}}\mathbf{u}_b$;
- (b) manipulator control sub-task using $\tilde{\mathbf{H}}_m\tilde{\mathbf{R}}^n\mathbf{u}_m$.

Thus a full decoupling of the base attitude dynamics from the manipulator dynamics can be achieved. Therefore, we can use the reaction null space component in order to perform joint velocity minimization that will not alter the angular momentum distribution whatsoever. In order to achieve that, let us specify the control inputs in the following way [82];

$$\mathbf{u}_b = -\mathbf{K}_b\omega_b \quad ; \quad \mathbf{u}_m = -\mathbf{K}_m\dot{\phi}_m$$

where \mathbf{K}_m and \mathbf{K}_b are positive-definite gain matrices for manipulator motion and base damping. Substituting them back into (5.3), the control law becomes:

$$\boldsymbol{\tau}_m^{rnsc} = -\tilde{\mathbf{H}}\mathbf{K}_b\boldsymbol{\omega}_b - \tilde{\mathbf{H}}_r\boldsymbol{\tau}_r + \bar{\mathbf{c}}_n - \tilde{\mathbf{H}}_m\tilde{\mathbf{R}}^n\mathbf{K}_m\dot{\boldsymbol{\phi}}_m \quad (5.5)$$

The first term of (5.5), guarantees that the manipulator will “absorb” all the angular momentum from the base, and the last one will perform joint velocity minimization. The second component ($\tilde{\mathbf{H}}_r\boldsymbol{\tau}_r$) accounts for the acceleration change of the reaction wheels. The nonlinear term $\bar{\mathbf{c}}_n$ performs feedback linearization.

It should be noted that, in (5.5) there is no term accounting for the inertia characteristics of the target satellite. During the post-impact phase the target will be in contact with the end-effector, nevertheless, even without taking this into account, with proper choice of the two gain matrices, stable base attitude can be achieved.

The computational burden when a control law at acceleration level is applied is generally high. This might be considered as a drawback. In the next subsection we propose a remedy to this problem introducing a control law at velocity level.

5.2 Distributed Momentum Control

The angular momentum conservation equation has linear form at velocity level. It is much simpler than the equation of motion at acceleration level, and still fully expresses the system dynamics. This permits the formulation of a control law with simpler structure compared to the *reaction null space control* (RNSC) [82] from the previous section. By taking into consideration the *coupling wrench theorem* (see Section 4.2), we propose the following control:

$$\dot{\boldsymbol{\phi}}_m^d = \tilde{\mathbf{H}}_{bm}^+(\tilde{\mathbf{H}}_{bm}\dot{\boldsymbol{\phi}}_m + \tilde{\mathbf{H}}_b\boldsymbol{\omega}_b) \quad (5.6)$$

where $\dot{\boldsymbol{\phi}}_m^d$ is the desired value for the manipulator joint velocities which would guarantee zero base attitude change. Equation (5.6) is called *distributed momentum control* (DMC). If applied for controlling the arm during the post-impact phase of a tumbling satellite capturing operation, (5.6) will guarantee minimal base attitude deviation. As can be seen DMC includes no information about the inertia characteristics of the target object, and its implementation is straightforward.

To begin with the derivation of (5.6), we note that the angular momentum of the target satellite can be expressed as:

$$\mathbf{L}_t = \tilde{\mathbf{H}}_{bt}\boldsymbol{\omega}_{bt} + \mathbf{r}_{bt} \times \mathbf{P}_t \quad (5.7)$$

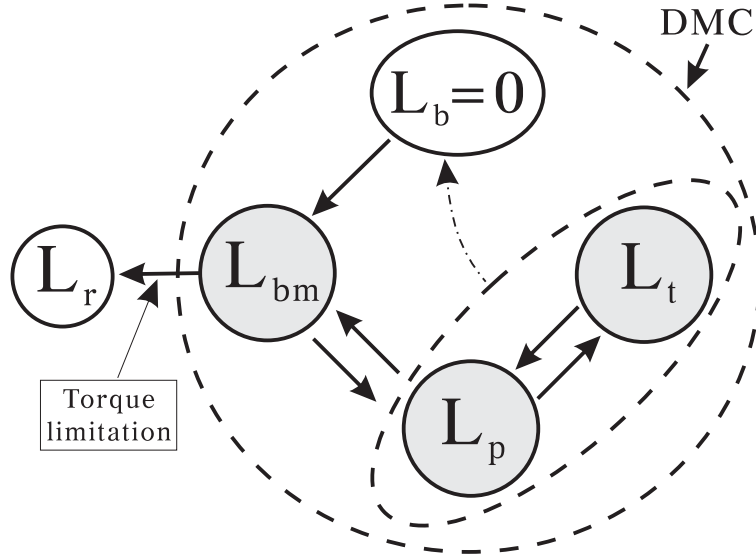


Figure 5.1: Angular momentum “flow” when DMC is used.

where subscript t shows that the variables describe the target satellite. Addition of (4.5) and (5.7) leads to:

$$\mathbf{L} + \mathbf{L}_t = \tilde{\mathbf{H}}_b \boldsymbol{\omega}_b + \tilde{\mathbf{H}}_{bm} \dot{\boldsymbol{\phi}}_m + \tilde{\mathbf{H}}_{br} \dot{\boldsymbol{\phi}}_r + \tilde{\mathbf{H}}_{bt} \boldsymbol{\omega}_{bt} + \mathbf{P}_f \quad (5.8)$$

where $\mathbf{P}_f = \hat{\mathbf{r}}_{bg} \mathbf{P} + \mathbf{r}_b \times \mathbf{P} + \mathbf{r}_{bt} \times \mathbf{P}_t$. Now substitution of (5.6) into (5.8) (noting that $\tilde{\mathbf{H}}_{bm} \tilde{\mathbf{H}}_{bm}^+$ is a unit matrix) leads to:

$$\tilde{\mathbf{H}}_b \boldsymbol{\omega}_b = 0$$

Hence, proving that if the manipulator is controlled using (5.6), it will “absorb” the angular momentum transferred to the base body, resulting in minimal attitude change.

Note that the utilization of the DMC is not limited only to the post-impact phase. If applied during the approach to the target, for the redistribution of angular momentum, it yields identical results to equation (4.21). This can be proved by equating the right hand sides of (4.21) and (5.6) to obtain the angular momentum conservation law (4.5). It should be noted that including a null space component in (5.6) is possible only in the case when the mass and inertia characteristics of the target satellite are known.

Fig. 5.1 depicts the angular momentum “flow” when DMC is applied. When the reaction wheels are not utilized the momentum is repeatedly exchanged only between \mathbf{L}_t , \mathbf{L}_{bm} and \mathbf{L}_p . Note that because \mathbf{L}_b is kept equal to zero at all times, \mathbf{L}_{bm} can become zero only when the system is at rest. Such state can be achieved if the unknown amount of momentum stored in \mathbf{L}_t , \mathbf{L}_{bm} and \mathbf{L}_p is transferred in the attitude devices.

The properties of DMC described above show that through the entire capturing operation only one simple control law could be utilized in order to perform:

- angular momentum redistribution during the approaching phase,
- base attitude minimization during the post-impact phase.

In the next two sections examples with both *reaction null space control* and *distributed momentum control* are included.

5.3 Application to single arm manipulator

For the simulations here, the torque profile for the reaction wheels as obtained in case S_{AB} (Fig. 4.11) is used. Again the manipulator is controlled using equation (4.21) (with $\mathbf{L} = 0$, and $\dot{\xi}_p = 0$). This leads to a partial bias momentum distribution in the chaser system. During the post-impact phase (starts at $t = 30$ sec.), while the remaining momentum is accommodated in the reaction wheels, DMC / RNSC is applied in order to maintain zero base attitude. The profile of the angular momentum in the reaction wheels, manipulator and target during the capturing operation is depicted in Fig. 5.2. As can be seen, after the contact with the target the attitude devices continue to accommodate the remaining momentum² until the manipulator and target come to a complete stop. In general, the utilization of both post-impact control laws can be done just for a limited amount of time since joint angle limitations could be reached. In this sense using the *bias momentum approach* during the approaching phase, reduces the amount of momentum left for accommodation after the contact. Hence, BMA facilitates the post-impact control.

During the post-impact phase the end-effector is in contact with the target object, hence, from the viewpoint of the chaser satellite a continuous external disturbance is exerted. In the case discussed here, the manipulator motion should guarantee the condition of the *coupling wrench theorem* in order for the base attitude to remain stationary. It should be noted that since the linear motion of the spacecraft is not controlled, the derivative of the coupling angular momentum ($\frac{d}{dt}\mathbf{L}_{bm}$) with respect to time is equal only to the reaction moments exerted on the base.

The resulting base attitude is depicted in Fig. 5.3. It shows that both post-impact controls used are successful in achieving minimal base attitude change without information about the mass or inertia characteristics of the target object.

It is interesting to note that, even though joint velocity minimization is performed³ when RNSC is applied, the joint velocity rates in the case when the manipulator is controlled using DMC are with lower magnitude. Comparison is made in Fig. 5.4-Fig. 5.5.

²Since $\mathbf{L}_{bm} = [2.46, 1.43, 0.41]$ Nms at the beginning of the post-impact phase, the remaining momentum to be stored in the reaction wheels is $[0.14, 1.57, 2.59]$ Nms.

³During the application of *reaction null space control*, the following gains were used:
 $\mathbf{K}_m = \text{diag}(10, 10, \dots, 10) \in R^{p \times p}$, $\mathbf{K}_b = \text{diag}(25, 25, 25) \in R^{3 \times 3}$.

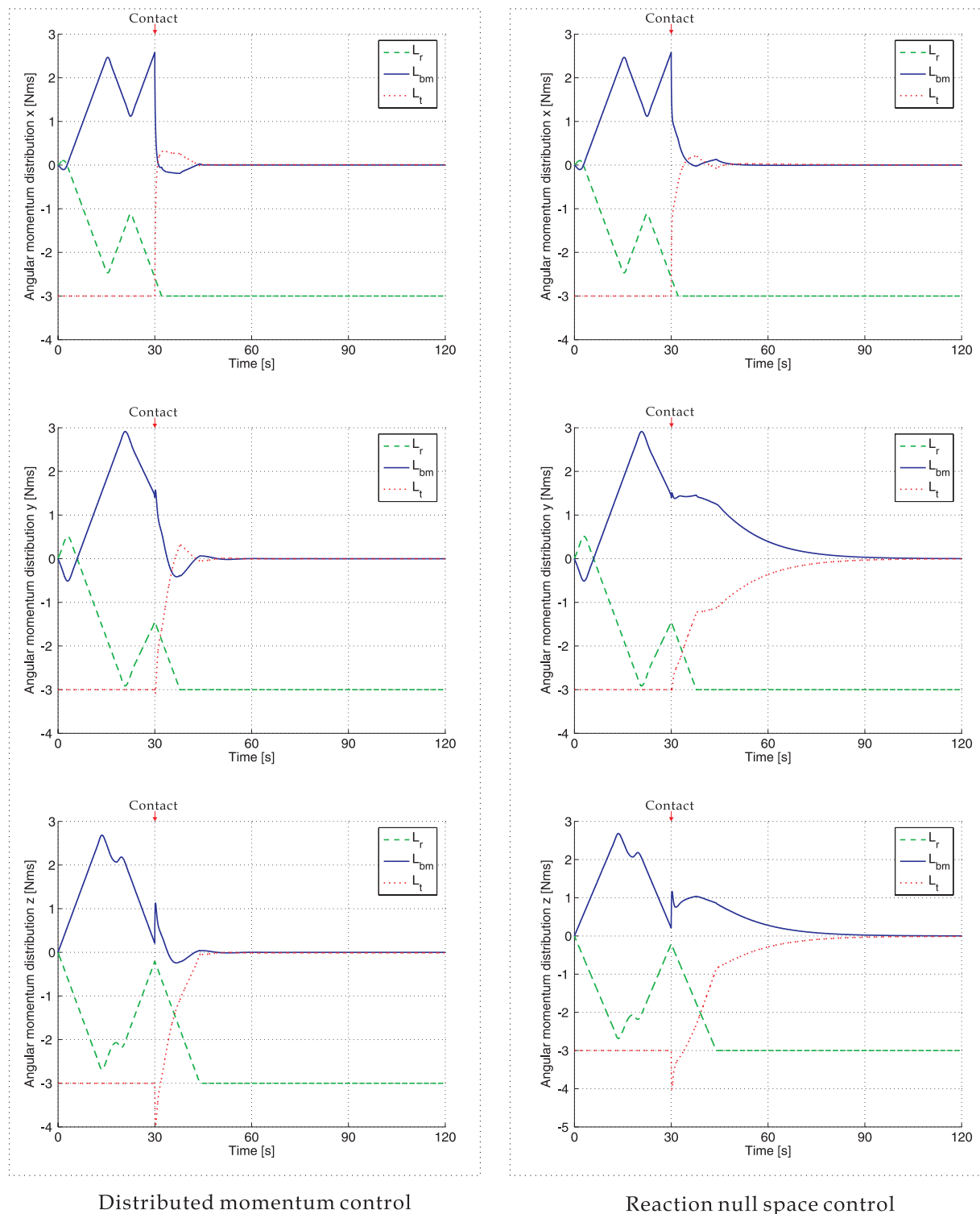


Figure 5.2: Angular momentum distribution when DMC and RNSC are used during the post-impact phase (x , y and z axis).

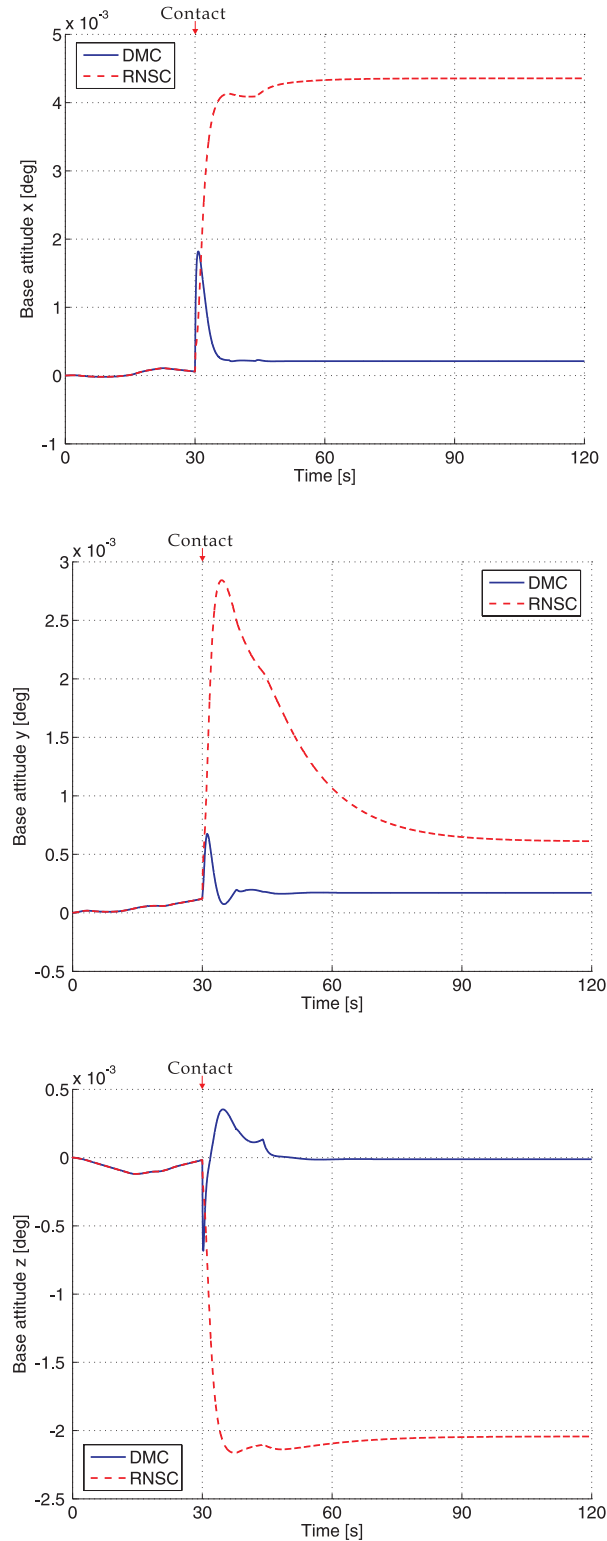


Figure 5.3: Base attitude comparison when DMC and RNSC are used (x , y and z axis).

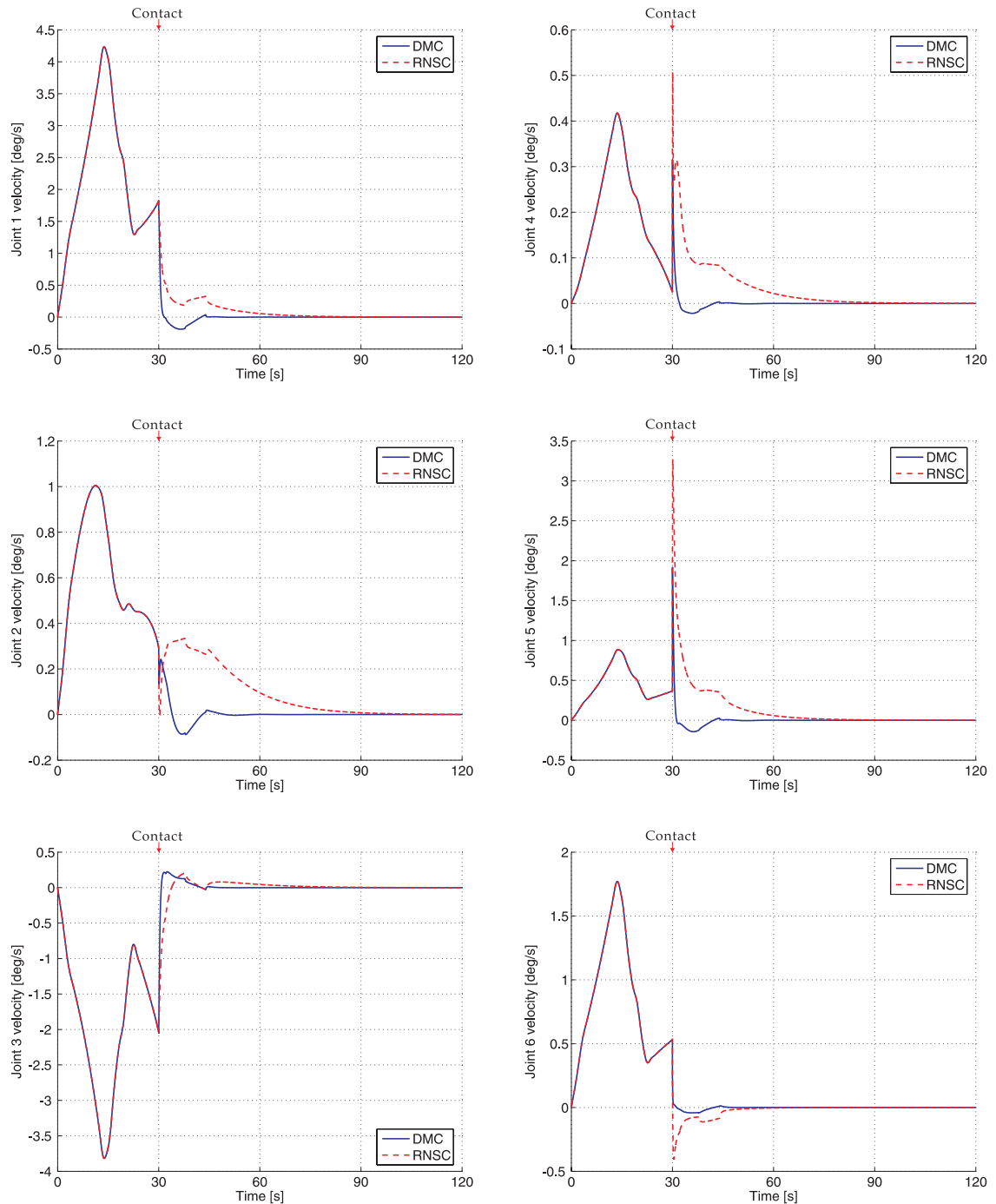


Figure 5.4: Joint (1-6) velocity rates when DMC and RNSC are used.

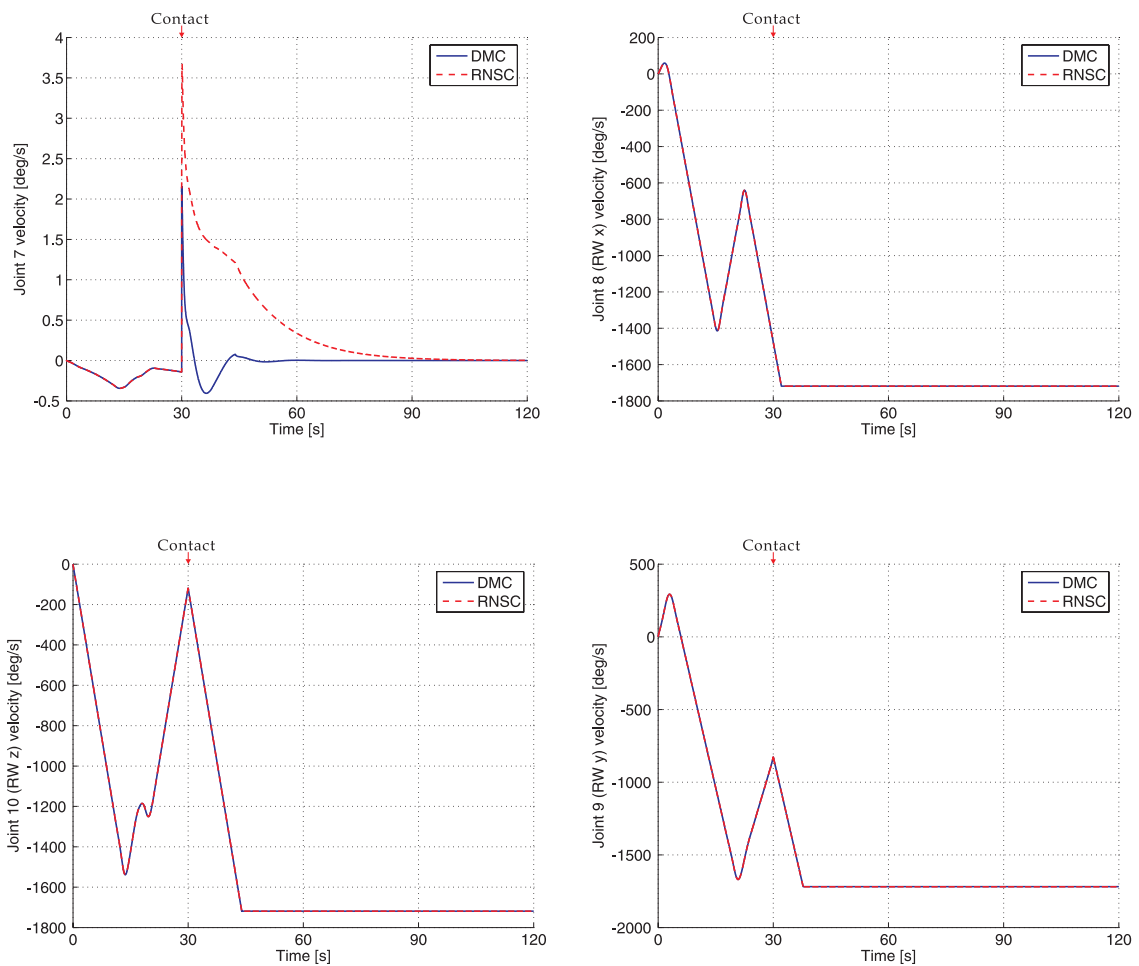


Figure 5.5: Joint (7-10) velocity rates when DMC and RNSC are used.

5.3.1 Utilization of gas/jet thrusters for attitude control

From the simulation results presented at the beginning of this section (Fig. 5.2-Fig. 5.5.) it becomes clear that the utilization of manipulator post-impact control for base attitude stabilization is advantageous. The discussion up to now was performed under the assumption that the available gas/jet thrusters are turned off. In this subsection however, this assumption will be dropped and thrust power will be used for base attitude control. The resulting system motion will be compared with the one when *distributed momentum control* is utilized. The aim of this subsection is to demonstrate the merits of using post-impact manipulator control even though powerful attitude devices are available.

Two cases will be considered:

- T** *approaching phase*: partial bias momentum
 post-impact phase: the manipulator joints are locked
 (altitude control via gas/jet thrusters, reaction wheels are not utilized);

- P** *approaching phase*: partial bias momentum
 post-impact phase: *distributed momentum control* is utilized.

In both cases **T** and **P**, during the approaching phase, the partial bias momentum distribution obtained after the application of *Step B* of the trajectory planning procedure in Section 4.5.2 is used (Fig. 4.10, case **S_{AB}**). This leads to a value of the coupling angular momentum $\mathbf{L}_{bm} = [2.46, 1.43, 0.41]^T$ Nms at the beginning of the post-impact phase ($t = 30$ sec.). The simulation in case **P** is the same as the one made in Section 5.3, nevertheless it will be recycled here as well, in order to make a clear comparison with the case when thrusters are used for base attitude control. As in Section 5.3 the target satellite has angular momentum $\mathbf{L}_t = [-3, -3, -3]^T$. As already noted, momentum distribution in the manipulator as the currently obtained is a favorable one, since the actual amount of momentum that needs to be redistributed during the post-impact phase is $\mathbf{L}_t + \mathbf{L}_{bm} = [-0.54, -1.57, -2.95]^T$.

Remark:

Again the utilization of the *bias momentum approach* during the approaching phase should be emphasized. It is clear that, managing the actually remaining angular momentum is much easier than doing so with the originally available one in the target satellite.

The main disadvantage of control strategies based on utilization only of powerful thrusters (as the one in case **T**), is the waste of expensive and nonrenewable resource as reaction jet's fuel. Furthermore, trying to suppress the base attitude motion without taking into consideration the nonlinearity effects resulting from the complicated system

dynamics might lead to unsatisfactory results from the viewpoint of attitude stabilization as well. On the other hand it should be considered that reaction jets with different capacity and accuracy exist. Not all spacecrafts are equipped with powerful thrusters. Furthermore, reaction controllers do not possess the same linear relationship between the input of the controller and its output torque (they are active in an *on-off mode*). Hence, it is difficult to perform the same fine attitude control as a manipulator arm does. It should be noted that, once momentum is stored in a system of reaction wheels its dumping can be performed using different methods. Some of them⁴ do not require the utilization of expensive thruster power. For more information about characteristics of attitude control systems see [105]. Although in practice thrusters are controlled using *bang-bang* or *pulse width modulation* based control, here for simplicity a PD feedback will be used.

The angular momentum profile in cases \mathbf{P} and \mathbf{T} is depicted in Fig. 5.6. The base attitude profiles are compared in Fig. 5.7. Although with small amplitude, in case \mathbf{T} the base oscillates. This however is not critical, since it is related to the gains for the PD controller. Finally, in Fig. 5.8 the torque applied by the thrusters is depicted. In total, the absolute value of the momentum change through the post-impact phase is $[1.12, 5.37, 7.35]$ Nms. This is in times more than the minimum necessary one $[-0.54, -1.57, -2.95]$ Nms. Such waist of fuel can is critical for the life of a spacecraft system, and should be avoided whenever possible. Hence, the utilization of post-impact control for the manipulator system is absolutely necessary requirement for future capturing missions.

⁴For example, magnetic unloading of the reaction wheels [105].

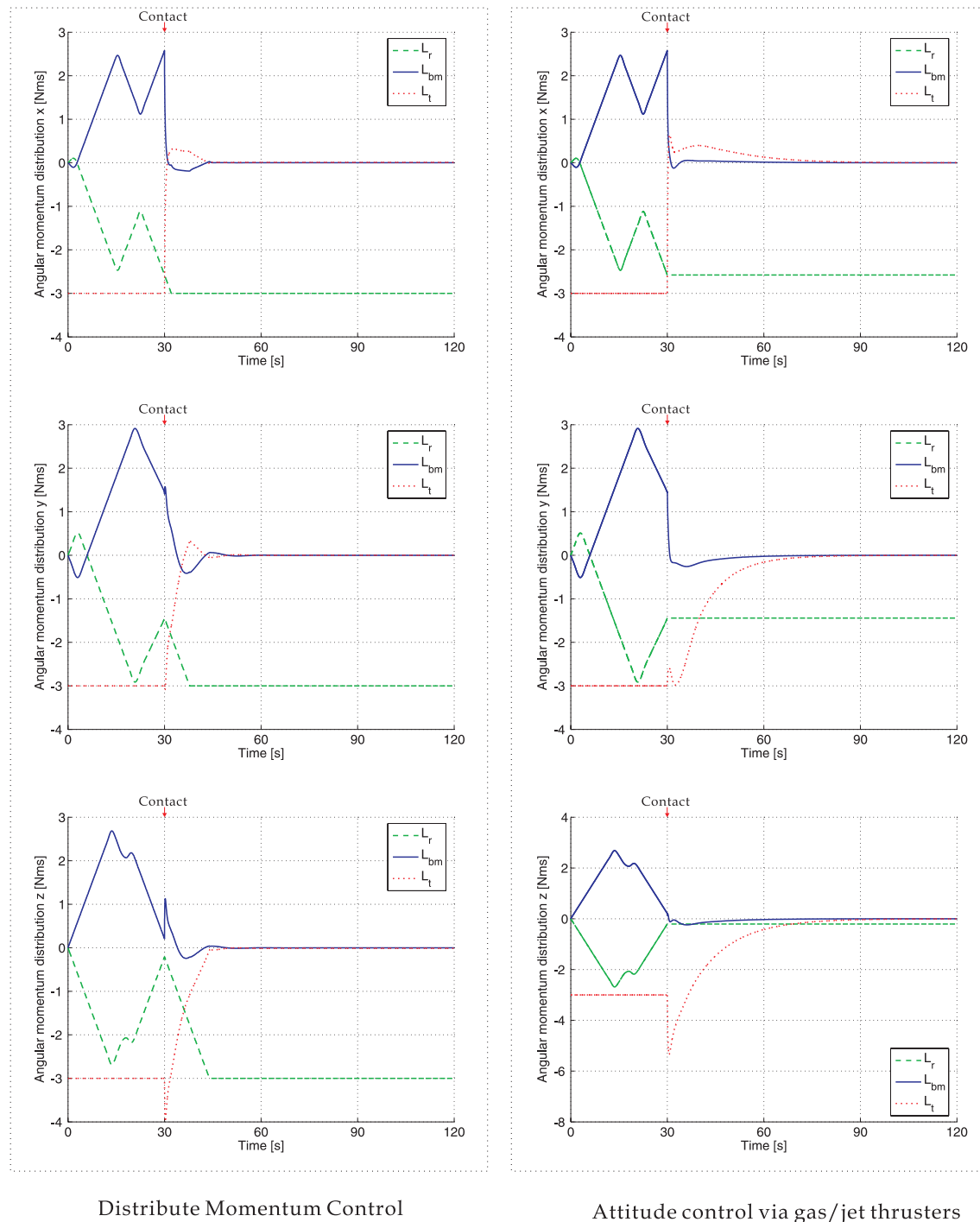


Figure 5.6: Comparison of angular momentum distributions in case of DMC, and attitude control via thrusters.

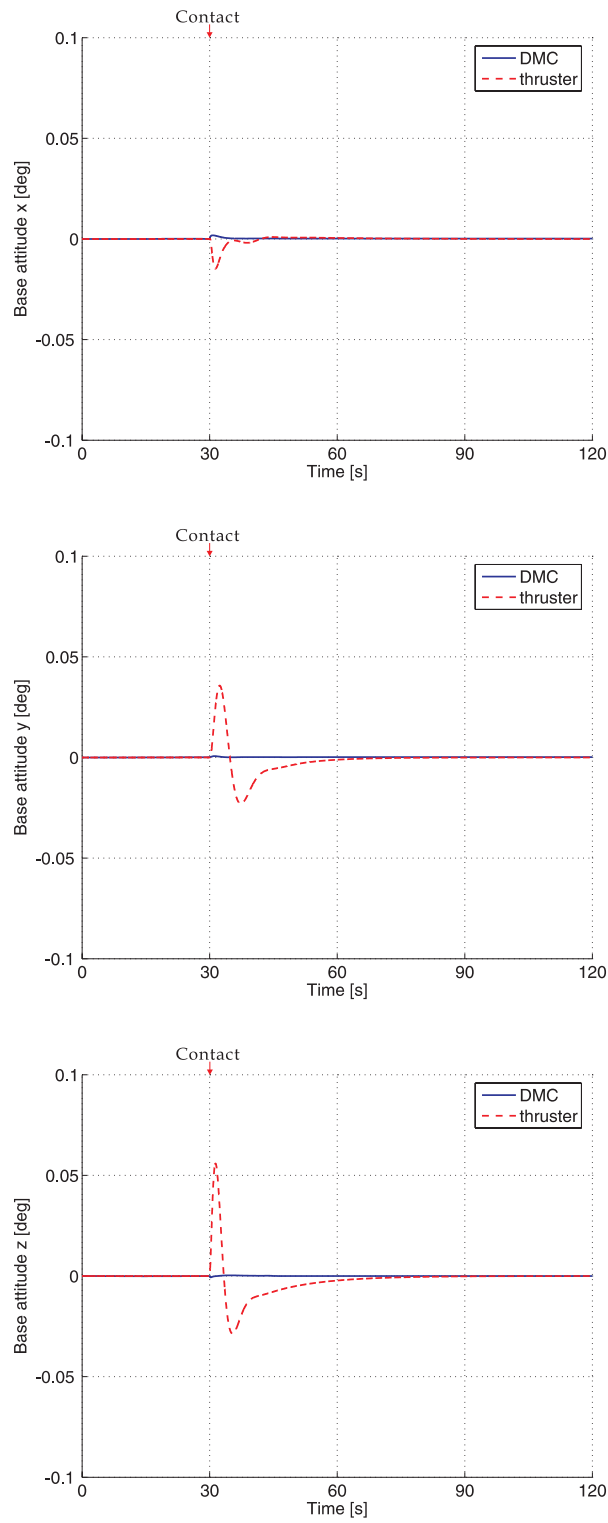


Figure 5.7: Comparison of the base attitude deviations in case of DMC, and attitude control via thrusters.

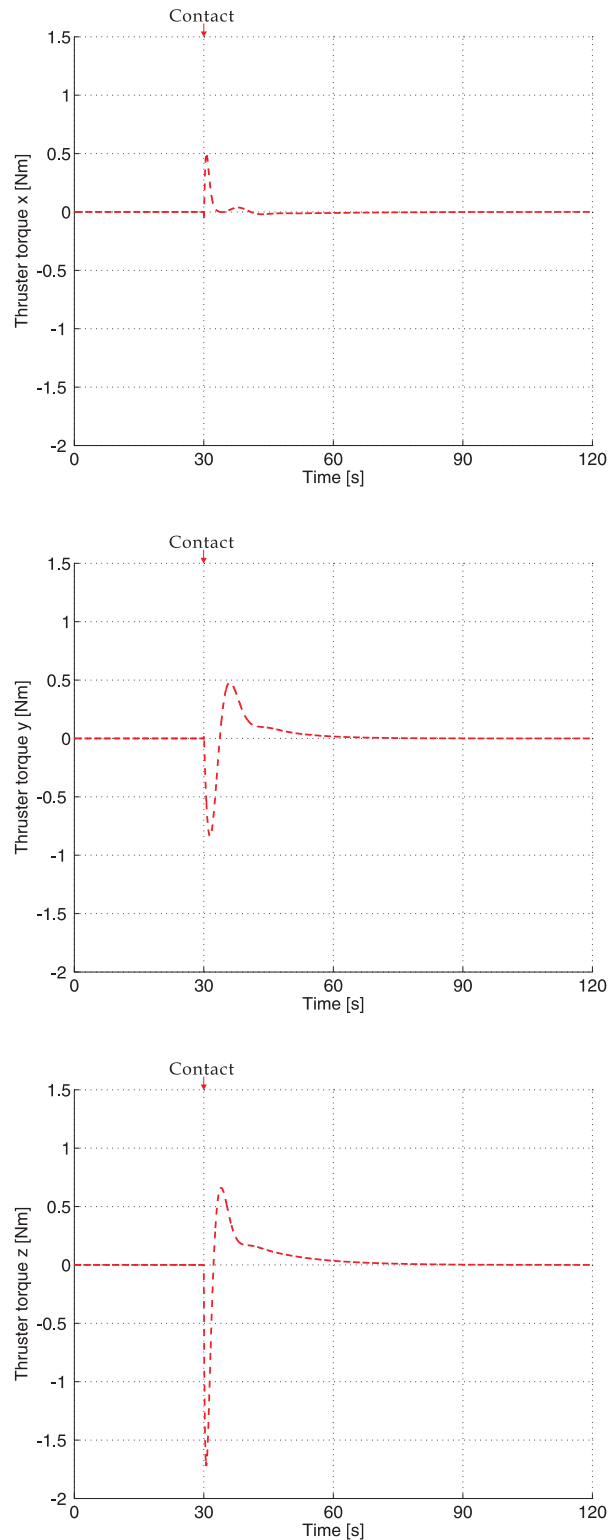


Figure 5.8: Torque applied by the thrusters.

5.4 Application to dual manipulator system

In this section a dual-arm manipulator is assumed to be mounted on the chaser spacecraft. The parameters of the system are included in Appendix F. Only the post-impact motion is considered and the manipulator is controlled using DMC.

As it was mentioned in Section 2.4.2, after a dual-arm manipulator system establishes contact with a target satellite a closed loop is formed. Hence, the remaining degrees of redundancy (DOR) are less than the DOF of the original system (before the capture). In such case, controlling only an independent set of joints is sufficient to guarantee minimal base deviation. Here, joints 1, 3 and 5 are (arbitrary) chosen to be this independent set⁵. The angular momentum profile for this case is depicted in Fig. 5.9⁶. Reaction wheels are not utilized to accommodate the momentum of the target satellite, and as a result the two manipulators perform continuous motion. The resulting base attitude change is depicted in (Fig. 5.10). Finally, the initial and final system configurations are compared in Fig. 5.11 (the actively controlled joints are indicated with red circle).

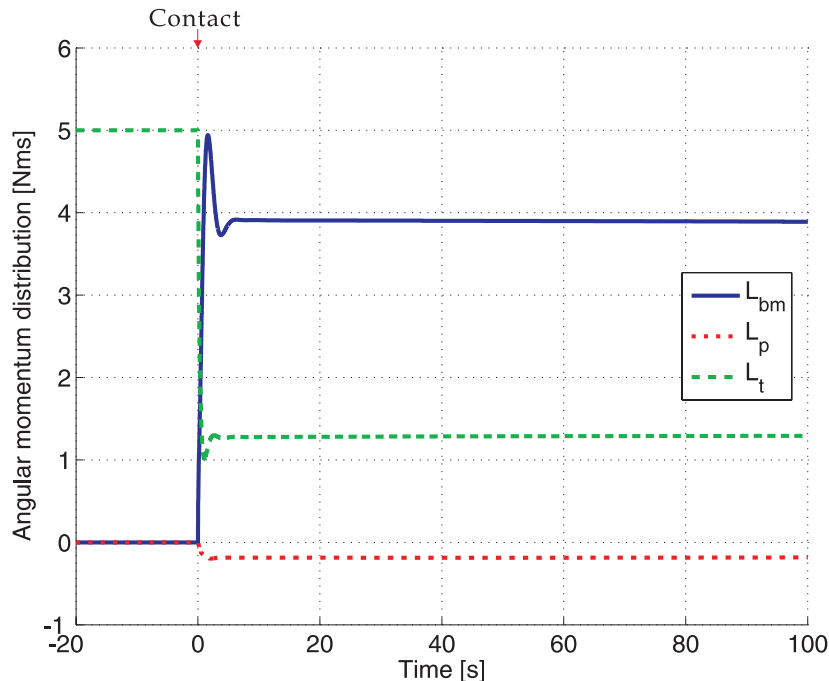


Figure 5.9: Angular momentum distribution for the dual-arm case.

⁵Choosing any set of joints does not alter the result, hence, in this sense controlling only one of the arms would be sufficient.

⁶The angular momentum in both manipulators is included in the profile of L_{bm} .

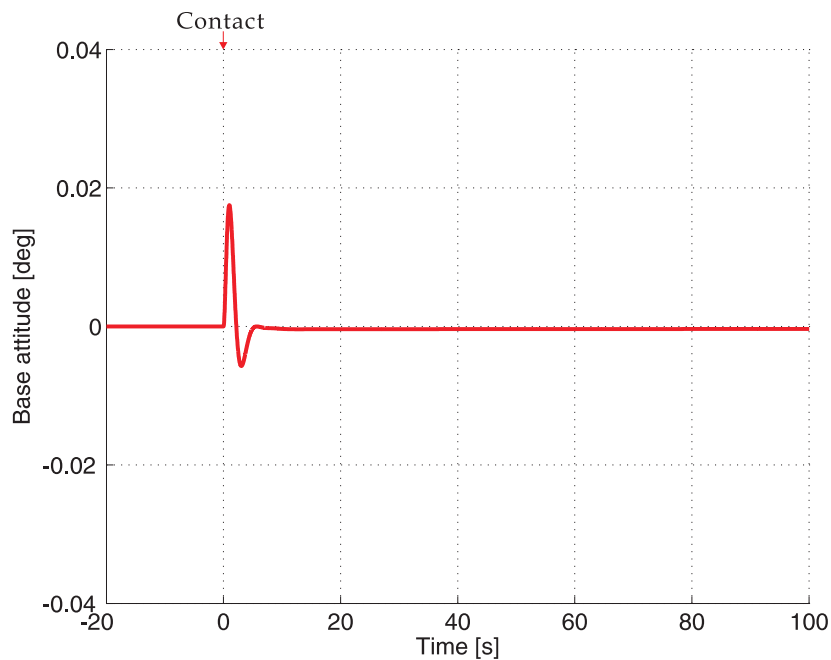


Figure 5.10: Base attitude deviation for the dual-arm case.

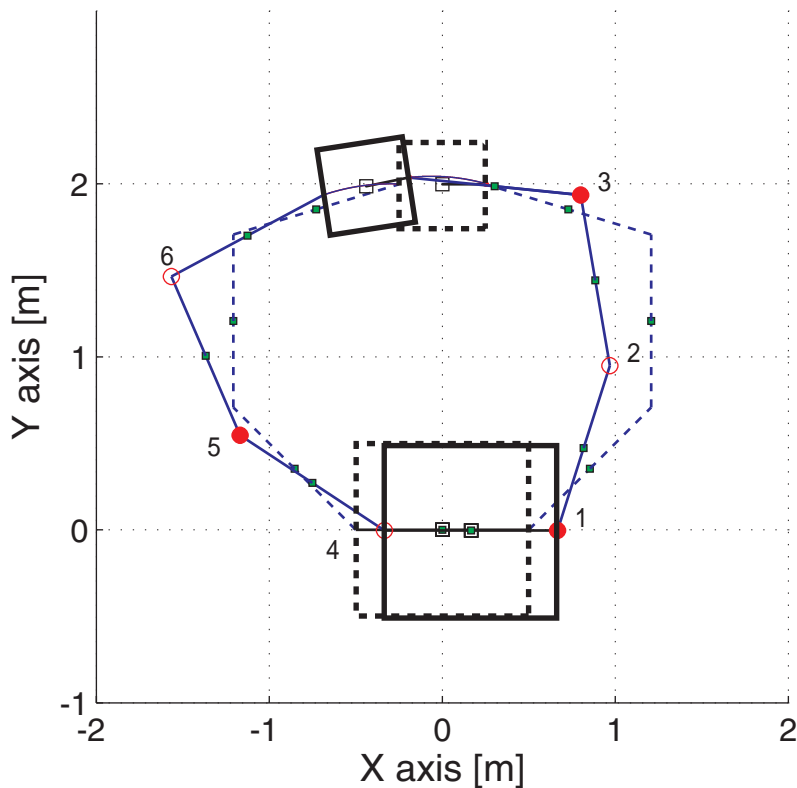


Figure 5.11: Initial and final manipulator configurations in the post-impact phase.

Chapter 6

Conclusions and future work

In this dissertation, several fundamental issues arising during the analysis of a satellite capturing operation are studied. A systematic treatment of different problems related to path and trajectory planning is made. The different phases of interaction between a chaser and target satellites are studied and solutions that might overcome practical difficulties are presented. In the sequel, the contents of this dissertation is summarized, and some possible directions for future research are proposed.

6.1 Summary

Chapter 1 introduces different problems that need to be dealt with in order to successfully perform servicing, inspection and assembling operations in orbit. A brief literature review of the dynamic modeling, planning and control strategies (related to a satellite capturing operation) introduced up to now is made. These serve as a motivation for the following study.

Chapter 2 includes a general formulation for the kinematics and dynamics of manipulator systems with open and closed-loop structure. During the derivation of the equations of motion a free-floating base body is assumed. The formulation is made using a set of independent coordinates that sufficiently describe the motion of the system of interest. The derived dynamical model is used as a framework for the remaining chapters of this thesis.

Chapter 3 includes some of the fundamental control concepts and strategies that are closely related to this study. It makes an overview of the concepts of reactionless manipulation, methods for redundancy resolution and task priority control.

Chapter 4 deals with the approaching phase of a satellite capturing operation. The first three sections introduce the problems that need to be solved, the assumptions upon which the study is made, and a generalization of the *coupling angular momentum* concept. This generalization is stated as a theorem, referred to as the *coupling wrench theorem*. It establishes a clear condition which if satisfied, the stationary state of the spacecraft base will be maintained in the presence of external forces/torques. This condition proves to be useful for the formulation of *favorable angular momentum distributions*, which if obtained during the manipulator approaching motion, lead to certain advantages from the viewpoint of base attitude control during the post-impact phase. Furthermore, the *coupling wrench theorem* is used in Section 5.2 for the formulation of a post-impact control law, that guarantees minimal base attitude deviation.

Section 4.4 deals with the problem of designing a reactionless path for a n DOF manipulator to a point in Cartesian space. Although the discussion is made from the viewpoint of stationary satellite capturing operation, the solution to such problem can have many practical applications. The concept of *Holonomic Distribution Control* (HDC) is introduced. It is pointed out that if the manipulator is controlled using HDC, simplifications to the path planning problem can be achieved. The newly introduced control is partially based on a strategy previously employed for solving the inverse kinematics problem for a redundant manipulator arm by partitioning the Jacobian matrix into *full rank* minors. In short, the main idea is to partition the manipulator joint variables into different sets. Each of these sets, referred to as *primitives*, has a degree of redundancy one with respect to the base attitude motion (one dimensional *distribution* in joint space is used). It was pointed out that by choosing different *primitives* to be used during different stages of the manipulator motion the planning process can be simplified significantly. The planning problem that needs to be solved when *holonomic distribution control* is employed is a typical nonlinear mixed-variables optimization problem. In order to find solution, a *mesh adaptive direct search algorithm* is used.

Up to now, utilization of manipulator pre-impact configuration for minimizing the base reactions, as a result of a force impulse applied at the end-effector, have been discussed by a number of researchers (as pointed out in Chapter 1). In the case when a force impulse (with known direction) is applied for an infinitesimally small time period, the above approach can yield satisfactory results. However, in the case of a continuous contact with a tumbling target satellite, where the magnitude and direction of the forces has to be assumed unknown, obtaining a pre-impact manipulator configuration is not advantageous. Section 4.5 deals with a tumbling target satellite capturing operation, where the idea of the *bias momentum approach* (BMA) is introduced. It is based on obtaining a favorable

angular momentum distribution in the chaser satellite before the contact with the target object. Advantages resulting from the application of this new approach are discussed. In addition, notes on its practical implementation are made. The problem of trajectory planning for the end-effector to a grasping point, positioned on the target satellite (when BMA is applied) is addressed. It should be noted that, for a general 3D manipulator system, trajectory planning for such case, is still a challenge for the research community¹. We utilize a *two step* method based on the utilization of numerical optimization techniques, which led us to satisfactory results in most of the cases studied. A discussion on the influence of the state variables utilized for the optimization procedure, on the algorithm convergence rate is made in Section 4.5.3. A numerical simulation using a seven DOF manipulator is performed in order to verify the presented control strategy.

Chapter 5 is dedicated to the post-impact phase of a capturing operation. Analysis of manipulator motions that result in maintaining the stationary state of the spacecraft's base in the presence of external forces is made, for this purpose we make use of the newly formulated *coupling wrench theorem* in Chapter 4. The concept of *distributed momentum control* (DMC) is introduced and compared with existing post-impact control strategies. A new form of the *reaction null space control* (RNSC) initially introduced in [82] is presented. In Section 5.3.1 a comparison between a strategy that makes use of manipulator post-impact control, and one that relies on gas/jet thrusters is made. It is shown that the utilization of powerful attitude devices does not necessarily lead to achieving best performance from the viewpoint of fuel consumption. Furthermore, it was pointed out that the *distributed momentum control* does not use information about the mass and inertia characteristics of the target satellite. Hence, from practical point of view its implementation is straightforward. The merit and validity of both *distributed momentum control* and *reaction null space control* are verified by numerical simulations. It was observed that although joint velocity minimization in the case of DMC, was performed only locally using the pseudoinverse solution, the resultant joint velocity rates have smaller magnitude as compared to the case when RNSC is applied.

6.2 Future work

It is my hope that this work will be helpful for further study and analysis of the problems underlying space manipulators during a satellite capturing operation. There are still a lot of problems and much remains to be done. Some of the possible future directions of research are summarized below:

¹Up to the knowledge of the author of this thesis.

- In my opinion experimental work needs to be done for the practical realization of the control algorithms proposed in this thesis. This might reveal different problems and directions for research.
- It is interesting to consider joint flexibility in the cases when *Bias Momentum Approach* or the two post-impact control laws introduced in Chapter 5 are applied.
- The utilization of gripper for the impact phase is absolutely necessary. Research in this direction could be valuable. When multi-fingered hand manipulator is used it is necessary to study how to optimize the grasping quality by controlling the contact trajectory. Problems related to the nonholonomic nature of the constraints that appear in the case mentioned above will occur.
- The problem of applying impedance control in the case when the manipulator is loaded with angular momentum is interesting.
- The utilization of dual-manipulator system for satellite capture is interesting especially from the viewpoint of trajectory planning during the approaching phase.
- The implementation of the path planning strategy presented in Chapter 4.4 for a 3D manipulator is an interesting direction of research. Furthermore, convergence analysis is necessary².
- As discussed in Section 4.4.1 a one dimensional *distribution* in joint space is always integrable. Therefore, there should be an algebraic function that spans a smooth one dimensional manifold (on which the manipulator motion evolves). Formulating such an algebraic constraint can be helpful from the viewpoint of planning.

²Currently I have been dealing with this problem.

Bibliography

- [1] Om P. Agrawal, and Y. Hu, “Global optimum path planning for a redundant space robot,” *The Robotic Institute CMU, Pittsburgh, Pennsylvania 15213*, CMU-RI-TR-91-15, December 1991.
- [2] S. K. Agrawal, G. Hirzinger, K. Landzettel, and R. Schwertassek, “A new laboratory simulator for study of motion of free-floating robots relative to space targets,” *IEEE Trans. on Robot. and Automat.*, vol. 12, no. 4, pp. 627-633, 1996.
- [3] J. Angeles, and S. Lee, “The formulation of dynamical equations of holonomic mechanical systems using a natural orthogonal complement,” *ASME J. Appl. Mech.*, vol. 55, pp. 243-244, 1998.
- [4] J. Angeles, “Fundamentals of Robotic Mechanical Systems: Theory, Methods, and Algorithms,” Second Edition, *Springer*, 2002.
- [5] M. Annapragada, and S. K. Agrawal, “Design and experiments on a free-floating planar robot for optimal chase and capture operation in space,” *Robotics and Autonomous Systems*, vol. 26, pp. 281-297, 1999.
- [6] W. Armstrong, “Recursive solution to the equations of motion of an n link manipulator,” *Proc. of the 5th World Congress on Theory and Machines and Mechanisms*, vol. 2, pp. 1343-1346, 1979.
- [7] H. Asada, and K. Youcef-Toumi, “Direct Drive Robots: Theory and Practice,” *MIT Press, Cambridge MA*, 1986.
- [8] U. Ascher, H. Chin, L. Petzold, and S. Reich, “Stabilization of constraint mechanical systems with DAEs and invariant manifolds,” *J. Mech. Struct. Machines*, 23, pp. 135-158, 1993.
- [9] U. Ascher, and L. Petzold, “Stability of computational methods for constrained dynamics systems,” *SIAM J. SISI*, 14, pp. 95-120, 1993.
- [10] U. Ascher, H. Chin, S. Reich, and S. Reich, “Stabilization of DAEs and invariant manifolds,” *Numer. Math.*, 67, pp. 131-149, 1994.
- [11] C. Audet, and J. E. Dennis, Jr., “Pattern Search Algorithms for Mixed Variable Programming,” *SIAM J. Optim.*, 11, (3), pp. 573-594, 1999.

- [12] C. Audet, and J. E. Dennis, Jr., "Mesh Adaptive Direct Search Algorithms for Constrained Optimization," *SIAM J. Optim.*, (to appear).
- [13] J. Baillieul, J. M. Hollerbach, and R. W. Brockett, "Programming and control of kinematically redundant manipulators," *Proc. 23rd IEEE Conf. Decision and Control, IEEE*, New York, pp. 768-774, 1984.
- [14] J. Baillieul, "Avoiding obstacles and resolving kinematic redundancy," *Proc. IEEE Int. Conf. on Robotics and Automation (ICRA)*, San Francisco, California, pp. 1698-1704, 1986.
- [15] J. Baumgarte, "Stabilization of Constraints and Integrals of Motion in Dynamical Systems," *Computer Methods in Applied Mechanics and Engineering*, 1, pp. 1-16, 1972.
- [16] U. Becker, and L. Kerstein, "An evolutionary approach towards unmanned orbit servicing," *Space Technology*, vol. 12, no. 1, pp. 45-56, 1992.
- [17] B. Benhabib, A. A. Goldenberg, and R. G. Fenton, "A solution to the inverse kinematics of redundant manipulators," *Journal of Robotic Systems*, 2, pp. 373-385, 1985.
- [18] A. Ben-Israel, and T. Greville, "Generalized Inverses: Theory and Applications," *John Wiley & Sons*, New York, 1981.
- [19] F. Caccavale, and B. Siciliano, "Kinematic control of redundant free-floating robotic systems," *J. Adv. Robot.*, vol. 15, pp. 429-448, 2001.
- [20] C. L. Chung, S. Desa, and C. W. deSilva, "Base reaction optimization of redundant manipulators for space applications," *The Robotic Institute CMU, Pittsburgh, Pennsylvania 15213, CMU-RI-TR-88-17*, September 1988.
- [21] R. Colbaugh, M. Trabatti, and K. Glass, "Redundant nonholonomic mechanical systems: characterization and control," *Robotica*, vol. 17, issue 02, pp. 203-217, 1999.
- [22] J. J. Craig, "Introduction to Robotics: Mechanics and Control," Second Edition, *Addison-Wesley Publishing Company, Reading, MA*.
- [23] X. Cyril, G. J. Jaar, and A. K. Misra, "The effect of payload impact on the dynamics of a space robot," *Proc. of IEEE/RSJ Int. Conf. on Intelligent Robots and Systems (IROS)*, Yokohama, Japan, pp. 2070-2075, 1993.
- [24] X. Cyril, G. J. Jaar, and A. K. Misra, "Dynamical modeling and control of a spacecraft-mounted manipulator capturing a spinning satellite," *Acta Astronautica*, vol. 35, no. 2/3, pp. 167-174, 1995.
- [25] C. Dickson, and R. H. Cannon, "Experimental results of two free flying robots capturing and manipulating a free-floating object," *Proc. of IEEE/RSJ Int. Conf. on Intelligent Robots and Systems*, Pittsburgh, PA, pp. 51-58, 1995.

- [26] D. N. Dimitrov, and K. Yoshida, "Utilization of the bias momentum approach for capturing a tumbling satellite," *Proc. of IEEE/RSJ Int. Conf. on Intelligent Robots and Systems (IROS)*, Sendai, Japan, pp. 3333-3338, September 28 - October 2, 2004.
- [27] D. N. Dimitrov, and K. Yoshida, "Momentum distribution in a space manipulator for facilitating the post-impact control," *Proc. of IEEE/RSJ Int. Conf. on Intelligent Robots and Systems (IROS)*, Sendai, Japan, pp. 3345-3350, September 28 - October 2, 2004.
- [28] R. V. Dubey, J. A. Euler, and S. M. Babcock, "An efficient gradient projection scheme for a seven-degree-of-freedom redundant robot with spherical wrist," *Proc. IEEE Int. Conf. on Robotics and Automation (ICRA)*, Philadelphia, Pennsylvania, pp. 28-36, 1988.
- [29] S. Dubowsky, and M. A. Torres, "Path Planning for Space Manipulators to Minimize Spacecraft Attitude Disturbance," *Proc. IEEE Int. Conf. on Robotics and Automation (ICRA)*, Sacramento CA, vol. 3, pp. 2522-2528, 1991.
- [30] S. Dubowsky, and E. Papadopoulos, "The kinematics, dynamics, and control of free-flying and free-floating space robotic systems," *IEEE Trans. on Robot. and Automat.*, vol. 9, no. 5, October 1993.
- [31] C. W. Gear, "Numerical Initial Value Problems in Ordinary Differential Equations," *Prentice-Hall Series in Automatic Computation*, 1971.
- [32] G. Gilardi, S. Kawamoto, and S. Kibe, "Angular motion control of non-cooperative satellites using a two-arm manipulator," *54th IAC, IAC-03-A.6.03*, Bremen, Germany, 2003.
- [33] G. Hart, "Multidimensional analysis: algebras and systems for science and engineering," Springer Verlag, 1995.
- [34] R. Hartshorne, "Algebraic Geometry," *Springer-Verlag*, Berlin, 1977.
- [35] U. Hillenbrand, and R. Lampariello, "Motion and parameter estimation of a free-floating space object from range data for motion prediction," *Proceeding of the 8th International Symposium on Artificial Intelligence and Robotics & Automation in Space (i-SAIRAS)*, 2005.
- [36] S. Hirose, and S. Ma, "Redundancy Decomposition Control for Multijoint Manipulator," *Proc. IEEE Int. Conf. on Robotics and Automation (ICRA)*, 1, pp. 119-124, 1989.
- [37] J. M. Hollerbach, "A recursive Lagrangian formulation of manipulator dynamics and a comparative study of dynamics formulation complexity," *IEEE Trans. Syst., Man., Cybern.*, SMC-10, pp 730-736, 1980.
- [38] P. C. Hughes, "Spacecraft Attitude Dynamics," *John Wiley & Sons*, 1986.

- [39] N. Inaba, and M. Oda, "Autonomous satellite capture by a space robot," *Proc. of IEEE/RSJ Int. Conf. on Intelligent Robots and Systems (IROS)*, San Fransisco, vol. 2, pp. 1169-1174, 2000.
- [40] G. Jaar, X. Cyril, and A. K. Misra, "Dynamic modeling and control of a spacecraft-mounted manipulator capturing a spinning satellite," *43rd Congress of the Int. Astronautic Federation, IAF-92-0029*, 1992.
- [41] S. Jacobsen, C. Lee, C. Zhu, and S. Dubowsky, "Planning of Safe Kinematic Trajectories for Free Flying Robots Approaching an Uncontrolled Spinning Satellite," *Proceedings of the ASME 27th Annual Biennial Mechanisms and Robotics Conference*, Montreal, Canada, September 2002.
- [42] S. Jacobsen, "Planning and Control During Robotic Satellite Capture," *MS Thesis, Department of Mechanical Engineering, MIT*, 2003.
- [43] J. Garcia de Jalón, J. Unda, and A. Avello, "Natural coordinates for the computer analysis of multibody systems," *Computer Methods in Applied Mechanics and Engineering*, vol. 56, pp. 309-327, 1986.
- [44] J. Garcia de Jalón, J. Unda, A. Avello, and J. M. Jimenez, "Dynamic analysis of three-dimensional mechanisms in natural coordinates," *ASME J. of Mechanisms, Transmissions and Automation in Design*, vol. 109, pp. 460-465, 1987.
- [45] J. Garcia de Jalón, E. Bayo, "Kinematic and dynamic simulation of multibody systems," Springer-Verlag, 1993.
- [46] J. Garcia de Jalón, E. Álvarez, and F. A. Ribera, "Improved dynamic formulations for the dynamic simulation of multibody systems," <http://mat21.etsii.upm.es/mbs/matlabcode/Mbs3dv1.0/mba3d.htm>
- [47] P. Jasiobedzki, M. Greenspan, and G. Roth, "Pose Determination and Tracking for Autonomous Satellite Capture," *Proceeding of the 6th International Symposium on Artificial Intelligence and Robotics & Automation in Space (i-SAIRAS)*, Canadian Space Agency, St-Hubert, Quebec, Canada, June 18-22, 2001.
- [48] H. Kamimura, S. Kawamoto, S. Nishida, H. Hashimoto, S. Kimura, H. Yamamoto, et al., "Detection and motion estimation of small target using color image processing," *24th ISTS*, Miyazaki, Japan, May 30 - June 6, 2004.
- [49] J. W. Kamman, and R. L. Huston, "Dynamics of constrained multibody systems," *ASME Journal of Applied Mechanics*, vol. 51, pp. 899-903, 1984.
- [50] T. R. Kane, and D. A. Levinson, "The use of Kane's dynamical equations in robotics," *Int. J. Robot. Automat.*, vol. 2, pp. 3-21, 1983.
- [51] T. Kane, P. Likins, and D. Levinson, "Spacecraft Dynamics," *McGraw-Hill*, 1983.

- [52] S. Kawamoto, K. Matsumoto, and S. Wakabayashi, "Ground experiment of mechanical impulse method for uncontrollable satellite capturing," *Proceeding of the 6th International Symposium on Artificial Intelligence and Robotics & Automation in Space (i-SAIRAS)*, Montreal, Canada, 2001.
- [53] S. S. Kim, "A subsystem synthesis method for efficient vehicle multibody dynamics," *Multibody System Dynamics*, 7, pp. 189-207, 2002.
- [54] D. King, "Space Servicing: Past, Present and Future," *Proceeding of the 6th International Symposium on Artificial Intelligence and Robotics & Automation in Space (i-SAIRAS)*, Montreal, Canada, 2001.
- [55] C. A. Klein, and S. Huang, "Review of pseudoinverse control for use with kinematically redundant manipulators," *IEEE Trans. Sys. Man Cybernetics SMC*, 13(3), pp. 245-250.
- [56] Y. Y. Kuen, "Geometry, dynamics and control of parallel manipulators," *Hong Kong University of Science and Technology*, Ph.D. Thesis, August 2002.
- [57] J.-C. Latombe, "Robot Motion Planning," *Kluwer Academic Publishers*, 1991.
- [58] S. M. Lavalle, "Planning Algorithms," <http://msl.cs.uiuc.edu/~lavalle/>
- [59] M. D. Lichter, and S. Dubowsky, "State, shape and parameter estimation of space objects from range images," *Proc. IEEE Int. Conf. on Robotics and Automation (ICRA)*, New Orleans, LA, April 2004.
- [60] J. Y. S. Luh, M. W. Walker, and R. P. C. Paul, "On-line computational scheme for mechanical manipulators," *J. Dyn., Syst., Meas, Contr.*, vol. 102, no. 1, pp. 69-76, 1980.
- [61] Y. Masutani, Y. Okada, T. Iwatsu, H. Ikeda, and F. Miyazaki, "Estimation of general three-dimensional motion of an unknown rigid body under no external forces and moments," *Advanced Robotics*, vol. 9, no. 6, pp. 675-691, 1995.
- [62] S. Matsumoto, et al., "Satellite capturing strategy using agile orbit servicing vehicle, Hyper-OSV," *Proc. IEEE Int. Conf. on Robotics and Automation (ICRA)*, Washington DC, pp. 2309-2314, 2002.
- [63] S. Matsumoto, S. Jacobsen, S. Dubowsky, and Y. Ohkami, "Approach Planning and Guidance for Uncontrolled Rotating Satellite Capture Considering Collision Avoidance," *Proceeding of the 7th International Symposium on Artificial Intelligence and Robotics & Automation in Space (i-SAIRAS)*, Nara, Japan, May 2003.
- [64] S. Matunaga, T. Kanzawa, and Y. Ohkami, "Rotational motion-damper for the capture of an uncontrolled floating satellite," *Cont. Eng. Practice*, vol. 9, pp. 199-205, 2001.
- [65] F. Mnif, and J. Ghommem, "Genetic algorithms adaptive control for an underactuated system," *Int. J. of computational cognition*, vol. 3, no. 1, pp. 12-20, March 2005.

- [66] S. Ali, A. Moosavian, and E. Papadopoulos, "Kinematic control of redundant free-floating robotic systems," *Journal of Advanced Robotics*, vol. 15, pp. 429-448, 2001.
- [67] R. Mukherjee, and M. Kamon, "Almost smooth time-invariant control of planar space multibody systems," *IEEE Trans. on Robot. and Automat.*, vol. 15, no. 2, April 1999.
- [68] R. W. Murray, Z. Li, and S. S. Sastry "A Mathematical Introduction to Robotic Manipulation," *CRC Press, Boca Raton, FL*, 1993.
- [69] H. Nagamatsu, T. Kubota, and I. Nakatani, "Capture strategy for retrieval of a tumbling satellite by a space robotic manipulator," *Proc. IEEE Int. Conf. on Robotics and Automation (ICRA)*, pp. 70-75, 1996.
- [70] Y. Nakamura, H. Hanafusa, and T. Yoshikawa, "Task-priority based redundancy control of robot manipulators," *Int. Journal of Robotics Research.*, vol. 6, no. 2, 1987.
- [71] Y. Nakamura, H. Hanafusa, "Optimal redundancy control of robot manipulators," *The Int. J. of Robot. Research*, vol. 6, no. 1, pp. 32-42, 1987.
- [72] Y. Nakamura, and M. Ghodoussi, "Dynamic Computation of Closed-Link Robot Mechanisms with Non-redundant and Redundant Actuators," *IEEE Trans. on Robot. and Automat.*, vol. 5, no. 3, June 1989.
- [73] Y. Nakamura, and R. Mukherjee, "Nonholonomic Path Planning of Space Robots via a Bidirectional Approach," *IEEE Trans. on Robot. and Automat.*, vol. 7, no. 4, August 1991.
- [74] Y. Nakamura, "Advanced Robotics: Redundancy and Optimization," *Addison-Wesley Publishing Company*, 1991.
- [75] Y. Nakamura, and R. Mukherjee, "Exploiting Nonholonomic Redundancy of Free-Flying Space Robots," *IEEE Trans. on Robot. and Automat.*, vol. 9, no. 4, August 1993.
- [76] Y. Nakamura, F. Sasaki, and S. Nakasuka, "Guidance and control of "Tethered retriever" for future on-orbit service missions," *24th ISTS*, Miyazaki, Japan, May 30 - June 6, 2004.
- [77] S. Nakasuka, and T. Fujiwara, "New method of capturing tumbling object in space and its control aspects," *Proc. IEEE Int. Conf. on Control Applications*, Kohala Coast, Hawaii, August 22-27, pp. 973-978, 1999.
- [78] S. Nakasuka, R. Funase, S. Kimura, F. Terui, K. Yoshihara, and T. Yamamoto, "Micro-LABSAT experiment of target motion estimation and tracking for future on-orbit service missions," *24th ISTS*, Miyazaki, Japan, May 30 - June 6, 2004.
- [79] D. Negrut, R. Serban, and F. A. Potra, "A topology based approach for exploiting sparsity in multibody dynamics. Joint Formulation," *Mechanics of Structures and Machines*, 25, pp. 379-396, 1997.

- [80] D. N. Nenchev, "Restricted Jacobian matrices of redundant manipulators in constrained motion tasks," *The Int. J. of Robot. Research*, vol. 11, no. 6, Dec 1992.
- [81] D. N. Nenchev, K. Yoshida, and M. Uchiyama, "Reaction null-space based control of flexible structure mounted manipulating systems," *Proc. 35th IEEE CDC*, Kobe, Japan, pp. 4118-4123, 1996.
- [82] D. N. Nenchev, and K. Yoshida, "Impact analysis and post-impact motion control issues of a free-floating space robot subject to a force impulse," *IEEE Trans. on Robot. and Automat.*, vol. 15, no. 3, pp. 548-557, June 1999.
- [83] D. N. Nenchev, and K. Yoshida, "Reaction null-space control of flexible structure mounted manipulator systems," *IEEE Trans. on Robot. and Automat.*, vol. 15, no. 6, pp. 1011-1023, Dec. 1999.
- [84] M. Oda, "Experiences and lessons learned from the ETS-VII robot satellite," *Proc. IEEE Int. Conf. on Robotics and Automation (ICRA)*, San Francisco, CA., April 2000.
- [85] S. Y. Oh, D. Orin, and M. Bach, "An inverse kinematic solution for kinematically redundant robot manipulators," *J. of Robotic Systems*, 1, pp. 235-249, 1984.
- [86] E. Papadopoulos, and S. Dubowsky, "Coordinated manipulator/spacecraft motion control for space robotic systems," *Proc. IEEE Int. Conf. on Robotics and Automation (ICRA)*, Sacramento, CA, pp. 1696-1701, April 1991.
- [87] E. Papadopoulos, and S. Dubowsky, "On the nature of control algorithms for free-floating space manipulators," *IEEE Trans. on Robot. and Automat.*, vol. 7, pp. 750-758, Dec. 1991.
- [88] E. Papadopoulos, "Path planning for space manipulators exhibiting nonholonomic behavior," *Proc. of IEEE/RSJ Int. Conf. on Intelligent Robots and Systems (IROS)*, Raleigh, North Carolina, pp. 669-675, July 7-10, 1992.
- [89] E. Papadopoulos, and S. Dubowsky, "Dynamic singularities in the control of free-floating space manipulators," *ASME J. Dyn. Syst., Meas., Contr.*, vol. 115, no. 1, pp. 44-52, Mar. 1993.
- [90] E. Papadopoulos, and A. Abu-Abed, "Design and Motion Planning for a Zero-Reaction Manipulator," *Proc. IEEE Int. Conf. on Robotics and Automation (ICRA)*, San Diego, California, pp. 8-13, May 1994.
- [91] E. Papadopoulos, and S. A. A. Moosavian, "Dynamics & Control of Multi-arm Space Robots During Chase & Capture Operations," *Proc. of IEEE/RSJ Int. Conf. on Intelligent Robots and Systems (IROS)*, Munich, Germany, pp. 1554-1561, September 12-16, 1994.
- [92] E. Papadopoulos, and K. Nanos, "On Configuration Planning for Free-floating Space Robots," 15th CISM-IFToMM Symposium on Robot Design, Dynamics and Control Montreal, Canada, June 14-18, 2004.

- [93] S. Di Pippo, "ASI's space programs," *Proceeding of the International Symposium on Artificial Intelligence and Robotics & Automation in Space (i-SAIRAS)*, Kobe, Japan, 1990.
- [94] R. D. Quinn, J. L. Chen, and C. Lawrence, "Redundant manipulators for momentum compensation in a micro-gravity environment," *AIAA Guidance, Navigation and Control Conference*, pp. 581-587, August 1988.
- [95] S. S. Rao, "Optimization Theory and Applications," 2nd ed., *John Wiley & Sons*, New York, 1984.
- [96] R. E. Roberson and J. Wittenburg, "A dynamical formalism for an arbitrary number of rigid bodies, with reference to the problem of satellite attitude control," *Proc. IFAC Congress, London*, 1966, Butterworth, London, 1968.
- [97] J. I. Rodriguez, J. M. Jiménez, F. J. Funes, and J. Garcia de Jalón, "Recursive and residual algorithms for the efficient numerical integration of multi-body systems," *Springer Science+Business Media B.V.*, vol. 11, no. 4, pp. 295-320, May 2004.
- [98] S. K. Saha, "Dynamic modeling of serial multi-body systems using the decoupled natural orthogonal complement matrices," *ASME J. Appl. Mech.*, vol. 66, no. 4, pp. 986-996, 1999.
- [99] Y. Sakawa, "Trajectory planning of a free-flying robot by using the optimal control," *Optimal Control Applications and Methods*, 20, pp. 235-248, 1999.
- [100] B. Schafer, R. Krenn, and B. Rebele, "On inverse kinematics and kinetics of redundant space manipulator simulation," *J. of Comput. and Applied Mechanics*, vol. 4, no. 1, pp. 53-70, 2003.
- [101] R. von Schwerin, "Multibody System Simulation. Numerical Methods, Algorithms and Software," *Springer*, 1999.
- [102] J. M. Selig, "Geometrical Methods in Robotics," *Springer*, 1995.
- [103] M. A. Serna, R. Avilés, and J. Garcia de Jalón, "Dynamic analysis of plane mechanisms with lower-pairs in basic coordinates," *Mechanism and Machine Theory*, vol. 17, pp. 397-403, 1982.
- [104] L. F. Shampine, "Numerical Solution of Ordinary Differential Equations," *Chapman & Hall Mathematics*, 1994.
- [105] M. J. Sidi, "Spacecraft dynamics and control: a practical engineering approach," *Cambridge University Press*, 1997.
- [106] R. P. Singh, and P. W. Likins, "Singular Value Decomposition for Constrained Dynamic Systems," *ASME Journal of Applied Mechanics*, vol. 52, pp. 943-948, 1985.
- [107] M. W. Spong, and M. M. Vidyasagar, "Robot Dynamics and Control," *John Wiley & Sons*, New York, 1989.

- [108] M. W. Spong, "Partial feedback linearization of underactuated mechanical systems," *Proc. of IEEE/RSJ Int. Conf. on Intelligent Robots and Systems (IROS)*, Munich, Germany, pp. 314-321, Sept. 1994.
- [109] G. Strang, "Linear algebra and its applications," *Academic Press, New York*, 1986.
- [110] M. A. Torres, and S. Dubowsky, "Minimizing Spacecraft Attitude Disturbance in Space Manipulator Systems," *AIAA Journal of Guidance, Control, and Dynamics*, vol. 15, no. 4, pp. 1010-1017, July-August, 1992.
- [111] Y. Tsuda, and S. Nakasuka, "New attitude motion following control algorithm for capturing tumbling object in space," *Acta Astronautica*, vol. 53, pp. 847-861, 2003.
- [112] Y. Umetani, and K. Yoshida, "Resolved motion rate control of space manipulators with generalized Jacobian matrix," *IEEE Trans. on Robot. and Automat.*, vol. 5, pp. 303-314, June 1989.
- [113] Z. Vafa, and S. Dubowsky, "On the dynamics of manipulators in space using the virtual manipulator approach," *Proc. IEEE Int. Conf. on Robotics and Automation (ICRA)*, pp. 579-585, 1987.
- [114] Z. Vafa, and S. Dubowsky, "The kinematics and dynamics of space manipulators: the virtual manipulator approach," *The International J. of Robotics Research*, vol. 9, no. 4, pp. 3-21, 1990.
- [115] Z. Vafa, and S. Dubowsky, "On the Dynamics of Space Manipulators Using the Virtual Manipulator, with Applications to Path Planning," *J. of the Astronautical Sciences, Special Issue on Space Robotics*, vol. 38, no. 4, pp. 441-472, 1990.
- [116] M. W. Walker, and D. M. Kim, "Satellite stabilization using space leeches," *Proc. IEEE Amer. Contr. Conf.*, San Diego, CA, pp. 1314-1319, May 23-25 1990.
- [117] L. B. Wee, and M. W. Walker, "On the dynamics of contact between space robots and configuration control for impact minimization," *IEEE Trans. on Robot. and Automat.*, vol. 9, pp. 581-591, Oct. 1999.
- [118] R. A. Wehage, "Application of matrix partitioning and recursive projection to O(N) solution of constrained equations of motion," *ASME Advances in Design Automation*, pp. 221-230, 1988.
- [119] J. Wittenburg, "Dynamics of Multibody Systems," *B.G. Teubner, Stuttgart*, 1977.
- [120] Y. Xu, "The measure of dynamic coupling of space robot systems," *Proc. IEEE Int. Conf. on Robotics and Automation (ICRA)*, Atlanta, Georgia, pp. 615-620, 1993.
- [121] K. Yamada, "Arm path planning for a space robot," *Proc. of IEEE/RSJ Int. Conf. on Intelligent Robots and Systems (IROS)*, Yokohama, Japan, pp. 2049-2055, 1993.
- [122] K. Yamada, S. Yoshikawa, and Y. Fujita, "Arm path planning of a space robot with angular momentum," *Journal of Advanced Robotics*, vol 9, no. 6, pp. 693-709, 1995.

- [123] M. Yamano, A. Konno, M. Uchiyama, and T. Miyabe, "Capturing a spinning object by two flexible manipulators," *Proc. of IEEE/RSJ Int. Conf. on Intelligent Robots and Systems (IROS)*, Takamatsu, Japan, 2000.
- [124] K. Yoshida, and R. Kurazume, "Modeling of collision dynamics for space free-floating links with extended generalized inertia tensor," *Proc. IEEE Int. Conf. on Robotics and Automation (ICRA)*, Nice, France, pp. 899-904, May, 1992.
- [125] K. Yoshida, and N. Sashida, "Modeling of impact dynamics and impulse minimization for space robots," *Proc. of IEEE/RSJ Int. Conf. on Intelligent Robots and Systems (IROS)*, Yokohama, Japan, pp. 2064-2069, July 1993.
- [126] K. Yoshida, "Space Robot Dynamics and Control: To Orbit, From Orbit, and Future, Robotics Research," *The Ninth International Symposium, Eds, Hollerbach, J.M, and Koditschek, D.E*, pp. 449-456, Springer, 2000.
- [127] K. Yoshida, "Engineering Test Satellite VII flight experiments for space robot dynamics and control: theories on laboratory test beds ten years ago, now in orbit," *Int. J. of Robot. Research*, vol. 22, no. 5, pp. 321-335, May 2003.
- [128] K. Yoshida, H. Nakanishi, H. Ueno, N. Inaba, T. Nishimaki, and M. Oda, "Dynamics, control and impedance matching for robotic capture of a non-cooperative satellite," *Advanced Robotics*, vol. 2, no. 2, pp. 175-198, 2004.
- [129] T. Yoshikawa, "Analysis and control of robot manipulators with redundancy," *1st Int. Symp. on Robotics Research*, Cambridge, MA:MIT Press, pp. 735-746.
- [130] S. Yoshikawa, and K. Yamada, "Impact estimation of a space robot at capturing a target," *Proc. of IEEE/RSJ Int. Conf. on Intelligent Robots and Systems (IROS)*, 1994.
- [131] S. Yoshikawa, and K. Yamada, "Impulsive control for angular momentum management of tumbling spacecraft," *24th ISTS*, Miyazaki, Japan, May 30 - June 6, 2004.
- [132] D. Zlatanov, and D. Nenchev, "On the use of metric-dependent methods in robotics," *Proc. of IDETC'05 ASME Int. Design Engineering Technical Conf. and Computers and Information in Engineering Conf.*, Long Beach, California, USA, Sept. 24-28, 2005.
- [133] <http://www.mathworks.com/access/helpdesk/help/toolbox/optim/ug/fmincon.html>
- [134] <http://www.afit.edu/en/enc/Faculty/MAbramson/nomadm.html>

Biography

Dimitar Nikolaev Dimitrov was born in Bulgaria, Sofia in 1975. He received the BEng and MSc from the Technical University - Sofia in 1996 and 1999, both in Electrical and Electronic Engineering. He is now pursuing the PhD degree at Tohoku University. His research interests include dynamics and control of serial and parallel manipulators, nonholonomic path planning, contact dynamics, multi-fingered robotics manipulation.

List of Publications

Journal

- [1] Dimitar Dimitrov, Kazuya Yoshida, “Control Strategies for the Approach and Post-Impact Motion of a Space Manipulator Capturing a Tumbling Satellite,” *submitted to IEEE Transactions on Robotics (under review)*.

Conference

- [1] Dimitar Dimitrov, Kazuya Yoshida, “Utilization of the Bias Momentum Approach for Capturing a Tumbling Satellite,” *Proc. of IEEE/RSJ Int. Conf. on Intelligent Robots and Systems (IROS)*, Sendai, Japan, pp. 3333-3338, Sep. 28 - Oct. 2, 2004.
- [2] Dimitar Dimitrov, Kazuya Yoshida, “Momentum Distribution in a Space Manipulator for Facilitating the Post-Impact Control,” *Proc. of IEEE/RSJ Int. Conf. on Intelligent Robots and Systems (IROS)*, Sendai, Japan, pp. 3345-3350, Sep. 28 - Oct. 2, 2004.
- [3] Dimitar Dimitrov, Kazuya Yoshida, “Utilization of Distributed Momentum Control for Planning Approaching Trajectories of a Space Manipulator to a Target Satellite,” *8th International Symposium on Artificial Intelligence, Robotics and Automation in Space (iSAIRAS)*, 2005.
- [4] Kazuya Yoshida, Tomohisa Oki, Dimitar Dimitrov “Distributed Angular Momentum Control of Space Robot Capturing a Tumbling Target,” *15th. Workshop on Astrodynamics and Flight Mechanics*, Sagamihara, Japan, 2005.
- [5] Dimitar Dimitrov, Kazuya Yoshida, “A Satellite-Capturing strategy with Bias Initial Momentum,” *ISTS*, Miyazaki, Japan, May 30 - June 6, 2004.
- [6] Dimitar Dimitrov, Kazuya Yoshida, “A Satellite-Capture strategy with Bias Initial Momentum,” *ISAS 13th Workshop on Astrodynamics And Flight Mechanics*, pp. 91-96, July 24-25 2003.

- [7] Pavlov V., N. Angelov, D. Dimitrov, "Two-dimensional driving unit with one kinematic redundant controlling movement," *Proc. of the Technical University - Sofia*, Vol. 50, Book 3, 1999 pp. 78-85.
- [8] Pavlov V., N. Angelov, D. Dimitrov, "Controlling the torque of the manipulator with kinematic redundant drive," *Robotics and Mechatronics conference*, Drianovo 1999.

In preparation

- [1] Dimitar Dimitrov, Kazuya Yoshida, "Utilization of Holonomic Distribution Control for Reactionless Path Planning," *includes the contents of Chapter 4.4.*

Appendix A

Derivation of $\dot{\mathbf{B}}_i$ and $\dot{\mathbf{b}}_i$

See Fig. 2.2 for more information about the symbols.

$${}^k\dot{\mathbf{B}}_i = \begin{bmatrix} \mathbf{0} & -\frac{d}{dt}\hat{\mathbf{p}}_i \\ \mathbf{0} & \mathbf{0} \end{bmatrix}$$

During the differentiation the $(\hat{\cdot})$ operator will be dropped for simplicity.

$$\begin{aligned} -\frac{d}{dt}(\mathbf{p}_i) &= -(\boldsymbol{\omega}_k \times \mathbf{t}_k + \boldsymbol{\omega}_i \times \mathbf{s}_i) \\ &= -(\boldsymbol{\omega}_k \times \mathbf{t}_k + \boldsymbol{\omega}_k \times \mathbf{s}_i + \mathbf{u}_i \times \mathbf{s}_i \dot{\phi}_i) \\ &= -(\boldsymbol{\omega}_k \times (\mathbf{t}_k + \mathbf{s}_i) + \mathbf{u}_i \times \mathbf{s}_i \dot{\phi}_i) \\ &= -(\boldsymbol{\omega}_k \times \mathbf{p}_i + \mathbf{u}_i \times \mathbf{s}_i \dot{\phi}_i) \end{aligned}$$

hence,

$${}^k\dot{\mathbf{B}}_i = \begin{bmatrix} \mathbf{0} & \hat{(\mathbf{p} \times \boldsymbol{\omega}_k - \mathbf{u}_i \times \mathbf{s}_i \dot{\phi}_i)} \\ \mathbf{0} & \mathbf{0} \end{bmatrix}$$

where $\hat{(\cdot)}$ denotes that after evaluation the expression in the brackets should be transformed into a skew symmetric matrix.

$$\begin{aligned} \dot{\mathbf{b}}_i &= \begin{bmatrix} \frac{d}{dt}(\mathbf{u}_i \times \mathbf{s}_i) \\ \frac{d}{dt}(\mathbf{u}_i) \end{bmatrix} \\ \frac{d}{dt}(\mathbf{u}_i) &= \boldsymbol{\omega}_k \times \mathbf{u}_i \end{aligned} \tag{A.1}$$

$$\begin{aligned} \frac{d}{dt}(\mathbf{u}_i \times \mathbf{s}_i) &= \frac{d}{dt}(\mathbf{u}_i) \times \mathbf{s}_i + \mathbf{u}_i \times \frac{d}{dt}(\mathbf{s}_i) \\ &= (\boldsymbol{\omega}_k \times \mathbf{u}_i) \times \mathbf{s}_i + \mathbf{u}_i \times (\boldsymbol{\omega}_i \times \mathbf{s}_i) \\ &= (\boldsymbol{\omega}_k \times \mathbf{u}_i) \times \mathbf{s}_i + \mathbf{u}_i \times (\boldsymbol{\omega}_k \times \mathbf{s}_i + \mathbf{u}_i \times \mathbf{s}_i \dot{\phi}_i) \\ &= (\boldsymbol{\omega}_k \times \mathbf{u}_i) \times \mathbf{s}_i + \mathbf{u}_i \times (\boldsymbol{\omega}_k \times \mathbf{s}_i) + \mathbf{u}_i \times (\mathbf{u}_i \times \mathbf{s}_i \dot{\phi}_i) \end{aligned}$$

The following term can be added to the above equation:

$$\boldsymbol{\omega}_k \times (\mathbf{u}_i \times \mathbf{s}_i) + \mathbf{u}_i \times (\mathbf{s}_i \times \boldsymbol{\omega}_k) + \mathbf{s}_i \times (\boldsymbol{\omega}_k \times \mathbf{u}_i)$$

Note that this term is equal to zero because for random vectors A , B and C the following relation always holds (it is called the *Jacobi identity*):

$$\mathbf{A} \times (\mathbf{B} \times \mathbf{C}) + \mathbf{B} \times (\mathbf{C} \times \mathbf{A}) + \mathbf{C} \times (\mathbf{A} \times \mathbf{B}) = 0$$

Canceling the equal terms with opposite signs one obtains:

$$\frac{d}{dt}(\mathbf{u}_i \times \mathbf{s}_i) = \boldsymbol{\omega}_k \times (\mathbf{u}_i \times \mathbf{s}_i) + \mathbf{u}_i \times (\mathbf{u}_i \times \mathbf{s}_i \dot{\phi}_i) = (\boldsymbol{\omega}_k + \mathbf{u}_i \dot{\phi}_i) \times (\mathbf{u}_i \times \mathbf{s}_i) \quad (\text{A.2})$$

Joining equations (A.1) and (A.2) results in:

$$\dot{\mathbf{b}}_i = \begin{bmatrix} (\boldsymbol{\omega}_k + \mathbf{u}_i \dot{\phi}_i) \times (\mathbf{u}_i \times \mathbf{s}_i) \\ \boldsymbol{\omega}_k \times \mathbf{u}_i \end{bmatrix}$$

Appendix B

Example for coordinate partitioning

Here, an example using the *Gauss Jordan elimination* for extracting an independent set of variables from a dependent one is made. Let us consider the linear system of equations

$$\begin{bmatrix} 0.75 & 0.63 & 0.75 & 0.54 & 0.62 \\ 0.76 & 0.06 & 0.76 & 0.48 & 0.07 \\ 0.80 & 0.63 & 0.80 & 0.44 & 0.51 \end{bmatrix} \begin{bmatrix} \dot{z}_1 \\ \dot{z}_2 \\ \dot{z}_3 \\ \dot{z}_4 \\ \dot{z}_5 \end{bmatrix} = 0 \quad (\text{B.1})$$

which is similar to the one in 2.16. Hence, the leading matrix (\mathbf{A}_z) can be considered to be a Jacobian matrix of a system of three constraint equations with respect to five dependent velocities $\dot{\mathbf{z}}$ ($\mathbf{A}_z \in R^{3 \times 5}$). Judging from the dimensions of \mathbf{A}_z it can be concluded that the independent set of variables has dimension *two*¹. In order to solve this linear system of equations one needs to determine two entries in the vector $\dot{\mathbf{z}}$ and then performing the necessary forward and backward substitutions to determine the values of the rest of the variables. The question is “*which two*”? The choice should satisfy only one condition and it is: the matrix formed by the remaining dependent variables (\mathbf{A}_z^d) should have full rank.

By inspection it can be noted that columns *one* and *three* of \mathbf{A}_z are the same. This implies that both \dot{z}_1 and \dot{z}_3 cannot be included in the set of dependent variables because the resulting $\mathbf{A}_z^d \in R^{3 \times 3}$ matrix will be rank deficient. Using the *Gauss Jordan elimination* method one can easily ensure full rank of \mathbf{A}_z^d simply by forming it from the columns of \mathbf{A}_z containing pivots. The result from partitioning \mathbf{A}_z in (B.1) is:

$$\mathbf{A}_z^p = \begin{bmatrix} 1 & 0 & 1 & 0 & -0.51 \\ 0 & 1 & 0 & 0 & 0.86 \\ 0 & 0 & 0 & 1 & 0.84 \end{bmatrix} \quad (\text{B.2})$$

¹Which coincides with the dimension of the null space of \mathbf{A}_z .

with pivots in columns *one*, *two* and *four*. These columns form a unit matrix. Hence, once the independent variables \dot{z}_3 and \dot{z}_5 are specified the calculation of the dependent ones is straightforward. Mathematically matrix \mathbf{A}_z^p can be written as:

$$\mathbf{A}_z^p = \begin{bmatrix} \mathbf{A}_z^d & \mathbf{A}_z^i \end{bmatrix} \quad (\text{B.3})$$

where \mathbf{A}_z^d contains columns *one*, *two* and *four* of \mathbf{A}_z^p , and \mathbf{A}_z^i includes the remaining ones. Rewriting equation (B.1) using the partitioned form one obtains:

$$\begin{bmatrix} \mathbf{A}_z^d & \mathbf{A}_z^i \end{bmatrix} \begin{bmatrix} \dot{\mathbf{z}}^d \\ \dot{\mathbf{z}}^i \end{bmatrix} = 0 \quad (\text{B.4})$$

$$\dot{\mathbf{z}}^d = \begin{bmatrix} \dot{z}_1 \\ \dot{z}_2 \\ \dot{z}_4 \end{bmatrix} \quad \dot{\mathbf{z}}^i = \begin{bmatrix} \dot{z}_3 \\ \dot{z}_5 \end{bmatrix}$$

Solving B.4 for $\dot{\mathbf{z}}^d$ results in:

$$\dot{\mathbf{z}}^d = -\mathbf{A}_z^{d-1} \mathbf{A}_z^i \dot{\mathbf{z}}^i \quad (\text{B.5})$$

Hence, the matrix \mathbf{R} that relates $\dot{\mathbf{z}}$ and $\dot{\mathbf{z}}^i$ is defined as:

$$\mathbf{R} = \begin{bmatrix} -\mathbf{A}_z^{d-1} \mathbf{A}_z^i \\ \mathbf{E}_2 \end{bmatrix} \quad (\text{B.6})$$

where $\mathbf{E}_2 \in R^{2 \times 2}$ is a unit matrix.

Since the *Gauss Jordan elimination* guarantees that the components of \mathbf{A}_z^d form a unit matrix the above equations becomes:

$$\mathbf{R} = \begin{bmatrix} -\mathbf{A}_z^i \\ \mathbf{E}_2 \end{bmatrix} \quad (\text{B.7})$$

The numerical result for \mathbf{R} is:

$$\mathbf{R} = \begin{bmatrix} -1 & 0.51 \\ 0 & -0.86 \\ 1 & 0 \\ 0 & -0.84 \\ 0 & 1 \end{bmatrix} \quad (\text{B.8})$$

Note that the unit matrix \mathbf{E}_2 is formed by rows 3 and 5 of \mathbf{R} . Respectively $-\mathbf{A}_z^i$ contains the first, second and fourth one.

Appendix C

Momentum conservation equation

Here, a general form of the momentum conservation equation for a free-floating robotic system is derived. It is a fundamental tool for the control of space manipulators and is extensively used through the thesis. It can give a direct relation between the manipulator and *base* motions which proves to be useful in many cases. Furthermore, since the momentum conservation equation is simpler compared to the equation of motion, its utilization for the development of computationally uninvolved control strategies is indispensable (see Section 5.2).

The variables used in the derivation are defined as follows (all of them are expressed in the inertial frame Σ_i);

m_i, \mathbf{I}_i - mass and inertia of body i ,

\mathbf{r}_i - position of the centroid of body i ,

\mathbf{v}_i - linear velocity of the centroid of body i ,

$\boldsymbol{\omega}_i$ - angular velocity of body i .

Variables with index $i = 0$ refer to the base body (Fig. C.1). The translational and rotational parts of the Jacobian matrices \mathbf{J}_m and ${}^b\mathbf{J}_m$ (see Section 2.4.1) will be denoted as follows:

$$\mathbf{J}_m^i \in R^{6 \times n} = \begin{bmatrix} \mathbf{J}_{Ti} \\ \mathbf{J}_{Ri} \end{bmatrix} \quad (i = 1, 2, \dots, n) \quad (\text{C.1})$$

$${}^b\mathbf{J}_m \in R^{6 \times n} = \begin{bmatrix} \mathbf{J}_{T0} \\ \mathbf{J}_{R0} \end{bmatrix} = 0 \quad (\text{C.2})$$

A) First the linear momentum \mathbf{P} will be considered:

$$\mathbf{P} = \sum_{i=0}^n m_i \mathbf{v}_i$$

Using (2.26) the above equation becomes:

$$\begin{aligned}
\mathbf{P} &= \sum_{i=0}^n m_i (\mathbf{v}_0 + \boldsymbol{\omega}_0 \times (\mathbf{r}_i - \mathbf{r}_0) + \mathbf{J}_{Ti} \dot{\boldsymbol{\phi}}) \\
&= \left(\sum_{i=0}^n m_i \right) \mathbf{v}_0 + \boldsymbol{\omega}_0 \times \left(\sum_{i=0}^n m_i \mathbf{r}_i \right) - \left(\sum_{i=0}^n m_i \right) \boldsymbol{\omega}_0 \times \mathbf{r}_0 + \left(\sum_{i=0}^n m_i \mathbf{J}_{Ti} \right) \dot{\boldsymbol{\phi}} \\
&= w \mathbf{v}_0 + \boldsymbol{\omega}_0 \times w \mathbf{r}_g - w \boldsymbol{\omega}_0 \times \mathbf{r}_0 + \mathbf{J}_{Tg} \dot{\boldsymbol{\phi}} \\
&= w \mathbf{v}_0 + w \boldsymbol{\omega}_0 \times \mathbf{r}_{0g} + \mathbf{J}_{Tg} \dot{\boldsymbol{\phi}}
\end{aligned} \tag{C.3}$$

where

$$\begin{aligned}
\sum_{i=0}^n m_i &= w & \sum_{i=0}^n m_i \mathbf{r}_i &= w \mathbf{r}_g & \mathbf{r}_{0g} &= \mathbf{r}_g - \mathbf{r}_0 \\
\mathbf{J}_{Tg} &= \sum_{i=1}^n m_i \mathbf{J}_{Ti}
\end{aligned} \tag{C.4}$$

The term $\mathbf{J}_{Tg} \dot{\boldsymbol{\phi}}$ represents the linear momentum of the center of mass of the manipulator (without base) as seen from the coordinate frame fixed in the base body.

B) Angular momentum \mathbf{L} around the origin of the inertial frame:

$$\mathbf{L} = \sum_{i=0}^n (\mathbf{I}_i \boldsymbol{\omega}_i + \mathbf{r}_i \times m_i \mathbf{v}_i)$$

Using (2.25) and (2.26) the above equation becomes:

$$\begin{aligned}
\mathbf{L} &= \sum_{i=0}^n \left[\mathbf{I}_i (\boldsymbol{\omega}_0 + \mathbf{J}_{Ri} \dot{\boldsymbol{\phi}}) + \mathbf{r}_i \times m_i (\mathbf{v}_0 + \boldsymbol{\omega}_0 \times (\mathbf{r}_i - \mathbf{r}_0) + \mathbf{J}_{Ti} \dot{\boldsymbol{\phi}}) \right] \\
&= \left(\sum_{i=0}^n \mathbf{I}_i \right) \boldsymbol{\omega}_0 + \left(\sum_{i=0}^n \mathbf{I}_i \mathbf{J}_{Ri} \right) \dot{\boldsymbol{\phi}} + \left(\sum_{i=0}^n m_i \mathbf{r}_i \right) \times \mathbf{v}_0 \\
&\quad - \sum_{i=0}^n m_i \mathbf{r}_i \times [(\mathbf{r}_i - \mathbf{r}_0) \times \boldsymbol{\omega}_0] + \left(\sum_{i=0}^n m_i \mathbf{r}_i \times \mathbf{J}_{Ti} \right) \dot{\boldsymbol{\phi}}
\end{aligned} \tag{C.5}$$

substituting $\mathbf{r}_{0i} = \mathbf{r}_i - \mathbf{r}_0$, and noting that $\mathbf{r}_{00} = 0$, $\mathbf{J}_{T0} \in R^{3 \times n} = 0$ and $\mathbf{J}_{R0} \in R^{3 \times n} = 0$ one obtains:

$$\begin{aligned}
\mathbf{L} &= w \mathbf{r}_g \times \mathbf{v}_0 + \left[\sum_{i=1}^n (\mathbf{I}_i - m_i \hat{\mathbf{r}}_i \hat{\mathbf{r}}_{0i}) + \mathbf{I}_0 \right] \boldsymbol{\omega}_0 + \sum_{i=1}^n (\mathbf{I}_i \mathbf{J}_{Ri} + m_i \hat{\mathbf{r}}_i \mathbf{J}_{Ti}) \dot{\boldsymbol{\phi}} \\
&= w \mathbf{r}_g \times \mathbf{v}_0 + \mathbf{I}_w \boldsymbol{\omega}_0 + \mathbf{I}_\phi \dot{\boldsymbol{\phi}}
\end{aligned} \tag{C.6}$$

where (\cdot) stands for a skew-symmetric representation of a three dimensional vector. Joining equations (C.3) and (C.6) leads to:

$$\begin{bmatrix} \mathbf{P} \\ \mathbf{L} \end{bmatrix} = \begin{bmatrix} w \mathbf{E}_3 & w \hat{\mathbf{r}}_{0g}^T \\ w \hat{\mathbf{r}}_g & \mathbf{I}_w \end{bmatrix} \begin{bmatrix} \mathbf{v}_0 \\ \boldsymbol{\omega}_0 \end{bmatrix} + \begin{bmatrix} \mathbf{J}_{Tg} \\ \mathbf{I}_\phi \end{bmatrix} \dot{\boldsymbol{\phi}} \tag{C.7}$$

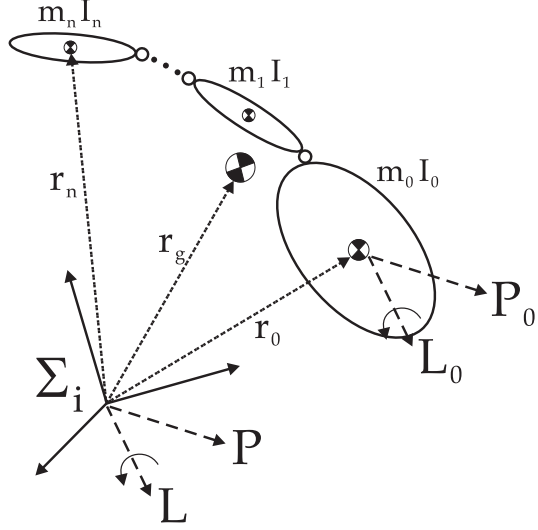


Figure C.1: Angular momentum expressed around different points. \mathbf{r}_0 and \mathbf{r}_g stand for the vectors from the inertial frame to the base and center of mass of the entire system, respectively.

where

$$\begin{aligned}\mathbf{I}_{\omega} &= \sum_{i=1}^n (\mathbf{I}_i - m_i \hat{\mathbf{r}}_i \hat{\mathbf{r}}_{0i}) + \mathbf{I}_0 \\ \mathbf{I}_{\phi} &= \sum_{i=1}^n (\mathbf{I}_i \mathbf{J}_{Ri} + m_i \hat{\mathbf{r}}_i \mathbf{J}_{Ti}) \dot{\phi}\end{aligned}$$

As already mentioned, equation (C.6) is the angular momentum of the system around the origin of Σ_i . From practical point of view, it is convenient to express it around the centroid of the base body (Fig. C.1).

B) Angular momentum \mathbf{L}_0 around the centroid of the base:

$$\begin{aligned}\mathbf{P}_0 &= \mathbf{P} \\ \mathbf{L}_0 &= \mathbf{L} - \mathbf{r}_0 \times \mathbf{P}\end{aligned}\tag{C.8}$$

The product $\mathbf{r}_0 \times \mathbf{P}$ becomes:

$$\mathbf{r}_0 \times \mathbf{P} = w \mathbf{r}_0 \times \mathbf{v}_0 - \sum_{i=1}^n m_i \mathbf{r}_0 \times [(\mathbf{r}_i - \mathbf{r}_0) \times \boldsymbol{\omega}_0] + \left(\sum_{i=1}^n m_i \mathbf{r}_0 \times \mathbf{J}_{Ti} \right) \dot{\phi}\tag{C.9}$$

Substituting (C.9) in (C.8) one obtains:

$$\begin{aligned} \mathbf{L}_0 &= \mathbf{L} - \mathbf{r}_0 \times \mathbf{P} = w(\mathbf{r}_g - \mathbf{r}_0) \times \mathbf{v}_0 + \left(\sum_{i=0}^n \mathbf{I}_i \right) \boldsymbol{\omega}_0 \\ &\quad + \sum_{i=1}^n m_i (\mathbf{r}_0 - \mathbf{r}_i) \times [(\mathbf{r}_i - \mathbf{r}_0) \times \boldsymbol{\omega}_0] + \left(\sum_{i=1}^n \mathbf{I}_i \mathbf{J}_{Ri} \right) \dot{\phi} + \left(\sum_{i=1}^n m_i (\mathbf{r}_i - \mathbf{r}_0) \times \mathbf{J}_{Ti} \right) \dot{\phi} \\ &= w\hat{\mathbf{r}}_{0g}\mathbf{v}_0 + \left[\sum_{i=1}^n (\mathbf{I}_i + m_i \hat{\mathbf{r}}_{0i}^T \hat{\mathbf{r}}_{0i}) + \mathbf{I}_0 \right] \boldsymbol{\omega}_0 + \sum_{i=1}^n (\mathbf{I}_i \mathbf{J}_{Ri} + m_i \hat{\mathbf{r}}_{0i} \mathbf{J}_{Ti}) \dot{\phi} \end{aligned} \quad (\text{C.10})$$

Joining equations (C.3) and (C.10) leads to:

$$\begin{bmatrix} \mathbf{P}_0 \\ \mathbf{L}_0 \end{bmatrix} = \begin{bmatrix} w\mathbf{E}_3 & w\hat{\mathbf{r}}_{0g}^T \\ w\hat{\mathbf{r}}_{0g} & \mathbf{H}_w \end{bmatrix} \begin{bmatrix} \mathbf{v}_0 \\ \boldsymbol{\omega}_0 \end{bmatrix} + \begin{bmatrix} \mathbf{J}_{Tg} \\ \mathbf{H}_{\omega\phi} \end{bmatrix} \dot{\phi} \quad (\text{C.11})$$

where

$$\mathbf{H}_\omega = \sum_{i=1}^n (\mathbf{I}_i + m_i \hat{\mathbf{r}}_{0i}^T \hat{\mathbf{r}}_{0i}) + \mathbf{I}_0 \quad (\text{C.12})$$

$$\mathbf{H}_{\omega\phi} = \sum_{i=1}^n (\mathbf{I}_i \mathbf{J}_{Ri} + m_i \hat{\mathbf{r}}_{0i} \mathbf{J}_{Ti}) \quad (\text{C.13})$$

Note that equation (C.12) is nothing else but the *parallel axis theorem* and the vector $\mathbf{H}_{\omega\phi}\dot{\phi}$ is the angular momentum of the manipulator as seen from the coordinate frame fixed in the base body. Using the newly obtained inertia matrices \mathbf{H}_ω and $\mathbf{H}_{\omega\phi}$ the expressions for \mathbf{P} and \mathbf{L} become:

$$\begin{bmatrix} \mathbf{P} \\ \mathbf{L} \end{bmatrix} = \begin{bmatrix} w\mathbf{E}_3 & w\hat{\mathbf{r}}_{0g}^T \\ w\hat{\mathbf{r}}_{0g} & \mathbf{H}_w \end{bmatrix} \begin{bmatrix} \mathbf{v}_0 \\ \boldsymbol{\omega}_0 \end{bmatrix} + \begin{bmatrix} \mathbf{J}_{Tg} \\ \mathbf{H}_{\omega\phi} \end{bmatrix} \dot{\phi} + \begin{bmatrix} \mathbf{0} \\ \mathbf{r}_0 \times \mathbf{P} \end{bmatrix} \quad (\text{C.14})$$

and using

$$\mathbf{H}_b \in R^{6 \times 6} = \begin{bmatrix} w\mathbf{E}_3 & w\hat{\mathbf{r}}_{0g}^T \\ w\hat{\mathbf{r}}_{0g} & \mathbf{H}_w \end{bmatrix} \quad (\text{C.15})$$

$$\mathbf{H}_c \in R^{6 \times n} = \begin{bmatrix} \mathbf{J}_{Tg} \\ \mathbf{H}_{\omega\phi} \end{bmatrix} \quad (\text{C.16})$$

equation (C.14) can be expressed as:

$$\begin{bmatrix} \mathbf{P} \\ \mathbf{L} \end{bmatrix} = \mathbf{H}_b \begin{bmatrix} \mathbf{v}_0 \\ \boldsymbol{\omega}_0 \end{bmatrix} + \mathbf{H}_c \dot{\phi} + \begin{bmatrix} \mathbf{0} \\ \mathbf{r}_0 \times \mathbf{P} \end{bmatrix} \quad (\text{C.17})$$

Equation (C.17) is just a different form of (C.7), nevertheless it is more convenient because the angular momentum resulting from \mathbf{P} is expressed in a separate term.

In many practical cases only the angular velocity of the base is of particular interest. Equation (C.17) can be reformulated explicitly only with respect to $\boldsymbol{\omega}_0$ as follows:

$$\begin{aligned}\mathbf{P} &= w\mathbf{E}_3\mathbf{v}_0 + w\hat{\mathbf{r}}_{0g}^T\boldsymbol{\omega}_0 + \mathbf{J}_{Tg}\dot{\boldsymbol{\phi}} \\ \mathbf{L} &= w\hat{\mathbf{r}}_{0g}\mathbf{v}_0 + \mathbf{H}_w\boldsymbol{\omega}_0 + \mathbf{H}_{\omega\phi}\dot{\boldsymbol{\phi}} + \mathbf{r}_0 \times \mathbf{P}\end{aligned}$$

\mathbf{v}_0 can be canceled out by pre-multiplication of the upper equation with $\hat{\mathbf{r}}_{0g}$ and then subtracting it from the lower one. This operation leads to:

$$\mathbf{L} - \hat{\mathbf{r}}_{0g}\mathbf{P} = (\mathbf{H}_w - w\hat{\mathbf{r}}_{0g}\hat{\mathbf{r}}_{0g}^T)\boldsymbol{\omega}_0 + (\mathbf{H}_{\omega\phi} - \hat{\mathbf{r}}_{0g}\mathbf{J}_{Tg})\dot{\boldsymbol{\phi}} + \mathbf{r}_0 \times \mathbf{P}$$

denoting $\tilde{\mathbf{H}}_b = \mathbf{H}_w - w\hat{\mathbf{r}}_{0g}\hat{\mathbf{r}}_{0g}^T$ and $\tilde{\mathbf{H}}_c = \mathbf{H}_{\omega\phi} - \hat{\mathbf{r}}_{0g}\mathbf{J}_{Tg}$ leads to:

$$\mathbf{L} = \tilde{\mathbf{H}}_b\boldsymbol{\omega}_0 + \tilde{\mathbf{H}}_c\dot{\boldsymbol{\phi}} + \mathbf{r}_g \times \mathbf{P} \quad (\text{C.18})$$

In [81] the term $\mathbf{H}_c\dot{\boldsymbol{\phi}}$ is called the *coupling momentum* and in [82] the term $\tilde{\mathbf{H}}_c\dot{\boldsymbol{\phi}}$ is referred to as the *coupling angular momentum*. $\mathcal{L} = \mathbf{H}_c\dot{\boldsymbol{\phi}}$ consists of both linear and angular part (\mathcal{L}^P and \mathcal{L}^L), nevertheless it should be noted that $\mathcal{L}^L \neq \tilde{\mathbf{H}}_c\dot{\boldsymbol{\phi}}$ because the latter one is expressed around the mass center of the system while the former one around the centroid of the base.

Appendix D

Components of the inertia matrix \mathbf{H}

Here the general structure of the inertia matrix \mathbf{H} will be shown. \mathbf{H} appears in the dynamical formulation for manipulators with tree structure (see Section 2.4.1).

The best way to reveal the components of \mathbf{H} is by example. Next, a n DOF manipulator attached to a free-floating base body will be considered. In Section 2.4.1 it was shown that for such case \mathbf{H} can be expressed as:

$$\mathbf{H} = \mathbf{R}^{oT} \mathbf{M} \mathbf{R}^o \quad (\text{D.1})$$

or

$$\mathbf{H} = \begin{bmatrix} {}^b\mathbf{J}_b^T & {}^b\mathbf{J}_m^T \\ {}^b\mathbf{J}_m^T & \mathbf{J}_m^T \end{bmatrix} \begin{bmatrix} \mathbf{M}_0 & \mathbf{0} \\ \mathbf{0} & \mathbf{M}_m \end{bmatrix} \begin{bmatrix} {}^b\mathbf{J}_b & {}^b\mathbf{J}_m \\ \mathbf{J}_b & \mathbf{J}_m \end{bmatrix} \quad (\text{D.2})$$

where the main diagonal of $\mathbf{M}_m \in R^{6n \times 6n}$ contains the mass and inertia matrices of the manipulator (see Section 2.4). Considering that ${}^b\mathbf{J}_b = \mathbf{E}_6$ and ${}^b\mathbf{J}_m = \mathbf{0} \in R^{6 \times n}$, after multiplication (D.2) becomes:

$$\mathbf{H} = \begin{bmatrix} \mathbf{M}_0 + \mathbf{J}_b^T \mathbf{M}_m \mathbf{J}_b & \mathbf{J}_b^T \mathbf{M}_m \mathbf{J}_m \\ \mathbf{J}_m^T \mathbf{M}_m \mathbf{J}_b & \mathbf{J}_m^T \mathbf{M}_m \mathbf{J}_m \end{bmatrix} \quad (\text{D.3})$$

The four components of the above equation have clear physical meaning. Each of them will be considered next:

A) By inspection it can be verified that the term $\mathbf{M}_0 + \mathbf{J}_b^T \mathbf{M}_m \mathbf{J}_b$ corresponds to the matrix \mathbf{H}_b derived in Appendix C equation (C.15). It is called the *global* inertia matrix of the base¹.

¹Often *global* will be dropped for simplicity, since usually from the context the reader can make a distinction whether \mathbf{I}_0 or \mathbf{H}_b is being referred (\mathbf{I}_0 is the moment of inertia of the base body around its center of mass expressed in the inertial frame).

B) The term $\mathbf{J}_b^T \mathbf{M}_m \mathbf{J}_m$ is the transposed of $\mathbf{J}_m^T \mathbf{M}_m \mathbf{J}_b$ ² and represents the coupling inertia matrix between the base and the manipulator. By inspection it can be verified that it is equivalent to \mathbf{H}_c derived in Appendix C equation (C.16).

C) The term $\mathbf{H}_\phi = \mathbf{J}_m^T \mathbf{M}_m \mathbf{J}_m$ represents the *global* inertia matrix of the manipulator. For example if the number of manipulator joints is $n = 2$ then the structure of \mathbf{H}_ϕ is as follows:

$$\mathbf{H}_\phi = [\mathbf{J}_{T1}^T \quad \mathbf{J}_{R1}^T \quad \mathbf{J}_{T2}^T \quad \mathbf{J}_{R2}^T] \begin{bmatrix} m_1 \mathbf{E}_3 & \mathbf{0} & \mathbf{0} & \mathbf{0} \\ \mathbf{0} & \mathbf{I}_1 & \mathbf{0} & \mathbf{0} \\ \mathbf{0} & \mathbf{0} & m_2 \mathbf{E}_3 & \mathbf{0} \\ \mathbf{0} & \mathbf{0} & \mathbf{0} & \mathbf{I}_2 \end{bmatrix} \begin{bmatrix} \mathbf{J}_{T1} \\ \mathbf{J}_{R1} \\ \mathbf{J}_{T2} \\ \mathbf{J}_{R2} \end{bmatrix}$$

where the translational and rotational parts of \mathbf{J}_m have been denoted as:

$$\mathbf{J}_m^i \in R^{6 \times n} = \begin{bmatrix} \mathbf{J}_{Ti} \\ \mathbf{J}_{Ri} \end{bmatrix} \quad (i = 1, 2)$$

After multiplication \mathbf{H}_ϕ becomes:

$$\mathbf{H}_\phi = m_1 \mathbf{J}_{T1}^T \mathbf{J}_{T1} + \mathbf{J}_{R1}^T \mathbf{I}_1 \mathbf{J}_{R1} + m_2 \mathbf{J}_{T2}^T \mathbf{J}_{T2} + \mathbf{J}_{R2}^T \mathbf{I}_2 \mathbf{J}_{R2} \quad (\text{D.4})$$

Rewriting (D.3) using the newly introduced symbols leads to:

$$\mathbf{H} = \begin{bmatrix} \mathbf{H}_b & \mathbf{H}_c \\ \mathbf{H}_c^T & \mathbf{H}_\phi \end{bmatrix} \quad (\text{D.5})$$

where $\mathbf{H}_b \in R^{6 \times 6}$, $\mathbf{H}_c \in R^{6 \times n}$ and $\mathbf{H}_\phi \in R^{n \times n}$. Substituting \mathbf{H}_b and \mathbf{H}_c with the expressions derived in Appendix C gives:

$$\mathbf{H} = \left[\begin{array}{c|c} w \mathbf{E}_3 & w \hat{\mathbf{r}}_{0g}^T \\ \hline w \hat{\mathbf{r}}_{0g} & \mathbf{H}_\omega \\ \hline \mathbf{J}_{Tg}^T & \mathbf{H}_{\omega\phi}^T \end{array} \right] \mathbf{H}_\phi \quad (\text{D.6})$$

The inertia matrix \mathbf{H} is symmetric, positive-definite and configuration dependent. Its components $\mathbf{H}_b(\mathbf{x}_b, \phi)$ and $\mathbf{H}_c(\mathbf{x}_b, \phi)$ in general depend on both the base position and orientation as well as manipulator configuration. $\mathbf{H}_\phi(\phi)$ however, depends only from the manipulator variables. This can be proved by inspecting its components in (D.4). For simplicity let us consider only the first one:

$$\mathbf{H}_{\phi_1} = m_1 \mathbf{J}_{T1}^T \mathbf{J}_{T1} + \mathbf{J}_{R1}^T \mathbf{I}_1 \mathbf{J}_{R1} \quad (\text{D.7})$$

using the latter term of equation (2.27), (D.7) becomes (see Fig. 2.2):

$$\mathbf{H}_{\phi_1} = m_1 (\mathbf{u}_1 \times \mathbf{s}_1)^T (\mathbf{u}_1 \times \mathbf{s}_1) + \mathbf{u}_1^T \mathbf{I}_1 \mathbf{u}_1 \quad (\text{D.8})$$

²Since \mathbf{M}_m is a symmetric matrix it is equal to its transpose. For more information on mass distribution see [22], [4].

all components from the above equation are expressed with respect to the inertial frame. It can be rewritten in the following form:

$$\begin{aligned}\boldsymbol{H}_{\phi_1} &= m_1 ({^iA_1} \boldsymbol{u}_1^1 \times {^iA_1} \boldsymbol{s}_1^1)^T ({^iA_1} \boldsymbol{u}_1^1 \times {^iA_1} \boldsymbol{s}_1^1) + ({^iA_1} \boldsymbol{u}_1^1)^T {^iA_1} \boldsymbol{I}_1^1 {^iA_1}^T ({^iA_1} \boldsymbol{u}_1^1) \\ &= m_1 [(\boldsymbol{u}_1^1 \times \boldsymbol{s}_1^1)^T {^iA_1}^T] [{^iA_1} (\boldsymbol{u}_1^1 \times \boldsymbol{s}_1^1)] + (\boldsymbol{u}_1^{1T} {^iA_1}^T) {^iA_1} \boldsymbol{I}_1^1 {^iA_1}^T ({^iA_1} \boldsymbol{u}_1^1) \\ &= m_1 (\boldsymbol{u}_1^1 \times \boldsymbol{s}_1^1)^T (\boldsymbol{u}_1^1 \times \boldsymbol{s}_1^1) + \boldsymbol{u}_1^{1T} \boldsymbol{I}_1^1 \boldsymbol{u}_1^1\end{aligned}$$

where iA_1 is a rotational matrix that relates the coordinate system Σ_1 fixed in the 1^{th} body to the inertial frame (${^iA_1}^T {^iA_1} = \boldsymbol{E}_3$), and superscript $(\cdot)^1$ means that the variable is expressed in Σ_1 .

Appendix E

Reduced equation of motion

With *reduced form* of the equations of motion, we imply a set of equations that account implicitly for some of the state variables: $\dot{\omega}_b$, \dot{v}_b or $\ddot{\phi}$. For example, equation (4.4) was formulated with respect to the joint accelerations $\ddot{\phi}$ and the base angular acceleration $\dot{\omega}_b$, by eliminating \dot{v}_b from equation (3.1). For convenience (3.1) will be rewritten in the following form:

$$\left[\begin{array}{cc|c} w\mathbf{E} & {w\hat{\mathbf{r}}_{bg}}^T & \mathbf{J}_{Tg} \\ w\hat{\mathbf{r}}_{bg} & \mathbf{H}_\omega & \mathbf{H}_{\omega\phi} \\ \hline \mathbf{J}_{Tg}^T & \mathbf{H}_{\omega\phi}^T & \mathbf{H}_\phi \end{array} \right] \begin{bmatrix} \dot{v}_b \\ \dot{\omega}_b \\ \ddot{\phi} \end{bmatrix} + \begin{bmatrix} \mathbf{c}_b^v \\ \mathbf{c}_b^\omega \\ \mathbf{c}_\phi \end{bmatrix} = \begin{bmatrix} \mathbf{0} \\ \mathbf{0} \\ \boldsymbol{\tau} \end{bmatrix} + \begin{bmatrix} \mathbf{J}_{bh}^{vT} \\ \mathbf{J}_{bh}^{\omega T} \\ \mathbf{J}_{\phi h}^T \end{bmatrix} \mathcal{F}_h \quad (\text{E.1})$$

where for simplicity only external wrenches acting at the tip of the end-effector (\mathcal{F}_h) are considered. \mathbf{J}_{bh} and $\mathbf{J}_{\phi h}$ are Jacobian matrices of the end-effector with respect to the motion of the base and manipulator plus reaction wheels, respectively¹. Solving the first (upper) equation of (E.1) and substituting into the lower two equations results in:

$$\left[\begin{array}{ccc} \tilde{\mathbf{H}}_b & \tilde{\mathbf{H}}_{bm} & \tilde{\mathbf{H}}_{br} \\ \tilde{\mathbf{H}}_{bm}^T & \tilde{\mathbf{H}}_m & \mathbf{0} \\ \tilde{\mathbf{H}}_{br}^T & \mathbf{0} & \tilde{\mathbf{H}}_r \end{array} \right] \begin{bmatrix} \dot{\omega}_b \\ \ddot{\phi}_m \\ \ddot{\phi}_r \end{bmatrix} + \begin{bmatrix} \tilde{\mathbf{c}}_b \\ \tilde{\mathbf{c}}_m \\ \tilde{\mathbf{c}}_r \end{bmatrix} = \begin{bmatrix} \mathbf{0} \\ \boldsymbol{\tau}_m \\ \boldsymbol{\tau}_r \end{bmatrix} + \begin{bmatrix} \tilde{\mathbf{J}}_{bh}^T \\ \tilde{\mathbf{J}}_{mh}^T \\ \tilde{\mathbf{J}}_{rh}^T \end{bmatrix} \mathcal{F}_h \quad (\text{E.2})$$

where

$$\begin{aligned} \tilde{\mathbf{H}}_b &= \mathbf{H}_\omega - w\hat{\mathbf{r}}_{bg}\hat{\mathbf{r}}_{bg}^T \in R^{3 \times 3} \\ \tilde{\mathbf{H}}_c &= [\tilde{\mathbf{H}}_{bm} \quad \tilde{\mathbf{H}}_{br}] = \mathbf{H}_{\omega\phi} - \hat{\mathbf{r}}_{bg}\mathbf{J}_{Tg} \in R^{3 \times n} \\ \tilde{\mathbf{H}}_\phi &= \begin{bmatrix} \tilde{\mathbf{H}}_m & \mathbf{0} \\ \mathbf{0} & \tilde{\mathbf{H}}_r \end{bmatrix} = \mathbf{H}_\phi - \frac{1}{w}\mathbf{J}_{Tg}^T\mathbf{J}_{Tg} \in R^{n \times n} \end{aligned}$$

¹Superscripts v and ω represent the part of a matrix corresponding to the base linear and angular motion, respectively.

$$\begin{aligned}\tilde{\mathbf{c}}_b &= \mathbf{c}_b^\omega - \hat{\mathbf{r}}_{bg} \mathbf{c}_b^v \\ \tilde{\mathbf{c}}_\phi &= \begin{bmatrix} \tilde{\mathbf{c}}_m \\ \tilde{\mathbf{c}}_r \end{bmatrix} = \mathbf{c}_\phi - \frac{1}{w} \mathbf{J}_{Tg}^T \mathbf{c}_b^v \\ \tilde{\mathbf{J}}_{bh}^T &= \mathbf{J}_{bh}^{\omega T} - \hat{\mathbf{r}}_{bg} \mathbf{J}_{bh}^{vT} \\ \tilde{\mathbf{J}}_{\phi h}^T &= \begin{bmatrix} \tilde{\mathbf{J}}_{mh}^T \\ \tilde{\mathbf{J}}_{rh}^T \end{bmatrix} = \mathbf{J}_{\phi h}^T - \frac{1}{w} \mathbf{J}_{Tg}^T \mathbf{J}_b^{vT}\end{aligned}$$

where subscripts m and r denote variables of the manipulator and reaction wheels, respectively. The symbols undefined here, can be found in Appendix C.

Using a similar approach as above, the base angular accelerations $\dot{\boldsymbol{\omega}}_b$ in (E.2) can be eliminated as well, to obtain the following equation of motion:

$$\mathbf{H}_\phi^g \ddot{\boldsymbol{\phi}} + \mathbf{c}^g = \boldsymbol{\tau} + \mathbf{J}_{\phi h}^{gT} \mathcal{F}_h \quad (\text{E.3})$$

Equation (E.3) is defined explicitly only with respect to the manipulator joint variables. It can be considered as a generalization of the fixed-base manipulator equation of motion, where the new matrices are defined as follows:

$$\begin{aligned}\mathbf{H}_\phi^g &= \mathbf{H}_\phi - \mathbf{H}_c^T \mathbf{H}_b^{-1} \mathbf{H}_c \\ \mathbf{c}^g &= \mathbf{c}_\phi - \mathbf{H}_c^T \mathbf{H}_b^{-1} \mathbf{c}_b \\ \mathbf{J}_{\phi h}^{gT} &= \mathbf{J}_{\phi h}^T - \mathbf{H}_c^T \mathbf{H}_b^{-1} \mathbf{J}_{bh}^T\end{aligned}$$

In [112], the matrix $\mathbf{J}_{\phi h}^g = \mathbf{J}_{\phi h} - \mathbf{J}_{bh} \mathbf{H}_b^{-1} \mathbf{H}_c$ (note that \mathbf{H}_b is symmetric) is referred to as *generalized Jacobian matrix*. It becomes identical to $\mathbf{J}_{\phi h}$ if the mass and inertia characteristics of the base body are infinitely big (which corresponds to the case of a fixed-base manipulator). By analogy the matrices \mathbf{H}_ϕ^g and \mathbf{c}^g can be referred to as *generalized inertia matrix* and *generalized nonlinear term*, respectively.

An alternative way to derive the *generalized Jacobian matrix* is by using the following system of equations (see Appendix C (C.17)²):

$$\begin{bmatrix} \mathbf{P} \\ \mathbf{L} \end{bmatrix} = \mathbf{H}_b \begin{bmatrix} \mathbf{v}_b \\ \boldsymbol{\omega}_b \end{bmatrix} + \mathbf{H}_c \dot{\boldsymbol{\phi}} + \begin{bmatrix} \mathbf{0} \\ \mathbf{r}_b \times \mathbf{P} \end{bmatrix} \quad (\text{E.4})$$

$$\begin{bmatrix} \mathbf{v}_h \\ \boldsymbol{\omega}_h \end{bmatrix} = \mathbf{J}_{bh} \begin{bmatrix} \mathbf{v}_b \\ \boldsymbol{\omega}_b \end{bmatrix} + \mathbf{J}_{\phi h} \dot{\boldsymbol{\phi}} \quad (\text{E.5})$$

²For consistency subscript 0 will be interchanged with b .

where \mathbf{v}_h and $\boldsymbol{\omega}_h$ are the linear and angular velocities of the end-effector. Expressing \mathbf{v}_b and $\boldsymbol{\omega}_b$ from (E.4) and substituting them in (E.5) leads to:

$$\begin{bmatrix} \mathbf{v}_h \\ \boldsymbol{\omega}_h \end{bmatrix} = \mathbf{J}_{\phi h}^g \dot{\boldsymbol{\phi}} + \mathbf{J}_{bh} \mathbf{H}_b^{-1} \begin{bmatrix} \mathbf{P} \\ \mathbf{L} - \mathbf{r}_b \times \mathbf{P} \end{bmatrix} \quad (\text{E.6})$$

The latter term of (E.6) is equal to zero if \mathbf{P} and \mathbf{L} are zero. Solving for $\dot{\boldsymbol{\phi}}$ leads to:

$$\dot{\boldsymbol{\phi}} = \mathbf{J}_{\phi h}^{g+} \left(\begin{bmatrix} \mathbf{v}_h \\ \boldsymbol{\omega}_h \end{bmatrix} - \mathbf{J}_{bh} \mathbf{H}_b^{-1} \begin{bmatrix} \mathbf{P} \\ \mathbf{L} - \mathbf{r}_b \times \mathbf{P} \end{bmatrix} \right) + (\mathbf{E} - \mathbf{J}_{\phi h}^{g+} \mathbf{J}_{\phi h}^g) \dot{\boldsymbol{\xi}} \quad (\text{E.7})$$

Even if the base body undergoes translational and rotational motion, and the momentum of the system is different from zero, by using (E.7) a desired end-effector velocity can be obtained. For more details about the solution of (E.6) see Section 3.1.1.

Appendix F

Parameters of the manipulators used

Here, the parameters of the two manipulator systems used in the numerical simulations are included.

F.1 3D 7 DOF manipulator

In the bigger part of the simulation results presented, a 7 DOF manipulator mounted on a free-floating base is used. All links are connected through rotational joints. The structure of the manipulator is depicted in Fig. F.1. Each joint is depicted by a blue circle and each link is represented by its centroid. The geometrical structure of the manipulator is in Table F.1. It includes information about the distance from the centroid of each link to the *input* and *output* joints. J_i stands for Joint i , ($i = 0, 1, 2, \dots, n$) where $n = p + 3$, $p = 7$ and 3 represents the three reaction wheels (RW) (Link 0 is the base body). The output of Link 7 is the end-effector (EE). All distances are expressed in the coordinate system fixed in Link i . The mass and inertia characteristics of the system are in Table F.2. Finally the relative orientation of the coordinate system fixed in joint i and the one fixed in the input joint for the parent body¹ of joint i is given in Table F.3. Note that the Z axis is the joint axis of rotation depicted by a dotted line in Fig. F.1.

The characteristics of the target satellite used are;

$mass = 200 \text{ kg}$;

$principal moments of inertia = [150, 150, 150] [\text{kgm}^2]$.

¹If i is an output joint for body k , body k is the parent of joint i .

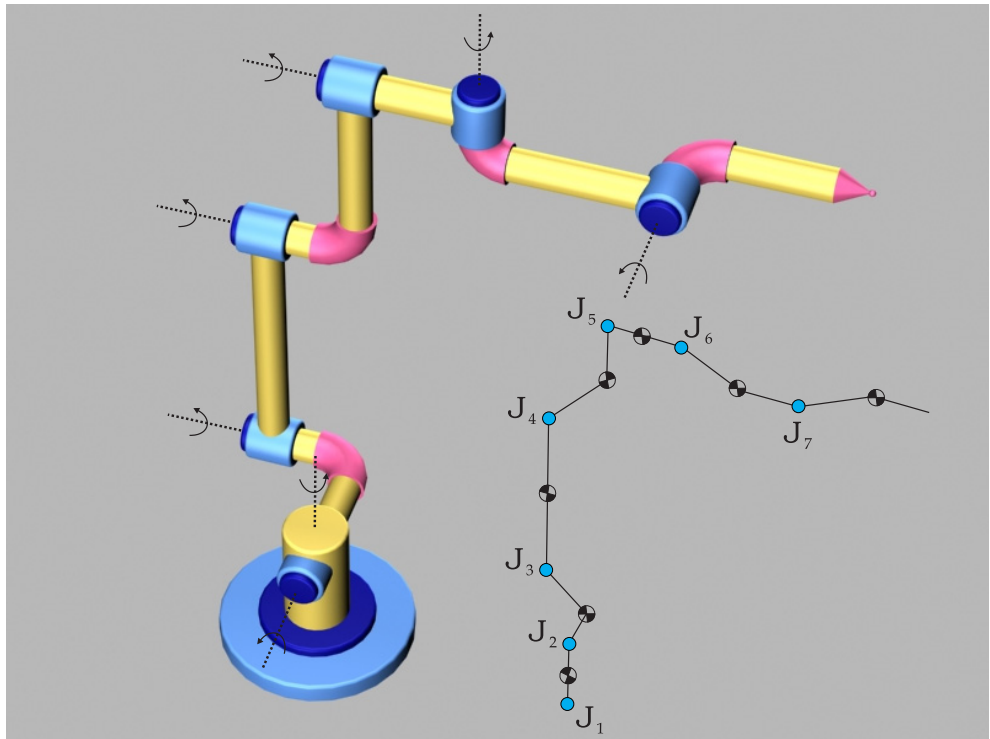


Figure F.1: 3D 7DOF manipulator

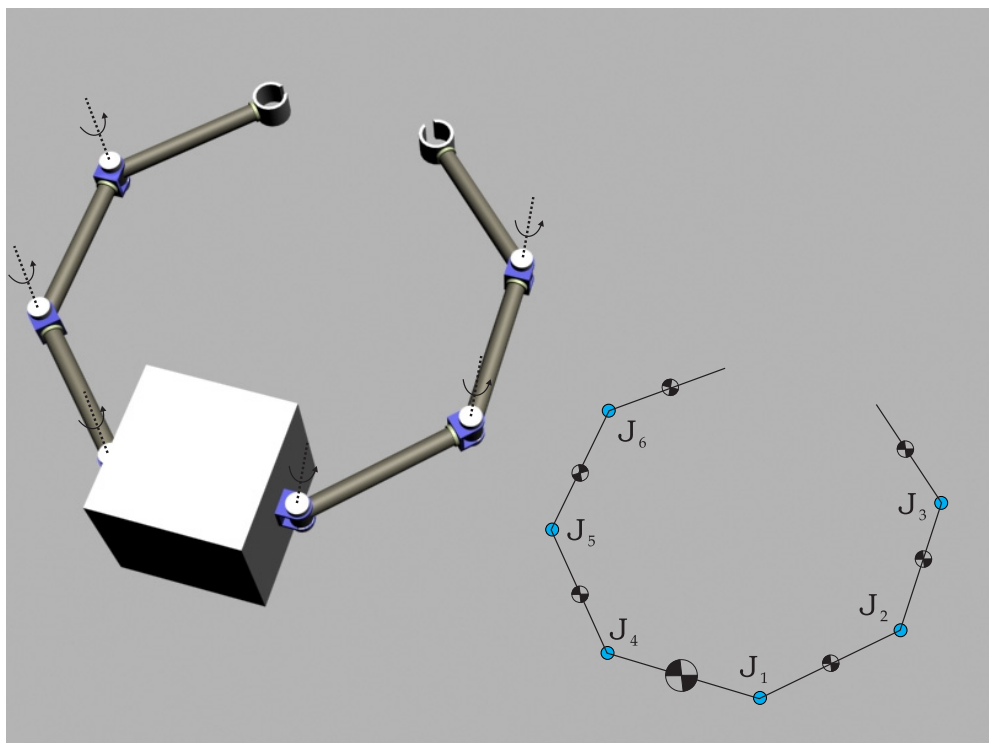


Figure F.2: 2D 6DOF dual-arm

Table F.1: 7DOF Manipulator - kinematical structure.

	<i>Joint IN [x,y,z] (m)</i>	<i>Joint OUT [x,y,z] (m)</i>
Link 1	[0, 0, -0.175] (J_1)	[0, 0, 0.175] (J_2)
Link 2	[0, 0, -0.2] (J_2)	[0, 0.275, 0.2] (J_3)
Link 3	[0, 0.435, 0] (J_3)	[0, -0.435, 0] (J_4)
Link 4	[0, 0.315, 0.275] (J_4)	[0, -0.315, 0] (J_5)
Link 5	[0, 0, 0.18] (J_5)	[0, 0, -0.18] (J_6)
Link 6	[0, -0.2750, -0.16] (J_6)	[0, 0.2750, 0] (J_7)
Link 7	[0, -0.266, -0.2] (J_7)	[0, 0.266, 0] (EE)
Link 0	-	[0.65, 0, 0.75] (J_1)
Link 0	-	[1, 0, 0] (J_8) RW_x
Link 0	-	[0, -1, 0] (J_9) RW_y
Link 0	-	[0, 0, -0.75] (J_{10}) RW_z

Table F.2: 7DOF Manipulator - mass and inertia parameters.

	Ixx(kgm²)	Iyy	Izz	Ixy	Ixz	Iyz	mass(kg)
Link 0	1200.00	1200.00	1200.00	0	0	0	1000.00
Link 1	1.22	0.51	1.33	-0.07309	0.00071	0.1132	35.01
Link 2	2.10	1.38	2.36	0	-0.00214	0	30.00
Link 3	0.10	3.38	3.36	0	-0.00214	0	22.69
Link 4	0.43	2.27	1.91	0	-0.6328	0	21.38
Link 5	0.39	0.40	0.07	0	0.01675	0	16.75
Link 6	0.57	0.60	0.13	0	-0.2313	0	26.17
Link 7	0.17	0.24	0.14	0.000781	-0.0145	-0.000137	18.07
RW_x	0.10	0.10	0.10	0	0	0	1.00
RW_y	0.10	0.10	0.10	0	0	0	1.00
RW_z	0.10	0.10	0.10	0	0	0	1.00

Table F.3: 7DOF Manipulator - Axis of rotation of each joint.

	J_1 [deg]	J_2	J_3	J_4	J_5	J_6	J_7	J_8	J_9	J_{10}
X	0	0	-90	0	0	-90	0	0	-90	0
Y	0	90	0	0	0	0	90	90	0	0
Z	0	0	-90	0	0	0	0	0	0	0

F.2 Planar 6 DOF dual-arm system

In Section 5.4 a planar manipulator system with two robotic arms (each 3 DOF) mounted on a free-floating base is used. Their structure is depicted in Fig. F.2. The geometry as well as mass and inertia characteristics of the system are in Tables F.4 and F.5.

Table F.4: 6DOF Manipulator - kinematical structure.

	<i>Joint IN [x,y,z] (m)</i>	<i>Joint OUT [x,y,z] (m)</i>
Link 1	[-0.5, 0, 0] (J_1)	[0.5, 0, 0] (J_2)
Link 2	[-0.5, 0, 0] (J_2)	[0.5, 0, 0] (J_3)
Link 3	[-0.5, 0, 0] (J_3)	[0.5, 0, 0] (EE)
Link 4	[0.5, 0, 0] (J_4)	[-0.5, 0, 0] (J_5)
Link 5	[0.5, 0, 0] (J_5)	[-0.5, 0, 0] (J_6)
Link 6	[0.5, 0, 0] (J_6)	[-0.5, 0, 0] (EE)
Link 0	-	[0.5, 0, 0] (J_1)
Link 0	-	[-0.5, 0, 0] (J_4)

Table F.5: 6DOF Manipulator - mass and inertia parameters.

	I_{xx}(kgm²)	I_{yy}	I_{zz}	I_{xy}	I_{xz}	I_{yz}	mass(kg)
Link 0	1250.00	1250.00	1250.00	0	0	0	1000.00
Link 1	33	33	33	0	0	0	100
Link 2	33	33	33	0	0	0	100
Link 3	33	33	33	0	0	0	100
Link 4	33	33	33	0	0	0	100
Link 5	33	33	33	0	0	0	100
Link 6	33	33	33	0	0	0	100